Identification and Analysis of *Rab8* Mutants: Genetic Enhancers of a *Drosophila* Model of Frontotemporal Dementia

Ryan John Hatcher West

PhD

University of York
Department of Biology

October 2013

Abstract

Frontotemporal dementia (FTD) is a progressive neurodegenerative disease associated with preferential atrophic degeneration of the frontal and temporal lobes of the brain. It is the second most prevalent early onset dementia, after Alzheimer's disease, displaying an average age of onset between 45 and 65 years. FTD has a strong genetic association, with a positive familial history in approximately 50% of cases and autosomal dominance in up to 20%. One gene associated with the disease is *Chromatin Modifying Protein 2B* (*CHMP2B*). *CHMP2B* encodes a key component of Endosomal Sorting Complex Required for Transport III (ESCRT-III), which in turn is involved in the biogenesis of multivesicular bodies at the late endosome. Here we demonstrate *Rab8* mutants dominantly enhance toxicity of the FTD *CHMP2B* mutation *CHMP2B*^{Intron5}, when expressed in the *Drosophila* eye. Characterisation of neuronal morphology, at the larval neuromuscular junction, reveals *Rab8* mutants display significant synaptic overgrowth, coupled with a reduction in synaptic bouton size. This abnormal morphology can be rescued by overexpressing wildtype *Rab8* pre-synaptically, demonstrating a neuronal complement of Rab8 to be essential for normal synaptic growth. We also demonstrate that TGF-β signalling and JNK signalling, known regulators of synaptic assembly and function, are necessary for the unrestricted synaptic growth seen. Furthermore we identify the endosomal JNK scaffold POSH and the JNKKK TAK1 as a novel regulators of synaptic growth. Taken together these findings implicate *Rab8* as a novel enhancer of *CHMP2B*^{Intron5} toxicity in a *Drosophila* model of FTD and as a potent regulator of synaptic growth. In addition they suggest a potential role for innate immune responses in the regulation of synaptic development.

Table of Contents

List of Tables and Figures

Tables

Figures

Acknowledgements

I would like to take this opportunity to thank everyone who has supported me throughout the course of my PhD.

Firstly I would like to thank my supervisor Sean Sweeney for first introducing me to *Drosophila* research and for his continued patience and support. I would also like to thank him for always being there with his guidance and advice and for always being happy to discuss beer, music and life outside the lab.

I would also like to thank Chris Elliott who, throughout the course of my project, has always been available with his support and advice. I also extend my thanks to all members of both the Sweeney and Elliott labs past and present.

I would like to acknowledge all of our collaborators that have made this work possible, including Fen-Biao Gao, Yubing Lu and Bruno Marie. I extend my gratitude to members of my TAP committee, Betsy Pownall and Gonzalo Blanco and to members of the Technology facility who have always been available with their advice and guidance. In particular I thank Meg Stark for assisting me with all aspects of TEM.

I thank all my friends, especially those in York who have made my time here the enjoyable experience it has been. I thank my family for their continued support and ensuring I have a roof over my head. Finally I would like to thank Sarah who has put up with me through everything and has always been there.

Declaration

I hereby declare that all work presented within this thesis is my own work except for when stated within the text or figures.

1. Introduction

1.1.Rationale

Frontotemporal dementia (FTD) is, after Alzheimer's disease (AD), the second most prevalent form of early onset dementia (Ratnavalli et al., 2002). There are estimated to be 800,000 dementia sufferers in the UK, creating a financial burden of approximately £23 billion per year and putting a significant strain upon the NHS (Kane and Cook, 2013; Lakey et al., 2012). One quarter of all hospital beds are occupied by someone with dementia (Kane and Cook, 2013; Lakey et al., 2012). With an increasing life expectancy, associated with improved health care, these figures are set to increase dramatically with the number of dementia sufferers expected to reach 1 million by 2021 costing £50 billion per year by 2038 (Kane and Cook, 2013; Knapp, 2007; Lakey et al., 2012). As such there is a real demand for greater understanding of the molecular and genetic mechanisms underlying dementia pathology, in order to develop new therapeutic options and combat the burden of dementia. In this investigation a *Drosophila* model of FTD, associated with a mutation in the *Chromatin modifying protein 2B* (*CHMP2B*) gene locus, was used to identify novel factors that influence disease pathology. In addition analysis looked to elucidate the molecular mechanisms in which these factors are involved. One such factor identified was the small GTPase Rab8 (Ras-related proteins in brain 8). The main aim of this investigation was to characterise the role of Rab8 in the regulation of neuronal development and identify the mechanisms contributing towards the unregulated synaptic growth phenotype displayed in *Rab8* mutants. In addition this investigation looks to determine whether these mechanisms contribute towards the Role of *Rab8* as a modifier of *CHMP2B*.

1.2. Frontotemporal Dementia

1.2.1. Clinical Characteristics of Frontotemporal Dementia

Frontotemporal Dementia is a comprehensive term referring to a group of distinct clinical syndromes affiliated with frontotemporal lobar degeneration (FTLD), a progressive neurodegenerative disease associated with preferential atrophic degeneration of the frontal and temporal lobes of the brain (Chauvire et al., 2007; Fukui, 2009; Quaid, 2011). Clinical variants of FTD display highly heterogeneous symptoms, associated with the broad clinico-pathological spectrum of the disease (Seelaar et al., 2011). As such FTD syndromes are commonly classified, based upon the most predominant and earliest presenting syndromes, into three distinct categories; behavioural variant FTD (bvFTD), semantic dementia (SD) and progressive non-fluent aphasia (PNFA) (Josephs et al., 2011; Pan and Chen, 2013). These three syndromes show distinct clinical traits, characterised by behavioural aberrations including disinhibition and loss of volition, progressive decline in word association and semantic memory, and disturbances to motor speech and syntax, for bvFTD, SD and PNFA respectively (Chauvire et al., 2007; Ichikawa and Kawamura, 2009; Leyton and Hodges, 2010). In addition to these main classifications the FTD spectrum may also present with additional phenotypes associated with progressive supranuclear palsy (PSP), corticobasal degeneration (CBD) and Frontotemporal dementia with motor neuron disease (FTD-MND) (Josephs et al., 2006; Pan and Chen, 2013; Seelaar et al., 2007).

The most prevalent variant of FTD, estimated to account for 50 % of all FTD cases, is bvFTD (Piguet et al., 2011). It most commonly presents with insidious behavioural and personality alterations including apathy, disinhibition, emotional blunting, loss of empathy, irritability, neglect for personal hygiene and aggression (Bathgate et al., 2001; Merrilees et al., 2010; Piguet et al., 2011; Snowden et al., 2001). Whilst typically less pronounced than behavioural aberrations patients may also present with deterioration of cognitive function, most notably displaying deficits in executive function (Diehl-Schmid et al., 2011; Rascovsky et al., 2011). Additionally patients may display impaired working

memory whilst, in contrast to Alzheimer's disease, visuospatial function is conserved (Rascovsky et al., 2011). Clinical presentation of bvFTD displays a distinct overlap with that of motor neurone disease (MND) with ~ 40 % of MND patients presenting behavioural and cognitive deficits associated with bvFTD and 15 % of bvFTD patients also presenting with MND (Bak and Hodges, 2001; Lomen-Hoerth, 2004). In contrast to bvFTD SD and PNFA, collectively termed primary progressive aphasias, are classified as language variants of FTD. SD or temporal variant FTD is typically characterised by asymmetric atrophy of the anterior temporal lobes (Chan et al., 2001; Rosen et al., 2002). Patients displaying predominantly left-sided atrophy typically present with fluent aphasia manifesting in a progressive decline in word association and comprehension associated with semantic memory, whilst retaining syntax (Chan et al., 2001; Seeley et al., 2005). Those suffering from predominantly right-sided atrophy present with behavioural perturbations that overlap with bvFTD (Seeley et al., 2005). Progressive atrophic degeneration typically spreads to affect contralateral temporal lobes after an average of 3 years, resulting in presentation of a range of symptoms associated with degeneration of both lobes (Brambati et al., 2009; Maguire et al., 2010; Seeley et al., 2005). In contrast to SD, patients presenting with PNFA show conservation of semantic memory and display limited behavioural aberrations. PNFA is, instead, characterised by a progressive decline in motor speech and syntax, displaying speech apraxia and expressive agrammatism (Rohrer et al., 2010).

Despite distinct classification criteria it is apparent that significant overlap in clinical presentation can occur between disease variants, with more significant overlap occurring in latter stages of disease progression. Such presentation can be attributed to increasingly diffuse atrophic degeneration occurring throughout the frontal and temporal lobes as the disease progresses.

1.2.2. Neuropathology of Frontotemporal Dementia

All FTD variants are characterised by distinct FTLD associated pathology, the major hallmark of which is selective focal atrophy of the frontal and temporal cortices of the brain (Janssen et al., 2005). Such gross atrophy displays progressive neuronal loss, spongiosis and variable degrees of gliosis throughout layers II and III of the frontal and temporal cortices (Holm et al., 2007; Mackenzie et al., 2006; Mann, 1998; Vanderzeypen et al., 2003). Adjacent regions of white matter may also display axonal and myelin loss accompanied by gliosis. Variability within the topographical patterns of focal atrophy seen in FTLD can, in part, be implicated in the heterogeneity of clinical symptoms presenting in FTD. However neuropathology in FTD shows further heterogeneity in the accumulation of distinctive proteins into neuronal inclusions within the brain (Mackenzie et al., 2010; Urwin et al., 2010b). The presence of such inclusions leads to further sub-classification of FTD, based on the predominant component of the neuronal inclusions seen, into 3 main categories; Tau-Positive FTLD (FTLD-Tau), Trans-activation response (TAR) DNA-binding protein 43 (TDP-43) positive FTLD (FTLD-TDP) and Fused in sarcoma (FUS) positive FTLD (FTLD-FUS) (Mackenzie et al., 2010; Urwin et al., 2010b).

FTLD-TDP, currently believed to be the most prevalent subtype of FTD, accounts for approximately 50 % of all FTD cases (Goedert et al., 2012). It is characterised by the presence of tau-negative, TDP-43- and ubiquitin-positive neuronal inclusions, occurring most prevalently in layer II neurons of the frontal and temporal cortices, as well as abundantly in the hippocampal dentate gyrus (Armstrong et al., 2012; Mackenzie et al., 2011). It is estimated that 50 % of bvFTD cases are associated with FTLD-TDP (Josephs et al., 2011). FTLD-Tau, characterised by the presence of neuronal inclusions composed predominantly of hyperphosphorylated tau protein, is the second most prevalent subtype of FTD, accounting for approximately 45 % of all cases (Boxer et al., 2013). It is implicated in ~ 40 % of bvFTD cases and ~ 70 % of PNFA cases (Josephs et

al., 2011). FTLD-FUS is considerably less prevalent, accounting for less than 10 % of FTD cases (Goedert et al., 2012). FTLD-FUS inclusions show a distribution and morphology pattern similar to that seen in FTLD-TDP (Rabinovici and Miller, 2010). FTLD-FUS cases, however, show significant focal atrophy within the caudate region of the brain and display a very early onset of symptoms, with a mean onset of 38 years of age (Josephs et al., 2010; Neumann et al., 2009). Whilst FTLD-TDP, FTLD-Tau and FTLD-FUS are the 3 major sub-classes a small number of FTD cases have been identified in which inclusions show tau-, TDP-43- and FUS-negative, ubiquitin-positive inclusions, termed FTD-UPS, or show no discernable inclusions, termed FTLD-ni (Urwin et al., 2010b).

1.2.3. Epidemiology and Aetiology of Frontotemporal Dementia

FTD is commonly implicated as the second most prevalent form of early onset dementia, occurring under 65 years of age, with an average age of onset between 46 and 65 and the youngest reported case being just 21 (Snowden et al., 2004)(Snowden et al., 2002). Epidemiological studies estimate incidence rates to range from between 2.7 and 15.1 cases per 100 000 adults aged under 65 (Ratnavalli et al., 2002). Interestingly a number of these studies have proposed incidence levels to be greater than previously thought, including a significant prevalence amongst those of advanced age. Cases in individuals over 65 account for 20 - 25 % of all cases (Ahmad et al., 2009; Arvanitakis, 2010; Borroni et al., 2010; Galimberti and Scarpini, 2010). Taken together this suggests FTD to be an under-diagnosed cause of dementia.

The aetiology of FTD remains largely unknown with the majority of cases being sporadic, without defined cause. However despite this, unlike Alzheimer's disease, FTD shows a strong genetic association with 40 - 50 % of cases showing a familial history of the disease and ~ 20 % of cases showing an autosomal dominant mode of inheritance (Chow et al., 1999a; Rosso et al., 2003a; Talbot and Ansorge, 2006). Of all the variants of FTD bvFTD shows the

strongest familial history whilst SD shows the least familial association (Goldman et al., 2005).

1.2.4. Genetic Causes of Frontotemporal Dementia

To date 7 predominant gene loci have been implicated in FTD of which 3 are believed to account for the majority of familial FTD cases; the *Microtubule Associated Protein Tau* (*MAPT*), *Progranulin* (*GRN*) and *Chromosome 9 Open Reading Frame 72* (*C9ORF72*) gene loci (Baker et al., 2006; Cruts et al., 2006; DeJesus-Hernandez et al., 2011; Hutton et al., 1998; Renton et al., 2011). A much smaller subset of FTD cases are associated with mutations in 4 other loci; the *Valosin Containing Protein* (*VCP*), *TAR DNA Binding protein 43* (*TARDBP*) *Fused in Sarcoma* (*FUS*) and *Charged Multivesicular Body Protein 2B* (*CHMP2B*) genes (Borroni et al., 2009; Skibinski et al., 2005; Van Langenhove et al., 2010; Watts et al., 2004). There has also been reported possible involvement of the *Apolipoprotein E* (ApoE) and *Presenillin*-1 (PSEN1) gene loci (Bernardi et al., 2011; Seripa et al., 2011).

1.2.5 CHMP2B a Core Component of The Endosomal Sorting Complex Required for Transport III (ESCRT-III)

Mutations in the *CHMP2B* gene locus have been associated with rare autosomal dominant cases of FTD linked to chromosome 3 (FTD-3) (Skibinski et al., 2005). During the course of this investigation focus will, predominantly, be upon on FTD associated with mutations in this *CHMP2B* gene. In addition this investigation looks to determine the role of *CHMP2B* in the regulation of cellular processes involved in the development and function of neurons, in both healthy and diseased states. *CHMP2B* encodes a core component of the Endosomal Sorting Complex Required for Transport III (ESCRT-III), one of 4 heteromeric ESCRT complexes (Table 1.1) that comprise the fundamental machinery involved in cargo-recognition and membrane-deformation events essential to a number of diverse cellular processes (Carlton, 2010; Skibinski et al., 2005;

Stuffers et al., 2009; Wollert et al., 2009b). These include cellular abscission, viral budding, exosome secretion, autophagy and the biogenesis of multivesicular bodies (MVB's) (Ariumi et al., 2011; Elia et al., 2011; Filimonenko et al., 2007a; Tamai et al., 2010).

Table 1.1. ESCRT Complexes and Their Constituent Components.
* = Core component

	Subunit		
	Yeast	**Human**	***Drosophila***
ESCRT-0	Vps27	HRS/HGS	HRS
	HSE1	STAM1	STAM
		STAM2	
ESCRT-I	Vps23	TSG101	TSG101
	Vps28	H-Vps28	Vps28
	Vps37	Vps37A	Vps37A/Mod(r)
		Vps37B	Vps37B
		Vps37C	
		Vps37D	
	MVB12	MVB12A	CG7192
		MVB12B	
ESCRT-II	Vps22	EAP30/Snf8	Lsn
	Vps25	EAP20	Vps25
	Vps36	EAP45	Vps36
ESCRT-III	Vps46	CHMP1A	
		CHMP1B	CHMP1
	Vps2*	CHMP2A*	Vps2*
		CHMP2B*	CHMP2B*
	Vps24*	CHMP3*	Vps24*
	Vps32/Snf7*	CHMP4A*	Shrub*
		CHMP4B*	
		CHMP4C*	
	Vps60	CHMP5	CG6259
	Vps20*	CHMP6*	Vps20*

MVB formation occurs through the sequential activity of ESCRT's 0-III allowing the deformation, invagination and scission of the late endosome limiting membrane to form intraluminal vesicles (ILV's) that act as segregation compartments into which ubiquitinylated endosomal cargo proteins can be sorted and loaded into (Fig. 1.1.) (Carlton, 2010; Filimonenko et al., 2007b; Gruenberg and Stenmark, 2004b; Piper and Katzmann, 2007b). This process forms a central point in both the endocytic and autophagic degradative

trafficking pathways (Fig. 1.2.) that, through targeted sorting and degradation of cellular components, are fundamental to normal cellular homeostasis.

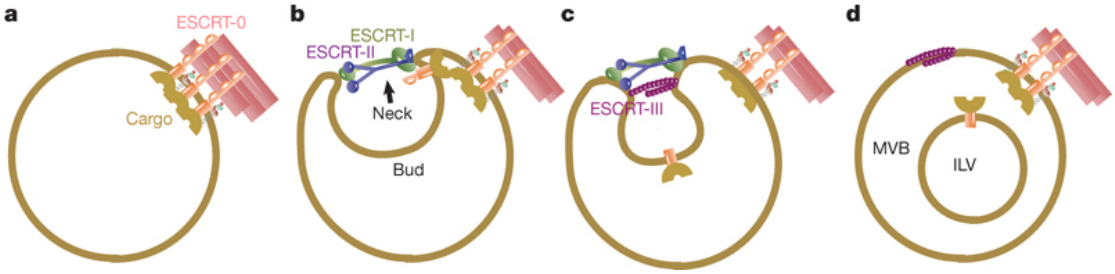

Figure 1.1. Multivesicular Body Biogenesis
MVB biogenesis occurs through the sequential activity of ESCRT's 0-III. First ESCRT-0 self assembles and clusters cargo at the early endosome (a). This is followed by recruitment of ESCRT's I and II, which may prop open the membrane neck (b). ESCRT-II then recruits ESCRT-III, via the Vps20 subunit, allowing membrane scission to occur (c). Finally, post scission, cargo is internalized into intraluminal vesicles (ILV's) and ESCRT-III remains on the external membrane until it is recycled by Vps4 (d). Reproduced from Wollert and Hurley, 2010 (Wollert and Hurley, 2010).

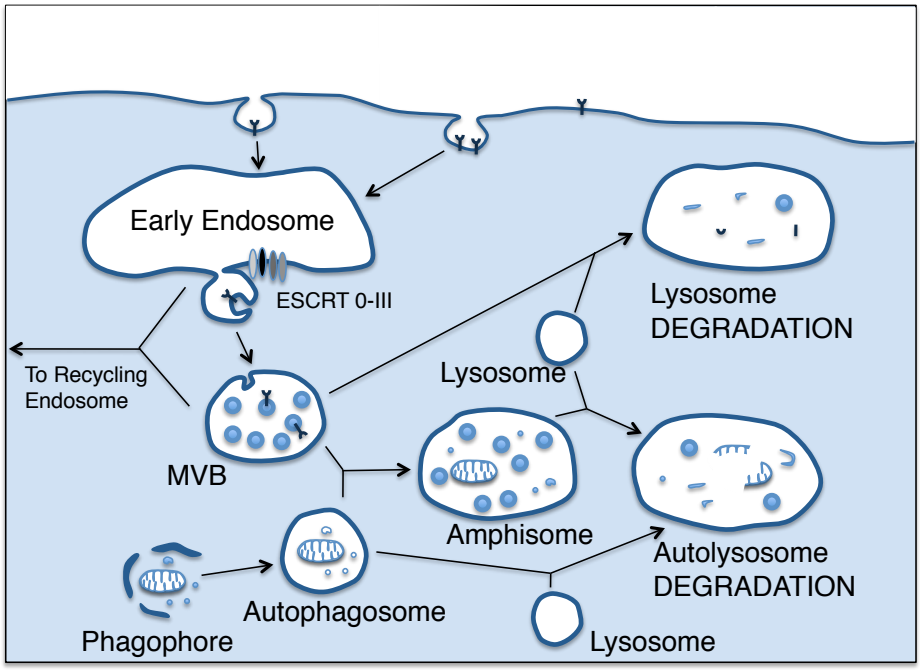

Figure 1.2. Multivesicular Bodies Form a Central Point in Both the Endosomal-Lysosomal and Autophagic Trafficking Pathways.
Multivesicular body (MVB) biogenesis occurs through the sequential activity of ESCRT's 0 – III acting to deform and invaginate the plasma membrane of early endosomes, forming MVB's. MVB's act as a nexus in both the endosomal-lysosomal and autophagic degradative pathways, which are essential for cellular homeostasis. In order to degrade endosomal cargo MVB's fuse with the lysosome. Alternatively MVB's can fuse with autophagosomes forming autolysosomes, where content is degraded. Autophagosomes can also fuse directly with the lysosome, however this typically occurs less frequently. Endosomal cargo can also be targeted for recycling to the recycling endosome either directly or via MVB formation.

Of all the ESCRT complexes (Table 1.1.) both *in vivo* and *in vitro* studies suggest that ESCRT-III is arguably the most important, fundamental to membrane deformation and scission events and involved in all known ESCRT dependent processes (Henne et al., 2011; Henne et al., 2013; Schmidt and Teis, 2012; Wollert et al., 2009a). Unlike ESCRT's 0-II ESCRT-III only transiently assembles upon the endosome and is unable to form a stable complex within the cytoplasm, where the core subunits (Table 1.1.) auto-inhibit, forming stable inactive monomers (Bajorek et al., 2009; Merrill and Hanson, 2010; Teis et al., 2008; Zamborlini et al., 2006). Autoinhibition is achieved through conformational orientation in which the negative C-terminus, of each component, obstructs a 7nm hairpin structure that is essential for membrane binding and dimerisation (Bajorek et al., 2009; Merrill and Hanson, 2010; Zamborlini et al., 2006). ESCRT-III assembly, into an active filamentous structure, is initiated through ESCRT-II induced activation of CHMP6/Vps20 leading to the cascading assembly of ESCRT-III (Teis et al., 2008). This occurs through a series of conformational changes that alleviate autoinhibition and promote oligomerisation and membrane association. Active ESCRT-III is then capable of recruiting deubiquitinases, allowing for ubiquitin recycling, and inducing membrane deformation events (Schmidt and Teis, 2012).

Recent evidence suggests that CHMP2B not only promotes recruitment of other components to the plasma membrane, during MVB biogenesis, but also has a fundamental role in the membrane deformation events (Bodon et al., 2011b; Hanson et al., 2008). Bodon et al. (2011) demonstrate that over expression of *CHMP2B* promotes its recruitment to the plasma membrane where polymerization into protruding helical structures directly interacting with the inner leaflet of the membrane bilayer induces membrane constriction (Bodon et al., 2011b). This evidence supports previous hypotheses that suggest ESCRT-III proteins act to catalyse membrane fission events through the formation of membrane deforming hemi-spherical structures during MVB biogenesis (Fabrikant et al., 2009). Despite this the exact mechanism by which CHMP2B and the ESCRT-III complex functions in membrane remodelling remains yet to be fully elucidated.

1.2.6. The Role of CHMP2B in Frontotemporal Dementia

Biogenesis of MVB's and normal trafficking through the endosomal-lysosomal and autophagic-lysosomal trafficking pathways, to which MVB's act as a nexus (1.2.), are essential for the maintenance of normal cellular homeostasis and the regulation of diverse biological processes (Guillaumot et al., 2010; Ryter et al., 2013; Schneider and Zhang, 2010). As such perturbation to normal MVB biogenesis and the ESCRT machinery, fundamental for their formation, has been implicated in a range of disease's including cancer, infectious diseases and neurodegenerative disease, including Parkinson's, Huntington's and FTD (Schneider and Zhang, 2010; Stuffers et al., 2009; Urwin et al., 2010a; Wollert et al., 2009b).

The first mutation implicating CHMP2B in FTD was identified in 2005 in a large Danish cohort suffering from autosomal dominant, familial frontotemporal dementia associated with chromosome 3 (FTD-3) (Skibinski et al., 2005). It was demonstrated that all affected members of this large cohort displayed the same G-to-C transition within the splice acceptor site of exon 6, of the CHMP2B gene (Lindquist et al., 2008; Skibinski et al., 2005). This mutation resulted in aberrant mRNA splicing, leading to the formation of two novel transcripts, $CHMP2B^{\Delta 10}$ and $CHMP2B^{Intron5}$ (Lindquist et al., 2008; Skibinski et al., 2005). Furthermore these transcripts were shown to be present in the brains of patients at 10 % and 35 % of wildtype CHMP2B transcript levels, respectively (Urwin et al., 2010a). Subsequently, upon translation these transcripts result in the formation of two aberrant, C-terminally truncated proteins with their terminal 36 amino acids replaced by either a 29 amino acid nonsense sequence, in $CHMP2B^{\Delta 10}$, or a single valine residue, in $CHMP2B^{Intron5}$ (Lindquist et al., 2008; Skibinski et al., 2005). Subsequently further CHMP2B mutations have been identified in FTD patients outside of this original Danish kindred (Momeni et al., 2006; van der Zee et al., 2008). These include an autosomal dominant Belgian pedigree displaying the *CHMP2B* mutation $CHMP2B^{Q165X}$ and an Afrikaner family presenting with a potential disease causing mutation, $CHMP2B^{R186X}$ (Momeni et al., 2006; van der Zee et al., 2008). Interestingly the Afrikaner mutation

(*CHMP2B*^{R186X}) was only observed in unaffected family members and not their affected relatives (Momeni et al., 2006). Therefore the pathogenesis of this mutation remains unclear. For the *CHMP2B*^{Q165X} and *CHMP2B*^{R186X} mutations Glutamine-165 or Arginine-186, respectively, are substituted for a premature stop codon. As such both mutations also result in the formation of novel C-terminally truncated CHMP2B proteins, suggesting a common mechanism behind pathology associated with CHMP2B mutants; C-terminal truncation of the CHMP2B protein. Subsequent studies corroborate this hypothesis revealing a functional role of the CHMP2B C-terminus in CHMP2B's interaction with the AAA ATPase Vacuolar Protein Sorting 4 (Vps4) (Stuchell-Brereton et al., 2007). This interaction occurs via association of Microtubule Interacting and Transport (MIT) domains on Vps4 with a MIT interacting motif (MIM) located in the C-terminus of CHMP2B (Stuchell-Brereton et al., 2007). This subsequently promotes the recruitment of Vps4 which, in turn, catalyses the disassembly of the ESCRT-III complex. As such, the C-terminal truncation of CHMP2B results in a loss of the Vps4 interacting MIM, resulting in an aberrant failure of CHMP2B to dissociate from the ESCRT-III complex, maintaining ESCRT-III in an endosomally bound and "active" state. Substantiating this recent studies have shown that models of FTD, associated with the *CHMP2B*^{Intron5} mutation, show that CHMP2B^{intron5} forms an abnormal complex with the ESCRT-III component mSnf7-2, leading to abnormal accumulation of autophagosomes and dendritic retraction prior to neurodegeneration (Lee et al., 2007). As previously stated the C-terminus of all the core ESCRT-III components, including CHMP2B, are also involved in autoinhibition of the inactive monomers located within the cytosol. As such it is reasonable to infer that C-terminally truncating CHMP2B mutations also prevent autoinhibition therefore further promoting activity of CHMP2B.

1.3. Using *Drosophila* to Model Frontotemporal Dementia Associated With CHMP2B Mutations

1.3.1. *Drosophila* As a Model Organism

Drosophila melanogaster, the common fruit fly, has been utilised as a model organism for over a century, since the pioneering work by Thomas Hunt Morgan at the University of Columbia, USA. During this time *Drosophila* have become the most extensively utilised genetic model organism and a powerful tool for the elucidation of complex cellular and molecular mechanisms involved in a broad range of biological processes. These include cellular signalling, the cell cycle, the development of the nervous system, behaviour, development and even human diseases, where it is estimated that "…about 75 % of known human disease genes have a recognizable match in the genome of fruit flies" (Reiter et al., 2001; Roote and Prokop, 2013). Furthermore due to the high degree of evolutionary conservation seen between *Drosophila* and mammalian systems, despite evolutionarily diverging ~ 700 million years ago, work in *Drosophila* has laid fundamental foundations for further progression of research in mammals (St Johnston, 2002). *Drosophila* have become valued as a powerful research tool for a plethora of reasons. Firstly they are relatively cheap and easy to maintain under laboratory conditions. They display rapid generation times, ~ 10 - 12 days at room temperature, and produce large numbers of genetically identical progeny, facilitating high-throughput experiments. They have relatively short lifespans, 40 to 120 days depending upon diet and stress, allowing for easy study of age related disorders (Bonner and Boulianne, 2011). Furthermore they possess a complex and well characterised nervous system capable of displaying intricate behaviours, including learning and memory (Hirth, 2010; Margulies et al., 2005; McGuire et al., 2005; Ofstad et al., 2011). Finally, and perhaps most importantly, *Drosophila's* greatest asset is it's genetic potential. Not only has the entire *Drosophila* genome of ~13600 genes, located across just 4 chromosomes and displaying low redundancy, been sequenced since 2000, but there exists a plethora of powerful genetic tools available to manipulate *Drosophila* in a way unrivalled in any other organism (Adams et al., 2000).

1.3.2. Genetic Tools in *Drosophila*

The genetic power and tractability of *Drosophila* is optimized by the sophisticated genetic toolbox available for their manipulation. Traditionally, prior to the sequencing of the *Drosophila* genome in 2000, genetic manipulation relied, predominantly, upon forward genetic approaches (St Johnston, 2002). Using such approaches mutations are randomly generated and then screened based upon a specific phenotype of interest. Random mutations can be induced by a number of methods. For example flies can be fed ethyl methane sulphonate (EMS), which typically induces point mutations, or subjected to ionizing radiation to induce chromosomal rearrangements (Lewis, 1968; Muller, 1927). Alternatively one can use transposable elements, such as *P*-elements, to perform insertional mutagenesis in which transposable elements are “hopped” randomly into genes, disrupting their function (Ryder and Russell, 2003; St Johnston, 2002). This approach is often advantageous as the gene being affected can be easily identified using the *P*-element as a tag. However *P*-elements are inefficient mutagens, favouring transcriptionally active genes where the chromatin is more open, therefore generating “hot-spots” and not saturating the genome (St Johnston, 2002).

Whilst forward genetics has proven highly successful in the study of gene function, the sequencing of the *Drosophila* genome has led to an expansion of the *Drosophila* genetic toolbox through more favourable reverse genetic approaches (Adams and Sekelsky, 2002). Despite this forward genetics remain important due to their ability to generate allelic series of mutations, ranging from nulls (amorphs) to weak partial loss of function mutations (hypomorphs) (St Johnston, 2002). In contrast to forward genetics reverse genetics is based on the principle of mutating specific, known genes and observing the resultant phenotypes, thus allowing elucidation of gene function. Some reverse genetic approaches also rely upon forward genetic approaches, such as chemical or transposon mediated mutagenesis, that have been modified to allow targeting of specific genes. For example *P*-elements inserted near to a known gene of interest can be mobilized, allowing excision of the *P*-element and the generation of a double stranded DNA break (Adams and Sekelsky, 2002). Inaccurate repair

of such breaks will often occur, allowing deletion of the gene sequence flanking the *P*-element insertion site and generating a specific null mutant. In order to prevent loss of such mutations through homologous recombination Drosophilist's utilise what are known as balancer chromosomes (See section 1.3.4.). The use of transposable elements has proven highly versatile in *Drosophila* genetics with them also being utilized to allow misexpression of genes, using *P*[EP]-elements, or to characterize the temporal and spatial expression of genes through enhancer trapping (O'Kane and Gehring, 1987) (for reviews see Adams and Sekelsky, 2002 and Ryder and Russell, 2003). They also allow for the generation of transgenic fly lines via transposon mediated transformation (Rubin and Spradling, 1982). This process involves the insertion of a gene of interest into a plasmid between two p-element ends followed by the microinjection of this construct, along with a transposase, into syncytial blastoderm embryos (See section 2.5.). Typically the gene of interest will be inserted into a construct containing an Upstream Activator Sequence (UAS), allowing implementation of the *Drosophila* tissue specific expression system known as the UAS/GAL4 system (see section 1.3.3.). This system can also be used to implement alternative reverse genetic approaches, as opposed to those that rely upon modifications to classical forward genetic methods, for example RNA interference (RNAi) (Hammond et al., 2001). Based upon known gene sequences it is now possible to design double stranded RNA's against specific genes, allowing for target silencing of homologous genes through RNAi mediated degradation of cognate messenger RNA (mRNA) (Dietzl et al., 2007).

1.3.3. The UAS/GAL4 System

The UAS/GAL4 system is a powerful genetic tool that allows the ectopic expression of any gene sequence with a remarkable degree of flexibility, allowing for precise study of gene expression. It was initially developed as a tool in *Drosophila* by Andrea Brand and Norbert Perrimon, in 1993, and has since become one of the most reliable and useful tools in *Drosophila* genetics (Brand and Perrimon, 1993). The system relies upon two components. Firstly GAL4, a transcriptional activator derived from yeast, that is expressed in a tissue or cell

specific manner and, secondly, a transgene under the control of the Upstream activator sequence (UAS) to which GAL4 binds, activating expression. Through expressing these two individual components in different flies they can easily be brought together, promoting controlled ectopic gene expression in a cell/tissue specific manner, through a straightforward cross (Fig. 1.3.).

Progressive modifications and adaptations to the original GAL4 system have created a highly versatile and powerful suite of genetic tools that allow for highly regulated temporal and spatial control of gene expression within *Drosophila*. These include the abilities to selectively antagonize GAL4 using GAL80 and temperature sensitive GAL80's, the ability to temporally regulate expression using a series of heat shock promoters associated with GAL4 or GAL80 and inducible Gal4's which can be activated through feeding specific ligands to larvae (Elliott and Brand, 2008; Han et al., 2000; Matsumoto et al., 1978).

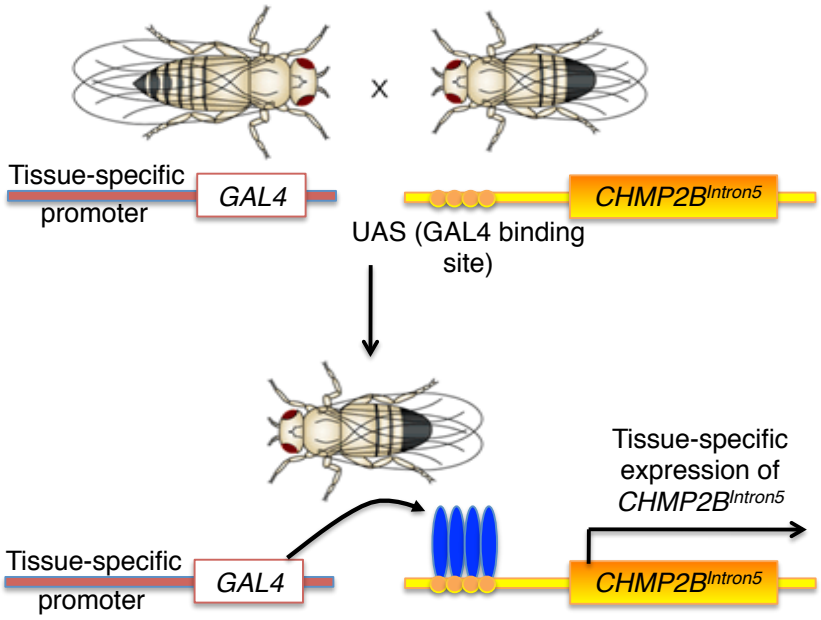

Figure 1.3. The UAS/GAL4 system Allows Ectopic Gene Expression in A Controlled Tissue Specific Manner
The UAS/GAL4 system is a bipartite system in which one line expresses GAL4 under the control of a tissue specific promoter and the other contains a gene of interest (in this example CHMP2B^{Intron5}) downstream of the UAS to which GAL4 binds. These 2 components are brought together by crossing the fly lines, giving progeny in which the gene of interest is expressed only in those cells or tissue types expressing the GAL4 protein.

1.3.4. Balancer Chromosomes

Balancer chromosomes have become an essential tool in *Drosophila* genetics, conveying 3 fundamental properties; they prevent homologous recombination, they are homozygously deleterious to survival and they carry dominant markers. The advantage of which is that they can be used to maintain a heterozygous mutation within a strain of *Drosophila* and that this mutation can be easily followed during mating schemes using the balancer chromosome markers on the alternative allele (for a review see Roote and Prokop, 2013) (Roote and Prokop, 2013).

In order to prevent homologous recombination in *Drosophila* females (it does not occur in males) balancer chromosome contain multiply inverted chromosomal segments. These multiple inversions allow chromosomes to segregate normally, however prevent synapsis between homologous chromosomes. If recombination does occur the presence of chromosomal fragment duplication and deletions results in lethality. This property, along with the homozygous lethality of balancers, is essential for the maintenance of heterozygous mutations in *Drosophila* stocks.

The second beneficial function of balancer chromosomes is that they convey dominant markers, characterised by a distinct phenotype, that allow researchers to easily follow a specific balancer and therefore the mutation that is on the alternative allele during a crossing scheme (Fig. 1.4).

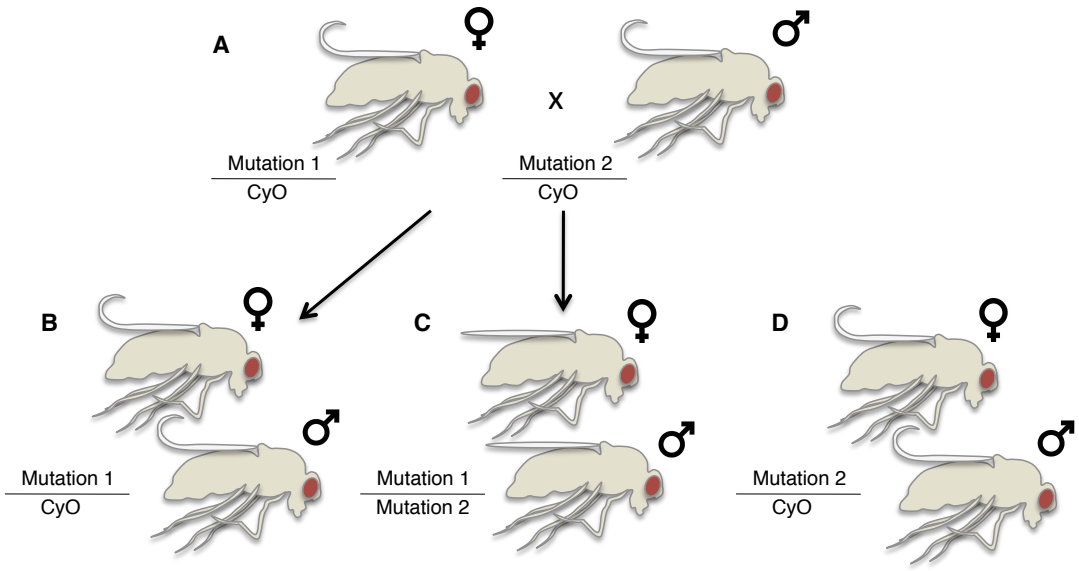

Figure 1.4. Balancer Chromosomes Allow Following of Mutations During Chromosomal Segregation
Balancer chromosomes allow researchers to select flies of the desired genotype during crossing schemes. For example in this cross parent flies carrying the desired mutations are crossed together (A) with the goal of obtaining progeny processing both mutations (C). Parent flies (A) each possess one of the desired mutations on the second chromosome with the balancer chromosome CyO on the alternative allele. The CyO balancer carries a dominant marker giving adults curly wings. Therefore following crossing chromosomal segregation produces progeny possessing either curly (B & D) or straight (C) wings. Those with curly wings must possess the balancer chromosome whilst equally those with straight wings must be the desired genotype possessing both mutation 1 and mutation 2 (one on each allele of chromosome 2). As such balancers allow the researcher to follow alleles and obtain flies of the desired genotype during crossing schemes.

1.3.5. Using *Drosophila* to Study Neurodegeneration and Human Neurodegenerative Disorders

Whilst human genetic studies have contributed significantly in the identification of genetic loci implicated in neurodegenerative diseases they show limited potential in the dissection of molecular pathways contributing to disease development and progression. Furthermore there are a number of technical and ethical constrains that limit the use of human participants in the study of disease. The majority of studies that do use humans to study neuropathology occur *post mortem*, providing limited insight into early disease pathology. As such, in order to elucidate the underlying pathogenic mechanisms associated with disease and develop approaches to prevent, stop, ameliorate or even reverse disease progression we must develop reliable models of neurodegenerative diseases. As the most tractable and highly utilized genetic

model organism *Drosophila* have already proven highly successful in the study of neurodegenerative disorders including Alzheimer's disease, Parkinson's Disease, Lysosomal Storage Disorders (LSD's), Huntington's Disease, Trinucelotide repeat disorders, Hereditary Spastic Paraplegia and Amyotrophic lateral Sclerosis (ALS) (Cao et al., 2008; Chakraborty et al., 2011; Huang et al., 2005; Jung and Bonini, 2007; Marsh et al., 2003; Milton et al., 2011; Moloney et al., 2010; Orso et al., 2005; Watson et al., 2008; Weiss et al., 2012; Whitworth, 2011; Whitworth et al., 2006; Yu and Bonini, 2011).

One of the strengths of *Drosophila* in the modelling of neurodegenerative diseases is the conservation of human disease causing genes within *Drosophila*. For example 5 of the 7 core loci implicated in FTD have a *Drosophila* orthologue (Table 1.2.). Furthermore *Drosophila* show limited genetic redundancy, allowing for a more specific dissection of gene function than in other metazoan organisms.

Table 1.2. Conservation of Frontotemporal Dementia Disease Loci in *Drosophila*

Human Loci	Drosophila Orthologue	% Homology (amino acids)
MAPT	Tau	24
GRN	-	-
C9ORF72	-	-
VCP	TER94	83.63
CHMP2B	CHMP2B	52.75
TARDBP	TBPH	56
FUS	Caz	54.62

One system that has proven effective in the elucidation of genes that regulate neuronal development and function, with an emphasis on dissecting pathological mechanisms involved in neurodegenerative diseases, is the *Drosophila* neuromuscular junction (NMJ)

1.3.6. The *Drosophila* Larval Neuromuscular Junction as a Model Synapse

The *Drosophila* neuromuscular junction is a well characterised model synapse that has proven a highly amenable and successful tool for the study of synaptic

development and neurotransmission. Like with most *Drosophila* models this has been, in part, due to the unrivalled genetic tractability of the system, allowing precise manipulation and dissection of the molecular mechanisms involved in synaptic assembly and function. Furthermore, unlike vertebrate NMJ's which are cholinergic, *Drosophila* NMJ's are, like vertebrate central synapses, glutamatergic, showing significant conservation of molecular components (Broadie and Bate, 1993b; DiAntonio et al., 1999; Wu et al., 2010). However, in contrast to the vertebrate central synapse, each pre-synaptic motor neuron and it's associated post-synaptic muscle are distinctly identifiable, accessible and invariable (Broadie and Bate, 1993b; DiAntonio et al., 1999; Johansen et al., 1989; Wu et al., 2010). As well as this distinct pattern of distribution it is apparent that individual NMJ subtypes also display a largely archetypal structure characterized by stereotypical arborisation, size, bouton number and synaptic strength (Campbell and Ganetzky, 2012; Landgraf and Thor, 2006). As such specific NMJ's can be easily identified and reliably compared between flies and, therefore, a number of specific NMJ's have become standardized, well characterised model synapses. For example Muscle 6/7 in hemi-segment A3 (Fig. 1.5), which is innervated by one of 5 RP neurons (RP1-5), RP3.

Another benefit of the *Drosophila* NMJ is that it is highly amenable to analysis by well established physiological, genetic, anatomical and cell biological approaches. For example immunohistochemistry and electron microscopy allow for dissection of the structure and anatomy of the NMJ whilst the use of FM (frequency-modulated) dyes and classical electrophysiology provide insight into physiological function (Imlach and McCabe, 2009; Verstreken et al., 2008).

Therefore the *Drosophila* NMJ provides an accessible, amenable model synapse, representative of the glutamatergic vertebrate central synapse, for the study and dissection of molecular mechanisms involved in normal synaptic development and neurotransmission *in vivo.*

1.3.7. Anatomy of the *Drosophila* NMJ

The *Drosophila* larval body plan displays a predominantly segmented structure, comprised of 14 segments; 3 defining the head and mouthparts, 3 thoracic segments and 8 within the abdominal region (Fig. 1.5.A.) (Va et al., 2009; Wolpert, 2007). The development of these segments is strictly regulated and from segment A2-A7 this regulation shows a highly conserved molecular and genetic program, leading to the formation of 6 almost identically organized, bilaterally symmetrical segments (Hoang and Chiba, 2001; Keshishian et al., 1996; Landgraf et al., 2003b). Each of these segments can be further divided into the two bilaterally symmetrical hemi-segments, comprised of 30 distinct syncytial muscles (Fig. 1.5.B) (Hoang and Chiba, 2001). Within this abdominal region (A2-7) the majority of motor neurons have been extensively characterized, starting from their developmental origins within the neuroectoderm (Budnik, 2006; Landgraf et al., 1997). As such individual motor neuronal connections, to specific muscles, and the morphological and structural characteristics of these NMJ's have been well described, providing significant insights into the *Drosophila* larval motor neuronal system and, consequently, the regulation of synaptic assembly and function.

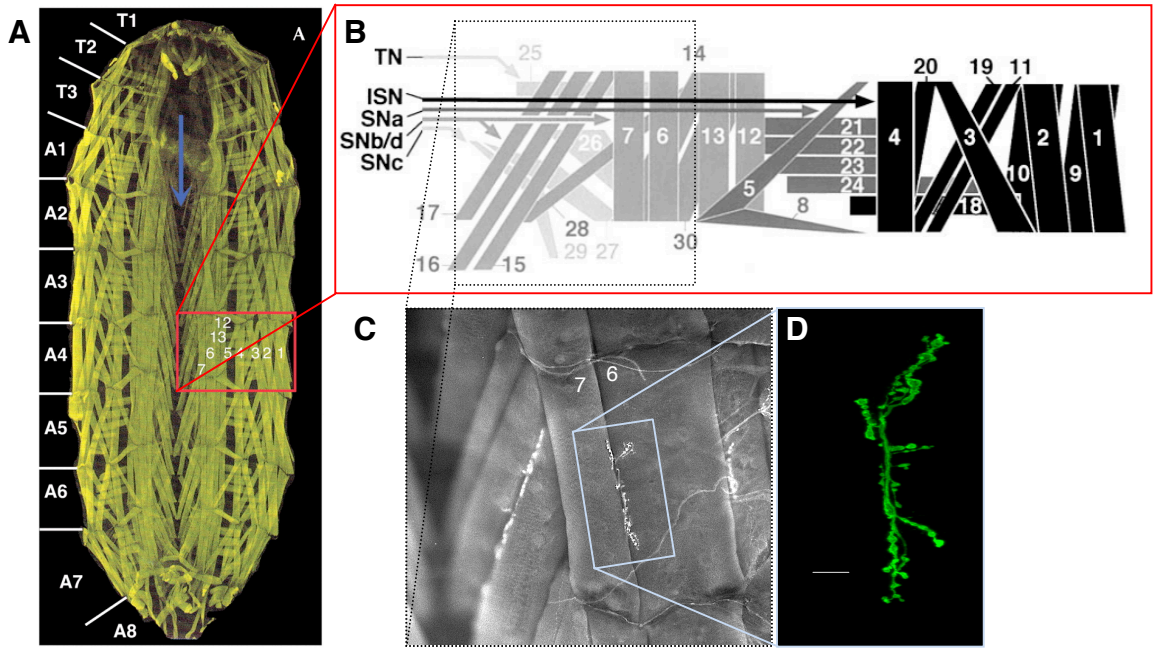

Figure 1.5. The *Drosophila* Larval Neuromuscular Junction.
(**A**) The Drosophila larval body plan is comprised of 14 segments, 3 defining the head and mouth, 3 thoracic segments (T1-T3) and 8 abdominal segments (A1-A3) (modified from Zhang and Stewart, 2010 (Zhang and Stewart, 2010)). (**B**) Each abdominal segment A2-A7 is

comprised of 2 bilaterally symmetrical hemi-segments containing 30 distinct muscles (modified from Hoang and Chiba, 2001 (Hoang and Chiba, 2001)). (**C-D**) Hemi-segments A2-A7 have been extensively studied with a number of specific NMJ's, for example muscle 6/7 hemi-segment A3 (c-d), becoming model synapses.

Motor neuronal cell bodies are located proximally to the larval central nervous system (CNS), within the outer cortex of the ventral nerve cord (VNC). Each uni-polar cell body presents two neuronal projections (neurites). The first projects into the neuropil region of the VNC where it forms a distinct dendritic arbour, that with other motor neuronal dendrites form a myotopic map, comparable to the motor columns seen in the vertebrate spinal cord (Landgraf et al., 2003a). The second projection is that of the axon which projects through one of 6 nerve branches (transverse nerve (TN), intersegmental nerve (ISN), segmental nerves (SN) a-d) (Fig. 1.5.B) before defasciculating in a stereotypical pattern to innervate its specific target muscle (Budnik, 2006; Hoang and Chiba, 2001). 32 known and well characterised motor neurons have been demonstrated to innervate the 30 muscle of each abdominal hemi-segment (Fig. 1.5.B) (Budnik, 2006; Collins and DiAntonio, 2007; Hoang and Chiba, 2001). The interface between the motor neuron and the target muscle is the NMJ and is characterized by a branched synaptic terminal comprised of a chain of varicosities known as synaptic boutons (Johansen et al., 1989). Each bouton, in turn, contains multiple pre-synaptic release sites known as active zones (Zito et al., 1999). The majority of NMJ's in *Drosophila* are classical glutamatergic (type-I) NMJ's, capable of evoking an excitatory contractile response within the post-synaptic muscle (Prokop, 2006). However there also exist non-classical type-II and type-III terminals, which display a functional role in neuromodulation, as well as other significantly less understood synaptic terminals (Prokop, 2006). In this investigation we are focusing upon classical type-I glutamatergic NMJ's.

The development of type-I glutamatergic NMJ's, from here on in referred to simply as NMJ's, is highly regulated, allowing for tight control of synapse number, and thus synaptic strength. As such NMJ's display a well characterised, archetypal morphology with a relatively consistent pattern of branching, NMJ size and number of synaptic boutons for each specific muscle type. Such invariability allows for the application of quantitative approaches in

the characterization of NMJ morphology, allowing dissection of molecular mechanisms involved in the regulation of NMJ assembly and function through the identification of perturbations in specific *Drosophila* mutants. NMJ's can be broadly classified into two populations based upon the morphology of their synaptic boutons, type-I small (type-Is) and type-I big (type-Ib) (Gramates and Budnik, 1999; Prokop, 2006). Type-Is NMJ's are, as the name suggests, characterized by small synaptic boutons, typically 1-1.5 µm in diameter as opposed to the larger 3-5 µm diameter boutons of type-Ib terminals (Atwood et al., 1993; Prokop, 2006). In addition, type-Is boutons tend to contain a plethora of variable sized vesicles, including large clear and dense cored vesicles. In contrast type-II boutons predominantly contain small, 30-40 nm, clear vesicles (Prokop, 2006). In comparison to type-Is boutons type-Ib's also display a greater number of mitochondria, are typically located closer to the NMJ branch point than type-Is boutons and present a larger subsynaptic reticulum (SSR) (Ataman et al., 2006b). The SSR is a feature characteristic to type-I NMJ's (Ataman et al., 2006b). It is comprised of complex convolutions of the post-synaptic muscle plasma membrane, which envelops the bouton, embedded with post-synaptic molecules, including glutamate receptors (GluR's), cell adhesion molecules and scaffolding proteins (Ataman et al., 2006b). Whist the SSR remains poorly understood in terms of function, it has been implicated as a local site for GluR translation whilst Syndapin has been implicated in regulating its biogenesis (Ataman et al., 2006b; Kumar et al., 2009).

1.3.8. Development and Plasticity of the NMJ

Growth, development and maintenance of the *Drosophila* larval NMJ is a highly dynamic process, requiring continuous remodelling in response to both muscle growth and to exogenous signals, allowing for modulation of synaptic strength in an activity dependent manner (Fuentes-Medel et al., 2009). Remodelling of the NMJ is, like most developmental processes, highly regulated by a variety of interconnected, intricate and bi-directional signalling pathways from both the pre- and post-synaptic terminals. During development to the larval 3rd instar

stage the muscle surface area will increase in size by approximately 100 times, with a 10 fold increase in bouton number between the first and third instar stages (Keshishian et al., 1993; Schuster et al., 1996). Throughout this growth process the larval NMJ must undergo a period of significant dynamic development, with growth paralleling that of the muscle. In contrast muscle growth is, with the exception of glutamate receptor clustering at the post synaptic density (PSD), relatively independent of innervation by the nervous system (Broadie and Bate, 1993a).

The initial formation of the NMJ begins approximately 13 hours post egg laying (PEL) (at 25°C) when the axonal growth cone of the newly developing motor neuron contacts the myopodia of its specific target muscle (Broadie and Bate, 1993b; Yoshihara et al., 1997). It is at approximately this time that the first electrical activity is detectable from central motor neurons (Baines and Bate, 1998). Upon interaction the developing growth cone undergoes remodelling, initially expanding across a large surface area of the muscle, the pre varicosity stage (~ 16.5 - 18.5 hours PEL), before constricting to form a distinct branched mature NMJ structure, characterized by definitive varicosities (~ 18 - 19 hours PEL) (Broadie and Bate, 1993b; Yoshihara et al., 1997). Prior to the interaction between the developing axonal growth cone and the muscle the development of the pre- and post-synaptic components are autonomous of each other. For example it has been shown that functional glutamate receptors are present within the muscle in the absence of neuronal innervation whilst *twist* mutants, displaying a complete loss of muscles due to a failure in mesoderm formation, are still capable of axonal outgrowth and the formation of morphologically normal presynaptic active zones (Broadie and Bate, 1993b; Currie et al., 1995; Prokop et al., 1996). Subsequently, following interaction of the developing growth cone with it's target muscle, the development and continuous homeostatic modulation of synaptic size and strength, in response to external cues, is regulated by a series of bi-directional pre- and post-synaptic signalling pathways. These include morphogenic signalling pathways such as wingless and transforming growth factor beta (TGFβ) signalling as well as intracellular signals such as mitogen-activated protein kinase (MAPK) cascades and the

regulation of signalling cascades by cell adhesion and scaffolding proteins such as Fasciclin II (Fas II) and Discs large (Dlg).

1.3.9. TGFβ Signalling During NMJ Development

TGF-β signaling has been demonstrated as fundamental to normal NMJ assembly and function, in *Drosophila,* with mutants defective in normal TGF-β signaling displaying synaptic undergrowth, whilst up-regulation of TGF-β signaling promotes an overgrowth phenotype (Aberle et al., 2002; Rawson et al., 2003; Sweeney and Davis, 2002). TGF-β signaling acts through a complex signaling cascade in which TGF-β ligands, including TGF-β's, activins and bone morphogenic proteins (BMP's) bind type II transmembrane receptors. These in turn recruit type I receptors, forming a tetrameric receptor complex in which type II receptors phosphorylate type I receptors. Activated type I receptors are then capable of activating receptor SMAD's (R-SMADs) which, following association with a cofactor SMAD (co-SMAD), proceed to the nucleus to regulate gene transcription. The acronym SMAD is a portmanteau of *Drosophila* MAD (mothers against decapentaplegic (dpp)) and *Caenorhabditis elegans* SMA (small body size). In *Drosophila* there are 3 known type-I receptors (Thick Veins, Baboon and Saxophone), 2 type-II receptors (Punt and Wishful thinking), 2 R-SMADs (MAD and SMAD on the X), 1 Co-SMAD (Medea), a single inhibitory SMAD (Daughters against DPP (dad)) and 7 TGFβ ligands (Marques, 2005). The TGF-β ligand implicated in TGF-β signalling regulating NMJ development is glass bottom boat (gbb), a BMP family protein (Marques et al., 2003; McCabe et al., 2003). Gbb is post-synaptically derived, being secreted by the muscle and providing a retrograde signal from the muscle to the motor neuron that allows coalescence of pre- and post-synaptic growth (Marques, 2005; Marques et al., 2003; McCabe et al., 2003). Muscle secreted gbb binds pre-synaptic type-I receptors Thick veins (Tkv) and Saxophone (sax), signaling through the type-II receptor Wishful thinking (wit) and SMAD's MAD and Medea (Fig. 1.6.) (Collins and DiAntonio, 2007; Marques, 2005; McCabe et al., 2003; Rawson et al., 2003). This pathway has been comprehensively dissected with

gbb, sax, Tkv, wit, MAD and Medea mutants all displaying a significant reduction in NMJ size coupled with perturbed synaptic transmission and aberrations to normal synaptic ultrastructure, including detachment of synaptic membranes and floating T-bars (Aberle et al., 2002; Marques et al., 2002; Marques et al., 2003; McCabe et al., 2004; Rawson et al., 2003; Sweeney and Davis, 2002). Furthermore it has been shown that these aberrations can be alleviated through pre-synaptic rescue experiments, confirming that gbb is acting retrogradely activating a TGFβ signaling cascade within the pre-synaptic motor neuron (McCabe et al., 2004). This is further supported by observations that normal phospho-SMAD localization to the motor neuronal nucleus is perturbed in TGFβ signaling mutants (Marques et al., 2003). Conversely it has been demonstrated that mutations to genes that are likely involved in the down regulation of TGFβ signaling via endosomal-lysosomal trafficking, such as *spinster* (*spin*) show significant NMJ overgrowth that is dependent upon normal TGFβ signaling (Sweeney and Davis, 2002). As such there is significant evidence that the TGFβ signaling pathway, which shows clear conservation between flies and mammals, plays a fundamental role in coupling pre- and post-synaptic growth, via retrograde signaling, during NMJ development.

1.3.10. JNK Signalling During NMJ Development

A number of mitogen activated protein kinase (MAPK) signalling cascades have been implicated in neuronal plasticity, with mutants in MAPK pathways displaying defects in learning and memory and long-term potentiation (LTP) (Kelleher et al., 2004; Moressis et al., 2009). Furthermore research has show these pathways play an important role in the regulation of synaptic development, including that of the *Drosophila* NMJ, where alterations in MAPK activity have been shown to influence NMJ size and strength (Collins et al., 2006; Milton et al., 2011).

One MAPK pathway identified as a potent regulator of synaptic growth and function, in *Drosophila*, is that of the Jun N-terminal kinase (JNK)/activator protein-1 (AP-1) signal transduction pathway (Fig. 1.6.) (Collins et al., 2006;

Milton et al., 2011). The central component of this pathway is JNK, which was initially identified as an evolutionarily conserved stress activated kinase (Hibi et al., 1993). The JNK pathway has been shown to be activated by a range of both endogenous and environmental insults including DNA damage, oxidative stress, immune challenges, UV irradiation and heat stress (Derijard et al., 1994; Hibi et al., 1993; Milton et al., 2011; Pantos et al., 2003; Silverman et al., 2003; Yoshida et al., 2005). For example recent work in the Sweeney lab has shown that reactive oxygen species (ROS) induce an activation of the JNK/AP-1 pathway, promoting synaptic overgrowth in *Drosophila* (Milton et al., 2011). In response, individual stress stimuli have been shown to selectively activate specific JNK Kinase Kinase's which, in turn, propagate a kinase cascade, through JNK kinases, leading to the phosphorylation and activation of JNK. JNK in turn has a number of downstream targets, including AP-1. AP-1 is a dileucine zipper transcription factor composed of hetero- or homo-dimers of Fos and Jun, which in *Drosophila* are termed kayak and jun-related antigen (Jra) respectively (Halazonetis et al., 1988; O'Shea et al., 1989; Rauscher et al., 1988). Upon activation AP-1 has been demonstrated to induce a variety of stimuli and tissue specific responses including apoptosis, autophagy and cell proliferation (Guo et al., 2012; Lauricella et al., 2006; Shaulian and Karin, 2001). As such the JNK/AP-1 pathway has been identified as a conserved a highly versatile stress response pathway.

In *Drosophila* it has been shown that the JNK/AP-1 pathway is a potent regulator of NMJ assembly and function. For example Sanyal et al. demonstrated that increased motor neuronal, but not muscle, expression of Fos and Jun was sufficient to induce significant increases in bouton number (Sanyal et al., 2002). Similarly Etter at al. (2005) showed that neuronal overexpression of an activated JNK Kinase, Hemipterous, induced a 30 % increase in bouton number at the NMJ (Etter et al., 2005). Furthermore it has also been shown that mutations in *highwire (hiw)*, a neuronally expressed E3-ubiquitin ligase required for inhibition of the JNK Kinase Kinase wallenda (wnd), display significant synaptic overgrowth that can be alleviated by inhibition of *wnd* (Collins et al., 2006). As previously mentioned work in the Sweeney lab has

also shown that inhibition of the JNK/AP-1 pathway in both *Spin* mutants, which display an oxidative stress burden, and SOD mutants alleviates synaptic overgrowth phenotypes (Milton et al., 2011). These findings support previous hypotheses that suggest the JNK/AP-1 pathway may mediate synaptic development in response to stress stimuli such as oxidative stress.

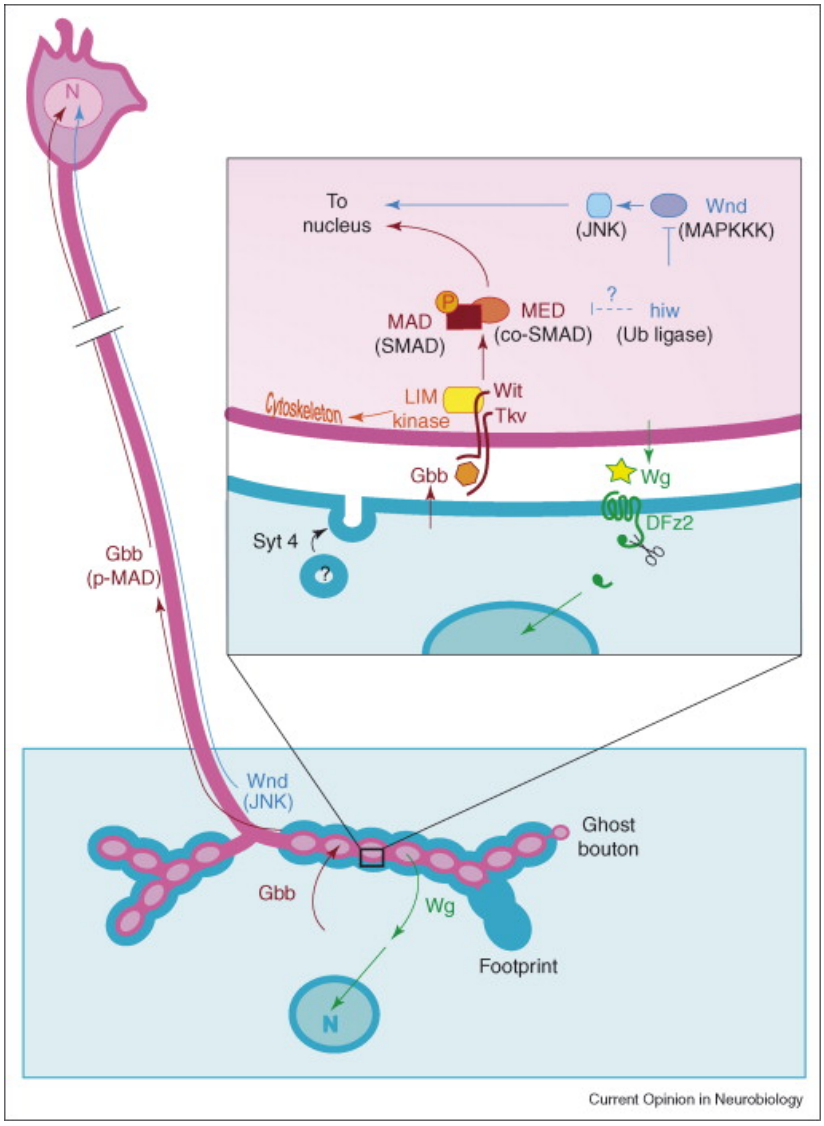

Figure 1.6. Signaling pathways regulating NMJ assembly and Development.
During development of the *Drosophila* larval NMJ the pre-synaptic nerve terminal (pink) innervates abdominal muscles (light blue) in the larval body wall. Development of the NMJ is regulated by a series of bi-directional interconnected signalling pathways including TGFβ and JNK. In the TGFβ pathway the BMP ligand Gbb (orange) is secreted by the muscle, signalling retrogradely to the pre-synaptic nerve terminal via type-I (Tkv) and type-II (Wit) TGFβ receptors. Gbb mediated activation of the receptors promotes phosphorylation of downstream SMAD proteins, which translocate to the nucleus in order to regulate transcription of genes involved in NMJ development. JNK signalling also contributes towards regulated development of the NMJ, acting to promote NMJ growth. Evidence suggests that JNK signalling is regulated by the E3 ubiquitin ligase hiw, which maintains restraint upon the JNK signalling pathway through targeting the JNKKK wnd for degradation by the proteasome. Reproduced from Collins and DiAntonio (2007)

1.3.11. Enhancer and Suppressor (Modifier) Screens

One of the greatest strengths of *Drosophila,* as a model organism, is it's ability to be utilised in high-throughput forward genetic screens that allow for the identification of genes involved in specific biological processes (for review see (St Johnston, 2002)). *Drosophila* screens were popularized by the revolutionary, Nobel prize winning, Heidelberg screens conducted by Christiane Nüsslein-Volhard and Eric Wieschaus in which, through screening of embryonic mutant phenotypes, they identified a series of genes that are essential to embryonic patterning (Nusslein-Volhard and Wieschaus, 1980). Whilst revolutionary such traditional screening approaches, for embryonic homozygous lethal mutations, only allow for identification of the earliest phenotype of a mutation and so do not always allow for elucidation of more extensive signal transduction pathways. As such since the pioneering work of Nüsslein-Volhard and Wieschaus numerous more advanced, elegant screening approaches have been devised, including enhancer and suppressor screens.

Enhancer and suppressor, or modifier, screens are based upon the principle that if a specific biological process is perturbed by a mutation then an organism may become "sensitised" to heterozygous mutations in secondary genes, affecting the same pathway, which would typically be recessive in a wildtype background (St Johnston, 2002). Generally loss of function mutations are recessive, with a 50% of wildtype complement usually being sufficient for normal development (St Johnston, 2002). However in a "sensitised" mutant background these same mutations may become dominant and therefore more easily identifiable. Using such an approach a mutation in a specific gene of interest, that gives a distinctive phenotype, can be the basis of large modifier screens in which second-site mutations that dominantly enhance or supress the primary mutant phenotype can be identified. This approach has a number of advantages over traditional genetic screens; firstly as mutants do not need to be made homozygous, as in traditional screens, an F_1 instead of F_3 screen can be performed, increasing both speed and throughput. Secondly mutations that are homozygously embryonic lethal can be screened to determine their functional

role in later developmental stages. Finally as no specific chromosomes have to be made homozygous there is no requirement for balancer chromosomes and so the entire *Drosophila* genome can be screened against the primary mutation. As such modifier screens have become a fundamental tool in the dissection of genetic interactions involved in specific pathways associated with an initial gene of interest.

1.3.12. The *Drosophila* Eye as a Model System for Unbiased Modifier Screens

The *Drosophila* eye has become one of the most popular and successful systems in which to conduct enhancer and suppressor screens (St Johnston, 2002). Using the UAS/GAL4 system it has proven possible to express mutant transgenes within the *Drosophila* eye, under the control of eye specific promoters such as the glass multimer reporter (GMR). The advantages of this specific spatial expression can be seen as three fold. Firstly the eye has a highly regular, organized structure (Fig. 1.7.) meaning that even minor perturbations become amplified and therefore discernable as significant changes to cell patterning (Mishra and Knust, 2013). Such distinctive phenotypes can easily be quantified allowing for easy identification of enhancers and suppressors of this initial phenotype. Secondly the structure and neuronal connections of the eye are well studied and characterised allowing for analysis of neuronal morphology (Raghu and Borst, 2011). Finally, and perhaps of greatest significance, the eye is dispensable for normal viability and reproduction, under laboratory conditions (Sang and Jackson, 2005). Therefore mutations that induce significant pathogenesis or are typically lethal in the whole organism can be expressed in the eye and degeneration easily visualized without lethality. As such modifier screens have proven robust and successful in the identification of novel genetic interactions influencing diseases. For example Pandey et al. (2007) utilised the *Drosophila* eye to identify Histone deacetylase 6 (HDAC6) as a modifier of neurodegeneration associated with Spinobulbar muscular atrophy (Pandey et al., 2007). Similarly Jackson et al (2002) demonstrated that tau hyperphosphorylation by Glycogen synthase kinase 3

(GSK-3) potentiated a tau eye model of neurodegeneration, a discovery that has proven important in the study of Alzheimer's disease (Jackson et al., 2002).

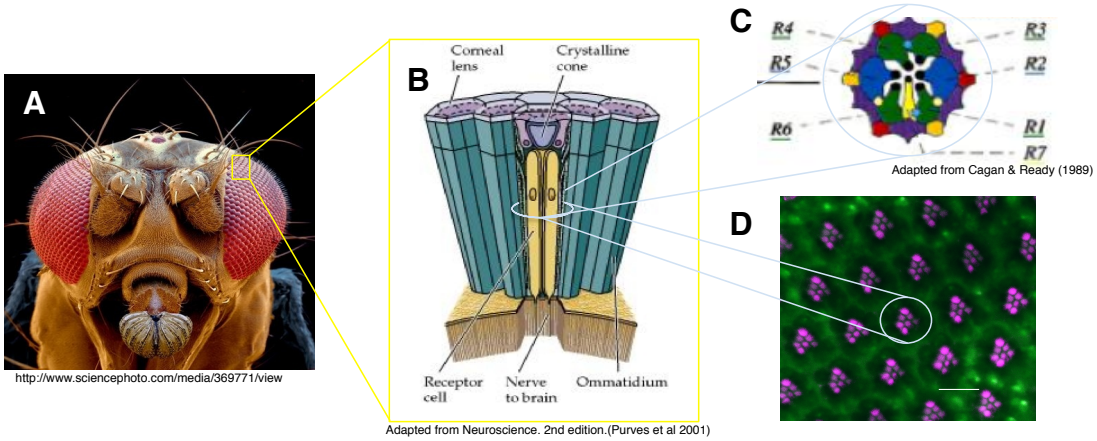

Figure 1.7. The *Drosophila* Compound Eye Exhibits a Highly Regular and Organised Structure
The *Drosophila* compound eye (**A**) consists of 760 virtually identical subunits termed ommatidia (**B**). Ommatidia are arranged into precise hexagonal arrays and each contains 8 photoreceptor cells, R1- R8 (**C**). Photoreceptor neurons are composed of 2 main sections, the cell body and the rhabdomeres. The rhabdomeres can be stained using phalloidin bound to a specific dye allowing visualisation of the eyes regular structure (**D**) only 7 of 8 rhabdomeres are distinctly visible as R7 lies directly above R8.

1.4. *Rab8*, An Enhancer of Frontotemporal Dementia?

In this investigation the *Drosophila* eye was used to perform modifier screens, looking for enhancers and suppressors of *CHMP2B*^{Intron5} toxicity associated with FTD. The majority of this investigation shall focus upon one potent enhancer, *Rab8*.

1.4.1. Rab Proteins

1.4.1.1. The Structure of Rab Proteins

Rab (Ras related in brain) proteins are small (20-25 kDa), monomeric G-proteins, constituting the largest subfamily of the Ras GTPase superfamily (Ng and Tang, 2008; Pfeffer, 2001; Stenmark, 2009; Zerial and McBride, 2001). In humans there are now more than 60 known Rabs, which can be divided into 14 Rab subfamilies (Schwartz et al. 2007, Diekmann et al., 2011). Over the past decade the structure of many Rab proteins, in both their GTP-bound active and

GDP-bound inactive states, have been determined, with the structure of at least one rab from each family having been elucidated (Hutagalung and Novick, 2011). As such it has been determined that, on the whole, Rab proteins show a typically conserved core structure, that is generally conserved across the entire Ras superfamily. This includes the presence of a 20 kDa catalytic GTPase fold composed of a six-stranded β-sheet, comprising of 5 parallel and one anti-parallel strands, flanked by 5 α-helices and containing 5 specific polypeptide loops that link the α-helices to the β-strands (Hutagalung and Novick, 2011; Pfeffer, 2005). These loops, classified as G1-G5, are the most highly conserved component of the GTPase fold and are functionally essential for guanine nucleotide binding and GTP hydrolysis (Okai et al., 2004). Within the catalytic domain there are also two distinct regions termed switch I and switch II which show nucleotide dependent conformational variability and are the only regions of Rab proteins to undergo conformational alterations essential to Rab function (Pfeffer, 2005). In a GDP-bound state the switch regions are typically disordered, adopting a highly ordered orientation upon GTP binding that allows Rab's to bind specific effectors in their "active" state (Pfeffer, 2005; Stroupe and Brunger, 2000).

As well as the N-terminal catalytic core Rab proteins also contain a hypervariable C-terminal domain, which early work implicated in the localisation of Rab's to specific target membranes (Chavrier et al., 1991). More recent evidence, however, suggests a more complex scenario in which multiple regions contribute towards localisation (Ali et al., 2004). In the majority of Rab proteins the C-terminal domain terminates with a distinctive cysteine rich motif (CC, CCX, CXC, CCXX or CCXXX) (Calero et al., 2003; Leung et al., 2007). This motif is required for recognition by Rab geranylgeranyl transferase (RabGGT) which catalyses the addition of prenyl groups, essential for membrane associate and anchoring of Rabs (Calero et al., 2003; Leung et al., 2007). A minority of Rab's possess an alternative CAAX motif more representative of other, non-Rab, Ras superfamily members (Calero et al., 2003; Leung et al., 2007).

1.4.1.2. The Function of Rab GTPases; Molecular Switches

As GTPases, Rab proteins function as molecular switches, cycling between conformationally distinct GTP-bound “active” and GDP-bound “in-active” states, which in turn influences association with effector proteins and localisation (Pfeffer, 2005; Stenmark, 2009). Cycling between GTP-bound and GDP-bound states occurs in process mediated by Guanine nucleotide exchange factors (GEF’s) and GTPase activating proteins (GAP’s) (Fig. 1.8.) and is associated with significant conformational alterations in two distinct variable regions, known as switch I and switch II (Zhu et al., 2010).

Newly synthesised Rab proteins are recognised by the Rab Escort Protein (REP) which, in turn, presents them to RabGGT (Fig. 1.8) (Alexandrov et al., 1994). RabGGT then acts to catalyse prenylation of the newly synthesized Rab through the addition of geranylgeranyl groups to one or two, most commonly two, cysteine residues within the hypervariable C-terminus of the Rab protein (Hutagalung and Novick, 2011). This irreversible addition of hydrophobic gernaylgeranyl groups acts to form an isoprenyl anchor, via which Rab proteins associate tightly with their target membrane. Furthermore it has been demonstrated that the prenyl groups of GDP-bound Rab proteins are recognised by GDP-dissociation inhibitor’s (GDI’s) which, therefore, masks the isoprenyl anchor and maintains a cytosolic, membrane dissociated localisation of the Rab protein (Grosshans et al., 2006; Rak et al., 2003). In addition to maintaining cytosolic localisation of Rab’s it has also been shown that GDI’s are actively capable of extracting Rab proteins from target membranes, via a ‘mobile effector loop’ comprised of an ordered loop of residues that, in the absence of prenyl groups remain disordered (Luan et al., 2000). Thus GDI’s may have a functional role in the retrieval of Rab proteins from target membranes and their relocation to their membrane of origin, a process that is essential for many Rab functions, such as delivery of vesicles from one compartment to another. In order for Rab’s to be specifically inserted into membranes it is essential to release them from the GDI complex and expose their isoprenyl anchor. Evidence suggests that this is mediated by another

family of proteins termed GDI Displacement factors (GDF's), which act to recognize Rab-GDI complexes and promote GDI displacement, exposing the isoprenyl anchor and allowing re-insertion into membranes (Dirac-Svejstrup et al., 1997; Hutagalung and Novick, 2011; Stenmark, 2009).

Once associated with their cognate membrane, through their isoprenyl anchor, GDP-bound inactive Rab proteins are activated by GEF's, which act to catalyse the exchange of GDP for GTP. It has been demonstrated that GEF's are capable of catalysing nucleotide exchange through varying mechanisms, although all appear to be based around the same basic principle. Association of GEF's with their Rab substrates occurs through direct interactions with the switch I, switch II and interswitch regions, promoting significant conformational changes within these domains (Stein et al., 2012; Wu et al., 2011). Conformational changes include displacement of aromatic residues that typically act to stabilise nucleotide binding from the switch I region (Wu et al., 2011). Through these conformational changes the nucleotide binding affinity of the Rab protein is reduced, facilitating displacement of GDP. Due to the high cytosolic concentration of GTP (~ 1 mM), 10 fold that of GDP, it rapidly associates with the Rab protein following GDP dissociation (Wu et al., 2011). Conformational changes to the switch regions, associated with GTP binding and activation of the Rab protein, allow interaction with multiple Rab effector proteins that are involved in diverse processes associated with distinct membrane trafficking pathways (Pfeffer, 2005). In order to return the Rab protein to its inactive state and continue the cycle bound GTP is hydrolysed to GDP through the endogenous GTPase activity of the Rab protein catalysed by GTPase activating proteins (GAP's) (Stenmark, 2009). Once again in an inactive GDP-bound state the Rab protein is once again a target for GDI, which can facilitate its extraction and relocation to its membrane of origin, allowing the cycle to continue.

Through this conformational cycling, and the specific localisation of different Rab's, and the effector proteins they activate and/or recruit, Rab proteins act as multifaceted organisers (Ng and Tang, 2008; Stenmark, 2009). As such they convey strict regulation to both rate and specificity for almost all trafficking

events occurring in eukaryotic cells (Ng and Tang, 2008; Stenmark, 2009). These events include vesicle transport, tethering and docking to target membranes and exocytosis, via interaction with cytoskeletal motor proteins, N-ethylmaleimide-sensitive factor (NSF) and Soluble NSF attachment protein receptor (SNARE) proteins, respectively (Ng and Tang, 2008; Pfeffer, 2001; Stenmark, 2009). When in a GTP-bound active state Rab proteins have been shown to activate and recruit numerous distinct effectors including motor proteins, tethering factors, adaptor proteins, kinase's and phosphatase's. They have even been shown to recruit and activate GEF's that proceed to activate other, downstream, Rab proteins (Knodler et al., 2010). Currently more than 70 Rab proteins have been identified in humans, each localised to distinct cytoplasmic membranes of intracellular vesicles and organelles involved in cellular endocytic and secretory pathways (Mercer and Helenius, 2009; Ng and Tang, 2008; Pfeffer, 2001; Stenmark, 2009). Such distinct intracellular localisations are fundamental to Rab functions, conveying specificity to trafficking pathways.

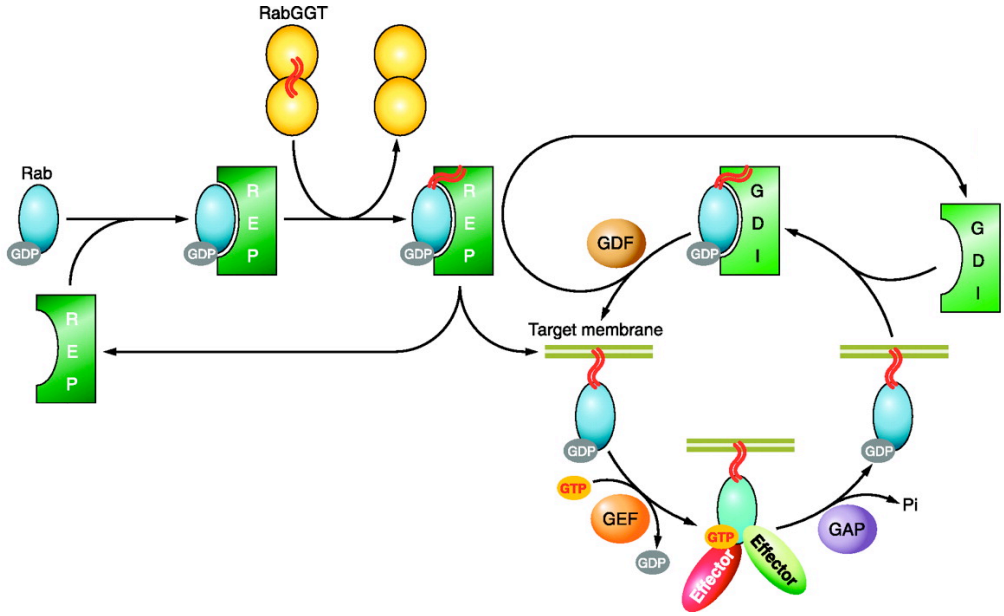

Figure 1.8. The Rab GTPase Regulatory Cycle.
GEF's catalyse the exchange of GDP for GTP through recognition of specific residues within the switch domain's and promoting conformational changes that facilitate the release of GDP. Conformational changes upon GTP binding and activation promote interaction with multiple Rab effector proteins involved fundamental to Rab function in membrane trafficking events. Bound GTP is hydrolysed to GDP through the GTPase activity of the Rab protein catalysed by GTPase activating proteins (GAP's), releasing free inorganic phosphate (P_i). Newly synthesised Rab proteins are recognised by the Rab Escort Protein (REP) and presented to Rab geranylgeranyl transferase (RabGGT) which prenylates the C-terminus forming an Isoprenyl anchor, essential

for membrane association. Genranlygeranylated, GDP-bound Rab proteins are recognized by the Rab GDP dissociation inhibitor (GDI), which extracts Rabs from their associated membrane and mask the isoprenyl anchor, therefore promoting cytosolic localisation and continued cycling by returning Rab proteins to their membrane of origin. Evidence suggests that GDI Displacement factors (GDF's) recognize Rab-GDI complexes and promote GDI displacement, exposing the isoprenyl anchor and allowing re-insertion into membranes. (Adapted from Hutagalung and Novick, 2011).

1.4.1.3. The Role of Rab GTPases in Disease

As multifaceted organisers and master regulators of diverse cellular trafficking events it is clear how perturbation to Rab function, either directly or through their interacting proteins, may easily lead to disease. Corroborating this a growing body of research has implicated Rab GTPases, and their interacting proteins, in a large number of disparate human diseases ranging from multifactorial diseases such as type 2 diabetes to genetic disorders such as Crohn's disease and infectious pathogenic diseases including measles and influenza (Amorim et al., 2011; Murray et al., 2005; Ohira et al., 2009; Thong et al., 2007). It has also become apparent that a large number of neurodegenerative diseases show aberrant Rab function. Rab GTPases and their interacting proteins, their function and their association with specific neurological and neurodegenerative diseases are summarized in Table 1.3. Despite their well characterised role in such a range of diseases the potential of Rab GTPases, and their interacting proteins, as therapeutic targets remains an area of uncertainty, requiring significant further investigation.

Table 1.3. The Role and Function of Rab GTPases and Their Interacting Proteins in Neurodegenerative Diseases.

Protein	Localisation, Function	Disease	Associated Symptoms	Role in Disease	Source(s)
Rab1	ER to Golgi complex trafficking	Parkinson's Disease	Motor Symptoms (resting tremor, bradykinesia, hypokinesia, gait dysfunction), visual deficits, dementia	Alpha synuclein (αSyn) induced toxicity and disrupted ER-to-Golgi transport can be rescued by overexpression of Rab1.	(Cooper et al., 2006)
Rab3a	Exocytosis, neurotransmitter release	Parkinson's Disease	Motor Symptoms (resting tremor, bradykinesia, hypokinesia, gait dysfunction), visual deficits, dementia	Rab3a interacts with αSyn in brain extracts from mutant PD, but not wildtype mice.	(Aligianis et al., 2005; Dalfo et al., 2004; Gitler et al., 2008)
Rab3 GAP	Rab3 GAP, exocytosis	Warburg Micro Syndrome	Ocular Defects (microphtalmos, microcornea, congenital cataracts), neurodevelopmental defects (mental retardation, spastic cerebral palsy, microcephaly) and hypothalamic hypogenetalism	Germline-inactivating mutations in the genes encoding the regulatory catalytic subunit Rab3GAP1 have been demonstrated to lead to disease.	(Aligianis et al., 2005)
		Matsolf Syndrome	Similar to above but milder, including mild mental retardation, cataracts and hypogonadism	Mutations in the non-catalytic subunit Rab3GAP2 have been identified in patients.	(Aligianis et al., 2006)
Rab4a	Early and recycling endosomes (fast recycling)	Alzheimer's Disease	Cortical Atrophy, Dementia	Increased expression and altered localization of Rab4 is seen in AD patient brains, as well as animal and cellular models.	(Ginsberg et al., 2011; Ginsberg et al., 2010)

Table 1.3. The Role and Function of Rab GTPases and Their Interacting Proteins in Neurodegenerative Diseases.

Protein	Localisation, Function	Disease	Associated Symptoms	Role in Disease	Source(s)
		Niemann Pick	Hepatosplenomegaly, thrombocytopenia, neurological defects (ataxia, dysarthria, dysphagia)	Elevated endosomal cholesterol levels in Niemann-pick inhibit Rab4 and perturb membrane recycling	(Choudhury et al., 2004)
Rab5a	Early endosomes, Clathrin-coated vesicles	Alzheimer's Disease	Cortical Atrophy, Dementia	Rab5 is selectively up-regulated in the frontal cortex, hippocampus and basal forebrain of AD patients.	(Ginsberg et al., 2011)
		Parkinson's Disease	Motor Symptoms (resting tremor, bradykinesia, hypokinesia, gait dysfunction), visual deficits, dementia	Rab5 interacts with αSyn in brain extracts from mutant PD, but not wildtype mice.	(Dalfo et al., 2004)
Rab7	Late endosomes	Charcot-Marie-Tooth Disease Type 2B	Sensory Neuropathy and peroneal muscular atrophy	4 Rab7 mutations have been identified in independent CMT2B kindred. Mutant Rab7 is preferentially GTP-bound and shows reduced GTP hydrolysis.	(De Luca et al., 2008; McCray et al., 2010; Verhoeven et al., 2003)
		Alzheimer's Disease	Cortical Atrophy, Dementia	Rab7 is selectively up-regulated in the frontal cortex, hippocampus and basal forebrain of AD patients.	(Ginsberg et al., 2011; Ginsberg et al., 2010)
		Batten Disease	Visual degeneration, seizures, psychomotor disturbances, behavioural aberrations, echolalia	*CLN3* is mutated in Battens disease. The CLN3 protein has been show to form a complex with Hook1 and Rab7.	(Agola et al., 2011) (Luiro et al., 2004)

Table 1.3. The Role and Function of Rab GTPases and Their Interacting Proteins in Neurodegenerative Diseases.

Protein	Localisation, Function	Disease	Associated Symptoms	Role in Disease	Source(s)
Rab8	TGN to basolateral membranes, Recycling endosome	Huntington's Disease	Chorea, dystonia, cognitive degeneration, behavioural aberrations	The Rab8-optinurin complex is disrupted in Huntington's Disease, leading to perturbations to post-Golgi trafficking.	(del Toro et al., 2009; Hattula and Peranen, 2000)
		Alzheimer's Disease	Cortical Atrophy, Dementia	Rab8 is down-regulated in cells expressing mutations associated with Alzheimer's disease	(Kametani et al., 2004a)
		Parkinson's Disease	Motor Symptoms (resting tremor, bradykinesia, hypokinesia, gait dysfunction), visual deficits, dementia	Rab8 interacts with αSyn in brain extracts from mutant PD, but not wildtype mice. Rab8A suppresses toxicity in neuronal models of PD.	(Dalfo et al., 2004; Gitler et al., 2008)
Rab9	Late endosomes, TGN	Niemann Pick C	Hepatosplenomegaly, thrombocytopenia, neurological defects (ataxia, dysarthria, dysphagia)	Cholesterol accumulation sequesters Rab9 in an inactive form in NPC Cells.	(Ganley and Pfeffer, 2006)
		Batten Disease	Visual degeneration, seizures, psychomotor disturbances, behavioural aberrations, echolalia	*CLN3* is mutated in Battens disease. The CLN3 protein has been show to form a complex with Hook1 and Rab9.	(Agola et al., 2011) (Luiro et al., 2004)
Rab11	Recycling endosome (slow recycling), TGN	Huntington's Disease	Chorea, dystonia, cognitive degeneration, behavioural aberrations	Huntington's mice display impaired GDP-to-GTP exchange for Rab11 whilst expression of a dominant	(Li et al., 2009b; Li et al., 2009c)

Table 1.3. The Role and Function of Rab GTPases and Their Interacting Proteins in Neurodegenerative Diseases.

Protein	Localisation, Function	Disease	Associated Symptoms	Role in Disease	Source(s)
				negative Rab11 induces Huntington's like neuropathology and symptoms. Patient fibroblasts also display impaired Rab11-dependent vesicle formation.	
		Charcot-Marie-Tooth Disease Type 4C	Sensory Neuropathy and peroneal muscular atrophy	Disease causing mutations within *SH3TC2* result in a failure of SH3TC2 to associate with Rab11, inhibiting recycling endosome localization.	(Roberts et al., 2010)
		Batten Disease	Visual degeneration, seizures, psychomotor disturbances, behavioural aberrations, echolalia	*CLN3* is mutated in Battens disease. The CLN3 protein has been show to form a complex with Hook1 and Rab11.	(Agola et al., 2011) (Luiro et al., 2004)
Rab23	Autophagosomes	Carpenter Syndrome	Mental retardation, congenital heart disease, obesity, polydactyly, brachydactyly, cranial abnormalities	Carpenter Syndrome patients show mutations in Rab23 associated with dysregulated hedgehog signalling.	(Eggenschwiler et al., 2001; Jenkins et al., 2007)
GDIα	Brain enriched GDI	X-Linked non-specific mental retardation	Mental Retardation	Mutations in the GD1 gene, which encodes the brain enriched GDI GDIα, have been identified in patients suffering from the disease.	(D'Adamo et al., 1998)
Alsin	Rab5 GEF	ALS	Progressive motor deficits and muscle atrophy	ALS2/Alsin is mutated in Jeuvenile ALS (ALS2)	(Yang et al., 2001)

1.4.1.4. Rab8

Rab8 is a small, approximately 207 amino acid and 23 kDa, protein of the Rab subfamily of Ras GTPases. In humans it has two isoforms, Rab8A and Rab8B, showing 83 % homology with the majority of variation occurring within the hypervariable C-terminal domain (Armstrong et al., 1996; Heidrych et al., 2008; Schollenberger et al., 2010). Functional differences between the two isoforms remain poorly understood, although more is known about the function of Rab8A in vesicular trafficking events than Rab8B, the function of which remains unclear. Experimental evidence suggests there to be significant differential patterns of tissue expression between Rab8A and Rab8B (Chen et al., 2001). For example it has been demonstrated that Rab8B show's greatest expression in the brain and spleen whilst, in contrast, Rab8A displays low expression within these regions (Chen et al., 2001). It has also been suggested that expression of Rab8A and Rab8B may be regulated by different transcription factors, differentiating their function. In contrast to humans *Drosophila* only possess a single Rab8 isoform, displaying approximately 80 % homology to human Rab8 (www.genecards.org). *Drosophila* Rab8 is encoded by the *Rab8* gene located at cytological interval 76D2-76D3 on the left arm of chromosome 3 (www.flybase.org).

In contrast to the majority of Rab proteins, but in keeping with the majority of other proteins belonging to the Ras superfamily, Rab8 contains a C-terminal CAAX motif, in which A typically represents an aliphatic residue and X any amino acid (Joberty et al., 1993; Leung et al., 2007). In Rab8A the CAAX motif is CVLL whilst in Rab8B it is CSLL, with *Drosophila* Rab8 displaying CSLL, homologous to Rab8B (Joberty et al., 1993). The presence of this CAAX motif means that Rab8 is only mono-prenylated by a single geranylgeranyl modification to the cysteine residue of the CAAX motif, whereas the majority of Rab proteins are prenylated twice within CC, CXC or CCXX motifs (Leung et al., 2007). In a study by Leung et al. 2007 it was demonstrated that this CAAX motif was essential for post-prenylation carboxyl methylation of Rab8 and that this post-prenyl modification was essential for regulating the cycle of Rab8 membrane association and retrieval (Leung et al., 2007).

Rab8 has been strongly implicated in the regulation of numerous membrane trafficking pathways including membrane recycling, exocytosis and ciliogenesis (Ang et al., 2004; Grigoriev et al., 2011a; Hattula et al., 2006; Knodler et al., 2010). Furthermore it has been suggested that through this regulation Rab8 is fundamental to the development of polarised cells and the regulation of cell shape (For a review see Peränen, 2011) (Peranen, 2011). For example studies using over expression of *Rab8, Rab8*-eGFP or constitutively active *Rab8,* in various cell types, have shown induction of significant alterations to cellular morphology, characterised by the formation of distinct cellular protrusions (Peränen et al., 1996). Furthermore a significant body of research has implicated Rab8 in ciliogenesis (Follit et al., 2010; Knodler et al., 2010; Leung et al., 2007; Nachury et al., 2007a; Yoshimura et al., 2007). For example Nachury et al. (2007) demonstrated that depletion of the Rab8 GEF Rabbin8, via siRNA, resulted in a significant reduction of ciliogenesis (Nachury et al., 2007a). Furthermore Knödler et al., 2010 showed the Rab11-Rab8 cascade to be essential in cilia formation.

As well as its implication in the regulation of cellular morphology and the formation of cellular protrusions, such as cilia, Rab8 has also been shown to play an important role in the endosomal recycling pathway. For example Hattula et al. (2006) demonstrated Rab8 to be essential for trafficking, but not internalization or recycling, of components to the recycling endosome. In this study they showed that depletion of Rab8, via siRNA, results in a failure to traffic transferrin (Tfn) and the transferrin receptor (TfnR) to peri-nuclear recycling endosomal compartments. In contrast expression of the constitutively active Rab8, Rab8-Q67L, resulted in an accumulation of Tfn and TfnR within the recycling endosome. Corroborating these findings it has also been shown that depletion of one of Rab8's effector proteins, optineurin, also inhibits trafficking of Tfn to the recycling endosome compartment (Nagabhushana et al., 2010). Further substantiating a role for Rab8 in recycling endosomal traffic Rab8 has been shown to co-localise with EHD-1, EHD-3, Arf6, Myo5-b, MHC-I, β1 integrin and Rab11, all of which have been implicated in clathrin independent endocytic recycling (Hattula et al., 2006; Roland et al., 2007; Sharma et al., 2010; Sharma

et al., 2009). In a study by Henry and Sheff, 2008, it was also concluded that in fully polarized cells Rab8 regulates the traffic of newly synthesized basolateral proteins to the plasma membrane, via the recycling endosome, but does not regulate endocytic cargo (Henry and Sheff, 2008). This supports previous findings that suggest that recycling endosomes may act as a trafficking intermediate between the golgi and plasma membrane (Ang et al., 2004). Further implicating Rab8 in endosomal trafficking it has also been shown that Rab8 depletion results in a perturbation to normal trafficking leading to an accumulation of cholesterol within late endosomes, whilst overexpression of Rab8 is capable of rescuing cholesterol accumulation in Niemann-pick type C cells (Linder et al., 2007). Cholesterol accumulation has also been shown to specifically inhibit Rab4 dependent endosomal recycling (Choudhury et al., 2004).

A role for Rab8 in normal endosomal trafficking events has also been demonstrated through the identification that Rab8 knockdown mice show lysosomal accumulation, associated with perturbed apical hydrolase localization and microvilli shortening in the gut (Sato et al., 2007b). Furthermore del Toro et al. (2009) showed that mutations within the *huntingtin* (*htt*) gene disrupted post-golgi trafficking to the lysosome through a delocalization of the Rab8-Optineurin complex from the Golgi, leading to lysosome perturbation (del Toro et al., 2009).

Rab8 has also been implicated in exocytosis with Rab8 forming stable associations with exocytic vesicles, in a Rab6 and MICAl3 dependent manner, in order to regulate their efficient docking and fusion (Grigoriev et al., 2011b). Substantiating these findings a recent study implicates Rab8, acting alongside Rab11 and Myo5B, in the promotion of stretch induced exocytosis in bladder umbrella cells (Khandelwal et al., 2013). In contrast it has previously been shown that Rab8 but not Rab11 knockdown inhibited MT1-MMP exocytic traffic, implicating Rab8 but not Rab11 in the regulation of exocytosis (Bravo-Cordero et al., 2007).

Taken together these studies suggest a role for Rab8 in the regulation of normal endocytic trafficking, a process that is essential and conserved amongst all

eukaryotic cells. Furthermore they implicate Rab8 as essential in the development of polarised cells, such as neurons.

1.4.1.5. The Role of Rab8 in Neurons

Numerous studies suggest a functional role for Rab8 during normal neuronal development and maintenance. For example Huber et al (1995) suggested that Rab8 is important for membrane trafficking in developing neurons, demonstrating that antisense oligonucleotide suppression of Rab8 prevented exocytic vesicle formation and neurite outgrowth, inhibiting maturation of 95% of cultured rat hippocampal neurons (Huber et al., 1995b). Inhibition of neurite outgrowth coupled with reduced levels of Rab8 has also been demonstrated in cells expressing mutant presenillin-1, further implicating Rab8 in neuronal development (Kametani et al., 2004b). Corroborating the role of Rab8 in regulating neurite extension it has also been shown that Rab8 localises close to, and directly associated with, the PSD where it acts sequentially with Rab11, but in distinctly separate spatial functions, in the regulated cycling and delivery of AMPA receptors into dendritic spines (Brown et al., 2007b; Gerges et al., 2004b). Furthermore Rab8 expression decreases mGluR1a-mediated inositol phosphate formation and neuronal calcium release in a Protein kinase C (PKC) dependent manner (Esseltine et al., 2012). Additionally *Rab8* expression also appears to decrease endocytosis of mGluR1a receptors from the cell surface. Studies have also shown that Rab8 interacts with and regulates transport of α2B- and β2-adrenergic receptors, with expression of dominant negative Rab8 significantly reducing expression of the adrenergic receptors within the dendrites of cultured primary thalamic neurons (Dong et al., 2010).

In a recent study it was shown that the evolutionarily conserved Nuclear Dbf2-related (NDR) 1/2 kinase pathway, which is involved in the regulation of polarized development, regulates morphogenesis of dendritic spines (Ultanir et al., 2012). In this study it was demonstrated that inhibition of NDR1/2 via a kinase dead dominant negative or siRNA resulted in perturbed spine morphology coupled with reduced synaptic function both in cultured cells and *in*

vivo. Furthermore it was also shown that Rabin8, a Rab8 GEF and NDR1/2 substrate, was essential for normal dendritic spine morphogenesis with expression of a non-phosphorylatable Rabin8 showing perturbations to dendritic spine morphology, in keeping with the loss of function of NDR1/2. In a very recent study it was also shown that inhibition of Rabin8 phosphorylation by NDR2 resulted in the accumulation of Rab11 positive vesicles at the peri-centrosome (Chiba et al., 2013).

It has also been shown that perturbation to Rab8 function can lead to neurodegeneration. For example Moritz et al., 2001 demonstrated that expression a dominant negative Rab8 canine transgene, Rab8-T22N, led to rapid degeneration of the highly polarised photoreceptor neurons in *Xenopus laevis* (Moritz et al., 2001).

As well as showing a role in neuronal development, with perturbation causing neurodegeneration Rab8 trafficking pathways have also been implicated in a number of diseases, including neurodegenerative diseases.

1.4.1.6. The Role of Rab8 In Neurological and Neurodegenerative Diseases

To date there have been no mutations within either the Rab8A or Rab8B genes that have been directly associated with any diseases. However numerous Rab8 interacting proteins have been implicated in human pathologies. These pathologies include Bardet-Biedl syndrome, microvillus inclusion disease, polycystic kidney disease, MND, Joubert syndrome, Lowe syndrome, Parkinson's Disease, Cancer, Alzheimer's disease, retinal degeneration, glaucoma, Huntington's disease and viral infections (Bachmann-Gagescu et al., 2011; Coon et al., 2012; Dalfo et al., 2004; Del Bo et al., 2011; del Toro et al., 2009; Gitler et al., 2008; Kametani et al., 2004b; Nachury et al., 2007b; Parkhitko et al., 2011; Sato et al., 2007a; Vaibhava et al., 2012). Implication in such a broad spectrum of diseases suggests a greater understanding of Rab8 function may provide significant insight into disease pathology and potential treatment.

A large number of diseases associated with Rab8 interacting proteins show neurodegenerative pathology. For example Oculocerebrorenal syndrome of lowe (Lowe Syndrome/LS), a rare X-linked recessive disorder, presents with mental retardation, as well as other non-neurological symptoms. LS is associated with mutations in the *OCRL1* gene, which encodes the inositol-5-phosphatase OCRL1, and has been implicated in Rab8 and IPIP27 dependent cellular trafficking events (Coon et al., 2012). This is further substantiated by the identification that OCRL1 interacts with Rab8 directly and that mutations in the OCRL1 Rab8 binding domain are associated with LS (Hou et al., 2011). Rab8 has also been shown to interact with mutant α-syn, with over expression of Rab8 alleviating toxicity associated with mutant α-syn in neuronal models of Parkinson's disease (Dalfo et al., 2004; Gitler et al., 2008). Similarly it has also been shown that Abelson Helper Integration Site 1 (AHI1), the encoding gene for which is mutated in the neurological condition Joubert syndrome, also interacts with Rab8 (Hsiao et al., 2009; Valente et al., 2006). AHI1 knockdown cells show a destabilization of Rab8 resulting in a failure to localize correctly, leading to disruption of endocytic trafficking between the plasma membrane and Golgi (Hsiao et al., 2009). Rab8 has also been implicated in Alzheimer's disease where it has been shown that mutant presenilin perturbs transport of the Amyloid Precursor Protein (APP) and causes a depletion of Rab8 protein in cells (Kametani et al., 2004a). Rab8 has also been associated with Huntington's disease where it has been shown that mutations in the *htt* gene result in a disruption to the Rab8-optineurin complex, leading to aberrations in post Golgi trafficking to lysosomes (del Toro et al., 2009).

These studies demonstrated that Rab8, and it's interacting proteins, play a fundamental role in the regulation of intracellular trafficking events that are fundamental to normal cellular homeostasis and development, especially within polarized cell types such as neurons. Furthermore they reveal that perturbation to these processes can lead to numerous human diseases, including a large subset that display neurological pathology. As such they suggest that Rab8 plays an important role in neuronal function, a greater understanding of which may help us in the treatment of diseases, such as frontotemporal dementia.

1.5. Aims

- To perform enhancer and suppressor screens, using a *Drosophila* model of FTD in which *CHMP2B*^{Intron5} is expressed in the *Drosophila* eye, in order to identify novel modifiers of *CHMP2B*^{Intron5} toxicity.

- To characterize mutations in *Rab8*, a potent enhancer of *CHMP2B*^{Intron5} toxicity

- To determine the mechanism that contributes to unregulated synaptic growth seen in *Rab8* mutants

- To characterize a *Drosophila* model of FTD associated with *CHMP2B*^{Intron5} and determine whether mechanisms involved in unregulated growth in *Rab8* mutants also contribute to *CHMP2B*^{Intron5} toxicity.

2. Materials and Methods

2.1. *Drosophila* Husbandry and Genetics

2.1.1. *Drosophila* Stocks

Drosophila stocks were purchased from Bloomington *Drosophila* Stock Centre (Indiana University, Bloomington, U.S.A), the *Drosophila* Genetic Resource Center (Kyoto Institute of Technology, Kyoto, Japan) and the Vienna *Drosophila* RNAi Centre (VDRC; Institute of Molecular Biotechnology, Vienna, Austria). Additional stocks were generated as part of this work or kindly provided by members of the *Drosophila* community. A detailed summary of stocks can be found in Table 2.1. All stocks, without exception, obtained from outside sources were quarantined for at least 2 generations and were routinely inspected for the presence of mites. Alternatively, stocks were transferred onto fresh media on consecutive days for 4-5 days and inspected for mites. Post-quarantine, mite free stocks were transferred to the stock rooms.

Stocks were raised at either 18°C or 25°C and were transferred to fresh medium every 4 or 2 weeks, respectively. All experimental crosses were raised at 25°C, giving a generation time of ~ 10 - 12 days (egg to adult).

Table 2.1. Stocks Used During The Course of This Investigation
Summary of stocks used during this work. Only primary stocks are listed; double balance stocks, stocks combining multiple genetic elements listed below, recombinations of genetic elements listed below and deletion stocks used for screening are not included for brevity.

Stock	Chromosome	Description	Source
Wildtypes			
Canton S (CS)	n/a	Wildtype, red eyes	Sweeney Lab Stock
W^{1118} (w^{-})	n/a	Wildtype, white eyes	Sweeney Lab Stock
Balancer Stocks			
FM6-GFP/Y	First	First Chromosome Balancer	Kornberg Lab (UCSF, USA)
FM7-GFP/Y	First	First Chromosome Balancer	Kornberg Lab (UCSF, USA)
CyO/Sco	Second	Second Chromosome Balancer	Sweeney Lab Stock
CyO-GFP/Sco	Second	Second Chromosome Balancer	Kornberg Lab (UCSF, USA)
TM3/TM6b	Third	Third Chromosome Balancer	Sweeney Lab Stock
TM3/TM6b-GFP	Third	Third Chromosome Balancer	Kornberg Lab (UCSF, USA)
CyO-GFP/If;TM6b/MKRS	Second and Third	Second and Third Chromosome Balancer	Kornberg Lab (UCSF, USA)
CyO/If;TM6b/MKRS	Second and Third	Second and Third Chromosome Balancer	Sweeney Lab Stock
Gal4 Stocks			
GMR-Gal4/CyO-GFP	Second	Glass multimer reporter; eye specific driver	Bloomington Stock Centre
Act-Gal4/CyO-GFP	Second	Actin promoter; global driver	Bloomington Stock Centre
nSyb-Gal4/CyO-GFP	Second	Neuronal Synaptobrevin promoter; Pan-neuronal driver	Goodwin Lab (Oxford, UK)

Table 2.1. Stocks Used During The Course of This Investigation

Summary of stocks used during this work. Only primary stocks are listed; double balance stocks, stocks combining multiple genetic elements listed below, recombinations of genetic elements listed below and deletion stocks used for screening are not included for brevity.

Stock	Chromosome	Description	Source
OK6-Gal4/CyO-GFP	Second	Motor neuronal specific driver	O'Kane Lab (Cambridge, UK)
MHC-Gal4/TM6b	Third	Myosin Heavy Chain Promoter; Muscle specific driver	Goodman lab stock (UCSF, USA) (donation)
Rab8-Gal4/CyO-GFP	Second	Rab8 promoter	Hiesinger Lab (UT Southwestern, USA)
UAS Stocks			
UAS-CHMP2B^{Intron5}/CyO-GFP	Second	CHMP2B mutant transgene	Gao Lab (UMASS, USA) (Ahmad et al., 2009)
UAS-Shrub-GFP/CyO-GFP	Second	GFP tagged Shrub	Sweeney Lab Stock
UAS-Rab8/Cyo-GFP	Second	Second Chromosome Rab8 Insertion	Generated During This Investigation
UAS-Rab8/TM6b	Third	Third Chromosome Rab8 Insertion	Generated During This Investigation
UAS-Rab8-eGFP/TM6b	Third	Enhanced GFP tagged Rab8	Generated During This Investigation
UAS-Rab8-RNAi(a)/TM6b	Third	Rab8 RNAi	Sweeney Lab Stock
UAS-Rab8-RNAi(b)/TM6b	Third	Rab8 RNAi	VDRC (Vienna, Austria)
UAS-NTAP-Rab8/TM6b	Third	N-terminally TAP tagged Rab8	Generated During This

Table 2.1. Stocks Used During The Course of This Investigation

Summary of stocks used during this work. Only primary stocks are listed; double balance stocks, stocks combining multiple genetic elements listed below, recombinations of genetic elements listed below and deletion stocks used for screening are not included for brevity.

Stock	Chromosome	Description	Source
			Investigation
UAS-AliX/TM6b	Third	Wildtype ALG2 interacting protein X	Aigaki Lab (Tokyo Metropolitan University, Japan)
UAS-AliX-RNAi	Third	AliX-RNAi	Aigaki Lab (Tokyo Metropolitan University, Japan)
UAS-ALG2/CyO-GFP	Second	Wildtype Apoptosis linked gene 2	Aigaki Lab (Tokyo Metropolitan University, Japan)
UAS-POSH	Second	Wildtype Plenty of SH3's	Aigaki Lab (Tokyo Metropolitan University, Japan)
UAS-POSH^{MRing}/TM3	Third	POSH expressing a mutated zinc ring finger domain (C28S/C33S/C36S)	Aigaki Lab (Tokyo Metropolitan University, Japan)
UAS-HRS/TM6b-GFP	Third	Wildtype HRS/HGS	Bellen Lab (Howard Hughes Medical Institute, USA)
UAS-dTAK1	Third	Wildtype TGFβ-Activated Kinase 1	Stronach Lab (University of Pittsburgh, USA)

Table 2.1. Stocks Used During The Course of This Investigation

Summary of stocks used during this work. Only primary stocks are listed; double balance stocks, stocks combining multiple genetic elements listed below, recombinations of genetic elements listed below and deletion stocks used for screening are not included for brevity.

Stock	Chromosome	Description	Source
UAS-dTAK1^{K46R}/CyO-GFP	Second	TAK1 Dominant Negative	Stronach Lab (University of Pittsburgh, USA)
UAS-TAK1-RNAi	Third	TAK1-RNAi	Stronach Lab (University of Pittsburgh, USA)
UAS-EIF4-GFP/CyO-GFP	Second	Nuclear GFP	Bloomington Stock Centre
UAS-MCD8-GFP/CyO-GFP	Second	Membrane Localised GFP	Bloomington Stock Centre
UAS-Fos^{DN}	Second	Fos dominant negative	Bloomington Stock Centre
UAS-Atg1/TM6b	Third	Wildtype Atg1	Ganetzky Lab (University of Wisconsin, USA)
UAS-Atg5-RNAI	Second	Atg5-RNAi	VDRC (Vienna, Austria)
UAS-Atg7-RNAi	Second	Atg7-RNAi	VDRC (Vienna, Austria)
UAS-Atg18-RNAi	Second	Atg18-RNAi	VDRC (Vienna, Austria)
UAS-Atg5-GFP/TM6b	Third	GFP tagged Atg5	O'Kane Lab (Cambridge, UK)
UAS-Atg8-RFP/CyO-GFP	Second	RFP tagged Atg8/LC3	Hafen Lab (University of Zürich, Switzerland)
UAS-Rheb/CyO-GFP	Second	Wildtype Rheb	Hafen Lab (University of Zürich, Switzerland)
UAS-Rab4-RFP/CyO-GFP	Second	RFP tagged Rab4	Bloomington Stock Centre
UAS-Rab11-eGFP/CyO-GFP	Second	eGFP tagged Rab11	Bloomington Stock Centre

Table 2.1. Stocks Used During The Course of This Investigation

Summary of stocks used during this work. Only primary stocks are listed; double balance stocks, stocks combining multiple genetic elements listed below, recombinations of genetic elements listed below and deletion stocks used for screening are not included for brevity.

Stock	Chromosome	Description	Source
UAS-Spin-RFP/CyO-GFP	Second	RFP tagged Spinster	Sweeney Lab Stock
Mutant Stocks			
$Rab8^{1}$/TM6c	Third	EMS induced Rab8 point mutation	Bloomington Stock Centre
$Rab8^{2}$/TM6c	Third	EMS induced Rab8 point mutation	Kennison Lab (NIH, USA) (donation)
$Rab8^{3}$/TM6c	Third	EMS induced Rab8 point mutation	Kennison Lab (NIH, USA) (donation)
$Rab8^{Z3007}$/TM6b	Third	EMS induced Rab8 point mutation	Kennison Lab (NIH, UAS) (donation)
$Rab8^{B229}$/TM6b	Third	PBac{5HPw^{+}} P-element disruption of Rab8	Bloomington Stock Centre
$OCRL1^{C52}$/FM6-GFP	First	dOCRL1 loss of function, imprecise P-element excission	Sweeney Lab Stock
$OCRL1^{D40}$/FM6-GFP	First	dOCRL1 loss of function, imprecise P-element excission	Sweeney Lab Stock
$AliX^{EY10362}$/TM6b	Third	P{EPgy2}$AliX^{EY10362}$, AliX loss of function, (P-element activity)	Bloomington Stock Centre
$POSH^{74}$/CyO-GFP	Second	POSH Null	Stronach Lab (University of Pittsburgh, USA)
$POSH^{EP1206}$/CyO-GFP	Second	P{EP}$POSH^{EP1206}$, POSH loss of function, (P-element	Bloomington Stock Centre

Table 2.1. Stocks Used During The Course of This Investigation

Summary of stocks used during this work. Only primary stocks are listed; double balance stocks, stocks combining multiple genetic elements listed below, recombinations of genetic elements listed below and deletion stocks used for screening are not included for brevity.

Stock	Chromosome	Description	Source
		activity)	
$POSH^{EP2248}$/CyO-GFP	Second	P{EP}$POSH^{EP2248}$, POSH loss of function, (P-element activity)	Bloomington Stock Centre
HRS^{D28}/CyO-GFP	Second	EMS induced HRS loss of function	Bellen Lab (Howard Hughes Medical Institute, USA)
$TAK1^{2}$/FM6-GFP	First	EMS induced TAK1 loss of function	Bloomington Stock Centre
$TAK1^{179}$/FM6-GFP	First	EMS induced TAK1 loss of function	Bloomington Stock Centre
Wnd^{1}/TM6b	Third	EMS induced Wallenda loss of function	DiAntonio Lab (Washington University in St. Louis, USA)
Wnd^{3}/TM6b	Third	EMS induced Wallenda loss of function	DiAntonio Lab (Washington University in St. Louis, USA)
$Debra^{EP9}$/CyO-GFP	Second	P{EP}$Debra^{EP9}$, Debra loss of function, (P-element activity)	Bloomington Stock Centre
$Debra^{EY04764}$/CyO-GFP	Second	P{EPgy2}$Debra^{EY04764}$, Debra loss of function, (P-element activity)	Bloomington Stock Centre
Tkv^{7}/CyO-GFP	Second	EMS induced Thickveins loss of function	Sweeney Lab Stock
Tkv^{K16713}/CyO-GFP	Second	P{LacW}Tkv^{K16713} Thickveins loss of function (P-element activity)	Sweeney Lab Stock
$Dad^{\Delta IEL}$/TM6b	Third	Dad^{271-68} Loss of Function Mutant	Sweeney Lab Stock
Puc^{E69}/TM6b	Third	P{A92}Puc^{E69}, Puckered loss of function (P-element	Bloomington Stock Centre

Table 2.1. Stocks Used During The Course of This Investigation

Summary of stocks used during this work. Only primary stocks are listed; double balance stocks, stocks combining multiple genetic elements listed below, recombinations of genetic elements listed below and deletion stocks used for screening are not included for brevity.

Stock	Chromosome	Description	Source
		activity)	
$Atg1^{DG}$/TM6b	Third	$Atg1^{DG23110}$, Atg1 loss of function (P-element activity)	Bloomington Stock Centre
$Atg1^{PZ}$/TM6b	Third	P{PZ}$Atg1^{00305}$, Atg1 loss of function (P-element activity)	Bloomington Stock Centre
$Atg7^{D77}$/CyO-GFP	Second	Atg7 loss of function (P-element activity)	Fanto Lab (Kings College, London, UK)
$Atg18^{KG}$/TM6b	Third	$Atg18^{KG03090}$, Atg18 loss of function (P-element activity)	Bloomington Stock Centre
$Rheb^{261}$/TM6b	Third	EMS induced Rheb loss of function	Hafen Lab (University of Zürich, Switzerland)
$Rheb^{3M2}$/TM6b	Third	EMS induced Rheb loss of function	Hafen Lab (University of Zürich, Switzerland)
Other Stocks			
Df(3L)ED228/TM6b	Third	3L deletion covering Rab8	Bloomington Stock Centre
Df(3L)Excel6112/TM6b	Third	Deletion covering Atg18	Bloomington Stock Centre
Dad-LacZ/TM6b	Third	Dad Reporter	Bloomington Stock Centre

2.1.2. *Drosophila* Media

Unless otherwise stated stocks were raised on standard medium (25 g/l sucrose, 3.75 g/l agar, 0.125 g/l $CaCl_2$, 0.125 g/l $FeSO_4$, 0.125 g/l MnCl, 0.125 g/l NaCl, 2 g/l $KNaC_4H_4O_6{\cdot}4H_2O$). Following autoclaving the medium was cooled for 1 hour to ~ 45°C before addition of the antifungal agents Bavistin (1.5 mg/l in 100 % ethanol; BASF, Auckland, New Zealand) and Nipagin (0.7 mg/l in 100 % ethanol; Sigma, UK). 7 ml of medium was dispensed into 25x95 mm plastic vials (Dutscher Scientific, UK), which were subsequently plugged with cotton wool (Fisher Scientific, UK).

TGFβ experiments were performed on Nutri-Fly™ Bloomington Formulation medium (Genesee Scientific, San Diego, USA), which was prepared following the manufacturers instructions. Medium was dispensed (7 ml) into 25x95 mm plastic vials (Dutscher Scientific, UK), which were subsequently plugged with cotton wool (Fisher Scientific, UK).

Rapamycin experiments were performed on formula 4-24® instant *Drosophila* medium (Carolina Biological Supply Company, USA). Media was prepared by mixing 50:50 with dH_2O. 4-24® was used during Rapamycin drug treatment as the media does not require cooking, which could affect compound integrity, and Rapamycin could be readily mixed with water during preparation of the media.

When required in large numbers stocks were raised in 1/3 pint bottles on a maize based medium (119.0 g/l maize meal, 17.5 g/l yeast, 15.9 g/l agar, 103.2 g/l sucrose). Post-cooking of the primary ingredients media was cooled to ~45°C and the antifungal agents Nipagin (0.4mg/l in 100 % ethanol; Sigma, UK) and propionic acid (0.4 % v/v; Arcos Organics, Geel, Belgium) were added. The medium was then dispensed into 1/3 pint glass bottles and the bottles bunged using Flugs® (Dutscher Scientific, UK). Bottles containing medium were autoclaved at 121°C for 20 minutes

To encourage egg laying medium could be supplemented with dried yeast or yeast paste.

2.1.3. Anaesthesia

In order to identify gender and genotype adult *Drosophila* were anaesthetised on a porous gas pad using continuous administration of CO_2. Anaesthetised *Drosophila* were observed using a dissecting microscope (Zeiss Stemi-2000, Carl Zeiss AG, Germany). CO_2 was the primary method of anaesthesia, however ether was used for imaging of the *Drosophila* eye in the early stages of this investigation.

2.1.4. Crossing Techniques

Female *Drosophila* are capable of storing sperm, therefore in order to have a controlled genetic cross females must be isolated as virgins. At 25°C female flies will not mate within 8 hours of eclosion. Furthermore, newly eclosed flies display pale pigmentation, unexpanded wings and the presence of a meconium, visible through the abdominal cuticle, identifying them as virgins. Based on these principles virgin females can be collected by completely emptying vials in the morning and isolating any virgins based on the presence of the identifying features and then collecting any further females that eclose within the 8 hour window.

2.1.5. Modifier Screens

2.1.5.1 *Shrub*-GFP

Initial unbiased modifier screens were performed by crossing the GMR-Gal4, UAS-Shrub-GFP/CyO stock to all 257 individual deletion stocks in the DrosDel Deletion collection (University of Cambridge, Cambridge, U.K) (Ahmad et al., 2009). This collection represented ~75 % of the *Drosophila* Genome. The resultant eye phenotypes were classified as low (+) (< 15 black spots of melanisation), medium (++) (> 15 spots of melanisation but < 50 % of the eye affected) or high (+++) (> 50 % of the eye subjected to melanisation). Phenotypes were compared against GMR-Gal4, UAS-Shrub-GFP/CyO

outcrossed to *w*^{1118}. These initial screens were performed by Dr Sean Sweeney in collaboration with Dr Fen-Biao Gao (UMASS, Worcester, USA). Deletion regions identified as modifiers of the *Shrub*-GFP phenotype were subsequently narrowed using smaller deletions and, eventually, individual gene loci. Eyes were imaged under a dissecting microscope (Zeiss Stemi-2000, Carl Zeiss AG, Germany) using an attached AxioCam ERc 5s digital camera (Carl Zeiss AG, Germany) and Axiovison 4.8 software (Carl Zeiss AG, Germany).

2.1.5.2. *CHMP2B*^{Intron5}

Following the success of the initial modifier screens against *Shrub*-GFP more precise modifier screens were subsequently performed against *CHMP2B*^{Intron5} by crossing GMR-Gal4, UAS-CHMP2B^{Intron5}/CyO to 98 deletion stocks covering the entire left arm of chromosome 2 and 38 deletion stocks covering the entire left arm of chromosome 3 (Fig. 3.2.). For a schematic representation of the screen see Fig. 2.1. Deletion Stocks were a kind gift from John Roote (University of Cambridge, Cambridge, UK) and Guy Tear (Kings College, London, UK). Specific enhancers of *Shrub*-GFP and known genes of interest were also screened against *CHMP2B*^{Intron5} as part of targeted screens. Eyes were scored and imaged as for *Shrub*-GFP screens (above)

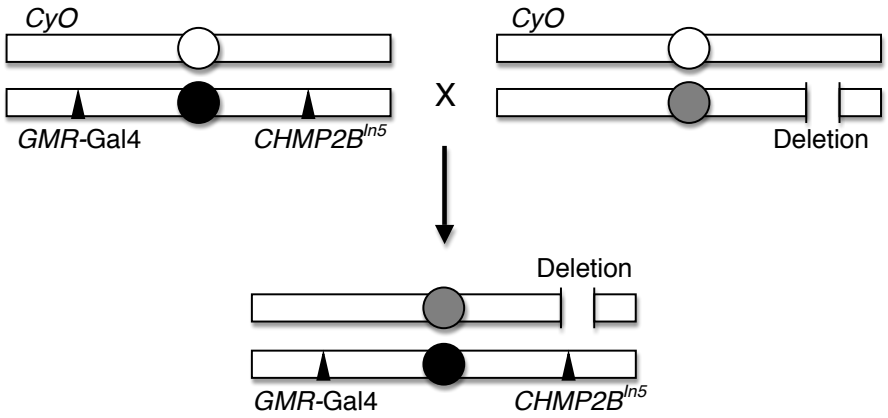

Figure 2.1. Schematic Representation of Modifier Screening Against the *CHMP2B*^{Intron5} Phenotype
GMR-Gal4, UAS-CHMP2B^{Intron5}/CyO flies were crossed to individual deletion stocks and the resultant eye phenotypes scored and compared to controls in order to identify modifiers of the eye phenotype.

2.1.6. Complementation Analysis

Complementation analysis was used to determine whether alleles of an identified locus belong to the same complementation group. A failure to complement suggests each mutation affects the gene of interest as complementation only occurs if mutations are within different genes. Complementation assays were performed by crossing different heterozygous balanced mutants, proposed to affect a specific gene (e.g *Rab8*), with each other and with a previously characterised mutant affecting that gene. Transheterozygous offspring were assayed for lethality or reduced viability, indicating a failure to complement. Complementation analysis was used during the characterisation of *Rab8* mutants, which display a distinct transheterozygous pharate lethal phenotype.

2.1.7. Recombination's

Homologous chromosomal recombination in *Drosophila* females was utilised in order to generate stocks in which two genetic components were present on the same chromosome arm, thus allowing the use of 3 or more genetic components on a single chromosome. For example this approach was used to recombine the $Rab8^{B229}$ piggyBac mutation with both MHC-Gal4 and the Puc-LacZ reporter constructs. Recombination was achieved by mating individual stocks with each other and selecting away from balancers to identify virgin female offspring carrying both genetic components (e.g $Rab8^{B229}$/*MHC*-Gal4). These offspring were subsequently crossed to balancer stocks for that chromosome and potential recombinant offspring selected. Selection was performed based on eye colour, where possible, as well as other characteristic phenotypes. The presence of the desired genetic components was confirmed via PCR or confirmation of GFP (see sections 2.4.1 and 2.4.2).

2.2. Immunohistochemistry and Imaging

2.2.1. Third Instar Larvae Dissection

Female third instar wandering larvae of the required genotype were transferred onto a sylgard dish (Silicone elastromere kit, DowCorning, MI, USA) and dissected in either PBS (137 mM NaCl, 2.7 mM KCl, 10 mM Na_2HPO_4 and 1.8 mM KH_2PO_4 in dH_2O) or Haemolymph-like buffer (HL3; 70 mM NaCl, 5 mM KCl, 1 mM $CaCl_2$.2H2O, 10 mM $NaHCO_3$, 5 mM trehalose, 115 mM sucrose and 5 mM BES in dH_2O). Dissections were performed using a dissecting microscope (Zeiss Stemi-2000, Carl Zeiss AG, Germany). Larvae were pinned, dorsal side up, at both the anterior and posterior ends using minuten pins (Austerlitz Insect Pins 0.1 mm diameter, Fine Science Tools, Heidelberg, Germany). An incision was made along the dorsal midline of the larvae from the posterior to anterior end using Vannas sprung straight bladed dissection scissors (Fine Science Tools, Heidelberg, Germany). Forceps were used to remove the internal organs, leaving the CNS *in situ*, and the muscle walls were pinned out. When only looking at NMJ's the CNS was removed. Larvae were fixed in 3.7 % formaldehyde (Sigma, UK) in PBS whilst pinned *in situ* for 7 min. When using antibodies for Glutamate receptors larvae were instead fixed in Bouins solution (Sigma, UK) for 2 min. Larval preps were unpinned, transferred to a 1.5 ml eppendorf tube and washed 3 times in 0.1 % PBS-T/PBT (0.1 % v/v triton X-100 in PBS)

2.2.2. Immunohistochemical Staining Larval NMJ's and VNC

Following preparation of *Drosophila* third instar larvae (See above) larval preparations were incubated in primary antibodies (see table 2.2.) in 0.1 % PBT at 4°C, overnight, in darkness with rocking. Following primary antibody incubation preparations were washed 3 times in 0.1 % PBT. Preparations were then incubated in secondary antibodies (see table 2.3.) in 0.1 % PBT for 1 hour, in darkness, with rocking at room temperature. Preparations were subsequently washed 3 times in 0.1 % PBT. Post-washing preparations were submerged in 70 % glycerol (70 % v/v in PBS) for 1-2 hours until all the air was

displaced from the preparations. Preparations were then mounted in Vectashield® (Vector Laboratories LTD, UK), cuticle side down upon a standard microscope slide. Cover slips were sealed in place using nail varnish.

Table 2.2. Primary Antibodies Used During The Course of This Investigation

Antigen	Dilution	Species/type	Source/Reference
Atg5	IF 1:300	Rabbit polyclonal	Novus Biological
Bruchpilot	IF 1:50	Mouse monoclonal	DSHB (NC82)
Discs large	IF 1:50	Mouse monoclonal	DSHB (4F3)
Elav	IF 1:50	Mouse monoclonal	DSHB (9F8A9)
Even Skipped	IF 1:50	Mouse monoclonal	DSHB (3C10)
Fasciclin II	IF 1:10	Mouse monoclonal	DSHB (3B43)
Futsch	IF 1:50	Mouse monoclonal	DSHB (22C10)
GluR IIa	IF 1:20	Mouse monoclonal	DSHB (8B4D2)
GluR IIb	IF 1:2500	Rabbit polyclonal	Di Antonio et al., (1999)
GluR III	IF 1:2500	Rabbit polyclonal	Di Antonio et al., (1999)
HRP	IF 1:200	Goat polyclonal, Cy3 Conjugate	Stratech scientific ltd.
HRS/HGS	IF 1:200	Guinea Pig polyclonal	Lloyd et al., 2002
Lac-Z	IF 1:1000	Rabbit polyclonal	Cappel Laboratories
Phosho-JNK	IF 1:1000	Rabbit polyclonal	Promega (V7931)
Phospho-MAD	IF 1:500	Rabbit polyclonal	Ten Dijke (PS1)
POSH	IF 1:20	Rabbit polyclonal	Tsuda et al., 2005
Rab8	IF 1:50	Rabbit polyclonal	Generated during this investigation
Rab11	IF 1:8000	Rabbit polyclonal	Tanaka and Nakamura., 2008
Repo	IF 1:50	Mouse monoclonal	DSHB (AD12)
Synaptotagmin	IF 1:2000	Rabbit monoclonal	Sweeney Lab
Ubiquitinylated proteins	IF 1:2000	Mouse monoclonal	Enzo Life Sciences (BML-PW8810-0500)

Table 2.3. Secondary Antibodies Used During The Course of This Investigation

Antibody	Dilution	Source/Reference
Goat anti-Rabbit Cy3	IF 1:200	Jackson ImmunoResearch
Goat anti-Rabbit Cy5	IF 1:200	Jackson ImmunoResearch
Goat anti-Rabbit FITC	IF 1:200	Jackson ImmunoResearch
Goat anti-Mouse Cy3	IF 1:200	Jackson ImmunoResearch
Goat anti-Mouse Cy5	IF 1:200	Jackson ImmunoResearch
Goat anti-Mouse FITC	IF 1:200	Jackson ImmunoResearch
Goat anti-Guinea Pig Cy3	IF 1:200	Jackson ImmunoResearch

2.2.3. *Drosophila* Retina Dissection

3 days post-eclosion adult flies of the correct genotype were anesthetised by CO_2 (see section 3.2.1.3). Flies were orientated ventral side up and, using forceps the thorax was gently grasped causing an extension of legs and proboscis. Whilst maintaining hold of the body forceps, were used to grasp the proboscis in order to gently remove the head. The body was discarded and the head submerged in a drop of HL3 on a sylgard dish. The eye was carefully dissected from the head. This is most easily done by teasing apart the connective tissue between the eye and the proboscis and working round gently tease the eye from the head. Eyes were transferred into a 0.5 ml eppendorf containing 3.7 % formaldehyde in PBS, for 40 min. Eyes were washed 3 times (5 min. with rocking) in 0.4 % PBS-T/PBT (0.4 % v/v triton X-100 in PBS). Post-washing eyes were transferred back onto a sylgard dish and, in a drop of PBS or PBT, any excess tissue and the lamina removed from the eyes. Eyes were transferred into a 0.5 ml eppendorf containing 0.4 % PBS-T and incubated at 4°C, overnight, in the dark with rocking in order to remove any auto-fluorescent pigment. Following incubation eyes were washed 3 further times in PBT (5 min. with rocking). Protocol modified from Williamson and Hiesinger (2010), (Williamson and Hiesinger, 2010).

2.2.4. Immunohistochemical Staining *Drosophila* Retinas

Following preparation (see above) *Drosophila* retinas were incubated in rhodamine conjugated phalloidin (1:100 in 0.4 % PBT) overnight, in darkness, with rocking at 4°C. After incubation eyes were washed 3 times in 0.4 % PBT before being submerged in 70 % glycerol (70 % v/v in PBS) for 1-2 h to displace any air from the preparation. Eyes were mounted in Vectashield® (Vector Laboratories LTD, UK) on a standard microscope slide. Coverslips were elevated, to avoid compressing the eye, on two 22 x 22 mm coverslips fixed either side of the preparations. Coverslips were sealed in place using nail varnish.

2.2.5. Microscopy and Image Analysis

2.2.5.1. Confocal Microscopy

Following immunohistochemical staining *Drosophila* larval NMJ's, brains and adult retinas were imaged using a Zeiss LSM 710 Axio Observer Z1 confocal microscope, using Zen 2009 software (Carl Zeiss AG, Germany). Whole NMJ's were imaged by taking Z-stack images, using a 63x oil immersion objective. Z-stacked projections of larval VNC's were imaged using a 40x oil immersion objective. Single focal plane images of *Drosophila* retinas were taken using the 40x oil objective. Both z-stack and single focal plane images were also taken using the 40x, 60x and 100x oil objectives during the course of this investigation. When taking confocal images for quantification of fluorescence all settings were kept the same between images.

2.2.5.2. Calculating Mean Normalised Bouton Number

Drosophila 3rd instar wandering larvae were dissected and immunohistochemically labelled (see sections 2.2.3. and 2.2.4.) using HRP-Cy3 to mark the nervous system and anti-synaptotagmin to label synaptic boutons. Synaptic bouton number, at muscle 6/7 and muscle 4, was assessed by counting the number of individual synaptotagmin positive swellings visible at each NMJ. Counts were made using the 40x objective on an Axiovert 200 invert fluorescence microscope (Carl Zeiss AG, Germany).

Synaptotagmin staining results in small amounts of background staining of the larval muscles. This was utilised to clearly image muscles 6/7 (see fig. 1.5.C) and 4 at hemi-segment A3 using the 10x objective and a AxioCam HRC camera (Carl Zeiss AG, Germany) connected to a Axiovert 200 invert fluorescence microscope (Carl Zeiss AG, Germany). Using ImageJ the width and length of the muscles was measured in pixels. A haemocytometer was imaged under the same conditions to allow conversion of pixel measurements to micrometres, which were then used to calculate the muscle surface area (MSA). The mean MSA of wildtype animals was used to normalise the bouton number of other

genotypes; the mean wildtype MSA was divided by the MSA of the muscle of interest and multiplied by the bouton number corresponding to the muscle of interest. As bouton number parallels MSA, normalisation in effect gives the bouton number expected if the muscle was a wildtype size. Any genotypes displaying a significantly different MSA from wildtypes are indicated.

2.2.5.3. Calculating Mean Normalised NMJ Length, Branch Number, Satellite Bouton Number and Synaptic Bouton Size

Confocal images of NMJ's at muscle 4 hemi-segment A3 were taken as described in section 2.2.5.1. and processed using ImageJ. The length of each NMJ was determined by tracing each NMJ using the NeuronJ ImageJ plugin and using the measure tracings setting. NMJ lengths were normalised via the same method as for bouton number, described above (section 2.2.5.2) and the mean normalised NMJ length determined for each genotype. Images were also used to calculate the branch number of each NMJ. Branches originating from the original nerve entry point were classified as primary branches with subsequent branches defined as strings of at least 2 consecutive boutons branching off from another branch (Jin et al., 2009). Branch numbers were normalised in the same way as bouton numbers and the mean normalised genotypic branch number calculated. Satellite boutons were defined as small supernumerary boutons budding from a central parent bouton (Dickman et al., 2006). Satellite bouton number was normalised as for bouton numbers. Synaptic bouton sizes were determined by measuring the diameter of each synaptotagmin positive swelling, measured across the widest point, for each NMJ. Bouton sizes were normalised and the mean normalised size calculated per genotype.

2.2.5.4. Assaying Pre-synaptic Retractions and Ghost Boutons

Analysis of pre-synaptic retractions was performed as previously described by Eaton et al. (2002) (Eaton et al., 2002). Larvae were dissected as described in section 2.2.1. and immunohistochemically labelled (see section 2.2.2.) using

both anti-Dlg, labelling the post-synaptic density, and anti-horseradish peroxidase (HRP), labelling the pre-synaptic terminal. Sites at which post-synaptic Dlg staining was observed in the absence of pre-synaptic HRP staining were classified as “post-synaptic footprints”, indicating a pre-synaptic retraction (Eaton et al., 2002). The number of NMJ’s displaying retractions was recorded per genotype. At the same time the presence of ghost-boutons, undifferentiated boutons that have failed to mature, was recorded. Ghosts were classified as boutons showing pre-synaptic HRP staining in the absence of post-synaptic Dlg (Ataman et al., 2006a; Packard et al., 2002). Analysis of pre-synaptic retractions and the presence of ghost boutons was performed using a 40x objective on an Axiovert 200 invert fluorescence microscope (Carl Zeiss AG, Germany).

2.2.5.5. Quantification of Nuclear and Cell Fluorescence.

ImageJ was used to calculate the corrected total cell immuno-fluorescence (CTCF) or corrected total nuclear immuno-fluorescence (CTNF) for P-MAD, Dad-LacZ, Puc-Lacz and HRS reporters within motor neurons. Third instar wandering larvae of the correct genotype were dissected as in section 2.2.1. and the CNS left *in situ*. Immunohistochemical staining of preparations was performed as in section 2.2.2. using the appropriate antibodies. All genotypes were stained within the same tubes. α-Eve was used to mark motor neuron nuclei within the VNC. Confocal microscopy was used to generate z-stacked images of the VNC’s (see section 2.2.5.1.) which were processed using imageJ. Confocal settings were kept the same for all images. Using the drawing tools in imageJ individual motor neuronal nuclei or cell bodies were selected and the area, integrated density and mean gray values measured. At least 3 measurements were also taken from surrounding regions to provide a mean background fluorescence reading. CTCF/CTNF was calculated using the following formula: CTCF = Integrated density – (Selected Area x Mean background fluorescence).

2.2.5.6. Transmission Electron Microscopy (TEM)

2.2.5.6.1. Fixation and Embedding of *Drosophila* Larval Muscles and Brains

Third instar wandering larvae were dissected as in section 2.2.1. and fixed (0.1 M sodium phosphate buffer ($NaPO_4$, pH 7.4), 1 % gluteraldehyde, 4 % methanol-free formaldehyde (pH 7.3)), whilst still pinned to the sylgard plate, for 7 mins. Larval preps were then transferred into 1.5 ml eppendorf tubes of fix and left rocking at 4°C overnight. Whole preps were subsequently washed 3x 10 mins in 0.1 M sodium phosphate buffer, rocking at room temperature (RT), before a 2 hour incubation in 1 % osmium tetroxide (1 % OsO_4 in 0.1 M $NaPO_4$, RT with Rocking). 3x 10 minute washes in dH_2O (RT with rocking) were performed prior to incubation in 1 % uranyl acetate (1 % in dH_2O, 4°C, overnight with rocking). 3x 10 minute washes in dH_2O were performed (RT with rocking) prior to dehydration. Preps were dehydrated in increasing concentrations of ethanol (30 %, 50 %, 70 %, 90 % and 3x 100 % in dH_2O, 15 mins each, RT with rocking), followed by 2x 15 min. incubation in propylene oxide (100 %, RT with rocking). 100 % propylene oxide and ethanol stocks used in this protocol were maintained dehydrated using a molecular sieve. Dehydrated preps were subsequently transferred to 7 ml glass snap top vials and incubated in increasing concentrations (25 %, 50 %, 75 % and 3x 100 %) of epon araldite resin (8 g agar 100, 18 g dodecenyl succinic anhydride **(**DDSA), 4 g araldite CY212, 0.75 ml dimethylbenzylamine (BDMA)) for 30 mins each at 37°C with rotation. Post resin incubation whole preps were removed and placed within a drop of 100 % epon araldite resin upon a sylgard dish. Fine tungsten needles were used to dissect out muscles of interest (muscle 6/7) and whole larval brains. These were then transferred into embedding moulds (Silastic J Kit, Dow, USA) half filled with pre-semi-polymerised (60°C 4-6 hours) resin. Moulds were then filled with un-polymerised resin and incubated at 60°C for 48 hours to complete polymerization. After 48 hours moulds were left to cool before removing the polymerized resin blocks.

2.2.5.6.2. Sectioning and TEM

Resin blocks containing the preparations were trimmed as close to the preparation as possible using a fine-toothed hacksaw. Blocks were then secured within a chuck and trimmed using a fine razor blade to leave a small, flat-topped pyramid surrounding the preparation. This reduces the subsequent cutting area. Blocks were typically trimmed to ~1/3 of the way through the VNC, from the posterior end, or ~1/3 through the muscle, from either the posterior or anterior end. This provides a start point close to the area of interest at which to begin sectioning. 1 µm sections were cut using glass knives upon a microtome (Leica Ultracut UCT). Sections were placed within a drop of water upon microscope slides and dried on a hot plate at 80°C. Sections were subsequently stained in toluidine blue (0.6 % in 0.3 % sodium carbonate, 80°C for ~5 seconds) rinsed in distilled water and again dried on the hot plate. Stained sections were analysed to confirm the region of interest and ascertain the quality of the preparation. Having determined positioning and quality fine sections (60-70 nm) were cut, as for 1 µm sections, and incubated in uranyl acetate (in 50 % ethanol, 10 mins at RT). Sections were subsequently submerged in distilled water to wash prior to staining in lead citrate in the presence of sodium hydroxide pellets (10 mins, RT) and rinsing in distilled water. Sodium hydroxide pellets are used to prevent excessive lead citrate precipitation. Sectioning was performed by M. Stark (Technology facility, York).

TEM imaging was performed using analySIS software on a TECNAI G^2 transmission electron microscope (120 kV). Quantification of the number and diameter of endosome-like vesicle structures was performed using ImageJ.

2.3. Physiological Analysis of *Drosophila* Larvae

2.3.1. Larval Locomotion Assay

The larval locomotion assay was conducted at 25°C and all equipment and reagents (e.g HL3, petri-dishes) used left to reach this temperature prior to use. Female third instar wandering larvae of the appropriate genotype were selected

and transferred into HL3 saline to wash off any debris. Using a fine, damp paintbrush 2-3 larvae were transferred onto the centre of a 90mm diameter petri-dish containing a thin layer of 2% agar and left to acclimatise. The petri dish was placed upon a black surface, providing optimal contrast, with a digital webcam (Creative labs, UK) vertically above, providing a birds-eye image. In the dark a light source was directed at the side of the petri-dish to elicit a crawling escape response. Upon initiation of crawling larvae were recorded for 120 sec. (0.2 frames sec^{-1}) using VirtualDub software. Locomotion was analysed using imageJ, with the median and thresh-track plugins, tracking larval movement (pixels $frame^{-1}$) across the X/Y coordinates. Distance travelled was calculated using Pythagoras' theorem ($\sqrt{((X_1-X_2)^2 + (Y_1-Y_2)^2)}$) and the mean velocity (pixels sec^{-1}) calculated. Velocity was converted to mm s^{-1} using a scale imaged under the same conditions.

2.4. Molecular Biology

2.4.1. Antibody Production

Drosophila Rab8 cDNA in the pOT2 plasmid vector was supplied to the York Protein Production Service (Technology Facility, York, UK) according to the required specifications. Briefly cDNA was subcloned into a plasmid vector containing a Glutathione S-transferrase (GST) tag. GST-tagged *Rab8* was expressed in *E*. Coli, extracted and purified via large scale glutathione sepharose purification. Purified GST tagged Rab8 protein was supplied to the Eurogentec Polyclonal Antibody Production service (Eurogentec, Belgium) in accordance with the required specifications. Briefly two separate rabbits were immunized with 100 µg of the supplied protein at 0, 14, 28 and 56 days, in accordance with the Eurogentec 87-Day classical immunization programme. Final bleed serum was aliquoted into 500µl aliquots in 1.5 ml eppendorf tubes and stored at - 80°C. When required individual aliquots were mixed 50:50 with glycerol and stored at 4°C.

2.4.2. Extraction of Genomic DNA

DNA was extracted from single adult flies by homogenisation in 50 µl of DNA extraction buffer (25 mM NaCl, 10 mM Tris-HCl pH 8.2, 1 mM EDTA, Proteinase K 200 µg/ml). Buffer can be stored aliquoted at - 20°C in the absence of proteinase K, which must be added fresh. Homogenate was incubated at 37°C for 30 min. prior to Proteinase K inactivation by incubation at 85°C, 10 min.. Centrifugation at 13000g for 3 min. in a bench-top centrifuge allowed separation of particulates. 1-2 µl of supernatant was used as a PCR template. Increased concentrations of DNA could be obtained by using multiple flies for extraction.

2.4.3. Polymerase Chain Reaction (PCR)

PCR reactions were run using PCR mastermix (Promega, UK; 25 U/ml *Taq* DNA polymerase, *Taq* Reaction Buffer, 200 µM of each dNTP, 1.5 mM $MgCl_2$) with 1 µM of each primer and 0.5-1 mg of genomic DNA (typically 1-2 µl from fly extraction) or 1-2 ng of plasmid DNA. Reactions were run as a total volume of 20 µl in a Techne TC512 PCR thermocycler (CamLab, UK), typically for 30 cycles. Annealing temperatures used were 5°C lower than the lowest primers melting temperature (T_m) with an extension time of 1 min. per kb (no less than 30 sec.). Primers were designed using Primer3 software and synthesised by Eurogentec (U.K).

2.4.4. DNA Agarose Gel Electrophoresis

The DNA products of PCR and restriction enzyme digestions were analysed via agarose gel electrophoresis. 1.4 % and 0.7 % agarose gels (in TAE; 40 mM Tris acetate, 1 mM EDTA, pH 8.3) were used for small (< 1kb) and large DNA products, respectively. Addition of SYBR® safe (Invitrogen, UK; 10 µl/100 ml) to the gel allowed for visualisation of the DNA using a blue light transilluminator. Bromophenol blue loading dye (0.25% w/v bromophenol blue, 30 % glycerol v/v in dH_2O) was added to DNA to assist loading. A 1 kb or 100 bp DNA ladder (0.5

µg/lane, NEB, UK) was run alongside DNA products in order to determine size. Gels were run at ~70-90 V.

2.4.5. DNA Purification; Gel Extraction

DNA products required for cloning or sequencing could be excised from electrophoresis gels using a sharp scalpel and visualisation by blue light. Gel slices were placed into 1.5 ml eppendorf tubes and processed in accordance with the QIAquick® gel extraction kit (Qiagen, UK) protocol. Following gel extraction DNA concentration could be ascertained using a NanoDrop ND-1000 spectrophotometer (Thermo Scientific, DE, USA) or by running a small quantity on an electrophoresis gel.

2.4.6. DNA Sequencing

DNA sequencing was used to confirm the generation of new transgenic flies (see section 2.5.) and to characterise the nature of *Rab8* mutant alleles. Samples were submitted, in accordance with provided guidelines, for sequencing by the Technology Facility Sequencing Service (York, UK) using a 3130XL Genetic Analyzer (Invitrogen, UK).

2.4.7. Bacterial Transformation and Amplification of Plasmid DNA

In order to generate new transgenic *Drosophila* lines *E. coli* was used to amplify both the original cDNA containing pOT2 plasmid and the pUASt plasmid containing the appropriate inserts following sub-cloning.

Both XL-1 Blue supercompetent and XL-10 Gold ultracompetent *E. coli* cells (Stratagene, CA, USA) were used, depending upon the antibiotic resistance of the plasmid. Transformation was achieved via heat-shock in accordance with the manufacturers instructions. Both protocols were, however, modified and

scaled to use 50 µl of cells as opposed to the recommended 100 µl. Luria broth (LB; 10 g/l tryptone, 10 g/l NaCl, 5 g/l yeast extract) was also used instead of SOC or NYZ^{+} media. For transformation of plasmid from a ligation mix 1 µl of the ligation reaction was used, as recommended. For transformation of a plasmid from a Whatman® FTA® disc 50 µl of cells were added directly to the disc following TE washing (see section 2.5.1.). Post transformation cells were plated on LB agar plates (20 g/l agar in LB broth) containing the appropriate antibiotics for antibiotic selection, either chloramphenicol (12.5 µg/ml) or ampicillin (200 µg/ml), in accordance with the manufacturers instructions. Plates were incubated at 37°C overnight.

Individual colonies were harvested from plates using a sterile pipette tip and transferred into a sterile 15 ml falcon tube containing 5 ml sterile LB broth and the appropriate antibiotic. Cultures were incubated at 37°C overnight (12-16 h) with vigorous shaking. Stocks of transformed *E. coli* were stored long-term at -80°C by addition of 50 % v/v sterile glycerol. Glycerol stocks were used to streak fresh plates when required.

In order to check for the presence of an insert within transformed colonies, for example following a ligation during sub-cloning, plasmid DNA must first be purified by miniprep (see section 2.4.9.1.) and then the insert presence determined by restriction enzyme digestion (see section 2.4.10.) and gel electrophoresis (see section 2.4.4.). For minipreps 2 ml of each overnight culture was pelleted via centrifugation at 13000 g (2 min., RT), supernatant removed and frozen at - 20°C. In order to ascertain those colonies most likely to have taken up the insert prior to miniprep, reducing the number of minipreps required, colony cracking could be performed using 15 µl of the overnight culture (see below).

2.4.8. Colony Cracking

Colony cracking was used as a quick method of screening large numbers of clones for those that are most likely to have taken up the insert. It relies upon

cell lysis using alkaline conditions and identification of positive clones based on electrophoretic mobility variance between supercoiled DNA plasmids containing the insert and those that don't. Insert carrying plasmids move slower. Inserts as small as 200 bp can be detected.

20 µl of bromophenol blue loading dye was added to 1 ml of 5x cracking buffer (25 g sucrose, 5 ml 5 M NaOH, 2.5 ml 10% SDS, 40 ml ddH_2O). 5 µl of cracking buffer + bromophenol blue loading dye was added to 5 µl of resuspension buffer (50 mM Tris-HCL pH 8.0, 10 mM EDTA, 100 µg/ml RNaseA) and mixed with 15 µl of overnight culture. The mixture was then loaded and run on an electrophoresis gel (see section 2.4.4.) using uncut empty plasmid as the control, no ladder is required. Alternatively single colonies can be patched and used directly for cracking instead of 15 µl of overnight culture. Those colonies containing plasmids carrying the insert will show an electrophoretic mobility difference to the control plasmid. The plasmid from these was purified via miniprep (see below).

2.4.9. Plasmid Purification

2.4.9.1. MiniPrep Purification

The QIAprep spin miniprep kit (Qiagen, UK) was used to purify up to 20 µg of molecular biology grade plasmid DNA from *E. coli*. Frozen pellets produced by centrifugation of 2 ml of overnight cultures (see section 2.4.6.) were processed in accordance with the manufacturers instructions. Plasmid DNA purified via this method was used during sub-cloning of Rab8 from the pOT2 plasmid to the pUASt plasmid (see section 2.5.)

2.4.9.2. MidiPrep Purification

To provide greater yields and purity of plasmid DNA (up to 200 µg of transfection-grade plasmid DNA), for example for microinjection of *Drosophila* embryos, plasmids were purified using the QIAGEN HiSpeed Plasmid Midi Kit.

Having confirmed the presence of the appropriate insert via colony cracking, miniprep, restriction enzyme digestion and gel electrophoresis 100 µl of the appropriate overnight culture (see section 2.4.7.) was used to inoculate 100 ml of LB broth containing the appropriate antibiotic. Alternatively, for optimal results, a single colony could be picked from a freshly streaked plate, streaked from the appropriate glycerol stock, and used to inoculate a 5 ml starter culture of LB broth and the appropriate antibiotic. Starter cultures were incubated for 8 h at 37°C with vigorous shaking before being used to inoculate a 100 ml culture (100 µl in 100 ml). 100 ml cultures were incubated at 37°C overnight with vigorous shaking. Following incubation 100 ml cultures were centrifuged at 6000 rpm for 15 min. at 4°C, the supernatant removed and the pellet frozen. The frozen pellet was processed in accordance with the QIAGEN HiSpeed Plasmid Midi Kit instructions.

2.4.10. Restriction Endonuclease Digestion

Plasmids contain restriction sites, typically within multiple cloning sites, that are specifically recognised by restriction enzymes. This means that restriction enzymes can be used to specifically cleave plasmids, allowing for excision and insertion of DNA fragments during sub-cloning. This approach was used to excise Rab8, eGFP and NTAP from the donor plasmids and cleave the recipient pUASt plasmid for their insertion. Restriction enzymes were also used to cleave plasmid DNA from transformed clones in order to check for the presence of the plasmid by gel electrophoresis. Restriction enzymes EcoRI, XhoI and NotI (Fermentas, UK) were used at concentrations indicated by the supplier. The required restriction enzymes were added to the appropriate buffer (Fermentas, UK) and DNA with a total reaction volume of 20 µl. DNA was used at an appropriate concentration to give at least 20 ng of the smallest fragment, post digestion. Reactions were incubated at 37°C for at least 1 h followed by 80°C for 20 min. to inactivate enzymes. Restriction products were run on an electrophoretic gel (see section 2.4.4.) and, if required, purified (see section 2.4.5.).

2.4.11. DNA Ligation

Purified DNA fragments, previously treated with restriction endonucleases, were ligated together and into cleaved vector plasmids using T4 DNA ligase. Ligation reactions were typically a 3:1 (insert:vector (ng)) ratio, determined using the following formula: Insert mass (ng) = 3 x (insert length bp/vector length bp) x vector mass (ng). DNA concentration was ascertained using a NanoDrop ND-1000 spectrophotometer (Thermo Scientific, DE, USA). 0.2 µl of T4 ligase (Fermentas, UK) was mixed with 2 µl of T4 buffer (Fermentas, UK) and the DNA in a total reaction volume of 20 µl. Reactions were incubated at 16°C overnight followed by a 10 min. 65°C inactivation.

2.4.12. Drosophila Larval X-Gal Staining

X-Gal staining was used to confirm recombination (see section 2.1.7.) of the *Puc*-LacZ reporter construct onto the same chromosome arm as *Rab8*^{B229}. 3rd instar wandering larvae from each potential recombinant stock were dissected as in section 2.2.1. Dissected larvae were fixed in 1 % glutaraldehyde (1 % in PBS) for 15 min. at room temperature, with rocking. Preparations were then washed in PBS (3x 10 min. RT, with rocking). Pre-warmed (37°C) LacZ staining buffer (20 mM $K_3[Fe(CN)_6]$, 20 mM $K_4[Fe(CN)_6]$, 2 mM $MgCl_2$, 0.03% NP-40) was mixed with fresh X-gal (1 mg/ml, 195 mM X-Gal in DMF) and applied to larval preparations. Preparations were incubated at 37°C for at least 30 min. until colour developed. Preparations were washed with PBS to halt staining.

2.5. Generation of Transgenic *Drosophila* Lines

2.5.1. Generation of *Rab8* pUASt Constructs

During the course of this investigation UAS-*Rab8*, UAS-eGFP-*Rab8* and UAS-NTAP-*Rab8* transgenic *Drosophila* stocks were generated. UAS-*OCRL1*, UAS-

VCP^{Q1} and UAS-*VCP*^{Q2} stocks were also generated via this process but do not feature in this investigation and so are not covered directly.

The Whatman® FTA® disc containing the Rab8 cDNA clone, within a pOT2 plasmid vector, was identified and isolated from the BDGP Gold collection (clone: LD44762). In a 0.5 ml eppendorf microfuge tube 50 µl of sterile 1X TE (10 mM Tris-HCl, 0.1 mM EDTA, pH 8.0) was added to the disc, mixed and removed within 2 seconds. Washing with TE is essential to remove chemicals used in the generation of the disc that will inhibit subsequent transformations. Prolonged exposure of the disc to TE will result in elution and loss of cDNA from the disc. Immediately after TE washing the disc was transferred to a pre-chilled 14 ml BD Falcon polypropylene round-bottom tube a kept on ice. 50 µl of chemically competent Xl-1Blue supercompetent cells (Stratagene, CA, USA) were added directly to the disc allowing transformation and amplification of the *Rab8*-pOT2 plasmid as described in section 2.4.7. For *Rab8*-pOT2 antibiotic selection was performed using chloramphenicol at a concentration of 12.5 µg/ml. Following amplification of the *Rab8*-pOT2 plasmid purification was performed as described in section 2.4.9.1. For the generation of the UAS-Rab8 construct Rab8 was amplified via PCR (see section 2.4.3.) from the POT2-Rab8 vector, introducing an upstream EcoRI restriction site and maintaining a downstream XhoI site (forward primer (EcoRI); CCTACCGCGAATTCACACAAAATG and reverse primer; CGTTAGAACGCGGCTACAAT). The *Rab8* fragment was purified via gel extraction (see sections 2.4.4. and 2.4.5.) and ligated (see section 2.4.11.) into the pUASt vector, which had been cut with EcoRI and XhoI (see section 2.4.10.). For the generation of the eGFP tagged UAS-Rab8 construct the eGFP tag was amplified via PCR (see section 2.4.3.) from an existing vector in the Sweeney lab collection using primers to introduce NotI and EcoRI restriction sites (forward primer (NotI); GATCCACCGGGCGGCCGCATGGTGAGC and reverse primer (EcoRI); CTCTAGAGTCGCGGCCGCTTGAATTCACAGCTC). The pUASt vector was cut using NotI and XhoI and purified via gel electrophoresis and gel extraction (see sections 2.4.4. and 2.4.5.). A three way ligation was performed (see section 2.4.11.) in order to directionally clone the eGFP tag and the previously PCR amplified and purified Rab8 fragment (EcoRI,

XhoI) into the pUASt vector, maintaining the open reading frame and with eGFP tag at the N-terminus of Rab8. For the generation of the N-terminally TAP tagged (NTAP) UAS-Rab8 construct a pUASt vector containing the TAP tag (Kyriakakis et al., 2008) was cut using EcoRI and XhoI (see section 2.4.10.) prior to purification via gel electrophoresis and gel extraction (see sections 2.4.4. and 2.4.5.). Purified, PCR amplified Rab8 (EcoRI, XhoI), as used for the UAS-Rab8 and UAS-eGFP-Rab8 constructs, was ligated into the pUASt-NTAP vector (see section 2.4.11.) maintaining the open reading frame. Following ligation of both the pUASt-eGFP-Rab8 and pUASt-NTAP-Rab8 constructs individual ligation reactions were used to transform XL-10 Gold Ultracompetent cells (Stratagene, CA, USA) (see section 2.4.7.) which were plated onto LB-agar plates containing 200 µg/ml ampicillin and incubated at 37°C, overnight. Single colonies were then picked and amplified in 5 ml 8 hour cultures (see section 2.4.9.2.). The colonies most likely to contain the insert were ascertained via colony cracking (see section 2.4.8.). Those identified by colony cracking were purified via mini-prep (see section 2.4.8.1.) and the presence of the insert confirmed via restriction endonuclease assessment (see section 2.4.10.). Having confirmed the presence of the insert 100 µl of the original 8 hour culture for that colony was used to seed a 100 ml overnight culture (37°C with shaking). Cultures were centrifuged at 6000 rpm for 15 min. at 4°C and the pellet used to purify the plasmid using the Qiagen Midi/Maxi kit (see section 2.4.9.2.).

2.5.2. Micro-Injection of *Drosophila* Embryos

Large quantities of w^{1118} embryos were generated by allowing a high density of w^{1118} adults to lay on apple-juice agar plates (40 g/l sucrose, 16 g/l agar, 20 % (v/v) apple juice) within a large embryo collection cage. Plates were changed every 24 h, seeded with yeast paste to promote egg laying and flies left to acclimatise for 48 h prior to embryo collection.

Embryos must be injected during the syncytial stage and so plates were changed every hour. Embryos were collected within the hour by gently loosening them from the plate, using a wet paintbrush, and transferring them

onto a piece of filter paper. Embryo's were sandwiched between 2 microscope slides lined with non-toxic double sided tape separated by 2 lengths of 15 A copper fuse wire laying perpendicular between the slides. Copper wires prevent too much pressure being applied to the embryos. Separation of the slides dechorionates the embryos.

A 5 mm strip of double sided tape was placed perpendicularly across a fresh microscope slide and dechorionated embryos transferred quickly, but carefully, to line up along the tape with their posterior overhanging. This process must be completed within 7-10 min. at RT to prevent embryos drying out. Embryo's were then covered with non-toxic, 19S technical grade oxygen-permeable voltaleff oil to prevent desiccation.

24 h prior to micro-injection ~ 6 µg of the pUASt construct to be injected was co-precipitated in 1/10th volume of 3 M NaOAc + 2 volumes of 100 % ice cold EtOH with 5 µg of the pπΔ2-3 transposase plasmid (Misra and Rio, 1990). Co-precipitation was incubated at - 20°C overnight followed by centrifugation at 13000g for 30 min.. Pellets were rinsed in 100 % ice cold EtOH and air dried. Pellets were re-suspended in 5 µl of Spradlings buffer (5 mM KCl, 0.1 mM NaH_2PO4, pH 7.8) (Rubin and Spradling, 1982; Spradling and Rubin, 1982). 2 µl of the suspension was loaded into a fine pulled glass needle which was loaded onto the micro-injection apparatus. After breaking the end of the needle to leave a sharp tip the slide of aligned embryos was placed on the apparatus with the posterior end facing the needle. Embryos were injected into the posterior end in order to target the posterior pole cells, which are progenitors to the gonads. The slide containing injected embryos was placed upon an apple-juice agar plate seeded with yeast paste in a box lined with damp tissue and left at 18°C.

2.5.3. Post-Microinjection Embryo Care

Larvae hatching from microinjected embryos were collected and transferred into vials of *Drosophila* medium. Virgin female and male micro-injected flies were collected post-eclosion and crossed to w^{1118} flies. As microinjection targets the

germ line those flies successfully transformed can be ascertained in the offspring (F^1). As the pUASt plasmid carries a mini-white gene the F1 offspring of successful transformants display a pigmented eye phenotype. Those displaying a pigmented eye were collected and crossed, individually, to w^{1118} flies in order to amplify numbers and generate a stock. The chromosome into which the plasmid had inserted was then determined (see below)

2.5.4. Identifying the Chromosome of Plasmid Insertion

Virgin females were isolated from the stocks generated via microinjection (see above) and crossed to w^- balancer chromosomes males for the second (CyO/Sco) or third (Tm6b/Tm3) chromosomes. If all male F1 progeny display pigmented eyes the insert must be on the first chromosome. If not on first offspring will display a mixture of un-pigmented and pigmented eyes. F1 offspring with pigmented eyes and carrying the appropriate balancer were collected and crossed, sibling to sibling, to each other. If the insertion site is on the same chromosome as the balancer all F2 offspring shall display a pigmented eye. If un-pigmented eyes are visible in the F2 generation the insert is not on that chromosome. The balancer prevents loss through homologous recombination.

2.6. Statistical Analysis

All statistical analysis was performed using JMP®7 (SAS Institute) statistical software. Unless otherwise stated the statistical tests performed were analysis of variance (ANOVA) with a post-hoc Dunnett's test to ascertain significance between individual genotypes and the wildtype control and post-hoc student t-tests to ascertain significance between individual genotypes. Error bars represent the standard error of mean (± SEM).

2.7. Bioinformatics and Computational Analysis

During the course of this investigation the following software and online resources were used. Unless otherwise stated default settings, assumptions and parameters were used.

For predicting the effect of amino acid substitutions upon protein structure and function:

- **PROVEAN** (**Pro**tein **V**ariation **E**ffect **An**alyzer) Protein v1.1.3. (http://provean.jcvi.org)

- **PolyPhen-2** (**Poly**morphism **Phen**otyping) v2.2.2. (http://genetics.bwh.harvard.edu/pph2)

- **ProSMS** (http://babel.ucmp.umu.se/prosms)

For Sequence Alignment:

- **ClustalX** v2.0.

For Image Processing:

- **Zen 2009 Lite Edition** v5.5. (Carl Zeiss Microimaging GmbH).
- **AxioVision** v4.8. (Carl Zeiss Microimaging GmbH).
- **AnalySIS** v2.18.
- **Virtual Dub** v1.5.10. (Avery Lee)
- **ImageJ** v1.46.
  Plugins:
  NeuronJ v1.4.2: plugin for facilitating the tracing and quantification of elongated image structures

  Straighten: plugin facilitating the straightening of filamentous particles, or any curved objects in an image

  Median: plugin used during larval locomotion assay

ThreshTrack: plugin used during larval locomotion assay

For Primer Design:

- **Primer 3** (http://www.bioinformatics.nl/cgi-bin/primer3plus/primer3plus.cgi)

DNA Chromatogram Viewer:

- **MacSequence View** v1.0. (GoToes)

3. Identification of Novel Modifiers of *CHMP2B*^{Intron5} Toxicity, Including the Dominant Enhancer *Rab8*

3.1 Introduction

Frontotemporal dementia (FTD) is the second most prevalent form of early-onset dementia, after Alzheimer's disease, displaying a mean age of onset between 46 and 65 (Ratnavalli et al., 2002; Snowden et al., 2002). It has been shown to present a strong genetic association with up to 50% of cases showing a positive familial history and 7 distinct gene loci implicated in disease pathology, to date (see section 1.2.4.) (Chow et al., 1999b; Rosso et al., 2003b). One of these genes is *CHMP2B*. *CHMP2B* has been identified as encoding a core component of ESCRT-III, one of 4 ESCRT complexes, 0-III, that act in numerically sequential order in the biogenesis of MVB's (Carlton, 2010; Skibinski et al., 2005; Stuffers et al., 2009; Wollert et al., 2009b). MVB's act as a nexus during both endosomal-lysosomal and autophagic degradative pathways, which are essential for homeostatic regulation within cells (Filimonenko et al., 2007a; Gruenberg and Stenmark, 2004a; Piper and Katzmann, 2007a; Wollert and Hurley, 2010). Perturbation to these trafficking pathways has been associated with a range of human pathologies including mucolipidosis, Danon disease, Antiphospholipid syndrome, Niemann Pick, Oculocerebrorenal syndrome of Lowe and FTD, to name a few (Coon et al., 2012; Huang et al., 2005; Kobayashi et al., 1998; Nishino et al., 2000; Skibinski et al., 2005; Vergarajauregui et al., 2008; Vergarajauregui and Puertollano, 2008). However, despite this, the molecular mechanism underlying these biological processes and their associated diseases remain to be fully elucidated. As such this study looks to identify novel factors implicated in frontotemporal dementia pathology, associated with CHMP2B dysfunction, and identify their roles within normal endosomal-lysosomal and autophagic processes.

In this chapter the *Drosophila* eye is utilised as a model system in which to identify novel modifiers of the FTD mutation *CHMP2B*^{Intron5}. Expression of *CHMP2B*^{Intron5} in the eye induced a clear phenotype, against which it is possible to screen for dominant modifiers of *CHMP2B*^{Intron5} toxicity. Using this approach we identified the small GTPase *Rab8* as a potent enhancer of *CHMP2B*^{Intron5} toxicity, along with the Rab8 effector protein OCRL1. It was also demonstrated that a number of CHMP2B interacting proteins implicated in JNK signalling act as potent modifiers of CHMP2B. As such this chapter provides a framework for the rest of this investigation, elucidating novel factors and their associated pathways as specific targets for further investigation. In this way we hope to identify novel factors implicated in FTD and elucidate the molecular mechanisms behind disease pathology.

3.2 Results

3.2.1 *Rab8* Mutants Dominantly Enhance *Shrub*-GFP Toxicity

Previous investigation has demonstrated that the *CHMP2B*^{Intron5} mutation results in a failure of CHMP2B to dissociate from the ESCRT-III complex (Han et al., 2012; Lee et al., 2007). Furthermore the toxic effects of *CHMP2B*^{Intron5}, leading to neurodegeneration and the accumulation of autophagosomes, have been associated with the formation of an abnormally avid complex between CHMP2B and mSnf7-2/Shrub, another ESCRT-III component that fails to dissociate from the complex (Han et al., 2012; Lee et al., 2007). In a study by Han et al. (2012) it was also demonstrated that the *CHMP2B* missense mutation *CHMP2B*^{T104N}, which occurs in the conserved Snf7 binding domain, results in a more avid association of CHMP2B with Snf7 and a reduced ability to associate with the ATPase Vps4 (Han et al., 2012). This supports previous findings suggesting that Vps4 is essential for dissociation of ESCRT-III components from the complex (Bodon et al., 2011a; Urwin et al., 2010a). It has also been demonstrated that the *CHMP2B*^{Intron5} mutation elicits an accumulation of Shrub in ubiquitin-positive late endosomes whilst depletion of shrub can also induce neurodegeneration (Lee et al., 2007). Work in the Sweeney lab, in collaboration with the Gao lab (UMASS, Worcester, USA), has identified that a Shrub-GFP

fusion protein acts as a dominant negative, antimorphic form of Shrub. In addition it has been demonstrated that when expressed in the fly eye *Shrub*-GFP phenocopies the degenerative phenotype associated with expression of *CHMP2B*^{Intron5} in the eye. As such one may postulate that the GFP tag on Shrub may act to perturb normal Vps4 mediated dissociation of the ESCRT-III complex, leading to pathology. Therefore, having observed pathology to associate with perturbation to normal Shrub-CHMP2B interaction dynamics and having demonstrated *Shrub*-GFP to phenocopy *CHMP2B*^{Intron5} initial modifier screens were performed against *Shrub*-GFP. These initial screens were performed by Sean Sweeney in collaboration with Fen Biao-Gao and Yubing Lu (UMASS, Worcester, USA) using 257 deletion stocks, representing ~ 75 % of the *Drosophila* genome, from the DrosDel collection (University of Cambridge, Cambridge, U.K) (Ryder et al., 2007). This initial screen identified 29 potential modifiers of the Shrub-GFP phenotype, including *Rab8 (*personal communication, Fen Biao-Gao and Yubing Lu, UMASS, Worcester, USA). Currently 2 of these potential modifiers, serpin 5 and syntaxin 12/13, have been investigated further and confirmed as modifiers of both *Shrub*-GFP and *CHMP2B*^{Intron5} toxicity (Ahmad et al., 2009). Here we look to do the same with *Rab8*.

Having identified *Rab8* as a potential modifier of *Shrub*-GFP toxicity, *Rab8* mutants were confirmed as potent enhancers of the *Shrub*-GFP phenotype. Here an allelic series of 5 *Rab8* mutants, a *Rab8* deficiency and 2 independent *Rab8*-RNAi lines were all shown to dominantly potentiate *Shrub*-GFP toxicity (Fig. 3.1. A&B). Each demonstrated a clear increase in the number of melanised spots present on the eye's surface, when compared to melanisation caused by *Shrub*-GFP alone (Fig. 3.1.A). Quantification of this phenotype reveals that 14.6 % of GMR-Gal4, *Shrub*-GFP/+ flies present with a "low" phenotype classification, with less than 15 melanised spots visible on the eye within 3 days of eclosion, whilst the remaining 85.4 % display a medium phenotype (more than 15 melanised spots but less than 50 % of the eye affected) (Fig. 3.1.B). In contrast expression of Rab8-RNAi, heterozygous mutants and a deficiency covering the Rab8 locus in a GMR-Gal4, *Shrub*-GFP/+ background resulted in a complete loss of any flies displaying a "low"

phenotype. Furthermore many of these genotypes potentiated toxicity sufficiently to display a “high” phenotype with > 50 % of the eye affected by melanisation (Fig. 3.1.B). Additionally it was also demonstrated that overexpression of *Rab8* was sufficient to partially rescue *Shrub*-GFP toxicity, with GMR-Gal4,*Shrub*-GFP/UAS-*Rab8* showing 35 % of flies to present with a low phenotype classification, with the remaining 65 % classified as “medium”. In the absence of *Shrub*-GFP no *Rab8* allele, when heterozygous in the presence of the GMR-Gal4 driver, induced an eye phenotype showing any variance from a wildtype eye (n = 100 per genotype). This indicates that *Rab8* mutants act purely as enhancers of Shrub-GFP toxicity.

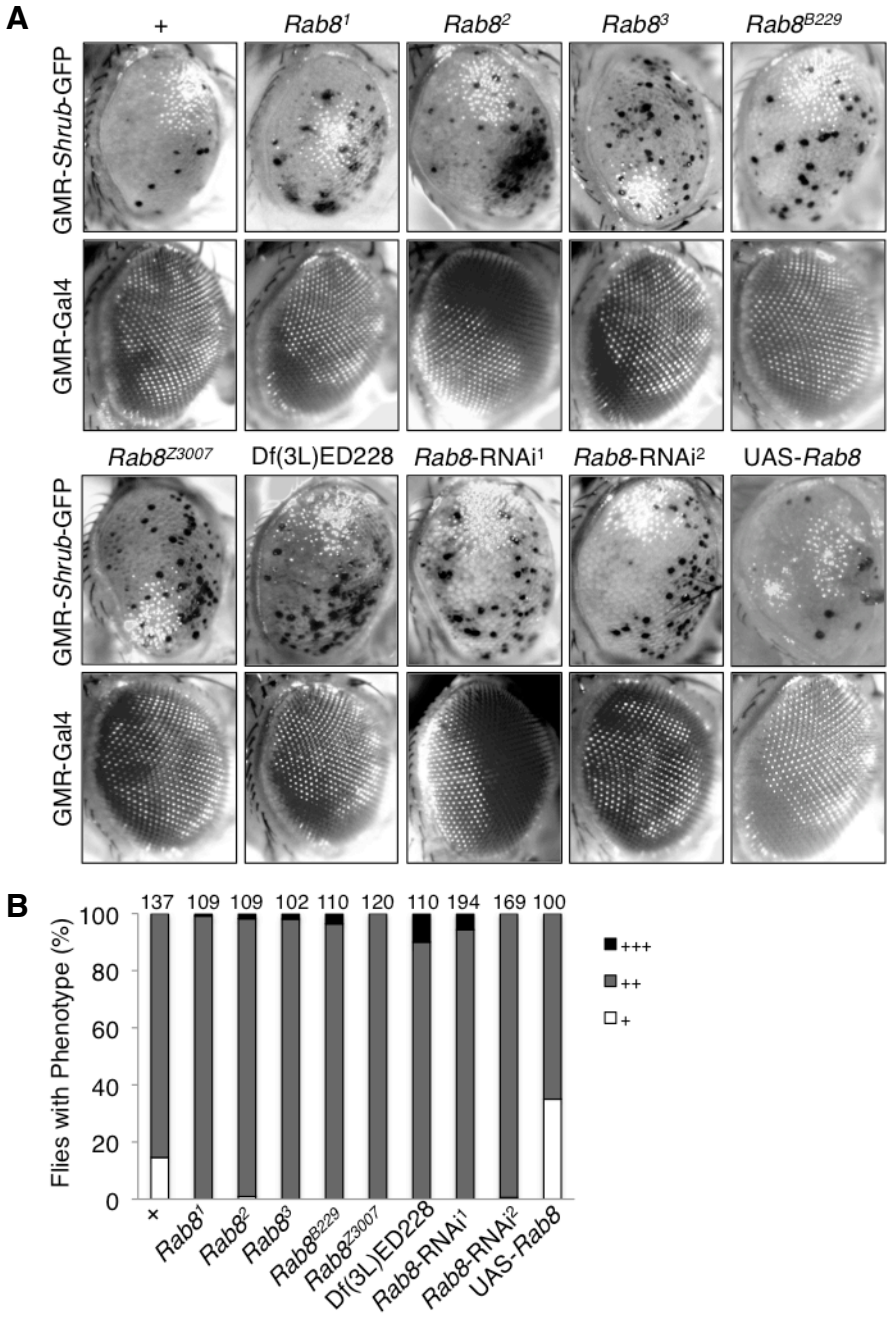

Figure 3.1. *Rab8* Mutants Dominantly Enhance *Shrub*-GFP Toxicity in the *Drosophila* eye
(**A**) Expression of *Shrub*-GFP in the fly eye, under the control of the eye specific driver GMR-Gal4, induces a distinct phenotype characterized by the presence of melanised spots across the eye's surface. Expression of *Rab8* mutants, a *Rab8* deficiency (Df(3L)ED228) and *Rab8*-RNAi's in a GMR-Gal4, UAS-*Shrub*-GFP background all potentiate Shrub-GFP toxicity, displaying an increase in melanisation. Overexpression of wildtype *Rab8* alleviates toxicity. (**B**) This phenotype is quantified as; white = low (+) phenotype (< 15 spots of melanisation), Grey = medium (++) phenotype (> 15 spots of melanisation but < 50 % of the eye affected), black = high (+++) phenotype (> 50 % of the eye affected by melanisation). No allele induced a perturbation to the wildtype eye phenotype in a GMR-Gal4 background, in the absence of $CHMP2B^{Intron5}$ (n = 100 per genotype).

3.2.2 *Rab8* Mutants Dominantly Enhance *CHMP2B*^{Intron5} Toxicity

Having confirmed *Rab8* as a dominant enhancer of toxicity associated with *Shrub*-GFP, a second modifier screen was performed in order to identify dominant enhancers and suppressors of the *CHMP2B*^{Intron5} phenotype. Part of this screen included a collection of 38 deletions covering most of the 3rd arm of chromosome 3 (Fig. 3.2.A). From these 38 deletions 3 were identified as extremely potent enhancers of *CHMP2B*^{Intron5} toxicity with over 50 % of flies displaying a "high" phenotype classification. One of the 3 most potent enhancer deletion regions was identified as Df(3L)ED228, a 701102bp deletion covering the cytological region between 76A1 and 76D2. Within this region there are 89 gene loci, including *Rab8* (Fig. 3.2.B).

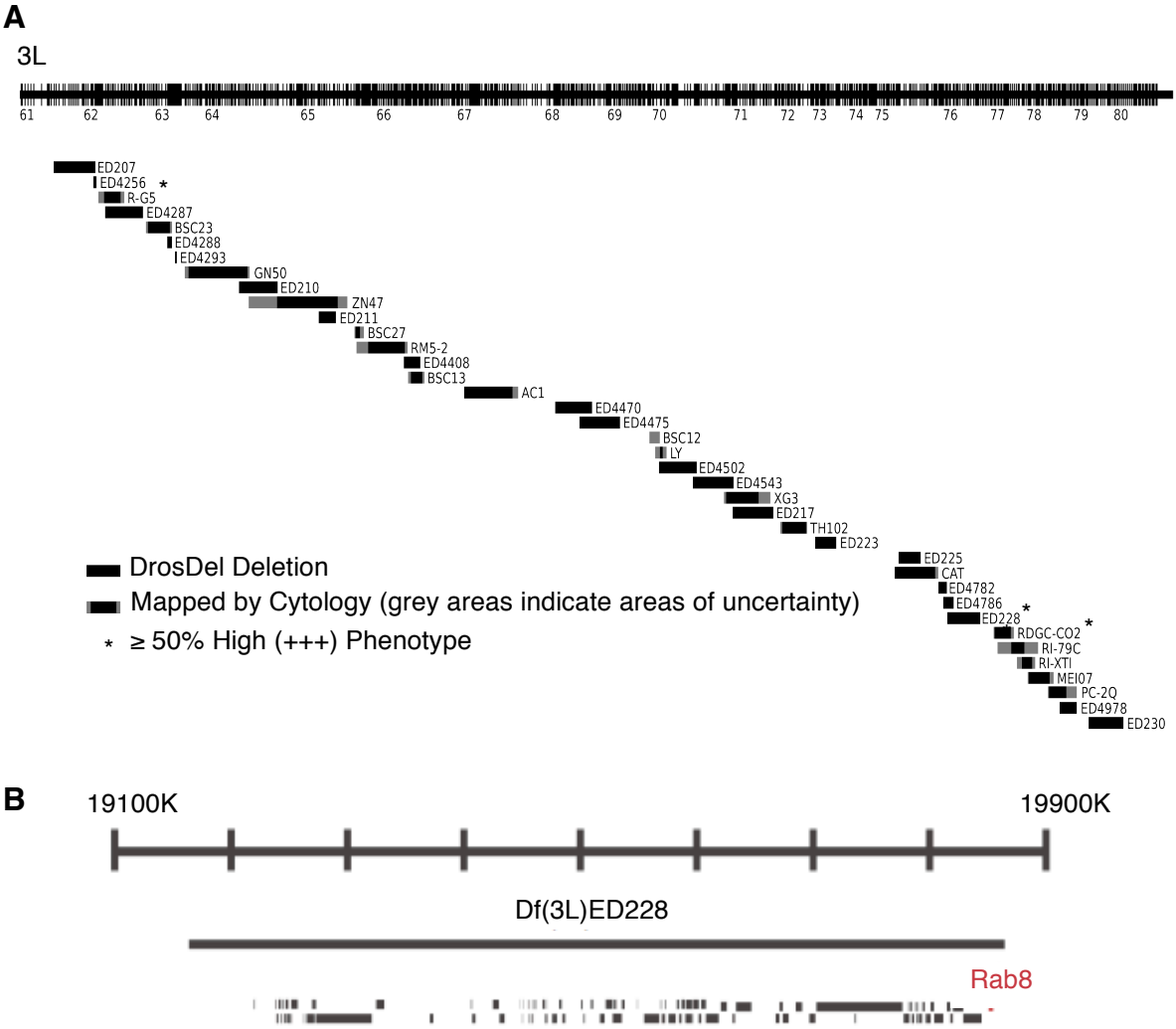

Figure 3.2. Deletion Coverage Map of Chromosome 3L
(**A**) Deletion coverage map of the left arm of chromosome 3 displaying those deletions that show the greatest enhancement of the *CHMP2B*^{Intron5} phenotype, with more than 50 % of flies presenting a "high" (more than 50 % of the eye covered by melanisation, +++) phenotype classification. (**B**) One of the 3 most potent enhancers of *CHMP2B*^{Intron5} toxicity is Df(3L)ED228 a 701102bp deletion covering 87 gene loci, including *Rab8*.

Having substantiated the role of *Rab8* as a dominant enhancer of *Shrub*-GFP and identified the deficiency region containing the *Rab8* gene loci as a potent enhancer of *CHMP2B*^{Intron5} toxicity investigation looked to determine whether *Rab8* acted as a dominant enhancer of *CHMP2B*. Here it is demonstrated that, as for *Shrub*-GFP, *Rab8* mutants dominantly enhance toxicity associated with the FTD causing *CHMP2B*^{Intron5} mutation (Fig. 3.3.A-B). Expression of *CHMP2B*^{Intron5} in the *Drosophila* eye, under the control of the eye specific GMR-Gal4 driver, induced a “medium” eye phenotype in 99.2 % of flies, with just 0.8 % presenting with a “high” phenotype classification (Fig. 3.3.B). Expression of the *Rab8*-RNAi, mutant and deficiency alleles in a GMR-Gal4, UAS-*CHMP2B*^{Intron5}/+ background potentiated toxicity with a notable increase in melanisation observed (Fig. 3.3.A). Quantification substantiated the role of *Rab8* alleles as enhancers of toxicity, inducing a high phenotype in 1 % (*Rab8*^{B229}) to 16.8 % (*Rab8*^{1}) of flies screened (Fig. 3.3.B). No low phenotype flies were observed in any genotype. In contrast overexpression of wildtype *Rab8* in a GMR-Gal4, UAS-*CHMP2B*^{Intron5}/+ background displayed a notable decrease in the melanisation phenotype observed (Fig. 3.3.A), with quantification revealing a “medium” phenotype in 100 % of flies screened (Fig. 3.3.B). This suggests that Rab8 may reduce *CHMP2B*^{Intron5} toxicity.

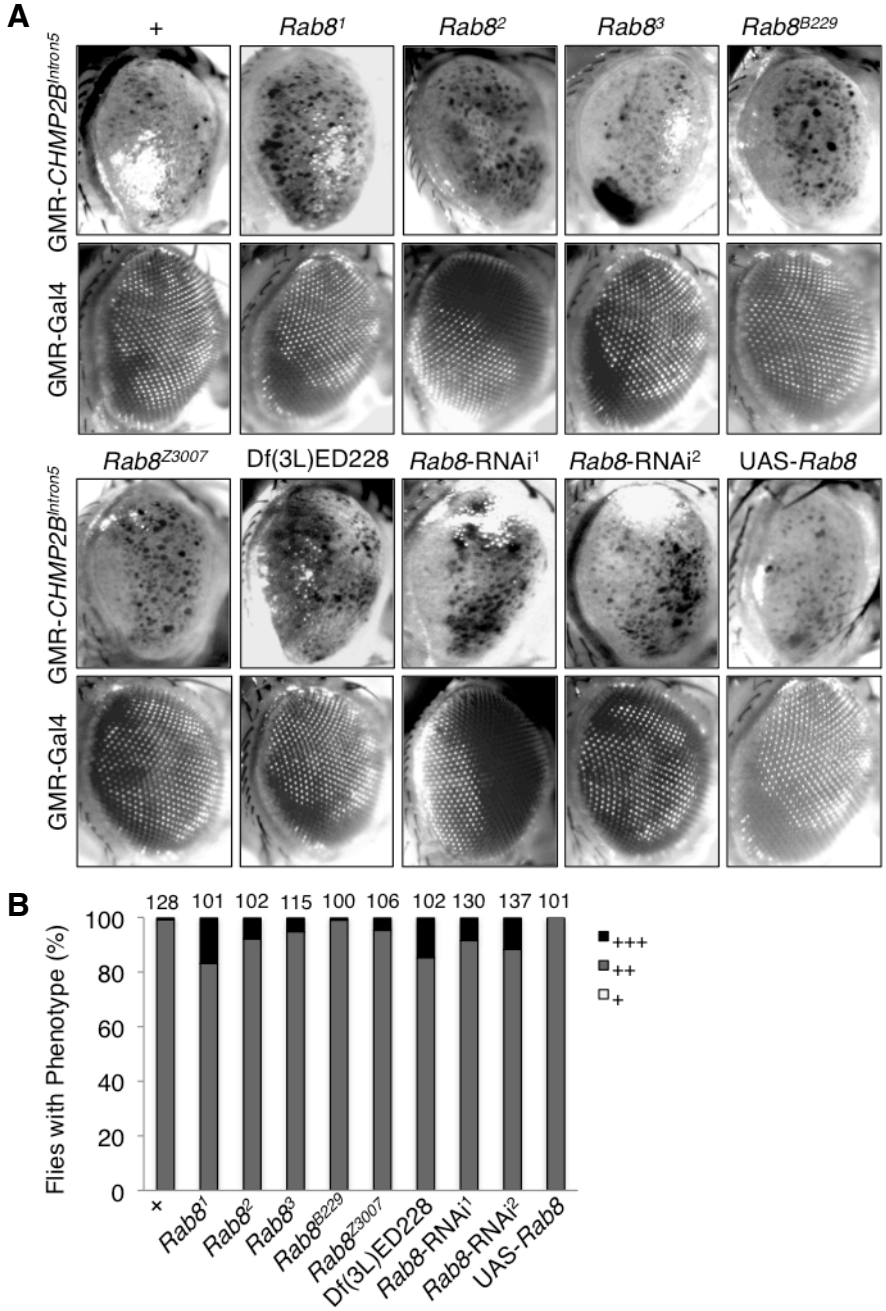

Figure 3.3. *Rab8* Mutants Dominantly Enhance *CHMP2B*^{Intron5} Toxicity in the *Drosophila* eye

(**A**) Expression of *CHMP2B*^{Intron5} in the fly eye, under the control of the eye specific driver GMR-Gal4, induces a distinct phenotype characterized by the presence of melanised spots. Expression of *Rab8* mutants, a *Rab8* deficiency (Df(3L)ED228) and *Rab8*-RNAi's in a GMR-Gal4, UAS-*CHMP2B*^{Intron5} background all potentiate toxicity, displaying an increase in melanisation. Overexpression of wildtype *Rab8* reduces toxicity. (**B**) This phenotype is quantified as; white = low (+) phenotype (< 15 spots of melanisation), Grey = medium (++) phenotype (> 15 spots of melanisation but < 50 % of the eye affected), black = high (+++) phenotype (> 50% of the eye affected by melanisation). No allele induced a perturbation to the wildtype eye phenotype in a GMR-Gal4 background, in the absence of *CHMP2B*^{Intron5} (n = 100 per genotype).

3.2.3 The *Rab8* Effector *OCRL* Dominantly Enhances *CHMP2B*^{Intron5} Toxicity

OCRL1 is an inositol 5-phosphatase encoded by the *OCRL* gene that has been associated with endosomal trafficking, cytokinesis and ciliogenesis (Ben El Kadhi et al., 2012; Coon et al., 2012). It has also been implicated in Rab8 and sesquipedalian/27 KDa inositol polyphosphate phosphatase-interacting protein (Ses/IPIP27) dependent trafficking through interaction with Rab8 (Coon et al., 2012; Noakes et al., 2011). Furthermore mutations in the OCRL1 Rab8 binding domain have been associated with Lowe syndrome, a neurodegenerative disorder (Coon et al., 2012). As such the interacting functions of Rab8 and OCRL1, particularly within endosomal trafficking events within neurons, are of significant interest. Here it is demonstrated that, like it's binding partner *Rab8*, *OCRL1* acts as a dominant enhancer of *CHMP2B*^{Intron5} toxicity. Previous work in the Sweeney lab has isolated a series of *OCRL1* mutant alleles, including *OCRL1*^{C52} and *OCRL1*^{D40}*.* These mutants were generated by imprecise P-element excision of the EPgy2 P-element within the 5' UTR of the P{EPgy2}*OCRL1*^{EY15890} stock. Subsequent analysis in both the Sweeney and Rodal (personal communication Avital Rodal, Brandeis University, MA, USA) labs has demonstrated both mutants to be loss of function mutants associated with deletions covering the OCRL1 start codon. Both *OCRL1* mutants *OCRL1*^{C52} and *OCRL1*^{D40} show a clear potentiation of toxicity when in a *CHMP2B*^{Intron5} background, displaying a clear increase in melanisation observed across the fly eye (Fig. 3.4.A). Quantification reveals 18.75 % and 60.6 % of flies to display a "high" phenotype in *OCRL1*^{C52} and *OCRL1*^{D40} flies, expressed in a GMR-Gal4, UAS-CHMP2B^{intron5}/+ background, respectively (Fig. 3.4.B). The remaining flies presented with a "medium" phenotype. In contrast 100 % of GMR-Gal4, UAS-CHMP2B^{intron5}/+ flies displayed a "medium" phenotype. *OCRL1*^{C52} and *OCRL1*^{D40} mutations alongside the GMR-Gal4 driver alone, in the absence of UAS-*CHMP2B*^{intron5}, induced no perturbation to a normal eye phenotype (n = 100 per genotype), indicating *OCRL1* is acting as a dominant enhancer of *CHMP2B*.

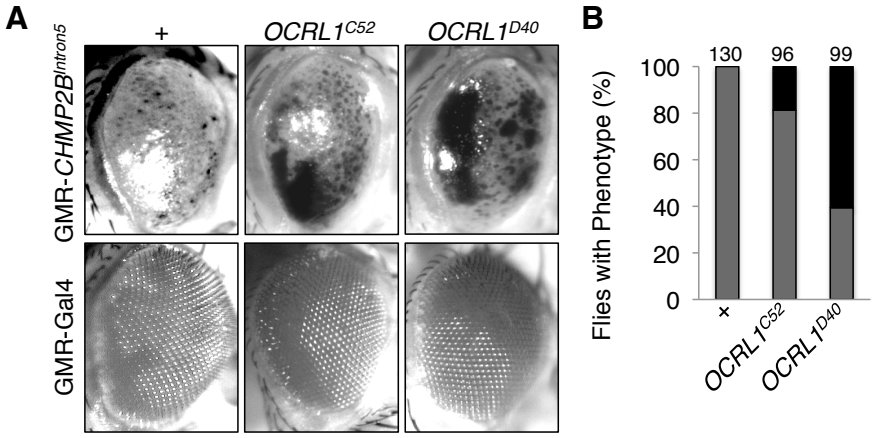

Figure 3.4. *OCRL1* Mutants Dominantly Enhance *CHMP2B*^{Intron5} Toxicity in the *Drosophila* eye
(**A**) *OCRL1* mutants *OCRL1*^{C52} and *OCRL1*^{D40} induce a notable potentiation of melanisation to the *Drosophila* eye when expressed in a GMR-Gal4,UAS-*CHMP2B*^{Intron5} background without perturbing the eye in their own right. (**B**) Expression of OCRL1 mutants in a GMR-Gal4,UAS-*CHMP2B*^{Intron5} background shows a significant increase in the proportion of flies presenting with a high phenotype. White = low (+) phenotype (< 15 spots of melanisation), Grey = medium (++) phenotype (> 15 spots of melanisation but < 50 % of the eye affected), black = high (+++) phenotype (> 50 % of the eye affected by melanisation). No allele induced a perturbation to the wildtype eye phenotype in a GMR-Gal4 background, in the absence of *CHMP2B*^{Intron5} (n = 100 per genotype).

3.2.4 ESCRT-III Interacting Proteins Involved in Innate Immunity and JNK Signalling Dominantly Enhance *CHMP2B*^{Intron5} Toxicity

In order to further elucidate potential pathways involved in *CHMP2B*^{Intron5} toxicity targeted modifier screens were performed looking at ESCRT-III interacting proteins and their associated pathways. Here it is demonstrated that ALG-2-Interacting Protein X (AliX) acts as a potent enhancer of *CHMP2B*. ALIX has been shown to interact with both ESCRT-I and ESCRT-III, via TSG101/Vps23 and Shrub/Snf7 respectively (Fisher et al., 2007; Kim et al., 2005b; Strack et al., 2003). It has also previously been implicated in MVB formation with AliX siRNA perturbing normal membrane remodelling events at the late endosome, most likely due to an inability to recruit the ESCRT machinery (Matsuo et al., 2004). AliX has also been shown to interact with lysobisphosphatidic acid (LBPA), which has been implicated in MVB biogenesis and has been demonstrated to be capable of inducing spontaneous formation of intraluminal vesicles within liposomes, *in vitro*, in the absence of any other proteins (Chevallier et al., 2008; Matsuo et al., 2004). ALIX siRNA also reduces cellular LBPA (Matsuo et al.,

2004). Expression of UAS-*Alix* in a GMR-Gal4, UAS-*CHMP2B*^{Intron5} background induces a high phenotype in 100 % of flies screened (Fig. 3.5.A-B). Flies also present with small, irregular eyes. In contrast inhibition of *AliX* via expression of an *AliX*-RNAi or an *AliX* mutant (*AliX*^{EY10362}) in the *CHMP2B*^{Intron5} background does not alleviate toxicity, instead a mild potentiation is observed. Thus any perturbation to *AliX* appears to enhance *CHMP2B*^{Intron5} toxicity, although overexpression acts as the most potent enhancer. No heterozygous *AliX* alleles affected the *Drosophila* eye in a GMR-Gal4 background, in the absence of *CHMP2B*^{Intron5} (n=100 per genotype), indicating the eye phenotype to result from a potentiation of *CHMP2B*^{Intron5} toxicity.

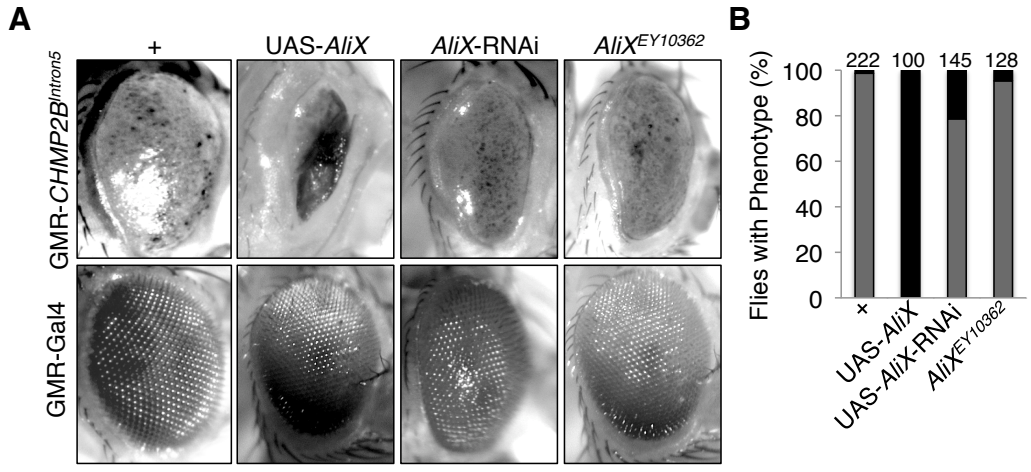

Figure 3.5. Overexpression of the CHMP2B Interacting Protein AliX Potentiates *CHMP2B*^{Intron5} Toxicity in the *Drosophila* eye
(**A**) Overexpression of UAS-AliX in a GMR-Gal4, UAS-*CHMP2B*^{Intron5} background induced a potent potentiation of *CHMP2B*^{Intron5} toxicity, displaying a clear increase in melanisation coupled with a shrunken eye phenotype. Expression of *AliX*-RNAi or the *AliX*^{EY10362} mutant mildly potentiated toxicity. None of the alleles perturbed the normal wildtype eye phenotype when expressed in a GMR-Gal4 background, in the absence of *CHMP2B*^{Intron5} (n = 100 per genotype). (**B**) Quantification of the eye phenotypes reveals a high phenotype classification in 100 % of GMR-Gal4, UAS-*CHMP2B*^{Intron5}/UAS-*AliX* flies with a lower high phenotype penetrance in RNAi and mutants. White = low (+) phenotype (< 15 spots of melanisation), Grey = medium (++) phenotype (> 15 spots of melanisation but < 50 % of the eye affected), black = high (+++) phenotype (> 50 % of the eye affected by melanisation).

Having identified such a potent enhancement of *CHMP2B*^{Intron5} toxicity through expression of UAS-*AliX* it was asked whether specific AliX interacting proteins had a role in the potentiation of *CHMP2B*^{Intron5} toxicity. As it's name suggest AliX interacts with Apoptosis-Linked Gene 2 (ALG2), which has also been shown to interact directly with ESCRT-I component TSG101, in a calcium dependent

manner (Mahul-Mellier et al., 2006; Okumura et al., 2009). In fact it has also been demonstrated that ALG2 has a calcium dependent role in the AliX-TSG101 interaction (Okumura et al., 2009). Furthermore, research has shown that ALG2 and AliX complex with Plenty of SH3's (POSH), a multi-domain JNK scaffold, in a calcium dependent manner (Tsuda et al., 2006). POSH in turn has been implicated as a functional component of regulated neuronal death in response to withdrawal of trophic factors and as a regulator of JNK signalling (Bruckner et al., 2001; Tsuda et al., 2006). Here it is demonstrated that disruption to normal ALG2 or POSH levels have a detrimental effect in the *Drosophila* eye, potentiating toxicity associated with the *CHMP2B*^{Intron5} mutation (Fig. 3.6.A-B). Whilst GMR-Gal4 induced expression of UAS-*ALG2* showed no variance from wildtype (100 % wildtype eye phenotype, n = 100) UAS-*ALG2* expression in a GMR-Gal4, UAS-*CHMP2B*^{Intron5} background induced a dominant enhancement of toxicity with 27.77 % of flies presenting with a high eye phenotype and the rest a medium phenotype (Fig. 3.6.B). This contrast with just 1.35 % high and 98.65 % medium phenotype in GMR-Gal4, UAS-*CHMP2B*^{Intron5}/+ flies (Fig. 3.6.B). Similarly overexpression of *POSH* also potentiated *CHMP2B*^{Intron5} toxicity with 17.65 % of flies presenting with a high phenotype (Fig. 3.6.B). GMR-Gal4 expression of UAS-*POSH* in the absence of *CHMP2B*^{Intron5} elicited a very mild rough eye phenotype in 100 % of flies (n = 100) (Fig. 3.6.A). Interestingly it was also observed that inhibition of POSH also actively enhanced *CHMP2B*^{Intron5} toxicity. For example UAS-*POSH*^{mring}, in which the putative zinc ring finger domain involved in E3 ubiquitin ligase activity was mutated, the *POSH* null *POSH*^{74} and *POSH* mutant expression all potentiated toxicity. Furthermore enhancement was, with the exception of the *POSH*^{EP2248} mutant, greater than that seen through overexpression of *POSH*. *POSH*^{EP1206} mutants in a GMR-Gal4 background, in the absence of *CHMP2B*^{Intron5}, show a mild rough eye phenotype in all flies screened (n = 100), all other mutants showed no variance from wildtype (n = 100 per genotype). The observation that both overexpression of UAS-*POSH* and the presence of the *POSH*^{EP1206} allele in a GMR-Gal4 background induced a rough eye phenotype can be explained by the nature of the *POSH*^{EP1206} mutant. *POSH*^{EP1206} is associated with an insertion of a P{EP} transposable element upstream of POSH, leading to an inhibition of *POSH* via insertional mutagenesis. However P{EP} elements also carry a UAS

sequence meaning that in the presence of a Gal4 promoter, such as the GMR-Gal4 used here, they can be used to induce regulated expression of the genes proximal to the insertion. In this case *POSH*^{EP1206} promotes expression of *POSH* giving a rough eye similar to that observed by *POSH* overexpression (Fig. 3.6A). *POSH*^{EP2248} which is also a P{EP} element is in the wrong orientation, in the minus orientation, to induce expression of POSH and so acts as a insertional mutagen.

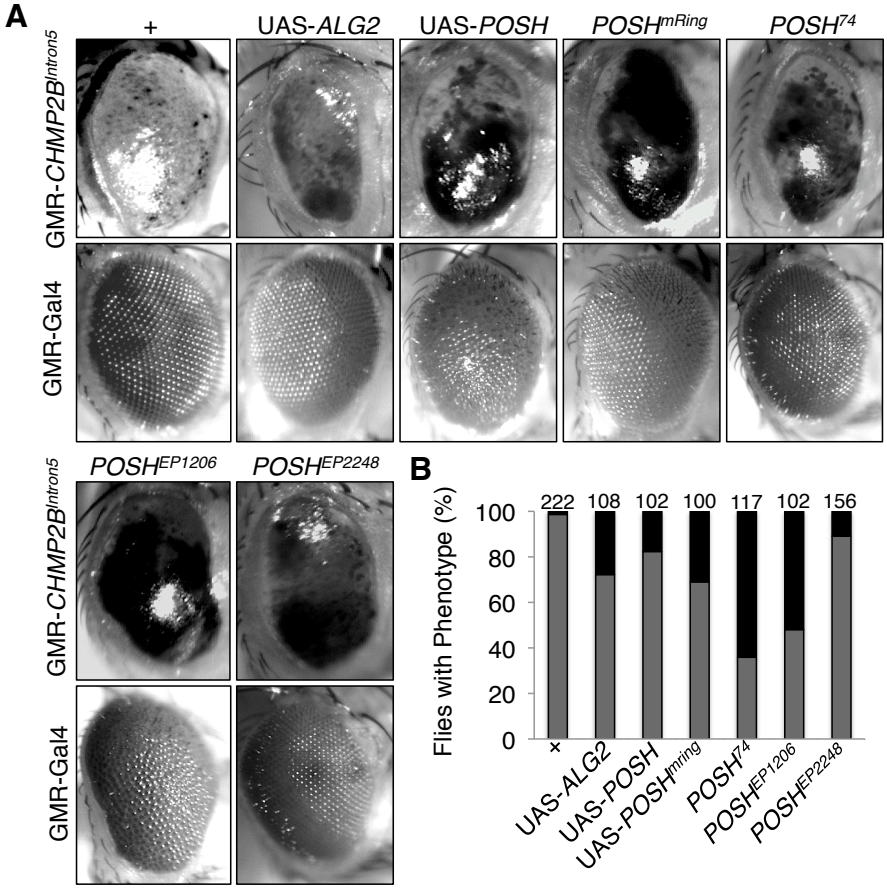

Figure 3.6. Perturbation to *ALG2* and *POSH* Potentiate *CHMP2B*^{Intron5} Toxicity in the *Drosophila* eye

(**A**) Overexpression of both *ALG2* and *POSH* or inhibition of *POSH* using UAS-*POSH*^{mring}, which has a mutated ring domain, a *POSH* null *POSH*^{74} or *POSH* mutants *POSH*^{EP1206} and *POSH*^{EP2248} all act to potentiate *CHMP2B*^{Intron5} toxicity. UAS-*POSH* and *POSH*^{EP1206} both mildly perturb the wildtype eye phenotype in a GMR-Gal4 background, in the absence of *CHMP2B*^{Intron5}, no other allele does (n = 100 per genotype). (**B**) Quantification reveals an increased penetrance of flies classified as presenting a high phenotype as a result of perturbation to POSH and ALG2 in a GMR-Gal4, UAS-*CHMP2B*^{Intron5} background with the greatest enhancement elicited by the *POSH* null, *POSH*^{74}. White = low (+) phenotype (< 15 spots of melanisation), Grey = medium (++) phenotype (> 15 spots of melanisation but < 50 % of the eye affected), black = high (+++) phenotype (> 50 % of the eye affected by melanisation).

Interestingly POSH has also been implicated in the targeted regulation of another essential ESCRT component Hepatocyte growth factor-regulated tyrosine kinase substrate (HRS/HGS), through its E3 ubiquitin ligase activity (Kim et al., 2006). Depletion of HRS has been shown to induce accumulation of ubiquitinylated proteins, in particular at early endosomes, leading to neurodegeneration (Tamai et al., 2008). Having demonstrated perturbation of *POSH* expression will elicit significant potentiation of $CHMP2B^{Intron5}$ toxicity it was asked whether *HRS* acts to enhance *CHMP2B* in a similar fashion. Here it is demonstrated that *HRS* acts as a potent enhancer of $CHMP2B^{Intron5}$ toxicity with both overexpression of *HRS* or depletion of *HRS*, using the HRS^{D28} loss of function mutation, causing significant potentiation to the melanisation phenotype (Fig. 3.7 A-B). Overexpression of UAS-*HRS* in a GMR-Gal4, UAS-$CHMP2B^{Intron5}$ mutant background induced a semi-lethal phenotype with the majority of flies dying within the pupal case as a result of significant degeneration of the eye. 100 % of flies surviving post-eclosion presented a “high” phenotype (Fig. 3.7.B). GMR-Gal4 expression of UAS-*HRS* in the absence of UAS-$CHMP2B^{Intron5}$ induced a very mild rough eye phenotype. As with *POSH* and *AliX* depletion of *HRS* also potentiated toxicity, however not as significantly as overexpression of *HRS*. HRS^{D28} loss of function mutants potentiated $CHMP2B^{Intron5}$ with 36.2 % of flies presenting with a high phenotype and the remainder a medium phenotype (Fig. 3.7.B). This is in contrast to GMR-Gal4, UAS-$CHMP2B^{Intron5}$/+ where 98.65 % of flies presented with a medium phenotype, the rest being high. HRS^{D28} mutants in a GMR-Gal4 background, in the absence of $CHMP2B^{Intron5}$, showed no variance from wildtype (n = 100).

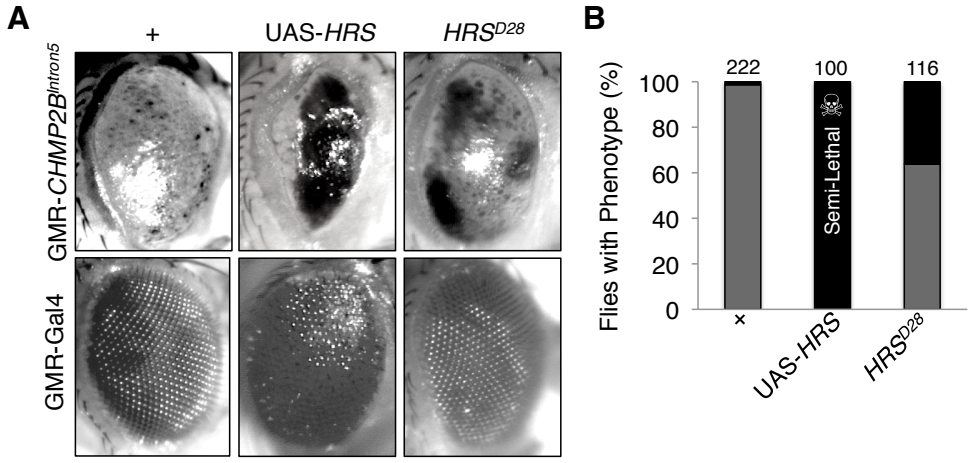

Figure 3.7. Overexpression of HRS Potently Enhances *CHMP2B*^{Intron5} Toxicity in the *Drosophila* eye
(**A**) Both overexpression and inhibition of *HRS* in a GMR-Gal4, UAS-*CHMP2B*^{Intron5} background potentiated toxicity, displaying a greater degree of melanisation across the eye. 85 % (n = 85/100) of GMR-Gal4, UAS-*CHMP2B*^{Intron5}/UAS-*HRS* flies died at a pupal stage as a result of severe retinal degeneration, those 15 % surviving to adulthood all presented with a "high" degenerative eye phenotype. Overexpression of UAS-*HRS* in the fly eye in the absence of *CHMP2B*^{Intron5} elicited a very mild rough eye phenotype in 100 % of flies, whilst the presence of *HRS*^{D28} in a GMR-Gal4/+ background showed no variation from the wildtype phenotype (n=100 per genotype). (**B**) Quantification of the phenotype indicates a clear potentiation by both overexpression and inhibition of HRS, with the most severe enhancement associated with overexpression. White = low (+) phenotype (< 15 spots of melanisation), Grey = medium (++) phenotype (> 15 spots of melanisation but < 50 % of the eye affected), black = high (+++) phenotype (> 50 % of the eye affected by melanisation).

Previous investigations have demonstrated that both POSH and HRS directly interact with and act as functional regulators of the transforming growth factor-beta-activated kinase 1 (Tak1) (Miura and Mishina, 2011; Tsuda et al., 2005). As such, having demonstrated both *POSH* and *HRS* as two of the most potent enhancers of *CHMP2B*^{Intron5} toxicity it was asked whether *TAK1* demonstrated a comparable enhancement. Here it is demonstrated that co-expression of wildtype *TAK1* (UAS-TAK1) alongside UAS-*CHMP2B*^{Intron5} in the *Drosophila* eye (GMR-Gal4) induces a lethal phenotype, with *Drosophila* dying at an early pupal stage, displaying melanisation throughout the pupae (Fig. 3.8.C). 100 % of flies presented a lethal phenotype. It was, however, also shown that UAS-*TAK1* expression in the absence of *CHMP2B*^{Intron5}, in a GMR-Gal4/+ background also elicited a pupal lethal phenotype in 100 % of cases (n=100) (Fig. 3.8.A). Lethality and the observation of melanisation throughout the pupae is indicative of an over activation of the innate immune system, associated with overexpression of *TAK1* and *TAK1's* known function as a positive regulator of innate immunity (Ajibade et al., 2013). Similarly to *HRS* it was also shown that

depletion of *TAK1* through expression of a *TAK1*-RNAi, a dominant negative *TAK1* (UAS-*dTAK1*^{K46R}) or using *TAK1* loss of function mutants (*TAK1*^{2} and *TAK1*^{179}) also potentiated *CHMP2B*^{Intron5} toxicity, however not to the point of lethality (Fig. 3.8. A-B). No other *TAK1* allele affected the eye in the absence of *CHMP2B*^{Intron5} (n=100 per genotype) (Fig. 3.8.A).

Having demonstrated that depletion of the JNKKK *TAK1*, via expression of a dominant negative *TAK1*, *TAK1*-RNAi or using the *TAK1*^{179} mutant, potentiated *CHMP2B*^{Intron5} toxicity it was asked whether the same effect was seen using an alternative JNKKK, in this case *wnd*. Here it is demonstrated that similarly to *TAK1* *wnd* mutants are capable of potentiating *CHMP2B*^{Intron5} toxicity (Fig. 3.8. A-B). As such this suggests that activation of JNK signalling may act to potentiate toxicity.

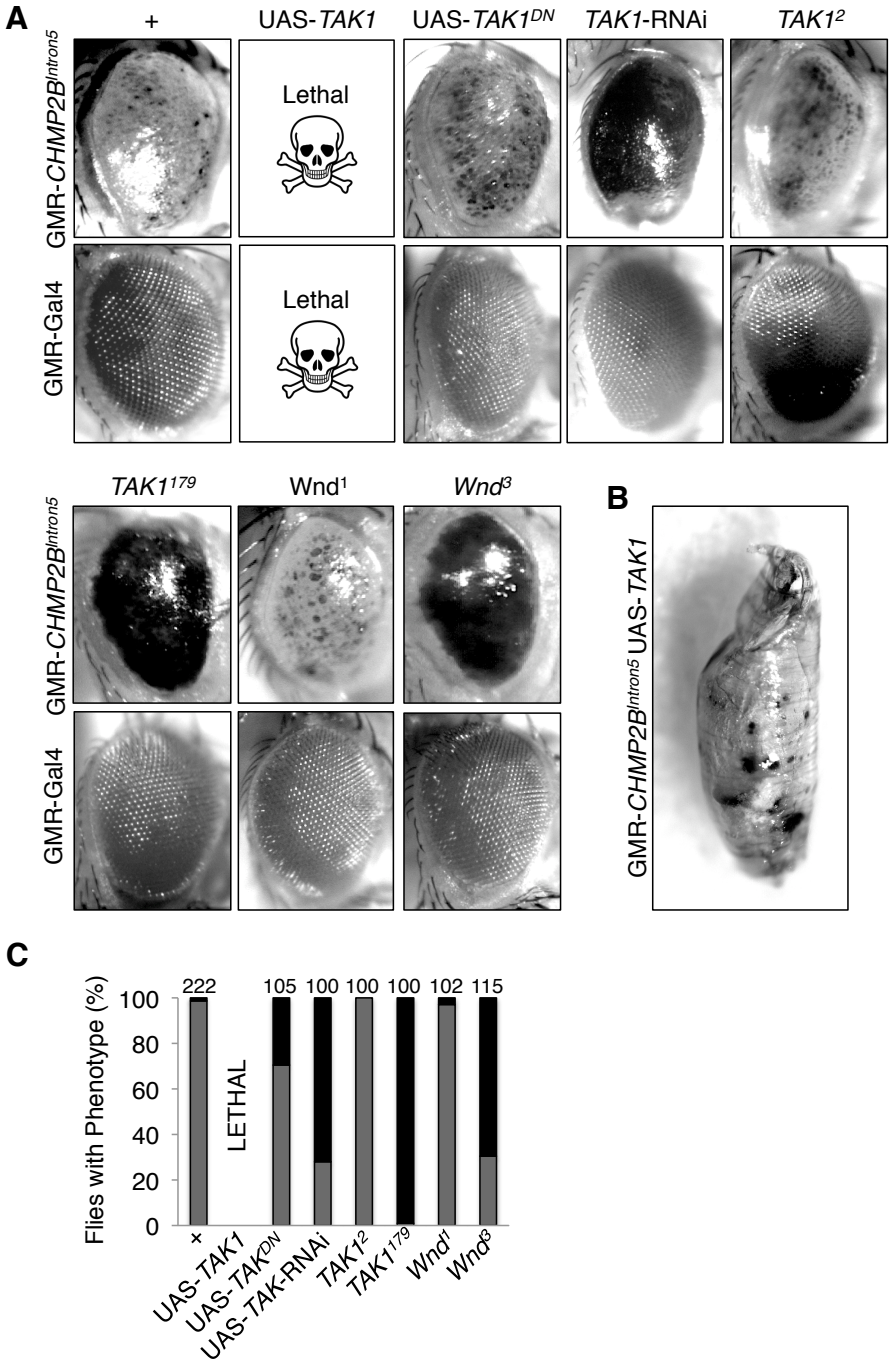

Figure 3.8. Perturbation of *TAK1* Potently Enhances *CHMP2B*^{Intron5} Toxicity in the *Drosophila* eye

(**A**) Perturbation to normal levels of *TAK1* via overexpression (UAS-*TAK1*) or inhibition, using a *TAK1* dominant negative, RNAi and loss of function mutants, in a GMR-Gal4, UAS-*CHMP2B*^{Intron5} background acts to significantly enhance *CHMP2B*^{Intron5} toxicity. *Wnd* loss of function mutations also potentiate *CHMP2B*^{Intron5} toxicity, most significantly by *Wnd*^{3}. UAS-*TAK1* in a GMR-Gal4 background, in the absence of CHMP2B^{Intron5} induced a lethal phenotype comparable to that seen in a *CHMP2B*^{Intron5} background in 100 % of flies. No other allele showed any variance from a wildtype eye phenotype in the absence of *CHMP2B*^{Intron5} (n = 100 per genotype). (**B**) Overexpression of *TAK1* in a GMR-Gal4, UAS-*CHMP2B*^{Intron5} or GMR-Gal4/+ background induced early pupal lethality characterised by melanisation throughout the pupae. This phenotype indicates a potent activation of innate immunity (**C**) Quantification reveals that with the exception of the *TAK1*^{2} and *Wnd*^{3} alleles all the alleles screened induced a clear increase in penetrance of the high phenotype, indicating both the *TAK1* and *wnd* JNKKK's as potent enhancers of *CHMP2B*^{Intron5} toxicity. White = low (+) phenotype (< 15 spots of melanisation), Grey = medium (++) phenotype (> 15 spots of melanisation but < 50 % of the eye affected), black = high (+++) phenotype (> 50 % of the eye affected by melanisation).

3.2.5. *Debra*, a Mediator of Lysosomal Degradation and Regulator of Long Term Memory, is a Dominant Enhancer of *CHMP2B*^{Intron5} Toxicity

During unbiased modifier screens of the *CHMP2B*^{Intron5} phenotype (see section 3.2.2.) a small deficiency region Df(2L)ED2809 covering 5306 bp at cytological position 21B1 was identified as a highly potent enhancer of toxicity. It was subsequently demonstrated that this deficiency region only contained two gene loci, Galectin and Debra (Determiner of breaking down of Ci activator). As such mutant alleles for both Galectin and Debra were screened against *CHMP2B*^{Intron5} revealing *Debra* to be a potent enhancer of *CHMP2B*^{Intron5} toxicity. *Debra* has been identified as encoding a 1077 amino acid protein that localises to the MVB, where it has been implicated as a mediator of protein polyubiquitination and degradation by the lysosome (Dai et al., 2003; Kottler et al., 2011). Debra has also been identified as playing a functional role during *Drosophila* long-term memory implicating lysosomal protein degradation in processes underlying synaptic plasticity and long-term memory (Kottler et al., 2011). Here it is demonstrated that heterozygous *Debra* mutants *Debra*^{EP9} and *Debra*^{EX04764} potentiate *CHMP2B*^{Intron5} toxicity, without having an affect on the eye phenotype on their own (n = 100 per genotype) (Fig. 3.9.A-B).

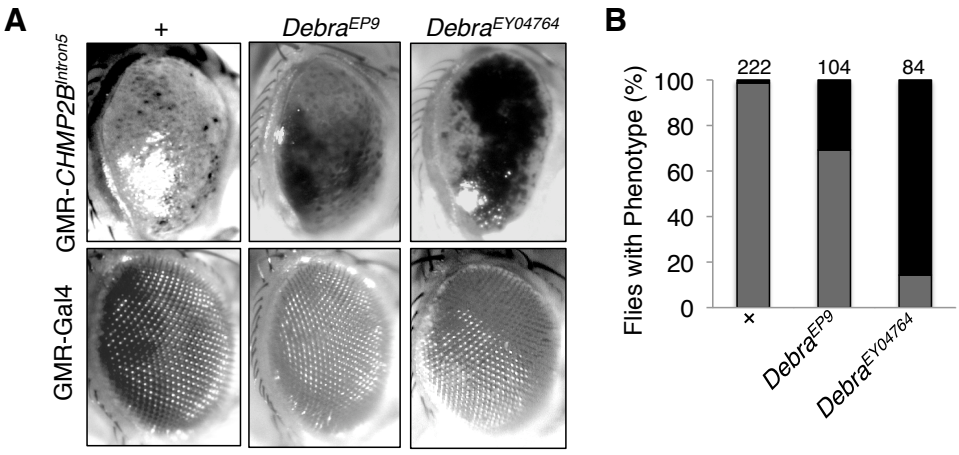

Figure 3.9. Modifier Screens Identify *Debra* as a Potent Enhancer of *CHMP2B*^{Intron5} Toxicity in the *Drosophila* eye
(**A**) *Debra* loss of function mutants in a GMR-Gal4, UAS-*CHMP2B*^{Intron5} background potentiate toxicity. Neither allele perturbs the wildtype eye phenotype in the absence of *CHMP2B*^{Intron5}, in a GMR-Gal4 background (n = 100 per genotype). (**B**) Quantification of the eye phenotypes reveals an increased penetrance of the high phenotype in *Debra CHMP2B*^{Intron5} double mutants. White = low (+) phenotype (< 15 spots of melanisation), Grey = medium (++) phenotype (> 15

spots of melanisation but < 50 % of the eye affected), black = high (+++) phenotype (> 50 % of the eye affected by melanisation).

3.3. Discussion

3.3.1. *Rab8*, a Novel Enhancer of Frontotemporal Dementia

Through unbiased modifier screens *Rab8* was initially identified as a potential enhancer of *Shrub*-GFP toxicity. The results described here corroborate this initial hypothesis, revealing that heterozygous *Rab8* mutants potently enhance toxicity associated with both *Shrub*-GFP and *CHMP2B*^{Intron5} toxicity. As such these results identify *Rab8* as a novel target for the study of FTD, in particular associated with endosomal perturbation.

Previous investigation has demonstrated that *CHMP2B*^{Intron5} toxicity is associated with a failure of CHMP2B to dissociate from the ESCRT-III complex, forming an abnormal, more avid association with Snf7-2/Shrub (Lee et al., 2007). Furthermore *Shrub*-GFP has been demonstrated to act as a dominant negative, phenocopying *CHMP2B*^{Intron5} toxicity. These results corroborate this previous finding, demonstrating that both *CHMP2B*^{Intron5} and *Shrub*-GFP present with a similar phenotype, when expressed in the *Drosophila* eye, and that both are equally affected by perturbation to *Rab8*. The observation that *Rab8* mutants potentiate both *Shrub*-GFP and *CHMP2B*^{Intron5} toxicity whilst overexpression of wildtype *Rab8* may reduce toxicity suggests that Rab8 functions in the same pathway as CHMP2B and Shrub.

Rab8 has been implicated in the clathrin independent endosomal recycling pathway where it has been shown to be recruited to the tubular endosomal recycling compartment (ERC) (Hattula et al., 2006; Vaibhava et al., 2012). It has also been demonstrated that the ERC plays an important role in the recycling of receptors back to the plasma membrane (Vaibhava et al., 2012). Depletion of *Rab8* has been shown to perturb normal trafficking events associated with membrane and receptor recycling through the recycling endosome (Hattula et al., 2006; Linder et al., 2007). As such one may postulate that perturbation to

Rab8 dependent endosomal recycling may perturb the normal dynamics of the entire endosomal trafficking pathway. For example lysosomal storage disorders, in which lysosome function is affected, result in “traffic jams”, burdening the endosomal pathway (Fraldi et al., 2010). Similar disruption as a result of perturbed recycling may explain why *Rab8* potentiates toxicity associated with mutations in *CHMP2B*, which is essential for MVB formation at the late endosome

Mutations in *Rab8* may also directly affect MVB biogenesis, which is regulated by normal ESCRT function. For example previous studies have shown that depletion of *Rab8* promotes cholesterol accumulation within late endosomes/lysosomes (Linder et al., 2007). Furthermore cholesterol has been demonstrated as critical for MVB formation and function (Kobuna et al., 2010). As such one may postulate that cholesterol accumulation within late endosomes may associate with a perturbation to normal MVB biogenesis at the late endosome. If correct and Rab8 plays an essential role in normal MVB formation this may also explain why *Rab8* mutants potentiate both *Shrub*-GFP and *CHMP2B*^{Intron5} toxicity

The observation that the *Rab8* effector, *OCRL1*, also potentiates *CHMP2B*^{Intron5} toxicity, in fact to a greater extent than *Rab8* mutants, may provide an insight into the role of *Rab8* as an enhancer of *CHMP2B*. OCRL1 has been shown to interact with numerous Rab proteins from different Rab families including Rab1, Rab5, Rab6 and Rab8 (Hou et al., 2011; Hyvola et al., 2006). However its greatest affinity is for Rab8 (Hou et al., 2011). It has also been demonstrated that the *OCRL1* F668V mutation, which is implicated in Lowe Syndrome, affects a key residue essential for Rab8 binding, leading to a 5.8 fold reduction in Rab8 binding affinity (Hou et al., 2011). The observation that this neurodegenerative disease causing mutation inhibits Rab8-OCRL1 interaction implicates this as a key complex in normal neuronal development and function. As such this substantiates a role for Rab8 in normal neuronal activity, supporting our observations that *Rab8* mutants enhance toxicity associated with another neurodegenerative disease causing mutation, *CHMP2B*^{Intron5}.

OCRL1 has also been implicated in Rab8 and Ses/IPIP27 dependent endocytic trafficking (Coon et al., 2012; Noakes et al., 2011). As such perturbation to either *Rab8* or *OCRL1* is likely to perturb this process and may explain the role of both as enhancers of *CHMP2B*. It is also interesting to note that Rab8, OCRL1 and Ses have all been shown to localise to the TGN (Choudhury et al., 2005; Dressman et al., 2000; Huber et al., 1993; Noakes et al., 2011). Depletion of Rab8 inhibits normal TGN to plasma membrane trafficking whilst Ses and OCRL1 depletion have been shown to inhibit endosome to TGN trafficking (Choudhury et al., 2005; Huber et al., 1995b; Noakes et al., 2011). As such it may be important to determine whether a perturbation to this trafficking pathway is specifically involved in potentiation of $CHMP2B^{Intron5}$ toxicity.

It is important to note that the two *OCRL1* mutations used in this study, $OCRL1^{D40}$ and $OCRL1^{C53}$, are yet to be fully characterised. Both mutations were generated by P-element mobilisation of the P{EPgy2} P-element within the 5' UTR region of the *Drosophila OCRL1* gene. Both mutations induced deletions covering the start codon of OCRL1, thus producing null-alleles. Whilst the C52 mutation has been mapped and shown to affect the first 6 exons of the OCRL1 gene resulting in a complete null, as shown by western blotting (personal communication Avital Rodal, Brandeis University, Massachusetts, USA) the D40 mutation has not been fully characterised. Work in the Sweeney Lab has shown the D40 deletion to remove the start codon for the upstream eukaryotic initiation factor 2B-epsilon (eIF-2Bε) gene, which may explain it's more potent enhancement of $CHMP2B^{Intron5}$ toxicity than the C52 mutation, which does not. Further investigation must look to further characterise these OCRL1 mutants as well as determine whether any other known OCRL1 mutations, such as the F668V mutation involved in Rab8 binding, potentiate $CHMP2B^{Intron5}$ toxicity.

Taken together these results demonstrate that mutations in *Rab8*, which has been implicated in neuronal development, and mutations in *OCRL1*, a Rab8 effector that has been implicated in the neurodevelopmental disorder Lowe Syndrome, both potentiate $CHMP2B^{Intron5}$ toxicity. As such this strongly implicates Rab8 and OCRL1, and their associated trafficking pathways, as

novel targets for the study of neuronal development and neurodegenerative diseases including both Lowe Syndrome and FTD.

3.3.2. Modifier Screens Identify Endosomal POSH and HRS Regulation of TAK1 as a Potential Novel Pathway Involved in *CHMP2B*^{Intron5} Toxicity

AliX has been shown to associate with the ESCRT machinery via direct interaction with both ESCRT-III component Shrub and ESCRT-I component TSG101 (Fisher et al., 2007; Kim et al., 2005b; Strack et al., 2003). Furthermore AliX has been implicated in MVB biogenesis through its interaction with LBPA, which plays a fundamental role in the formation of the intraluminal vesicles characteristic to MVB's (Chevallier et al., 2008; Matsuo et al., 2004). As such the observation that disruption to AliX, through both overexpression and depletion, potentiated *CHMP2B*^{Intron5} toxicity was unsurprising due to its likely effect in perturbing normal MVB biogenesis. However the observation that overexpression of AliX induces a more potent enhancement of *CHMP2B*^{Intron5} toxicity than depletion via RNAi or a loss of function mutation suggests that toxicity is associated with driving MVB formation. This supports the hypothesis that the *CHMP2B*^{Intron5} mutation promotes maintenance of CHMP2B in a permanently active state as a result of the C-terminal truncation preventing both CHMP2B autoinhibition and Vps4 mediated dissociation of the ESCRT-III complex. In this state ESCRT components are likely to become sequestered in complex, being unable to be recycled. Further support for the hypothesis that *CHMP2B*^{Intron5} toxicity is associated with driving MVB formation comes from the observation that overexpression of HRS, which promotes MVB formation, elicits the most potent enhancement of *CHMP2B*^{Intron5} toxicity, leading to a semi-lethal phenotype.

Further to the observation that *AliX* potentiates *CHMP2B*^{Intron5} toxicity these results also reveal a role for the AliX-ALG2-POSH complex, and it's interacting factors associated with innate immunity and JNK signalling, in *CHMP2B* mutant toxicity. Previous investigation in the Sweeney and Gao labs have demonstrated that CHMP2B may act as a mediator of innate immune

responses through regulation of Toll signalling (Ahmad et al., 2009). In this work it was demonstrated that Toll signalling, an activator of innate immune responses, was misregulated as a result of *CHMP2B*^{Intron5} toxicity, with *CHMP2B*^{Intron5} mutants displaying increased Toll activation (Ahmad et al., 2009). Furthermore *Serpin5*, a major regulator of Toll signalling, was identified as a modifier of the *CHMP2B*^{Intron5} phenotype (Ahmad et al., 2009). Results presented here provide support for the role of innate immunity in *CHMP2B*^{Intron5} toxicity. For example in addition to the role of HRS in MVB formation it has also been identified as a positive regulator of TAK1, a key regulator of innate immunity, interacting directly with TAK1 and localising it to the early endosome in order to promote its activation (Miura and Mishina, 2011). As such the observation that overexpression of *HRS* induces potent enhancement of *CHMP2B*^{Intron5}, eliciting a semi-lethal phenotype, may associate with an activation of *TAK1* and a potentiation of the innate immune response observed in *CHMP2B*^{Intron5} mutants. As such as well as promoting MVB formation *HRS* overexpression is likely to promote an increase in innate immune responses through induction of pathways downstream of TAK1, including the nuclear factor kappa-B (NFκB) and JNK signalling pathways (Tsuda et al., 2005). However whilst overexpression of *HRS* induced potent enhancement of toxicity, leading to lethality, the opposite cannot be said for depletion of *HRS* and *TAK1*. The results presented here demonstrate that inhibition of *HRS* and *TAK1*, with the exception of the *TAK1*^{2} mutant, elicit a potentiation of *CHMP2B*^{Intron5} toxicity, albeit not to the severity of overexpression. These findings suggest that TAK1 and HRS may be under tight regulation in order to maintain specific physiological levels, with perturbation either way affecting normal function. Such strict regulation may, in part, be controlled by POSH. Previous investigations have shown that POSH acts as a regulator of TAK1 mediated signalling, through its activity as an E3 ubiquitin ligase, targeting both HRS and TAK1 for proteasomal degradation (Kim et al., 2006; Tsuda et al., 2005). POSH also undergoes auto-inhibition, maintaining tight regulation upon its own activity (Tsuda et al., 2005). It must also be noted that whilst POSH inhibits the JNKKK *TAK1*, and therefore inhibits JNK signalling it has also been shown to act as a JNK scaffold and therefore promote JNK signalling (Xu et al., 2003). As such POSH has been shown to facilitate both rapid activation and inactivation of JNK

and NFKB signalling pathways and thus acts as a central component in maintaining this tightly regulated process (Tsuda et al., 2005; Tsuda et al., 2006; Xu et al., 2003). As such this may provide an explanation to why, similarly to HRS and TAK1, both overexpression and inhibition of POSH resulted in potentiation to *CHMP2B*^{Intron5} toxicity. What is apparent is that the *POSH* null, *POSH*^{74}, exhibits the most potent dominant enhancement of toxicity of all the *POSH* alleles, indicating an important role for POSH in the *CHMP2B*^{Intron5} induced phenotype.

Having demonstrated that altered expression of the JNKKK TAK1 potently affects *CHMP2B*^{Intron5} toxicity it was asked whether an alternative JNKKK *wnd*, which has been implicated in the regulation of synaptic growth, would act in the same manner (Collins et al., 2006). The results show that similarly to *TAK1* mutants *wnd* loss of function mutants display a variable effect upon *CHMP2B*^{Intron5} toxicity with *wnd*^{1} showing little variance from *CHMP2B*^{Intron5}/+ whilst the *wnd*^{3} mutation significantly enhances toxicity. This enhancement corroborates the suggestion that potentiation of toxicity may be associated with perturbation to normal JNK signalling. However due to the striking variance between the two alleles it is possible that one allele possesses a second site mutation affecting *CHMP2B*^{Intron5} toxicity. In order to elucidate whether *wnd* truly acts as a modifier of *CHMP2B* additional alleles need to be screened against CHMP2B.

Taken together the results presented here provide further support for the roll of innate immunity in *CHMP2B*^{Intron5} toxicity, potentially acting via endosomal localisation of TAK1 and POSH and their regulation of innate immune responses via the JNK signalling pathway. These results identify a series of interconnected novel factors associated with *CHMP2B*^{Intron5} toxicity that may provide the framework for further investigation into the molecular mechanisms associated with *CHMP2B* toxicity in FTD and other models of neurodegeneration.

It is also interesting to note that Rab8, AliX, POSH and the ESCRT machinery have all been shown to be manipulated by viruses in order to promote viral

budding and infection (Ariumi et al., 2011; Rowe et al., 2008; Shtanko et al., 2011; Votteler et al., 2009). As such it is possible to see how under normal physiological conditions each component may contribute to an innate immune response, potentially acting through TAK1, in response to a viral infection. As such this may provide some explanation as to why each potentiates *CHMP2B*^{Intron5} toxicity, which has previously been demonstrated to present an activated innate immune response.

3.3.3. Debra Implicates Perturbation to Normal Endosomal-Lysosomal Trafficking in *CHMP2B* Associated FTD

During unbiased modifier screens of the *CHMP2B*^{Intron5} phenotype *Debra* was identified as a potent enhancer of toxicity. Currently Debra remains relatively poorly understood, with no known mammalian orthologue. However work in *Drosophila* has identified that Debra localises to MVB's where it has a functional role in the regulation of lysosomal degradation (Dai et al., 2003; Khokhar et al., 2008; Kottler et al., 2011). For example it was demonstrated that Debra is involved in the targeting of the transcription factor Cubitus interruptus (Ci), a mediator of hedgehog signalling, to the lysosome for degradation (Dai et al., 2003). Furthermore it has been proposed that Debra's role in the regulation of protein degradation, via the lysosome, plays a fundamental role in the modulation of synaptic plasticity associated with long-term memory (Kottler et al., 2011). Support for this role in synaptic development can also be shown by the observation that Debra has been identified as interacting with IGF-II mRNA binding protein (Imp) and small nuclear ribonucleoprotein D3 polypeptide 18 kDa (SmD3), both of which have been implicated in synaptic growth and development of the nervous system (Boylan et al., 2008; Guruharsha et al., 2011; Schenkel et al., 2002). Interestingly Debra has previously been identified as a potent enhancer of both Ataxin-3 neurodegeneration associated with Spinocerebellar ataxia type-3 (SCA3) and *parkin* loss of function associated with Parkinson's disease (Bilen and Bonini, 2007; Fernandes and Rao, 2011). As such the results presented here provide further information to a growing body of evidence that suggests that Debra plays a fundamental role in normal

neuronal function, potentially acting at the MVB to regulate lysosomal degradation. In addition the observation that mutations in *Debra,* which has been implicated in MVB function and endosomal-lysosomal trafficking, potentiates *CHMP2B*^{Intron5} toxicity provides support to previous findings identifying HRS, which is also essential to MVB function, as a modifier of CHMP2B. As such this further implicates perturbation to endosomal-lysosomal trafficking pathways in *CHMP2B*^{Intron5} toxicity. Furthermore these results identify *Debra* as a novel enhancer of neurodegenerative disease, acting to enhance *Drosophila* models of Parkinson's disease, SCA3 and now FTD. As such this provides support for a role of protein degradation via the lysosome in synaptic plasticity and associated neurodegeneration as a result of endosomal-lysosomal defects.

Taken together this chapter provides a framework, identifying novel factors implicated in the enhancement of *CHMP2B*^{Intron5} toxicity. From this individual modifiers can be investigated further in order to identify their role in neuronal development and synaptic plasticity with the goal of elucidating pathways associated with normal synaptic development and those that may be perturbed during FTD. In the long term this may provide novel pathways in which to identify potential therapeutic targets for the treatment of FTD and other neurodegenerative diseases.

4. Characterisation of *Rab8* Mutants Identifies *Rab8* as a Potent Regulator of Synaptic Growth

4.1. Introduction

As discussed in Chapter 1 Rab8 is one of more than 60 identified Rab proteins belonging to the Rab subfamily of Ras GTPases (Diekmann et al., 2011; Schwartz et al., 2007). As a GTPase Rab8 acts as a molecular switch, cycling between active GTP-bound and inactive GDP-bound states. Through this conformational cycling, the specific localisation of different Rab's and the effector proteins they activate and/or recruit, Rab proteins act as multifaceted organisers (Ng and Tang, 2008; Stenmark, 2009). As such they convey strict regulation to both rate and specificity for almost all trafficking events occurring in eukaryotic cells (Ng and Tang, 2008; Stenmark, 2009).

Rab8 has been implicated in membrane trafficking events fundamental to polarised cell development and the regulation of cell shape. For example during membrane recycling, exocytosis and ciliogenesis (Follit et al., 2010; Nachury et al., 2007a; Peranen, 2011). Furthermore Rab8 has been implicated in essential trafficking events involved in normal neuronal development and maintenance. For example it has been shown to be important for neurite outgrowth as well as for the regulation of glutamatergic neurotransmitter receptor abundance at the cell surface (Brown et al., 2007a; Gerges et al., 2004a; Huber et al., 1995a). Rab8 has also been shown to be enriched within the nervous system, with the mammalian Rab8B isoform showing enrichment within the brain (Chan et al., 2011; Lau and Mruk, 2003).

Having identified *Rab8* mutants as a potent enhancer of toxicity associated with the FTD mutation *CHMP2B*^{Intron5}, the focus of this chapter is the characterization of *Rab8* mutants and their effects upon the nervous system. Previously, little characterisation of *Rab8* mutants in any model organism has been performed. Characterisation that has been carried out often focused upon the role of Rab8 in ciliogenesis as opposed to neurodegeneration. In fact the study of Rab8

function has often been hampered in higher organisms due both to genetic redundancy and the fact that Rab8 mutant mice die, within 3-4 weeks of birth, as a result of perturbations to normal ciliogenesis within the intestine (Sato et al., 2007a).

Here we identify and characterise *Rab8* mutations. The mutations we identify are shown to affect regions essential to protein function that are highly conserved across species, and across the Rab family of GTPase's. In addition mutations are demonstrated to cause significant perturbations to normal neuronal morphology, as observed using the *Drosophila* larval NMJ as a model system. These mutants are shown to display a general unregulated growth phenotype characterised by significant synaptic overgrowth, in terms of synaptic bouton number and NMJ length, with a reduction in synaptic bouton size. Furthermore *Rab8* mutants are shown to display major ultrastructural aberrations, despite showing limited perturbation at a histological level.

4.2. Results

4.2.1. Genetic Characterisation of *Rab8* Mutants; Identified Mutations in *Rab8* Affect Highly Conserved Amino Acid Residues.

Having demonstrated, in the previous chapter, that an allelic series of proposed *Rab8* mutants act to significantly enhance toxicity of the FTD causing mutation *CHMP2B*^{intron5} here we look to characterise the nature of these mutations. As mentioned in Chapter 1 classical forward genetic approaches often utilize random mutagenesis screens in which the *Drosophila* genome is subjected to mutagenesis, typically by ionizing radiation or chemicals such as EMS (St Johnston, 2002). The subsequent mutants can then be screened for a phenotype of interest. This approach produces a large number of mutants (~10^{-4}), many of which will not be involved in the investigators area of interest. As such unwanted mutants are often, subsequently, roughly mapped to complementation groups and donated to *Drosophila* stock centres. In such a way stock centres build up large collections of roughly mapped, but otherwise

uncharacterised, mutants. *Rab8* mutants $Rab8^{1}$, $Rab8^{2}$, $Rab8^{3}$ and $Rab8^{Z3007}$ are 4 such, EMS induced, uncharacterised mutations. Here complementation analysis was performed by crossing each of the proposed *Rab8* mutant genotypes to each other, as well as to the deficiency loci to which they have been mapped (Df(3L)ED228), and to Pbac{5HPw^{+}}Rab8^{B229} ($Rab8^{B229}$), a known *Rab8* mutant caused by a transposable element piggyBac insertion into the *Rab8* loci. Complementation analysis reveals that each mutation fails to complement each other, as well as the deficiency, (Table 4.1.) and results in a distinctive pharate lethal phenotype (Fig. 4.1.). This confirms that each mutation independently affects, and therefore maps to, the same gene. Failure to complement $Rab8^{B229}$ strongly suggests this gene to be *Rab8*. Furthermore lethality indicates the gene affected to be essential for normal development and survival. The distinctive late pharate lethal phenotype identified is one that has proven to be commonly associated with *Drosophila* models of neurodegenerative diseases, including Huntington's and Alzheimer's diseases (Colodner and Feany, 2010; Torroja et al., 1999; Weiss et al., 2012). In some instances a very small number of flies were capable of completing eclosion and escaping from their pupal case. However these flies showed a number of distinct physiological deficits including an inability to expand their wings, post-eclosion, coupled with almost complete immobility, remaining motionless upon the substrate and dying within 24 hours of eclosion. These flies were recorded as semi-lethal (Table 4.1). Lowering the temperature at which flies were raised (18°C instead of 25°C) showed a marginal increase in those flies classified as semi-lethal rather than pharate-lethal, although they still presented almost complete inactivity and died within 24 h of eclosion. Complementation analysis also reveals a reduced number, less than the ~ 33 % predicted by Mendelian laws of inheritance, of *Rab8* transheterozygous flies surviving to the pharate stage. Whilst there was no clearly distinct earlier stage at which larvae were dying these results suggest transheterozygous *Rab8* mutations convey a detrimental effect to survival, with those surviving past larval and pupal stages dying at the pharate stage.

Table 4.1. *Rab8* Mutant Alleles Fail to Complement Each Other

	$Rab8^{1}$	$Rab8^{2}$	$Rab8^{3}$	$Rab8^{Z3007}$	$Rab8^{B229}$	Df(3L) ED228
$Rab8^{1}$	-	Semi-Lethal	Semi-Lethal	Pharate Lethal	Pharate Lethal	Pharate Lethal
$Rab8^{2}$	-	-	Pharate Lethal	Pharate Lethal	Semi-Lethal	Pharate Lethal
$Rab8^{3}$	-	-	-	Pharate Lethal	Pharate Lethal	Pharate Lethal
$Rab8^{Z3007}$	-	-	-	-	Pharate Lethal	Pharate Lethal
$Rab8^{B229}$	-	-	-	-	-	Pharate Lethal
Df(3L) ED228	-	-	-	-	-	-

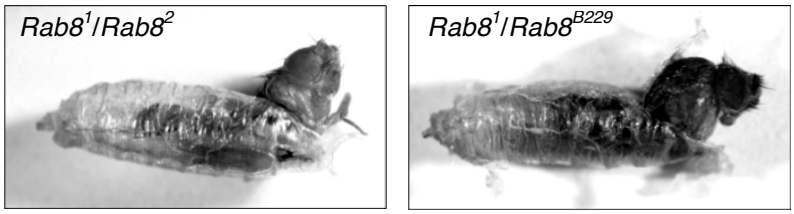

Figure 4.1. *Rab8* Mutants Display Pharate Lethality
Complementation analysis reveals that transheterozygous *Rab8* mutants display distinctive late pharate lethality, characterised by an inability of adult flies to complete eclosion, becoming trapped and ultimately dying semi-emerged from the pupal case.

With complementation analysis substantiating that all proposed *Rab8* alleles independently affect the same gene and that it is most likely *Rab8,* each of the 4 randomly induced *Rab8* mutant genotypes were sequenced in order to identify the nature of the mutations. Sequencing revealed each mutation to be caused by single, independent point mutations present within the *Rab8* gene locus (Fig. 4.2.). Three of these point mutations were C-to-T substitutions, typical of EMS induced mutagenesis which induces C/G-to-T/A transitions in 69.9-100 % of cases (Bentley et al., 2000; Blumenstiel et al., 2009; Cooper et al., 2008; Winkler et al., 2005). The other mutant, $Rab8^{Z3007}$, displays a T-to-A substitution. Such changes have been shown to be induced by EMS in *Drosophila* at a lower frequency (~ 15 %) (Cooper et al., 2008; Winkler et al., 2005).

Further analysis of these mutations demonstrates that each of the 4 point mutations result in an alteration to the *Drosophila* Rab8 amino acid sequence; $Rab8^{1}$: S17F, $Rab8^{3}$: T40I, $Rab8^{Z3007}$: M85K and $Rab8^{2}$: S95F. Functional analysis of the effect of these mutations upon protein stability and function, using in silico analysis, suggest all 4 mutations to be "probably damaging" and having a deleterious effect upon protein function (PolyPhen-2, PROVEAN). However only the $Rab8^{Z3007}$ mutation is predicted to cause a significant destabilisation to protein stability (ProSMS).

Further analysis reveals that these mutations affect residues that are both highly conserved across species (Fig. 4.3.) but also across the Rab sub-family of GTPases (Fig. 4.4.). Rab8 is highly conserved across species, with the only region of significant variation being the hyper variable C-terminal domain (Fig. 4.3.). It is also apparent that both the $Rab8^{1}$ and $Rab8^{3}$ mutations induce amino acid substitutions within 2 of the 5 highly conserved polypeptide loops, or G-domains G1-G5, that are essential to GTPase function (Okai et al., 2004). The $Rab8^{1}$ mutation falls within the G1 domain, a conserved motif comprising of the sequence GXXXXGKS/T (Bourne et al., 1991). $Rab8^{3}$ results in a substitution of the conserved threonine residue, within the G2 motif, that is responsible for Mg^{2+} binding (Bourne et al., 1991). In contrast the $Rab8^{2}$ and $Rab8^{Z3007}$ mutations fall in regions that, whilst conserved, are not obvious functional domains. As such it can be inferred that $Rab8^{1}$ and $Rab8^{3}$ mutations are most likely to be detrimental to Rab8 function through disruption of Rab8's normal GTPase activity, via direct perturbation of the GTPase domain. In contrast $Rab8^{Z3007}$ is suggested to destabilize the Rab8 protein, affecting normal function, whist the deleterious effect of the $Rab8^{3}$ mutations appears less definitive.

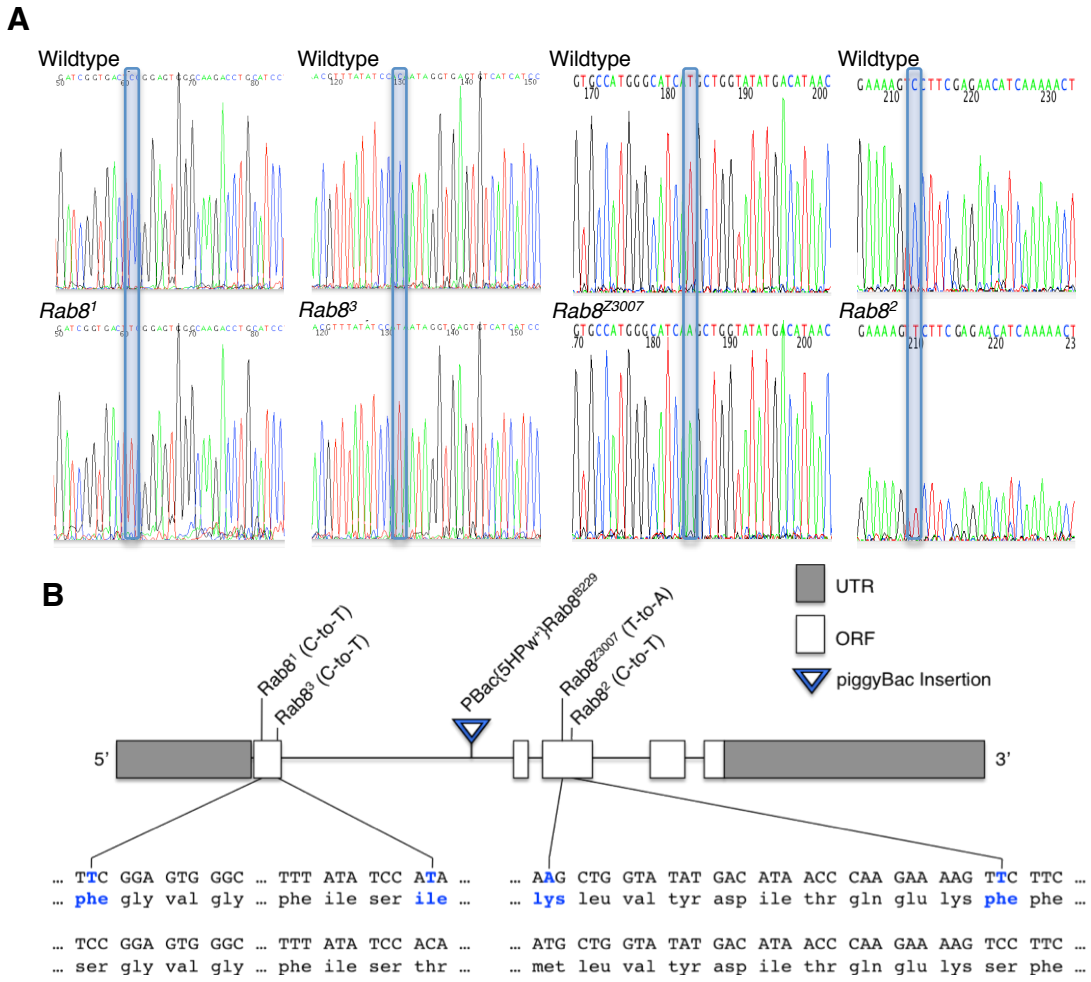

Figure 4.2. Identification of Point Mutations in the *Rab8* Locus.
Complementation mapping identified four specific ethyl methanesulfonate (EMS) induced mutations likely to be present within the *Rab8* gene locus. (**A**) DNA sequence analysis revealed each *Rab8* mutant genotype to be associated with single independent point mutations within the *Rab8* locus. (**B**) Mapping of these mutations identified their positions within the *Rab8* locus and revealed each mutation induced a specific alteration to the Rab8 amino acid sequence, highlighted in blue. The wildtype amino acid sequence is shown (bottom) for comparison.

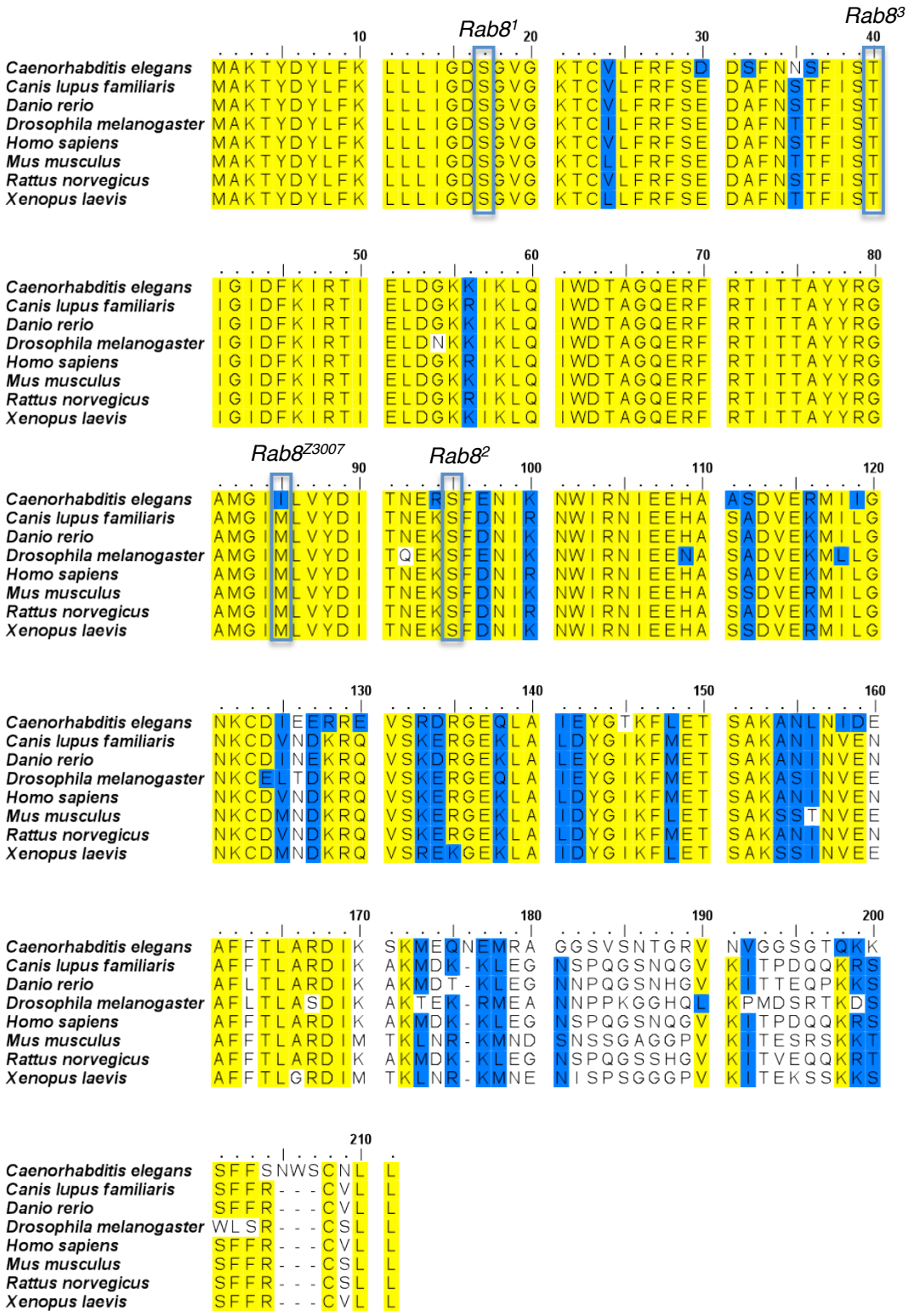

Figure 4.3. Identified Mutations in *Rab8* Affect Residues Conserved Across Species. Sequence alignment of Rab8 from different species. Location of *Rab8* mutants are shown. Rab8 is highly conserved across all species with the only region of variability being that of the hypervariable C-terminal domain. Yellow indicates regions of 100 % conservation, blue 80 % conservation. Accession numbers: *C. elegans*; BAD07034.1, *C. lupus*; CAB56776.1, *D. rerio*; AAI34060.1, *D. melanogaster*; BAD07038.1, *H. sapiens*; AAM21091.1, *M. musculus*; NP_075615.2, *R. Norvegicus*; AEJ31940.1 and *X. laevis*; NP_001087273.1.

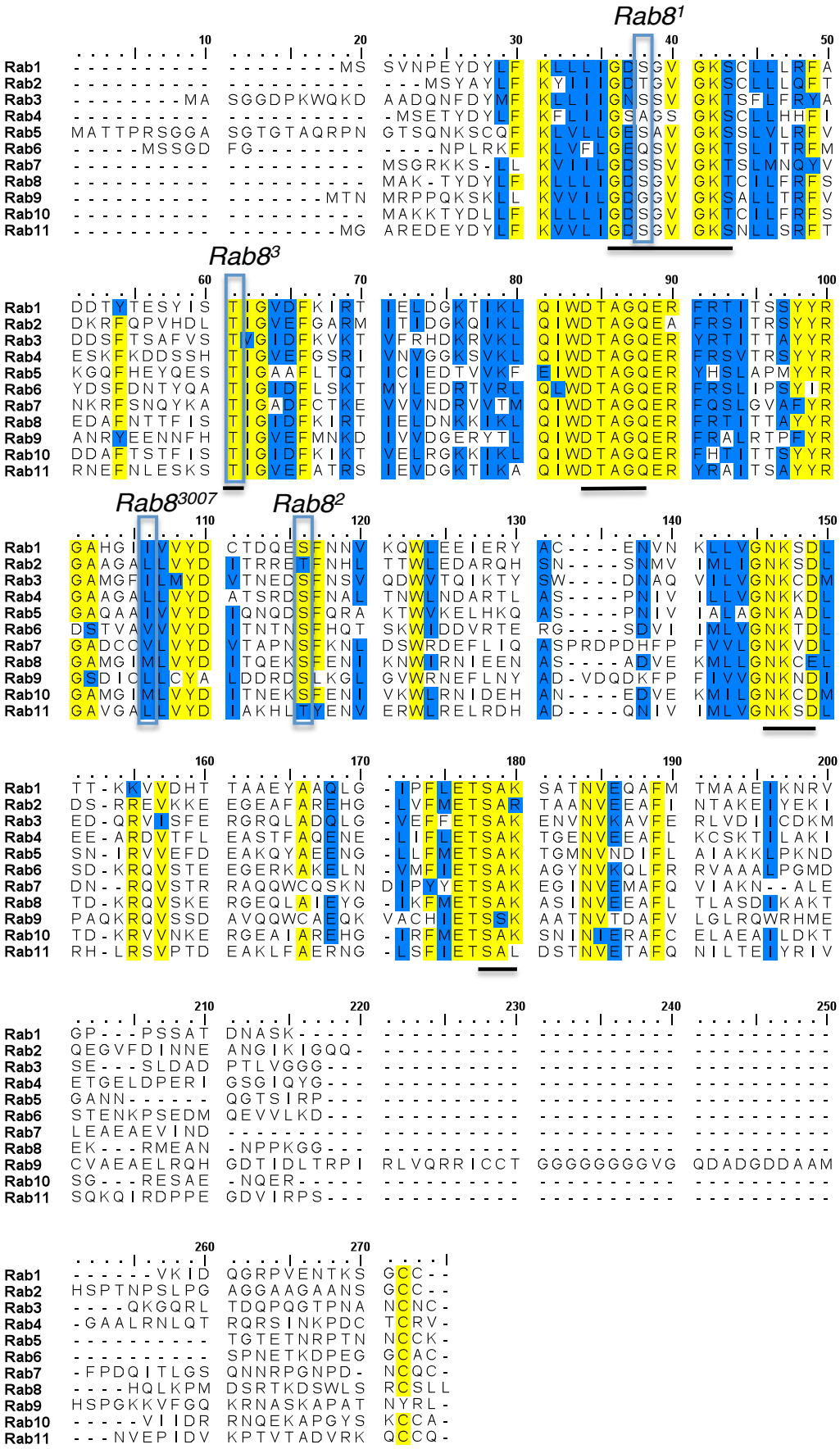

Figure 4.4. Mutations in *Rab8* Affect Functional Regions Highly Conserved Across The Rab Subfamily of GTPases

Sequence alignment of *Drosophila* Rab family members, showing the location of the identified mutations in *Rab8*. Underlined regions indicate the location of the 5 G-domains G1-5 in sequential order. Yellow indicates regions of 100 % conservation, blue 80 % conservation.

Accession numbers: Rab1; AAF55873.1, Rab2; BAA21706.1, Rab3; AAF58762.1, Rab4; AAF57831.1, Rab5; AAN85553.1, Rab6; AAF53168.1, Rab7; AAF56218.1, Rab8; BAD07038.1, Rab9; AAF53798.1, Rab10; AAF50924.1 and Rab11; BAA21708.1.

4.2.2. Rab8 is Neuronally Enriched and Expressed in *Drosophila* Motor Neurons

Having identified the nature of the mutations present within an allelic series of *Rab8* mutants this investigation looked to further characterise Rab8 by analysing the expression pattern of the *Rab8* gene. Using data obtained from the BDGP RNA *In situ* hybridization database it is clear that *Rab8* is ubiquitously expressed, in *Drosophila* embryos, with regions of enrichment within the CNS (Fig. 4.5.A). CNS enrichment is substantiated by data obtained from the FlyAtlas gene expression database (www.flyatlas.org) which reveals Rab8 to be enriched within the larval CNS and adult brain (Chintapalli et al., 2007; Robinson et al., 2013).

In order to further characterize *Rab8's* expression within the *Drosophila* third instar larval CNS nuclear (eif4-GFP, Fig. 4.5.B-C) and cell membrane (mcd8-GFP, Fig. 4.5.D) UAS-GFP markers were expressed under the control of the *Rab8* specific driver *Rab8*-Gal4 (Chan et al., 2011). Here it is demonstrated that *Rab8* is expressed in both neurons (Fig. 4.5.C) and glia (Fig. 4.5.B). However there appears to be a far greater number of elav positive cells co-localising with *Rab8* expressing cells than repo positive cells that do. This suggests that whilst expressed in both neuronal and glial cell types *Rab8* is predominantly expressed in neurons. In order to determine whether *Rab8* was expressed in the motor neurons responsible for the innervation of the dorsal muscle field even-skipped (eve) was used as a motor neuronal marker. Eve is expressed in pCC (posterior corner cell), fpCC (friend of pCC), aCC (anterior corner cell), RP2 and U/CQ neurons which, with the exception of pCC and fpCC interneurons, are all motor neurons (Bossing et al., 1996; Broadus et al., 1995; Landgraf et al., 2003a). All eve positive cells within the *Drosophila* third instar larval ventral nerve cord co-localised with cells positive for mcd8-GFP under the control of the *Rab8* driver (Fig. 4.5.D). Therefore *Rab8* must be expressed in

Drosophila larval motor neurons and so the NMJ can be utilised to study the role of Rab8 in neurons.

In order to further characterise the localisation and distribution of Rab8 both a Rab8-eGFP and an anti-Rab8 antibody were also generated (see sections 2.4.1. and 2.5.). Unfortunately neither was sufficient to elucidate a sub-cellular localisation of Rab8 with both demonstrating a diffuse and ubiquitous distribution pattern.

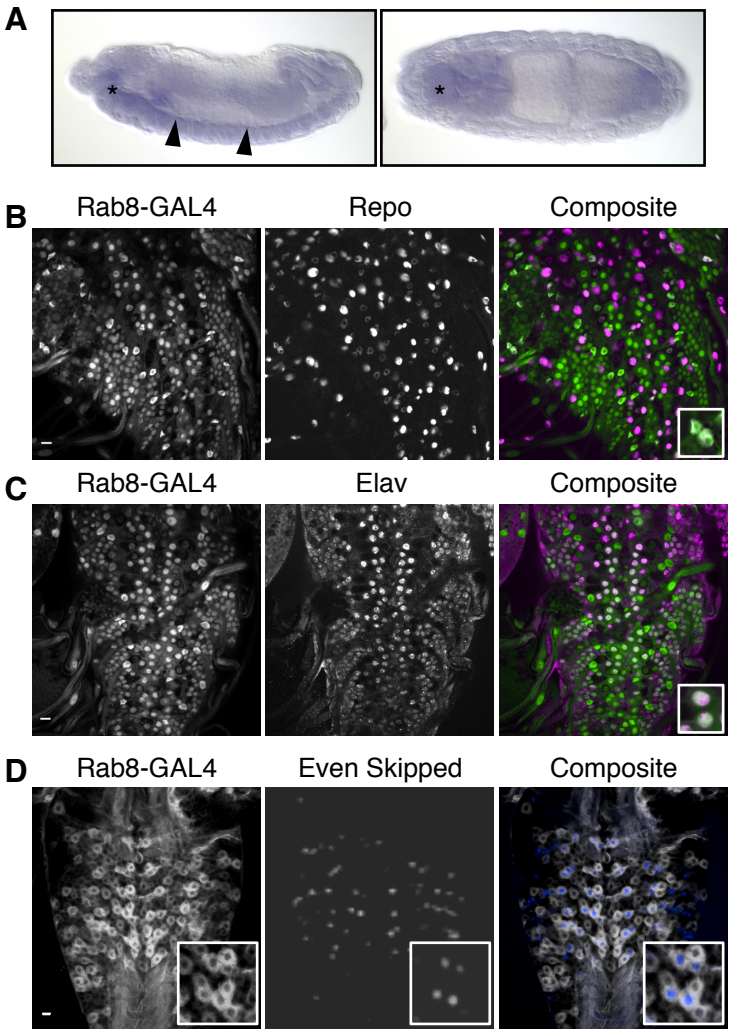

Figure 4.5. *Rab8* is Neuronally Enriched Displaying Expression Predominantly in Neurons, Although Also in Glia.
(**A**) Rab8 RNA *in situ* hybridization in a stage 13-16 *Drosophila* embryo (viewed from lateral (left) and dorsal (right) orientations) reveals *Rab8* expression to be ubiquitous, although enriched within the central nervous system, as seen in the embryonic brain (asterisks) and ventral nerve cord (arrow heads) (Image courtesy of and adapted from The Berkeley *Drosophila* Genome Project, (BDGP, 2013; Tomancak et al., 2002; Tomancak et al., 2007). (**B**) Rab8 is strongly expressed in some, but not all glial cells within the *Drosophila* third instar larval ventral nerve cord. Expression of the nuclear maker eif4-GFP under the control of the Rab8 specific driver Rab8-GAL4 partially co-localises with the glial marker anti-repo. (**C**) Rab8 shows pan-neuronal expression with Rab8-GAL4-eif4-GFP co-localising with the pan-neuronal marker anti-elav. (**D**) Rab8 is expressed in motor neurons. The aCC/pCC motor- and inter-neuron marker

anti-even skipped localises to cells expressing the membrane marker mcd8-GFP under the control of Rab8-GAL4, indicating Rab8 expression in both interneurons and motor neurons. Scale Bars = 10 μm.

4.2.3. *Rab8* Mutants Display Perturbed Synaptic Growth

4.2.3.1. *Rab8* Mutants Display a Significant Increase in Synaptic Bouton Number

Having identified that transheterozygous *Rab8* mutants display pharate lethality, characteristic of neurodegenerative disease models in *Drosophila*, and having shown *Rab8* to be expressed and enriched within the nervous system, this investigation looked to determine whether *Rab8* mutants showed any perturbation to normal neuronal morphology and function. Using the 3rd instar larval muscle 6/7, hemi-segment A3, NMJ as a model synapse here it was demonstrated that all 15 *Rab8* transheterozygous mutant genotypes display a significant increase in synaptic bouton number, compared to wildtype, indicative of synaptic overgrowth (Fig. 4.6.A-B). Heterozygous *Rab8* mutants showed no overgrowth phenotype. Synaptic bouton number was normalized against the wildtype control to account for variations in larval size and muscle surface area (MSA). It is well established that during synaptic growth and development the number of synaptic boutons increases proportionally to the muscle size (Lnenicka and Keshishian, 2000; Schuster et al., 1996). Here it was demonstrated that the majority of *Rab8* transheterozygous mutants showed no significant difference in MSA, compared to wildtype (Fig. 4.6C). Subsequently all mutants show a significant increase in bouton number both post-normalisation (Fig. 4.6.B) and prior to normalization (post-hoc Dunnett's comparison to wildtype $p < 0.001$ for all genotypes prior to normalization). Therefore all *Rab8* transheterozygous mutants display a synaptic overgrowth phenotype, characterised by a significant increase in synaptic bouton number.

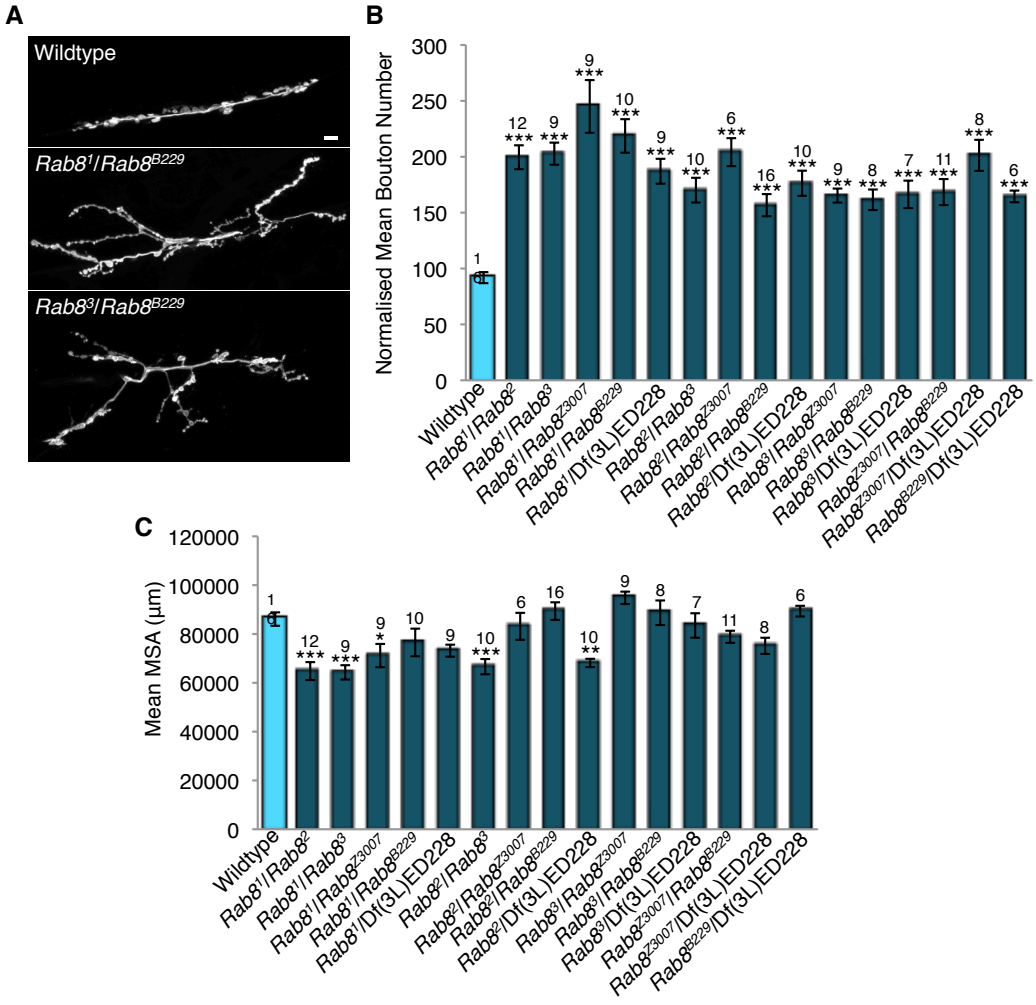

Figure 4.6. *Rab8* Mutants Display a Significant Increase in Synaptic Bouton Number
(**A-B**) All transheterozygous combinations of Rab8 mutants display a significant (ANOVA: F(d.f. 15) = 10.14; $p < 0.001$ with post hoc Dunnett's comparison to wildtype control, *** $p < 0.001$ vs WT) increase in synaptic bouton number at muscle 6/7, hemi-segment A3 of 3rd Instar larvae. Bouton number ranges from a 70.58 % to a 166.76 % increase in number compared to wildtype. Synaptic bouton numbers were normalised against wildtype to account for variations in muscle surface area (MSA). Scale bar = 10 µm. (**C**) *Rab8* transheterozygous mutants show significant variance in MSA between genotypes (ANOVA: F(d.f. 15) = 7.27; $p < 0.001$) with only 1/3 of genotypes showing significant variance from wildtype (post-hoc Dunnetts's comparison to wildtype control * $p < 0.05$, ** $p < 0.01$, *** $p < 0.001$).

4.2.3.2. Increased Bouton Number in *Rab8* Mutants Can be Rescued By Pre-Synaptic Expression of *Rab8*

Having established that *Rab8* mutants present a synaptic overgrowth phenotype, characterised by an increase in synaptic bouton number at muscle 6/7, analysis looked to determine whether this phenotype was conserved at alternative NMJ's and whether overexpression of wildtype *Rab8*, in specific tissues, could rescue the overgrowth phenotype observed. In order to perform

rescue experiments transgenic UAS-Rab8 *Drosophila* lines were first generated through microinjection of a pUASt construct, into which *Drosophila* Rab8 had been cloned, into w^{1118} *Drosophila* embryos (as described in section 2.5.). The pUASt plasmid construct contains UAS sequences upstream of the multiple cloning site, allowing for controlled expression of *Rab8* using the UAS/GAL4 system once integrated into the genome. Having isolated transformants, determined the chromosome onto which the transgene had inserted and stabilized individual stocks UAS-Rab8 could be expressed globally/ubiquitously (actin-Gal4), pan-neuronally (nSyb-Gal4) or post-synaptically in muscles (MHC-Gal4).

The $Rab8^{1}/Rab8^{B229}$ transheterozygous mutant genotype was selected as a genotype representative of all *Rab8* transheterozygous mutants. Analysis reveals that $Rab8^{1}/Rab8^{B229}$ mutants show an overgrowth phenotype, displaying a significant increase in synaptic bouton number, at muscle 4 (hemi-segment A3) comparable to that seen at muscle 6/7 (Fig. 4.7.A-C). Thus synaptic overgrowth appears to be conserved across NMJ‘s of differing size and morphology. It was also demonstrated that expression of UAS-*Rab8* under the control of the global driver actin-Gal4 was sufficient to rescue increased synaptic bouton number in $Rab8^{1}/Rab8^{B229}$ mutants at both muscle 4 and 6/7 (Fig. 4.7.A-C). Global rescues showed no significant difference from wildtype (Dunnett's post-hoc comparison to wildtype control; N/S) or actin-Gal4/UAS-Rab8 controls (Student t-test post-hoc comparison between groups; N/S) yet a significant difference from *Rab8* mutants (Student t-test post-hoc comparison between groups; $p < 0.001$).

Having confirmed overgrowth in *Rab8* mutants could be rescued by expression of wildtype *Rab8,* and having previously shown *Rab8* to be enriched within the CNS, rescue experiments were performed in order to elucidate whether a pre- and/or post-synaptic complement of Rab8 would be sufficient to rescue the increase in synaptic bouton number seen in *Rab8* mutants. Pan-neuronal, pre-synaptic, expression of UAS-*Rab8* was sufficient to completely rescue the increase in synaptic bouton number seen in *Rab8* mutants (Fig. 4.7.A-C); no significant difference in synaptic bouton number was seen between wildtype,

nsyb-Gal4/UAS-Rab8 control and nsyb-Gal4/UAS-Rab8;$Rab8^{1}$/$Rab8^{B229}$ mutant flies, at either muscle 6/7 or 4. However a significant difference was seen between the *Rab8* mutants and the neuronal rescues (Student t-test post-hoc comparison between groups; $p < 0.001$).

In contrast, muscle expression of UAS-*Rab8* was only sufficient to partially rescue the increase in synaptic bouton number seen in $Rab8^{1}$/$Rab8^{B229}$ mutants. At muscle 6/7 muscle rescues show a significant difference to *Rab8* mutants (Post-hoc students t-test; $p < 0.001$) with no significant variance from wildtype (Fig. 4.7.A-B). However in comparison to MHC-Gal4/UAS-*Rab8* controls muscle rescues show a significant difference (Post-hoc students t-test; $p < 0.001$) indicating an inability to completely rescue to control levels. Corroborating these findings analysis of muscle 4 NMJ's reveals that whilst muscle rescues show a significant difference from *Rab8* mutants (Post-hoc students t-test; $p < 0.01$) they show an equally significant variance from both wildtype (Post-hoc Dunnett's; $p < 0.001$) and MHC-Gal4/UAS-Rab8 controls (Post-hoc students t-test; $p < 0.001$) (Fig. 4.7.A&C).

Taken together these results demonstrate that expression of *Rab8* globally or pre-synaptically can completely rescue increased synaptic bouton number induced by the $Rab8^{1}$/$Rab8^{B229}$ transheterozygous mutation, however post-synaptic expression can only induce a partial rescue.

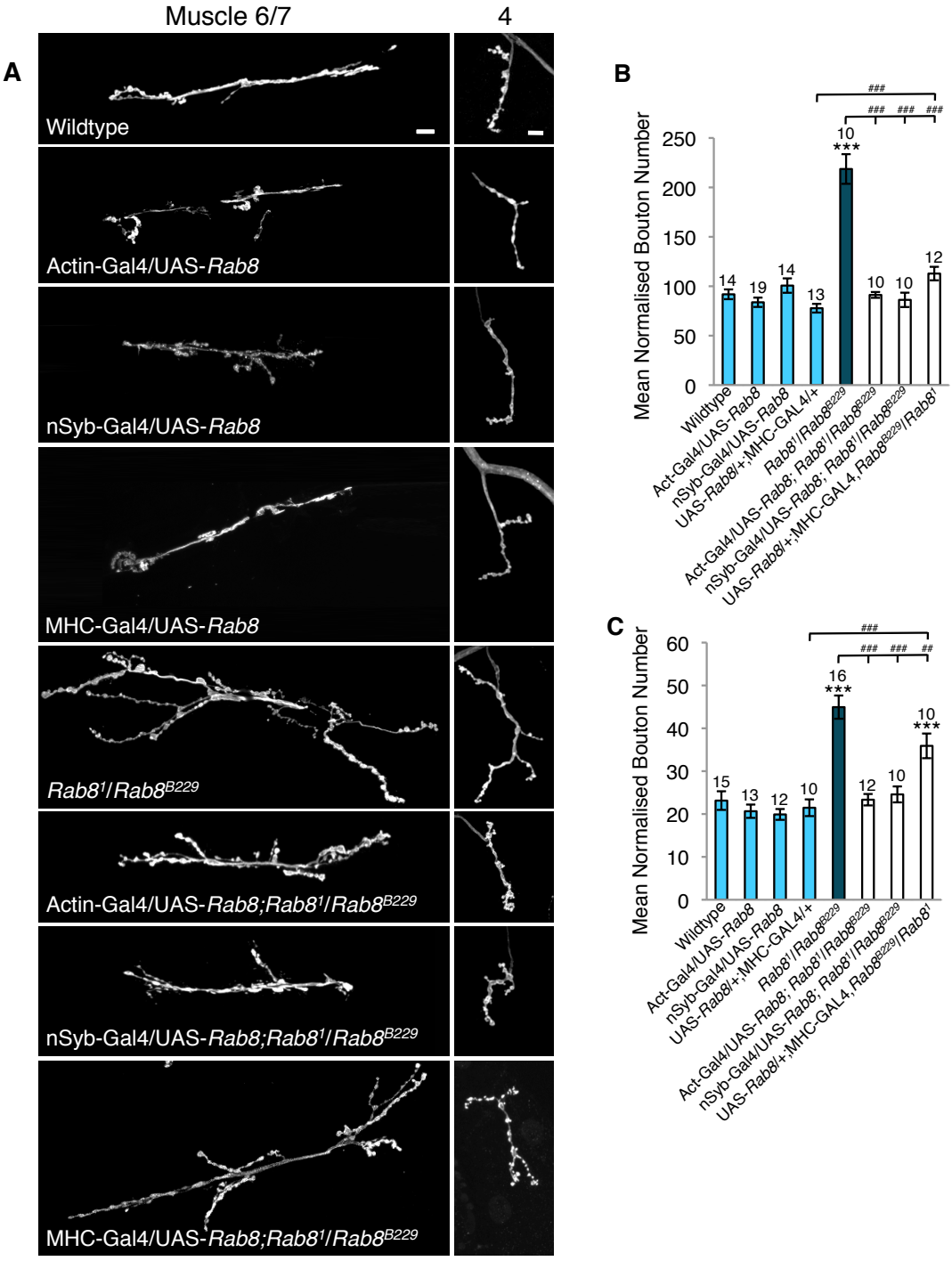

Figure 4.7. Pre-synaptic, Neuronal Expression of *Rab8* is Sufficient to Completely Rescue Increased Synaptic Bouton Number In *Rab8* Mutants.

(**A**) Confocal images show *Rab8* mutants display an overgrown NMJ phenotype that is conserved at both muscle 6/7 and 4, hemi-segment A3 of 3rd instar larvae. Overgrowth can be rescued by global (actin-Gal4) and pre-synaptic pan-neuronal (nSyb-Gal4) expression of wildtype Rab8. Post-synaptic (MHC-Gal4) expression of Rab8 only induces a partial rescue. Scale bars = 10 µm. (**B-C**) Quantification of normalized synaptic bouton number at muscle 6/7 (B) (ANOVA: $F(d.f.\ 7) = 36.8975$; $p < 0.001$ with post-hoc Dunnett's comparison to control (WT) *** $p < 0.001$ and post-hoc student t-test comparison between groups, ### $p < 0.001$) and muscle 4 (C) NMJ's. (ANOVA: $F(d.f.\ 7) = 19.95$; $p < 0.001$ with post-hoc Dunnett's comparison to control (WT) *** $p < 0.001$ and post-hoc student t-test comparison between groups, ### $p < 0.001$, ## $p < 0.01$).

4.2.3.3. *Rab8* Mutants Display Further Perturbation to Synaptic Growth, Including Increased NMJ length and Reduced Bouton Size

A significant increase in synaptic bouton number has been demonstrated in numerous *Drosophila* mutants including *spin*, *hiw*, *Rab11, endophilin, dap160* and *nervous wreck* (*nwk*) (Khodosh et al., 2006; O'Connor-Giles et al., 2008; Sweeney and Davis, 2002; Wan et al., 2000). However whilst these mutants all show a synaptic overgrowth phenotype in terms of synaptic bouton number they show significantly different NMJ morphologies. For example the endocytic mutants *Rab11*, *endophilin* and *dap160* are primarily characterised by a dramatic increase in satellite boutons, which contribute to the increase in synaptic bouton number seen (Dickman et al., 2006; Khodosh et al., 2006). Satellite boutons are classified as small supernumerary boutons that bud from a central parent bouton on the primary axon terminal (Dickman et al., 2006; Sarthi and Elefant, 2011). In contrast *hiw* mutants show a generalised overgrowth phenotype characterised by a significant increase in synaptic bouton number, overall NMJ length and number of branches, as well as a dramatic reduction in the size of synaptic boutons (Collins et al., 2006; Wan et al., 2000). *Spin* mutants display a similar, although not as dramatic overgrowth phenotype to *hiw* (Sweeney and Davis, 2002).

In order to comprehensively characterise the overgrowth phenotype seen in *Rab8* mutants NMJ morphology was further analysed based upon a range of attributes including NMJ length, branch number, number of satellite boutons, bouton size and cumulative bouton size. This analysis was all performed at muscle 4 (Hemi-segment A3), due its smaller and thus more amenable size.

Quantification of NMJ length reveals *Rab8* mutants ($Rab8^{1}/Rab8^{B229}$) to show a significant increase in NMJ length compared to wildtype (Dunnett's post-hoc comparison to wildtype $p < 0.001$) (Fig. 4.8.A). This increase in NMJ length (~ 173 % of wildtype) appears to be comparable to the increase in bouton number (~ 194 % of wildtype). As with synaptic bouton number the increase in NMJ length seen in *Rab8* mutants appears to be completely rescued by the global

expression of *Rab8*, with global rescues showing no significant variance from wildtype or actin-gal4/UAS-*Rab8* controls, whilst showing a significant difference to *Rab8* mutants (Post-hoc students t-test; $p < 0.01$) (Fig. 4.8.A). Similarly pre-synaptic pan-neuronal expression of *Rab8* is again sufficient to completely rescue the increase in NMJ length overgrowth phenotype (Fig. 4.8.A). No significant variance in NMJ length is seen between neuronal rescues and wildtypes or nSyb-Gal4/UAS-*Rab8* controls whilst rescues show a significant difference from the *Rab8* mutants (Post-hoc students t-test; $p < 0.05$). Substantiating the results for bouton number rescues expression of UAS-*Rab8* under the control of the MHC muscle driver in a *Rab8* mutant background is only sufficient to partially rescue increased NMJ length (Fig. 4.8.A). Muscle rescues show a small but significant variance from both wildtypes (Dunnett's post-hoc comparison to wildtype $p < 0.05$) and from the MHC-Gal4/UAS-*Rab8* controls (Post-hoc students t-test; $p < 0.05$) and no significant difference from Rab8 mutants. Despite showing no significant variance from *Rab8* mutants the rescues show a less significant variance from wildtype than *Rab8* mutants do, again indicating a partial rescue.

Whilst *Rab8* mutants display a significant increase in both NMJ length and synaptic bouton number they show no significant variance in branch number (Fig. 4.8.B), with no significant difference seen between any genotype and the wildtype control (Dunnett's post-hoc comparison to wildtype control).

In contrast to branch number, *Rab8* mutants display a significant increase in the number of satellite boutons (~ 329 % of wildtype) observed compared to wildtype (Dunnett's post-hoc comparison to wildtype $p < 0.01$) (Fig. 4.8.C). Again global rescues show no significant variance from wildtype or actin-Gal4/UAS-*Rab8* controls, yet a significant difference from *Rab8* mutants (post-hoc student t-test $p < 0.05$). Thus global expression of *Rab8* appears to rescue the increase in satellite bouton number seen in *Rab8* mutants. Similarly post-synaptic neuronal rescues show no significant variance from wildtypes or nSyb-Gal4/UAS-*Rab8* controls, indicating neuronal expression of *Rab8* rescues the increase in satellite bouton number seen in *Rab8* mutants (Fig. 4.8.C). However, whilst not significantly variant from controls neuronal rescues also

show no significant variance from *Rab8* mutants suggesting the rescue may only be partial. MHC-Gal4 driven muscle rescues on the other hand show no ability to rescue increased satellite bouton number, showing a satellite bouton number comparable to *Rab8* mutants and significantly different from wildtypes (Dunnett's post-hoc comparison to wildtype $p < 0.01$) (Fig. 4.8.C).

This data so far implicates *Rab8* as a regulator of NMJ growth and development with *Rab8* mutants displaying a significant increase in synaptic bouton number, satellite bouton number and NMJ length. Here it is further demonstrated that *Rab8* has a functional role in the regulation of normal NMJ growth with *Rab8* mutants displaying synaptic bouton sizes significantly reduced from wildtype (Dunnett's post-hoc comparison to wildtype $p < 0.01$) (Fig. 4.8.D). It was also demonstrated that pan-neuronal expression of UAS-*Rab8* induces an opposing effect, displaying significantly enlarged synaptic bouton sizes when compared to wildtype (Dunnett's post-hoc comparison to wildtype $p < 0.001$) (Fig. 4.8.D). In contrast global and muscle expression of UAS-*Rab8* in a wildtype background show no significant difference in bouton size, compared to wildtype. Both global and pan-neuronal expression of *Rab8* in a *Rab8* mutant background are sufficient to rescue reduced synaptic bouton size displaying no significant size difference when compared to wildtype and a significant difference to *Rab8* mutants (post-hoc student t-test $p < 0.001$) (Fig. 4.8.D). Global expression of *Rab8* in a *Rab8* mutant background also shows no significant bouton size difference from the actin-gal4/UAS-*Rab8* global controls. In contrast neuronal rescues show a significant difference to the nSyb-gal4/UAS-*Rab8* controls (post-hoc student t-test $p < 0.001$). As neuronal rescues show no variance from wildtype we can infer that this significant size difference observed is due to the enlarged bouton size seen in the neuronal controls.

Following the trend observed in other aspects of NMJ morphology it is demonstrated that whilst muscle expression of *Rab8* in a wildtype background has no effect on bouton size, showing no variance from wildtype (Dunnett's post-hoc comparison to wildtype control), muscle expression of *Rab8* in a *Rab8* mutant background does not rescue reduced bouton size, showing a significant variance from wildtype (Dunnett's post-hoc comparison to wildtype $p < 0.001$)

and MHC-gal4/UAS-*Rab8* controls (post-hoc student t-test $p < 0.001$) (Fig. 4.8.D). Interestingly muscle expression of *Rab8* in a *Rab8* mutant background actually shows a potentiation of the reduced bouton size, showing a significantly smaller bouton size than the Rab8 mutants (post-hoc student t-test $p < 0.001$) (Fig. 4.8.D).

With *Rab8* mutants displaying a significant increase in synaptic bouton number but a reduction in synaptic bouton size the question was asked as to whether they display a cumulative bouton size comparable to wildtypes. Here it is demonstrated that whilst boutons are significantly smaller the greater increase in bouton number means that *Rab8* mutants display a cumulative bouton size significantly larger than wildtypes (Dunnett's post-hoc comparison to wildtype $p < 0.001$) (Fig. 4.8.E). Again it is observed that both global and pan-neuronal expression of *Rab8* in a *Rab8* mutant background is sufficient to rescue the significantly increased cumulative bouton size seen in *Rab8* mutants, with rescues showing no significant difference to wildtypes or controls yet a significant difference to *Rab8* mutants (post-hoc student t-test $p < 0.001$ for both) (Fig. 4.8.E). Muscle expression of *Rab8* in a *Rab8* mutant background again appears to show only a partial rescue displaying a significant difference from *Rab8* mutants (post-hoc student t-test $p < 0.001$) and no significant difference from wildtypes, although a small variance from the MHC-gal4/UAS-*Rab8* control (post-hoc student t-test $p < 0.05$) (Fig. 4.8.E).

Taken together the results for characterisation of *Rab8* mutant NMJ morphology and rescue experiments suggests that *Rab8* mutants display a significant perturbation to normal NMJ growth and development, displaying a significant increase in bouton number, NMJ length, satellite bouton number and cumulative bouton size. They also display a reduction in bouton size, although no apparent variation in branching. Rescues also suggest that expression of *Rab8* globally and pre-synaptically is sufficient to rescue the morphological perturbations seen in *Rab8* mutants. In contrast muscle rescues were only capable of inducing, at best, a partial rescue.

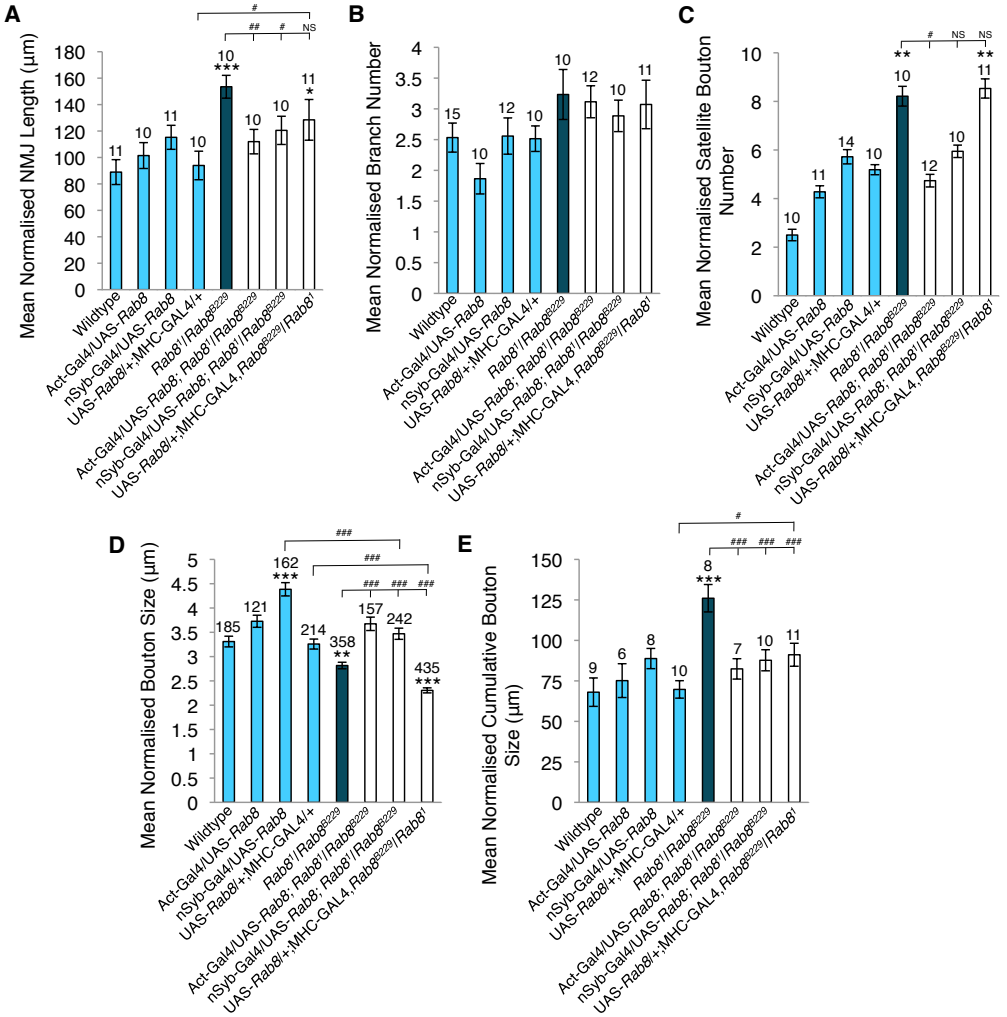

Figure 4.8. *Rab8* Mutants Display a Comprehensive Unregulated NMJ Growth Phenotype
Quantification of NMJ morphology at muscle 4, hemi-segment A3, of 3rd instar larvae. (**A**) *Rab8* mutants (*Rab8*^{1}/*Rab8*^{B229}) show a significantly increased mean normalized NMJ length (µm) that can be completely rescued by global (actin-gal4) and pre-synaptic pan-neuronal (nSyb-Gal4) expression of *Rab8*. Muscle expression (MHC-Gal4) of *Rab8* induces a partial rescue. (ANOVA: F(d.f. 7) = 5.2069; $p < 0.001$ with post-hoc Dunnett's comparison to control (WT) *** $p < 0.001$, * $p < 0.05$ and post-hoc student t-test comparison between groups, ## $p < 0.01$, # $p < 0.05$. (**B**) *Rab8* mutants show no significant variation in mean normalized branch number compared to wildtype controls (ANOVA: F(d.f. 7) = 2.2562; $p < 0.05$ with post-hoc Dunnett's comparison to control (WT), n/s between any genotype and WT. (**C**) *Rab8* mutants show a significant increase in the number of mean normalized satellite boutons compared to wildtypes. This increase can be rescued by global and pre-synaptic expression of *Rab8*, but not by post-synaptic *Rab8* expression (ANOVA: F(d.f. 7) = 2.6923; $p < 0.05$ with post-hoc Dunnett's comparison to control (WT), ** $p < 0.01$ and post-hoc student t-test comparison between groups, # $p < 0.05$. (**D**) *Rab8* mutants show significantly reduced mean normalized synaptic bouton size, compared to wildtypes. This overgrowth can be rescued by global and pre-synaptic expression of Rab8 but not by post-synaptic expression of *Rab8*, which actually potentiates reduced bouton size. Neuronal Expression of Rab8 induces a significant increase in synaptic bouton size, compared to wildtype. (ANOVA: F(d.f. 7) = 48.1829; $p < 0.001$ with post-hoc Dunnett's comparison to control (WT) *** $p < 0.001$, ** $p < 0.01$ and post-hoc student t-test comparison between groups, ### $p < 0.001$. (**E**) Despite showing reduced bouton size the mean normalised cumulative bouton size in *Rab8* mutants is significantly increased compared to wildtypes, a phenotype that can be completely rescued by global and neuronal expression of Rab8 and partially rescued by post-synaptic expression of Rab8 (ANOVA: F(d.f. 7) = 5.9508; $p < 0.001$ with post-hoc Dunnett's comparison to control (WT) *** $p < 0.001$ and post-hoc student t-test comparison between groups, ### $p < 0.001$, # $p < 0.05$.

Drosophila larval muscles are innervated by differential populations of synaptic boutons of variable size, for example type-Is and type-Ib (Gramates and Budnik, 1999). As such, having observed a reduction in mean normalised bouton size in *Rab8* mutants it proves useful to analyse the distribution of bouton sizes. Here it is demonstrated that not all *Rab8* mutant boutons are smaller, rather reduced mean bouton size is associated with an increase in the population of small, 2 to 3 µm diameter, boutons (Fig. 4.9.). These bouton sizes correspond approximately with those of type-Is boutons, however the estimated size of type-Is boutons varies between studies.

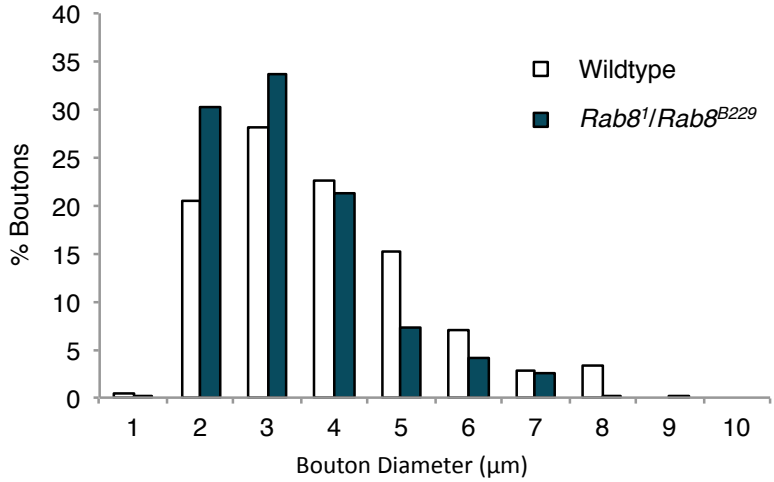

Figure 4.9. *Rab8* Mutants Display an Increased Percentage of Smaller Boutons
Frequency distribution of bouton sizes demonstrates that *Rab8* mutants show an increased percentage of boutons of 2-3 µm diameter whilst wildtypes show more larger diameter boutons.

4.2.4. *Rab8* Mutants Display Limited Disruption to Pre- and Post-Synaptic Markers at a Histological Level

Rab8 has, previously, been implicated in the regulated cycling and trafficking of AMPA receptors during both constitutive receptor recycling and during long-term potentiation events (Brown et al., 2007b; Gerges et al., 2004b). Furthermore expression of *Rab8* has been shown to increase mGluRIA cell surface expression, through antagonisation of receptor endocytosis, and attenuate intracellular calcium release, through inhibition of mGluRIA induced ionositol phosphate formation (Esseltine et al., 2012). Five ionotropic glutamate receptor subunits are expressed at the *Drosophila* NMJ, GluRIIA, GluRIIB, GluRIIC (also known as GluRIII), GluRIID and GlurIIE (Featherstone et al.,

2005). Each receptor forms a tetrameric complex composed of core subunits GluRC-E and either GluRIIA or GluRIIB (Featherstone et al., 2005). In order to determine whether Rab8 is involved in GluR trafficking and localisation at the *Drosophila* NMJ the localisation and distribution of these receptors was observed in *Rab8* mutants and compared to wildtypes. Here it is demonstrated that there is no obvious perturbation to GluRIIA or GluRIIB (Fig.4.10.) localisation and distribution at the NMJ in *Rab8* mutants. There was also no disruption seen to GluRIIC.

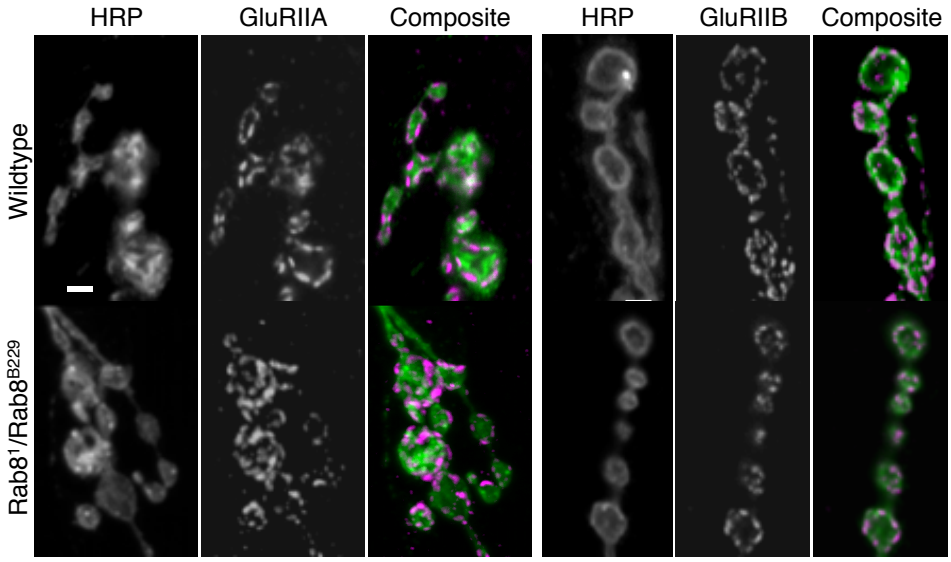

Figure 4.10. Glutamate Receptors at the Drosophila NMJ Show no Perturbation to Localisation and Distribution in *Rab8* Mutants.
Glutamate receptor distribution at the 3rd instar larval m6/7, hemi-segment A3, NMJ. HRP was used to stain the NMJ (green in composite). Scale Bar = 2 µm.

With no apparent perturbation to normal GluR localisation at the NMJ analysis turned to the pre-synaptic nerve terminal. Glutamate receptors cluster at the post-synaptic density directly apposing glutamatergic active zones, the sites of neurotransmitter release (Kim et al., 2012). Analysis of the presynaptic active zone marker nc82, which identifies the active zone protein bruchpilot, again showed no obvious disruption to normal bruchpilot distribution (Fig.4.11.). Similarly other presynaptic markers including the microtubule associated protein Futsch/22c10, a marker of presynaptic microtubule bundle integrity, and HRP showed no discernable perturbation in *Rab8* mutants. Neither did the pre- and post-synaptic cell adhesion molecule Fasciclin-II (Fas-II), which is essential for

postembryonic development of the NMJ (Kohsaka et al., 2007; Sanchez-Soriano and Prokop, 2005).

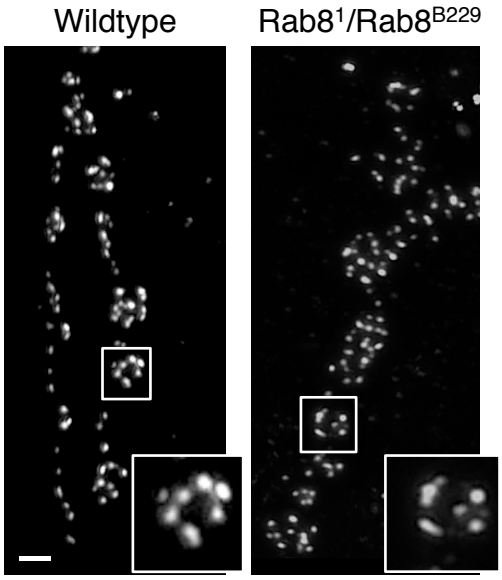

Figure 4.11. *Rab8* Mutants Display no Notable Disruption to Active Zone Localisation and Distribution.
Rab8 mutant larvae show no clear disruption to normal distribution and localisation of the active zone marker nc82, which labels bruchpilot, at the muscle 6/7 hemi-segment A3 NMJ of 3rd instar larvae. Scale Bar = 2 µm.

Structural alterations at the NMJ are an essential part of the dynamic processes associated with synaptic growth and remodelling, with synaptic boutons continuously added and eliminated at the NMJ (Chung and Barres, 2009; Fuentes-Medel et al., 2009). This allows for modulation of connectivity between the pre-synaptic nerve terminal and the post-synaptic muscle and is often regulated by neural activity (Chung and Barres, 2009; Fuentes-Medel et al., 2009). Interestingly it has been shown that addition of new synapses, at the NMJ, is a relatively wasteful process, associated with a production of significant amounts of pre-synaptic debris and the detachment of undifferentiated boutons known as “ghost boutons” (Fuentes-Medel et al., 2009). Production and clearance of debris and ghost boutons has been shown as fundamental to regulating normal NMJ expansion (Fuentes-Medel et al., 2009). Ghost boutons appear to be undifferentiated boutons that have failed to mature, containing some components of a mature bouton but remaining devoid of both pre- and post-synaptic compartments (Ataman et al., 2006a; Packard et al., 2002). They fail to recruit post-synaptic proteins or associate with the post-synaptic density

and, as such, are readily identifiable as synaptotagmin positive boutons lacking post-synaptic Dlg immunoreactivity (Ataman et al., 2006a; Packard et al., 2002). Dlg, a PDZ domain containing scaffolding protein and orthologue of mammalian PSD-95, has been implicated as a regulator of normal synaptic assembly and function through regulation of PSD assembly (Ataman et al., 2006b; Zhang et al., 2007). In order to determine whether increased synaptic expansion in *Rab8* mutants is associated with a perturbation to the normal clearance of undifferentiated ghost boutons the number of ghosts was compared between mutants and wildtypes. No variance was observed (Table. 4.2.). Identification of ghost-boutons also allows for simultaneous observation of synaptic retractions. As mentioned Dlg is a scaffolding protein within the PSD and has been implicated in the clustering and stabilization of GluRIIB, as well as regulating the expansion and development of the SSR. SSR development and clustering of proteins, including Dlg, within the PSD has been shown to require neuronal innervation of the muscle (Featherstone et al., 2002). As such it has been established that the presence of assembled highly organized Dlg at the PSD unapposed by a pre-synaptic terminal identifies a location where a pre-synaptic terminal formed and since retracted, this is termed a “footprint” (Eaton et al., 2002). Again it is demonstrated that *Rab8* mutants show no significant variation in the number of synaptic retractions observed when compared to wildtypes (Table. 4.2.).

Table 4.2. *Rab8* Mutants Shown no Variance in the Number of Ghost-boutons or Synaptic Retractions Observed, Compared to Wildtype

Genotype	NMJ’s Showing Ghost Boutons	NMJ’s Showing Synaptic Retraction
Wildtype	0/100	1/100 (1%)
$Rab8^{1}/Rab8^{B229}$	0/103	1/103 (0.97%)

4.2.5. *Rab8* Mutants Display Ultrastructural Aberrations

Having observed little disruption to either pre- or post-synaptic markers, at a histological level, the ultrastructure of *Rab8* mutants was examined. TEM analysis of individual synaptic boutons revealed that *Rab8* mutants displayed a significantly increased abundance of large clear vesicles (ANOVA: $F(d.f.\ 1) = 4.9635$; $p < 0.05$) (Fig. 4.12.A-B), a number of which contain further intralumenal vesicular structures, that can often be observed budding from the primary vesicle membrane (Fig. 4.12.D). Whilst visible in wildtype sections these large clear vesicles were significantly more abundant in mutant sections. Furthermore quantitative analysis reveals that these vesicles are, on average, significantly larger in *Rab8* mutants than wildtypes (ANOVA: $F(d.f.\ 1) = 55.1122$; $p < 0.001$) (Fig. 4.12.C).

At an ultrastructural level *Drosophila* active zones are characterised by the presence of electron dense membrane as well as electron dense specialisations known as T-bar ribbons or T-bars (Clarke et al., 2012; Zhai and Bellen, 2004). T-bars are so called due to their characteristic appearance in TEM sections, comprised of a pedestal with a large overhanging top giving rise to their T appearance. During analysis of TEM sections it was noted that numerous *Rab8* mutant sections showed the presence of T-bars containing 2 distinct pedestals, a phenotype that was never observed in wildtype sections (Fig. 4.12.E).

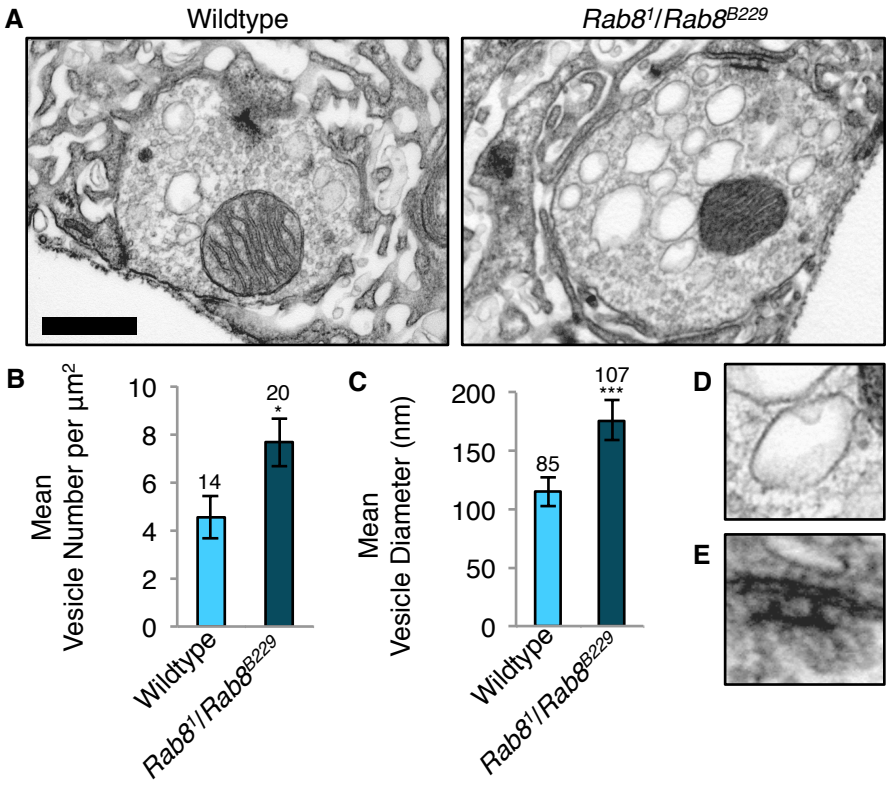

Figure 4.12. *Rab8* Mutants Show Large Clear Vesicles Within Synaptic Boutons
(**A**) *Rab8* mutant synaptic boutons at muscle 6/7, hemi-segment A3, of 3rd instar larvae show ultrastructural aberrations characterised by (**B**) a significant increase in large clear vesicles (ANOVA: $F(d.f.\ 1) = 4.9635$; $p < 0.05$) that display (**C**) a significant increase in mean diameter (ANOVA: $F(d.f.\ 1) = 55.1122$; $p < 0.001$). (**D**) Large clear vesicles often display smaller intralumenal vesicles seen budding from the primary diameter membrane. (**E**) *Rab8* mutants also display the presence of T-bar ribbons displaying double pedestal. Scale bar = 500 nm.

Further to ultrastructural perturbations seen within *Rab8* mutant boutons abnormalities were also observed within the CNS, within cell bodies in the VNC. Here a number of large, multi-lamellar, membranous, electron-dense structures were observed. These structures were often seen budding from the cell plasma membrane (Fig. 4.13. arrow head) and frequently contained smaller membranous structures and vesicles (Fig. 4.13. arrows). Such structures were rarely seen within wildtypes, and when they were they were typically smaller and less complex. Similar multi-lamellar structures were also observed within the muscles of *Rab8* mutants (Fig. 4.14.A-C). Furthermore large clear vesicle structures often containing small intraluminal vesicles similar, but much larger, to those observed within the *Rab8* mutant boutons were also observed in mutant muscles (Fig. 4.14.D-E).

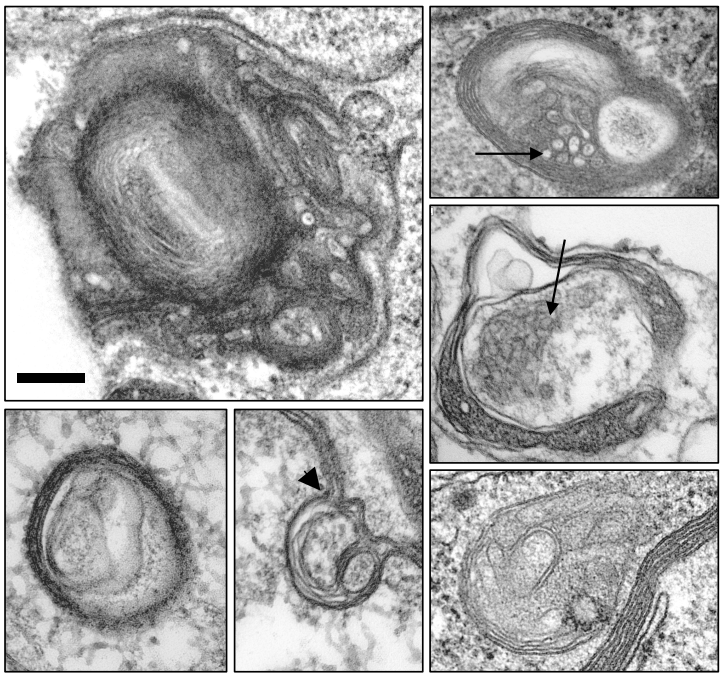

Figure 4.13. *Rab8* Mutants Display Large, Multi-lamellar, Membranous Structures Within Cell Bodies in the Ventral Nerve Cord
TEM analysis of cell bodies within the ventral nerve cord (VNC) of 3rd instar wandering larvae revealed that *Rab8* mutants display a large number of multi-lamellar structures, that can be seen budding from the cell membrane. Scale Bar = 200 nm.

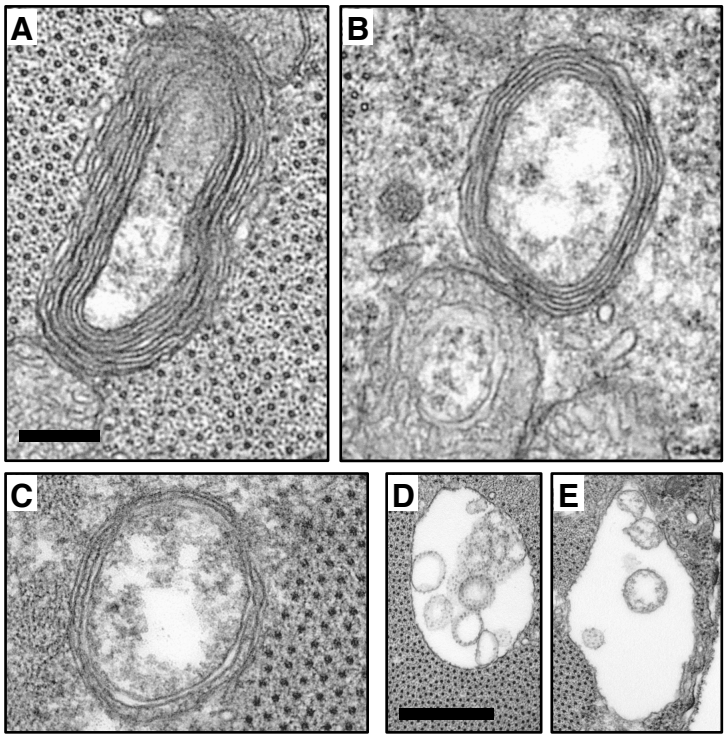

Figure 4.14. *Rab8* Mutants Display Large, Multi-lamellar, Membranous Structures and Large Vesicular Structures Within Abdominal Muscles
(**A-C**) *Rab8* mutants display large multi-lamellar structures and (**D-E**) clear vesicle structures within the muscles of 3rd instar wandering larvae. Scale Bars: A-C = 500 nm, D-E = 200 nm.

Additionally examination of *Rab8* mutant muscle ultrastructure also revealed a distinctive mitochondrial phenotype, characterised by mitochondria that appear stretched and interconnected by long projections. These mitochondria appear to have undergone division yet have failed to segregate through normal mitochondrial scission. Such mitochondria were observed, to different degrees of severity, within all *Rab8* mutants analysed, however were never seen in wildtypes. Mitochondria morphology appeared to only be perturbed within mutant muscles.

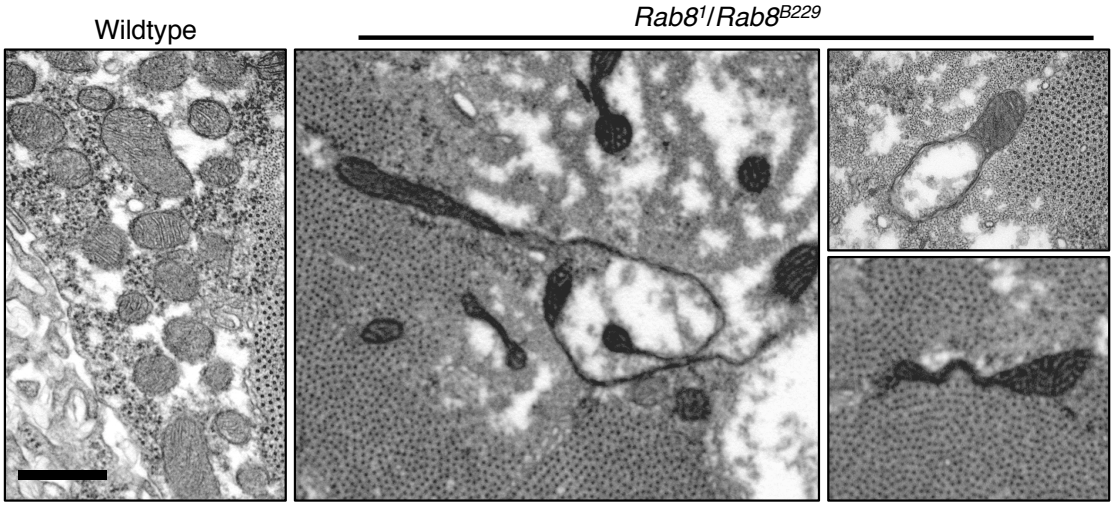

Figure. 4.15. *Rab8* Mutants Show Abnormal Mitochondrial Morphology Within Larval Muscles.
Drosophila 3rd instar wandering larvae show mitochondrial aberrations in Rab8 mutants. Muscle sections shown are from muscle 6/7, hemi-segment A3. Scale Bar = 200nm

4.2.6. *Rab8* Mutants Display Perturbations to Normal Endosomal-Lysosomal and Autophagic Markers

Having observed enlarged endosome-like vesicles and multi-lamellar structures, at an ultrastructural level, in *Rab8* mutants' investigation moved to determine whether mutants display a perturbation to normal endosomal-lysosomal and autophagic markers.

Previous investigation has identified a role for Rab8 in endocytic recycling, where it has been shown to localise to recycling endosomes (Hattula et al., 2006; Roland et al., 2007). It has also been demonstrated that recycling can

occur via different pathways. For example fast recycling occurs in a Rab4 and Rab35 dependent manner, trafficking components from the early endosome to the plasma membrane (Kouranti et al., 2006; Macia et al., 2012). In contrast slow recycling involves trafficking of cargo from the early endosome to an endosomal recycling compartment (ERC) (Grant and Donaldson, 2009). It has been proposed that this ERC forms during maturation of the early endosome with the main body of the early endosome becoming a MVB with tubular structures separating off to become the tubular ERC (Grant and Donaldson, 2009; Horgan et al., 2010). The ERC and the slow recycling pathway can be identified by the presence of Rab11 (Horgan et al., 2010). Here it is demonstrated that markers of both fast (Fig. 4.16.A-B) and slow (Fig. 4.17.A-C) recycling appear decreased in both the VNC and NMJ's of *Rab8* mutants. Rab4, and therefore fast recycling, appears to be more significantly depleted than Rab11 (slow recycling).

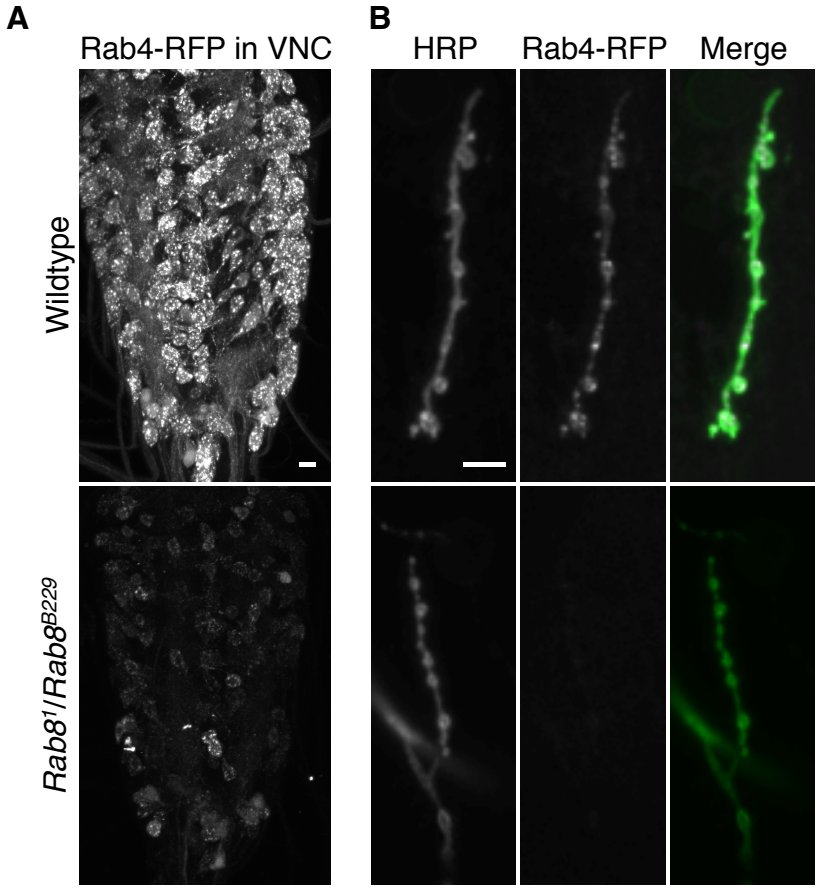

Figure 4.16. *Rab8* Mutants Display a Reduction in the Fast Endocytic Recycling Marker Rab4

Confocal immunofluorescence images of Rab4-RFP, expressed under the control of the pan-neuronal driver nSyb-Gal4, in (**A**) the ventral nerve cord and (**B**) NMJ of wildtype and *Rab8* mutant ($Rab8^{1}/Rab8^{B229}$) 3rd instar larvae. HRP is used as a marker of the NMJ. NMJ's are muscle 4,hemi-segment A3. Scale bars = 10 µm.

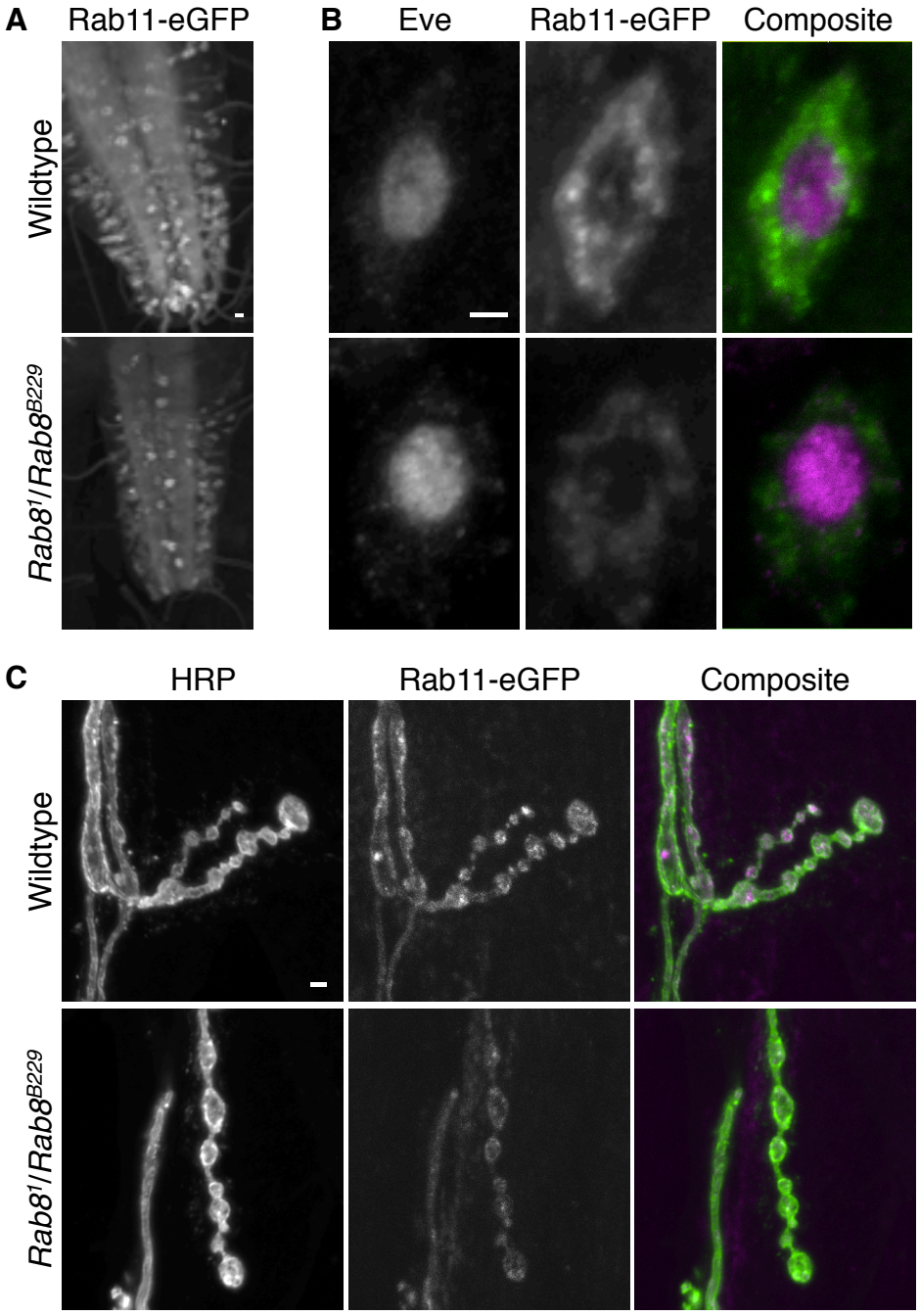

Figure 4.17. *Rab8* Mutants Display a Reduction in the Slow Endocytic Recycling Marker Rab11
Confocal immunofluorescence images of Rab11-eGFP, expressed under the control of the pan-neuronal driver nSyb-Gal4, in (**A**) the ventral nerve cord, (**B**) motor neuronal cell bodies and (**C**) NMJ's of wildtype and *Rab8* mutant ($Rab8^{1}/Rab8^{B229}$) 3rd instar larvae. Eve is used as a marker of motor neurons, HRP is used as a marker of the NMJ. NMJ's are muscle 6/7, hemi-segment A3. Scale bars; (**A**) = 10 µm, (**B-C**) = 2 µm.

In contrast to recycling endosome markers (Rab4-RFP and Rab11-eGFP) a marker of the late endosome (Spin-RFP) showed no variance between wildtype and *Rab8* mutants in either the VNC or NMJ. However a small reduction in the early endosome marker anti-Rab5 was observed at the NMJ (Fig. 4.18.).

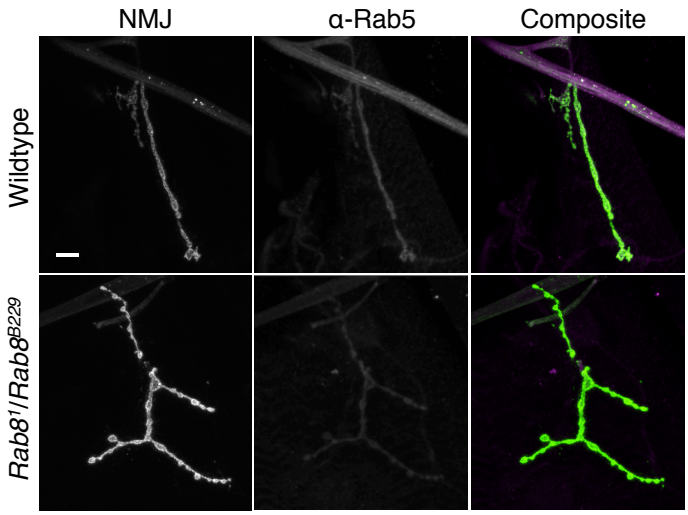

Figure 4.18. *Rab8* Mutants Display a Reduction in the Early Endosomal Marker Rab5 at the Larval NMJ
Confocal immunofluorescence images of anti-Rab5 at third instar larval, muscle 4, hemi-segment A3, NMJ's. NMJ is labelled with HRP. Scale bar = 10 µm.

Perhaps the most significant perturbation was observed in the late endosome/lysosome marker LAMP-GFP, which displayed aggregations throughout the VNC, predominantly in the neuropil region, and in axon bundles projecting from the VNC in *Rab8* mutants (Fig. 4.19.A). In addition to perturbations to endosomal and lysosomal-markers there was also demonstrated to be a significant diminution in the autophagosome marker Atg8-RFP, observed in the VNC of *Rab8* mutants, when compared to wildtypes (Fig. 4.19.B).

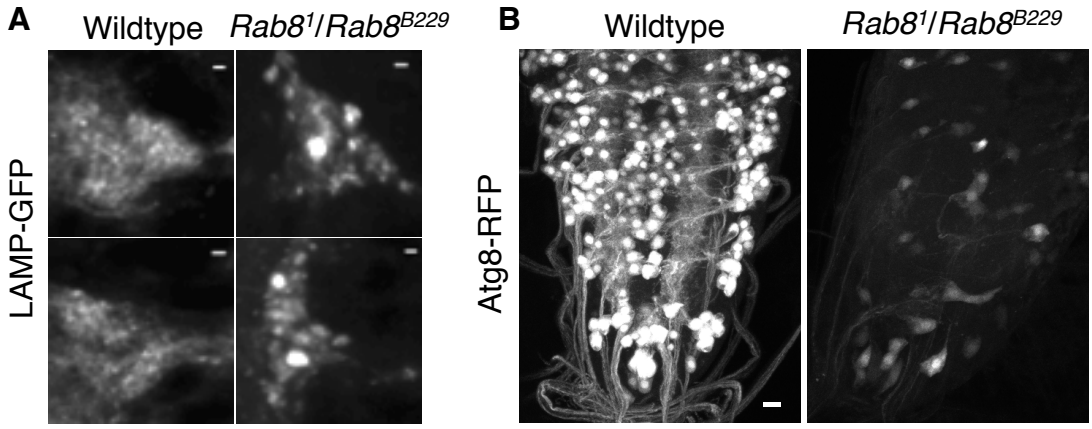

Figure 4.19. *Rab8* Mutants Display Abnormal Accumulations of the Late Endosome/Lysosome Marker LAMP and a Decrease in the Autophagosome Marker Atg8
Confocal immunofluorescence images of (**A**) the late endosomal/lysosomal marker LAMP-GFP, expressed under the control of the pan-neuronal marker nSyb-Gal4, focusing on accumulations within the neuropil. Scale Bar = 2µm. (**B**) The autophagosome marker Atg8/LC3-RFP, under the control of nSyb-Gal4, in the ventral nerve cord of 3rd instar larvae. Scale bar = 10 µm.

Taken together the results presented here demonstrate that *Rab8* mutants display a clear perturbation to normal endosomal-lysosomal and autophagic trafficking pathways. In comparison to wildtypes, mutants show an apparent diminution of recycling endosome (Rab4 and Rab11), early endosome (Rab5) and autophagosome (Atg8/LC3) markers. In addition they display an accumulation of late endosome/lysosome (LAMP) aggregations.

4.2.7. *Rab8* Mutants Display Perturbed Synaptic Transmission That Does Not Affect Physiological Crawling Behaviour

4.2.7.1. Unregulated NMJ Growth Does Not Affect Larval Crawling

Drosophila larval locomotion is a relatively complex and highly regulated behavioural process characterised by distinct subsets of behaviour, including linear crawling and burrowing (Heckscher et al., 2012). The former typically occurs when larvae are exploring their environment in search of nutrition or during an escape response, with larvae observed to crawl faster when starved (Koon et al., 2011; Steinert et al., 2006). Larval crawling occurs through bilaterally synchronized peristaltic waves of muscle contraction propagating longitudinally through abdominal segments along the larval body, in the direction of movement (Hughes and Thomas, 2007). For example from posterior to anterior when crawling forward. This process is highly coordinated through controlled communication and functional activity of both central and peripheral synapses, as well as functional muscle activity (Hughes and Thomas, 2007). It has, however, been shown that coordinated propagation can occur in the absence of sensory feedback and descending input from the brain due to regulation by autonomous neuronal circuitry associated with a central pattern generator (CPG) (Gjorgjieva et al., 2013). Larval crawling provides a robust measure of physiological output relating to NMJ activity, with crawling activity demonstrated to act as a modulator of NMJ growth (Tsai et al., 2012). Here it is demonstrated that the unregulated growth observed in all *Rab8* transheterozygous mutants does not correlate with perturbations to larval

crawling velocity, with only one transheterozygous *Rab8* mutant genotype displaying a significant reduction in larval crawling speed (Fig. 4.20.).

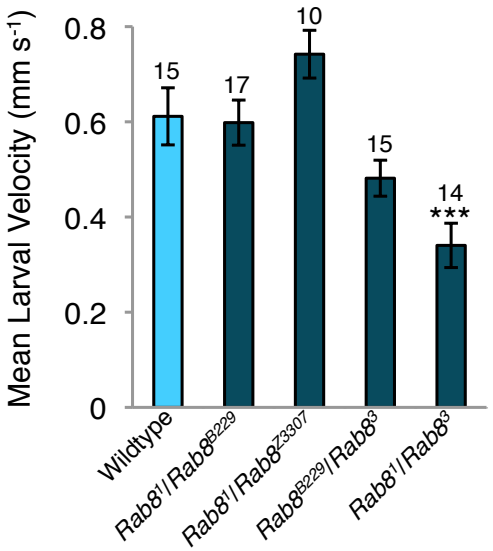

Figure 4.20. *Rab8* Mutants do Not Show a Conserved Perturbation to Locomotor Activity
Rab8 mutant third instar larvae show limited perturbation to normal NMJ physiological output with only one transheterozygous genotype ($Rab8^{1}/Rab8^{3}$) displaying a significant reduction in larval crawling speed (ANOVA: $F(d.f.\ 4) = 8.2890$; $p < 0.001$ with post-hoc Dunnett's comparison to control (WT); *** $p < 0.001$).

4.2.7.2. *Rab8* Mutants Show Aberrations to Normal Synaptic Transmission

Larval crawling provides a relatively simple and robust readout of physiological function. It is, however, a highly complex process regulated by intricate interconnected neural pathways and, as such, must be used in conjunction with other approaches in order to fully elucidate the effect of mutations upon normal neural function. Here electrophysiological recordings were used in order to determine the effect of mutant *Rab8* upon normal synaptic transmission. These recordings were conducted by Bruno Marie (University of Puerto Rico, Puerto Rico). Here it is shown that *Rab8* mutants ($Rab8^{1}/Rab8^{B229}$) display a significant reduction in the amplitude of mini excitatory post-synaptic potential's (mEPSP's) (student t-test $p < 0.001$) (Fig. 4.21.). A mEPSP correlates to the spontaneous fusion of a single synaptic vesicle with the pre-synaptic membrane, releasing neurotransmitter into the synapse, in the absence of presynaptic stimulation (Schwarz, 2006). This data also reveals that *Rab8* mutants display a significantly increased evoked EPSP amplitude (student t-test $p < 0.05$) coupled

with a significant increase in quantal content (student t-test $p < 0.001$). Quantal content can be defined as the number of effective synaptic vesicles released in response to presynaptic stimulation and can be quantified by measuring the EPSP and dividing it by the mEPSP (Schwarz, 2006). Taken together these data suggest that mutations in *Rab8* induce an aberration to normal synaptic transmission, associated with synaptic overgrowth, however normal physiological function, in terms of larval crawling, remains unaffected.

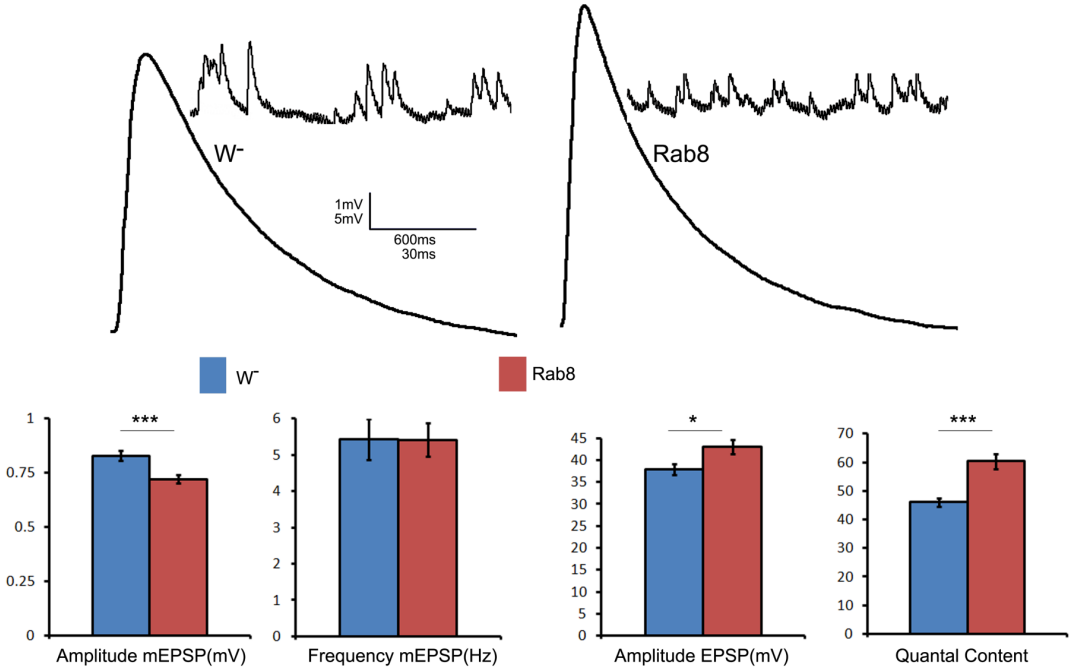

Figure 4.21. *Rab8* Mutants Display Aberrations to Normal Synaptic Transmission

Rab8 mutants ($Rab8^{1}/Rab8^{B229}$) display a significant reduction in normal mini excitatory post-synaptic potential (mEPSP) amplitude coupled with an increase in both EPSP amplitude and quantal content. The frequency of mEPSP's showed no variance from wildtypes (w^{-}). n = 20 per genotype. Statistical analysis = student t-test, *** $p < 0.001$, * $p < 0.05$. Electrophysiology and production of this figure was by Bruno Marie (University of Puerto Rico, Puerto Rico).

4.3. Discussion

4.3.1. Mutations in *Rab8* Affect Conserved Functional Domains and Are Detrimental to Survival

Currently there are very few *Rab8* mutants, within any *in vivo* system, in which to study Rab8 function. Furthermore, to a certain degree the study of Rab8 function in many higher organisms is hindered both by genetic redundancy and

the known role of Rab8 in ciliogenesis. For example it has been demonstrated that both *Rab8* mutant and knock-out mice present with shortening of microvilli within the intestines leading to a marked reduction in nutrient absorption, diarrhoea and, ultimately, premature death 3 to 5 weeks after birth (Sato et al., 2007a). In contrast *Drosophila* do not possess intestinal cilia with cilia restricted to just two specific cell types; spermatozoa and sensory neurons (Ma and Jarman, 2011). As such *Rab8* mutants in *Drosophila* may provide an insightful model in which to study the role of Rab8 outside of ciliogenesis and within other polarized cell types, such as neurons. This research presents, to our knowledge, the first known characterisation of *Rab8* mutants in *Drosophila*.

Complementation analysis reveals that all 4 randomly induced point mutations fail to complement one another as well as the $Rab8^{B229}$ piggyBac insertion, indicating each of these mutations affects *Rab8* gene function in their own right. Furthermore complementation reveals a distinct pharate lethal phenotype indicating that *Rab8* is essential for normal viability. Whilst Rab8 mutant mice die prematurely due to perturbations in nutrient uptake it can be hypothesised that this is not the cause of lethality in *Drosophila*. Late pharate lethality indicates that mutants are capable of progressing through the larval stages, at which point normal nutrient uptake is essential. Furthermore as mentioned previously *Drosophila* do not possess primary cilia within the intestine, eliminating perturbed ciliogenesis of intestinal villi as a cause of lethality. Instead lethality suggests a further essential role of *Rab8* in viability, potentially within the development of other polarized cell types such as neurons. Such a hypothesis is supported by observation of the pharate lethal phenotype, which has been commonly associated with *Drosophila* models of neuronal and/or muscle dysfunction (Colodner and Feany, 2010; Torroja et al., 1999; Weiss et al., 2012). This is corroborated by identification of neuronal perturbations in *Rab8* mutants, which shall be discussed in detail in the following section (4.3.2.).

Sequence analysis of *Rab8* mutants corroborates complementation analysis, demonstrating that each mutation independently affects the *Rab8* gene locus. Furthermore they provide significant insight into the effect of each mutation

upon *Rab8* function. For example both $Rab8^{1}$ and $Rab8^{3}$ display an alteration to amino-acid residues located within the G-domains, essential for normal GTPase activity. Interestingly whilst these results reveal the $Rab8^{1}$ mutation falls within the G1 motif the specific residue it affects is not conserved in the Rab family (Li and Liang, 2001; Urano et al., 2000). It has, however, been demonstrated that within other Ras-superfamily members including Ras, Rho and Ran this residue is a highly conserved and functionally important glycine (Li and Liang, 2001; Urano et al., 2000). The lack of conservation of this residue in Rab proteins has long been noted as surprising due to its importance in other Ras proteins (Li and Liang, 2001). It has, however, been noted that the same mutation as seen in $Rab8^{1}$, S17F, in Rab5 results in a significant loss of function, indicating that whilst not conserved in Rabs this residue is of functional significance (Li and Liang, 2001). In contrast to $Rab8^{1}$ the results show that the $Rab8^{3}$ mutation affects a highly conserved threonine residue, within the G2 motif, that has a proven essential role in Mg^{2+} binding and GTPase activity (Bourne et al., 1991). All Rab proteins require Mg^{2+} as a cofactor for GTPase activity (Zhang et al., 2000). For example it has been demonstrated that Mg^{2+} depletion abolishes GTP binding by Rab3, resulting in undetectable levels of intrinsic GTPase activity (Burstein and Macara, 1992; Zhang et al., 2000). Thus we can infer that the $Rab8^{3}$ mutation is likely to significantly perturb normal Rab8 GTPase function. Contrary to both the $Rab8^{1}$ and $Rab8^{3}$ mutations the effect of the $Rab8^{2}$ and $Rab8^{Z3007}$ mutations is far less obvious. The results of in silico analysis suggests that $Rab8^{Z3007}$ acts to destabilise Rab8 protein structure, however further analysis will have to be carried out to confirm the specific effects of this mutation upon protein structure. In contrast whilst both experimental evidence and in silico analysis demonstrate the $Rab8^{2}$ mutation to have a deleterious effect upon Rab8 function the cause of such an effect is unclear. In silico analysis suggests this mutation does not destabilize protein function however unlike $Rab8^{1}$ and $Rab8^{3}$ it does not fall within one of the 5 G-motifs fundamental for GTPase function. Further observations also show that this mutation does not fall within any known protein binding sites within the *Rab8* sequence. One may postulate that the nature of the amino acid substitution from a hydrophilic serine residue to a hydrophobic phenylalanine is likely to induce steric hindrance and perturb the normal protein.

Whist these findings provide a useful characterisation of the nature of each mutation, revealing a deleterious effect of each upon *Rab8* function further analysis will be required to fully elucidate their effect upon protein structure and function. During this investigation an antibody was raised against Rab8 (see section 2.4.1.) however it proved unsuccessful for determination of levels of Rab8 protein via western blotting in *Drosophila*. Similarly commercial Rab8 antibodies (BD, Transduction Laboratories) were unsuccessful for western blotting. As such whilst further analysis is required for determination of the effect of each mutation on protein structure and function the focus of this investigation is to determine the effect of these mutations on neuronal development and function and thus elucidate the role of Rab8 in neurons.

4.3.2 A Pre-Synaptic Complement of Rab8 is Essential For Normal NMJ Growth

It has previously been demonstrated that Rab8 is enriched within the nervous system, with the mammalian Rab8B isoform found in greatest abundance within the brain (Chan et al., 2011; Lau and Mruk, 2003). The results of this investigation substantiate these previous findings showing enrichment of Rab8 within the *Drosophila* nervous system. Furthermore they demonstrate *Rab8* to be expressed throughout the larval brain with significant expression within neurons, although also expressed in glia. Having identified this neuronal pattern of expression *Rab8* was subsequently shown to be expressed in motor neuronal subtypes. This allowed for use of the *Drosophila* larval NMJ as a model system to characterise the effects of *Rab8* mutations upon neuronal morphology and function.

Rab8 has been implicated in the development of polarised cells, including neurons. For example it has been demonstrated to be important for normal neurite outgrowth as well as the regulated cycling and delivery of AMPA receptors into dendritic spines (Brown et al., 2007a; Gerges et al., 2004a; Huber et al., 1995a). With this previous implication in neuronal development and having shown here that *Rab8* mutants display a pharate lethal phenotype, a

phenotype commonly implicated in neuronal or muscle dysfunction, it was investigated whether *Rab8* mutants showed any perturbation to normal NMJ development (Colodner and Feany, 2010; Torroja et al., 1999; Weiss et al., 2012). The results of this investigation implicate Rab8 as a potent regulator of normal NMJ development, with all transheterozygous *Rab8* mutants displaying a significant synaptic overgrowth phenotype at multiple model NMJ's (4 and 6/7).

Rab8 has previously been implicated in a "Rab cascade" acting sequentially with Rab11 in a number of biological processes conserved within eukaryotic cells (Khandelwal et al., 2013; Knodler et al., 2010; Westlake et al., 2011). For example in neurons Rab8 has been shown to act sequentially with Rab11 in the regulated cycling and delivery of AMPA receptors into dendritic spines (Brown et al., 2007b; Gerges et al., 2004b). Furthermore Rab11 has been implicated as a regulator of the Rab8 GEF, rabbin8 (Knodler et al., 2010). Rab8 and Rab11 have also been shown to act in combination to regulate slow recycling within the endocytic pathway (Grant and Donaldson, 2009; Rowe et al., 2008). As such it is interesting to observe that whilst *Rab8* and *Rab11* mutants both show significant synaptic overgrowth the overgrowth phenotype seen is significantly different between the two. For example whilst we show here that *Rab8* mutants display a general overgrowth phenotype, characterised by increased NMJ length, bouton number, satellite bouton number and cumulative bouton size, as well as reduced individual bouton sizes, *Rab11* mutants, in contrast, are characterised by an increase in branching and overproliferation of satellite boutons, a hallmark of endocytic mutants (Khodosh et al., 2006). These findings suggest that Rab8 and Rab11 may not necessarily act within the same pathway in the regulation of normal neuronal growth and development. Interestingly the overgrowth phenotype observed in *Rab8* is more akin to the overgrowth phenotypes observed in other *Drosophila* mutants, including the late endosomal/lysosomal protein *spin* and the E3 ubiquitin-protein ligase *hiw*. Analogous to *Rab8* mutants both *spin* and *hiw* mutants display an increase in synaptic bouton number and NMJ length coupled with a reduction in synaptic bouton size (Collins et al., 2006; Milton et al., 2011; Sweeney and Davis, 2002; Wan et al., 2000). In contrast, however, to *Rab8* mutants these mutants also

display an increase in branching. *Spin* and *Rab8* show similar sized overgrowths in terms of increased bouton number and NMJ length whilst overgrowth in *hiw* is significantly greater. The similarity in the overgrowth phenotypes seen in *Rab8*, *spin* and *hiw* mutants may suggest a conserved mechanism behind the overgrowth. This shall be explored in detail in the following chapter.

A notable difference between *spin* and *hiw* is their site of action in the regulation of synaptic growth. For example hiw has been shown to act entirely pre-synaptically whilst spin acts within both the pre- and post-synaptic compartments equally (McCabe et al., 2004; Sweeney and Davis, 2002; Wan et al., 2000). The experimental evidence presented here suggests that Rab8 acts predominantly within the presynaptic compartment with pre-synaptic expression of wildtype *Rab8* sufficient to rescue all aspects of the *Rab8* mutant overgrowth. In contrast post-synaptic expression of *Rab8* is only sufficient to partially rescue overgrowth, rescuing increased bouton number at muscle 6/7 but only partially rescuing increased bouton number at muscle 4. Similarly postsynaptic expression of *Rab8* also only partially rescues NMJ length, and cumulative bouton size whilst showing no ability to rescue increased satellite bouton number. This observation that post-synaptic expression of *Rab8* is capable of partially rescuing some aspects of the overgrowth phenotype, despite presynaptic expression completely rescuing overgrowth, suggests a possible post-synaptic function for Rab8 in the regulation of NMJ growth. This may be explained by the ultrastructural phenotypes observed in *Rab8* mutant muscles, discussed in detail in section 4.3.4. Here it was demonstrated that *Rab8* mutants show significant perturbations to normal mitochondrial morphology. Such mitochondrial disruption would likely cause significant levels of oxidative stress, which has previously been shown to induce synaptic overgrowth from a post-synaptic compartment, for example in *spin* mutants (Milton et al., 2011). Oxidative stress would likely act to potentiate overgrowth induced by pre-synaptic Rab8 dysfunction, in a non-autonomous manner. Similarly neuronal expression of *Rab8* would likely provide robust protection against postsynaptic oxidative stress, explaining why presynaptic expression of *Rab8* offers a complete rescue whilst a partial rescue can be induced by a postsynaptic

complement of Rab8. Alternatively Rab8 may have a role in the regulation of post-synaptic processes that provide a retrograde signal to the developing presynaptic nerve terminal with a degree of redundancy to the potent pre-synaptic signals. In order to elucidate the post-synaptic role of Rab8 in the regulation of NMJ development future investigation may look to determine whether Rab8 mutants present with an oxidative stress burden. For example by using the *cap'n'collar* glutathione S-transferase D (GST-D) GFP reporter construct (Sykiotis and Bohmann, 2008, 2010). GST-D is an antioxidant expressed under oxidative stress conditions and has been previously shown to be unregulated in *Drosophila* mutants displaying synaptic overgrowth associated with oxidative stress burdens (Milton et al., 2011; Sykiotis and Bohmann, 2008, 2010).

The observation that *Rab8* mutants display a reduced bouton size whilst presynaptic overexpression of *Rab8* in a wildtype background induces a significant increase in synaptic bouton size strongly substantiates a presynaptic role for Rab8 in the regulation of normal bouton development. This is further corroborated by the identification of significant perturbations to normal bouton ultrastructure in *Rab8* mutants, discussed in detail in the following section 4.3.3.

Interestingly *Rab8* mutants show no apparent gross perturbation to pre- or post-synaptic markers at a histological level. As such we can infer that unregulated growth is unlikely to be associated with perturbation to normal assembly of either presynaptic active zones or the postsynaptic density. Such an observation provides little support for the role of Rab8 in the regulated trafficking of AMPA receptors (Brown et al., 2007b; Gerges et al., 2004b). However from this we may infer that the unregulated growth phenotype observed is more likely to associate with perturbations to normal growth signalling pathways rather than being a compensation to account for disruptions to normal active zones or the PSD. The perturbation of growth signalling pathways in *Rab8* mutants is investigated in detail in the following chapter.

Taken together these findings implicate Rab8 as a potent regulator of normal synaptic growth at the *Drosophila* NMJ. Furthermore they demonstrate that,

although ubiquitously expressed, Rab8 enrichment within the nervous system associates with a predominantly presynaptic function in the regulation of normal synaptic growth and development. Furthermore unregulated growth is likely to associate with perturbed growth signalling in *Rab8* mutants.

4.3.3 *Rab8* Mutants Display Perturbed Endosomal-Lysosomal and Autophagic Trafficking

Ultrastructural analysis of pre-synaptic boutons revealed a significant increase in the size and abundance of large clear vesicle structures, often containing further intralumenal vesicles. These structures are clearly distinct from MVB's. However they show a notable similarity to structures previously observed in the synaptic boutons of *Drosophila* expressing a dominant negative Rab5, (Rab5S43N) under the control of the pan-neuronal driver elav-Gal4 (Fig. 4.22.) (Wucherpfennig et al., 2003). Such structures have also been observed in mammalian Rab5S43N models and have been identified as endocytic recycling intermediates associated with perturbation to normal homotypic endosome fusion, a process that is regulated by Rab5 (Bucci et al., 1992; Wucherpfennig et al., 2003).

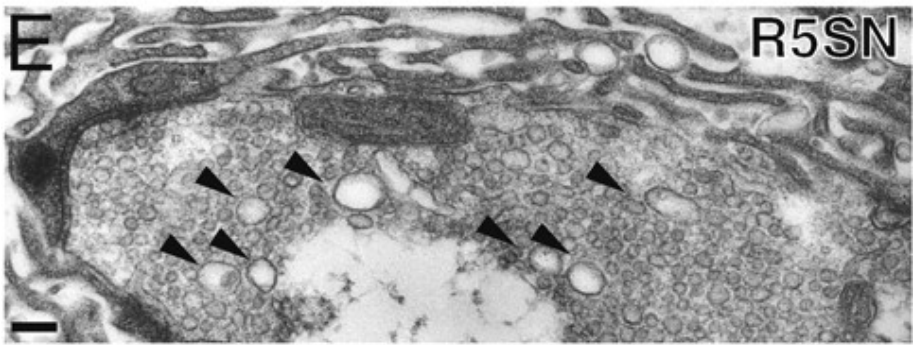

Figure 4.22. Expression of Dominant Negative Rab5 Neuronally Induces Accumulation of Endocytic Intermediates Identical to Those Observed in *Rab8* Mutants
Expression of the dominant negative Rab5 Rab5-S43N pan-neuronally using elav-Gal4 induced accumulation of endosomal intermediate structures with a distinct similarity to those observed in *Rab8* mutants. Scale Bar =100 nm. (Adapted From Wucherpfennig et. al (2003))

Similar structures have also been observed in Syndapin-I mutant mice (Koch et al., 2011). Syndapin-I has been identified as a neurally enriched isoform of

syndapin, a protein implicated in vesicle trafficking, neuronal morphogenesis and endocytosis, including clathrin-independent activity-dependent bulk endocytosis (ADBE), both pre- and post-synaptically (Quan and Robinson, 2013). During ADBE bulk endosomes are generated, through invagination of large regions of the plasma membrane, to form large endosomes (>100nm in diameter) (Quan and Robinson, 2013). Subsequently synaptic vesicles bud from activity dependent bulk endosomes forming a new population of synaptic vesicles to join the recycling pool. As such one might propose that the large endosome structures observed in *Rab8* mutants represent bulk endosomes associated with ADBE and that Rab8 has a role in regulation of this process. This supports previous hypotheses that Rab8 may act in an endosomal recycling process independent of clathrin mediated recycling. For example Rab8 has been shown to localize with Arf6, a known regulator of clathrin independent recycling (Hattula et al., 2006). Furthermore Rab8 has been implicated in the regulated delivery of AMPA receptors to dendritic spines, with evidence from *C. elegans* suggesting AMPA receptor pools are endocytosed in a clathrin independent, cholesterol dependent manner (Brown et al., 2007a; Gerges et al., 2004a; Glodowski et al., 2007). As previously mentioned Rab8 depletion has also been shown to induce endosomal accumulation of cholesterol (Linder et al., 2007). The observation of similar endosome-like structures in the muscles of *Rab8* mutants supports the hypothesis that these structures are more likely associated with endosomes than directly with a perturbation to normal synaptic vesicles. A perturbation to endosomal trafficking is supported by the results of immunofluorescence analysis of endosomal markers. The observation that both Rab4 and Rab11 recycling endosome markers appear decreased in *Rab8* mutants further supports a role for Rab8 in the recycling endosome pathway. It has also previously been shown, in separate studies, that depletion of Rab8 results in an accumulation of cellular cholesterol, which in turn inhibits Rab4 and disrupts normal membrane recycling (Choudhury et al., 2004; Linder et al., 2007). As such the results presented here support previous findings. Furthermore it has subsequently been shown that recycling endosomes contribute towards the formation of autophagosomes and as such an inhibition of endosomal recycling in *Rab8* mutants could explain the simultaneous decrease in autophagosome markers (Longatti et al., 2012; Puri

et al., 2013). It has also been shown that conversely, overexpression of the Rab8 effector optineurin regulates autophagosome formation, supporting the hypothesis that Rab8 is required for both endosomal recycling and autophagosome formation (Wild et al., 2011).

The observation of multi-lamellar, membranous structures in both the CNS and the muscles of *Rab8* mutants may further suggest a functional role for *Rab8* in the regulation of endosomal-lysosomal and autophagic processes. For example Lee et al. (2007) demonstrated that perturbation to normal ESCRT-III function, through depletion of the essential ESCRT-III component mSnf7-2 or expression of the FTD mutation *CHMP2B*^{Intron5}, induced significant neuronal degeneration, coupled with accumulation of autophagosomes. In this study they propose that autophagosome accumulation is likely the result of abnormal fusion between autophagosomes and late endosomes or lysosomes, and that this contributes to FTD pathogenesis. The autophagosome structures observed by Lee et al. (2007) show significant similarity to the multi-lamellar structures observed here in *Rab8* mutants (Fig. 4.23.). As such one may postulate that perturbation to normal autophagic processes in both *CHMP2B*^{Intron5} and *Rab8* mutants may explain why *Rab8* mutants potentiate the FTD toxicity of *CHMP2B*^{Intron5}, as well as *Shrub*-GFP. However as previously mentioned the autophagosome marker Atg8 was observed to be decreased in the VNC of *Rab8* mutants and therefore it is unlikely that these structures relate to mature autophagosomes. However one may postulate that these structures could represent immature autophagophore's or autophagic intermediates, supporting the idea that autophagosome formation may require the recycling endosome. Corroborating this hypothesis preliminary experiments have demonstrated that decreasing autophagy through introduction of the homozygous *Atg7* mutant *Atg7*^{D77}, in a *Rab8* mutant background, alleviates the *Rab8* mutant NMJ overgrowth phenotype. Future investigation shall look to further substantiate these findings through further genetic manipulation of the autophagic pathway in *Rab8* mutants whilst also looking to identify the nature and origin of multilamellar structures. Alternatively one may postulate that multilamellar structures may relate to cholesterol accumulation that has been previously identified to occur as a result of Rab8 depletion, leading to perturbations to normal endosomal

recycling (Choudhury et al., 2004; Linder et al., 2007). For example it has been shown that similar multilamellar structures are observed in NPC cells where they have been proposed to act as sites of cholesterol deposition as a result of defective NPC1, where they have also been associated with autophagosome formation (Choudhury et al., 2004; Linder et al., 2007; Longatti et al., 2012; Puri et al., 2013). Similar multilamellar structures have also been observed in *Drosophila* models of lysosomal dysfunction, including *spin* mutants.

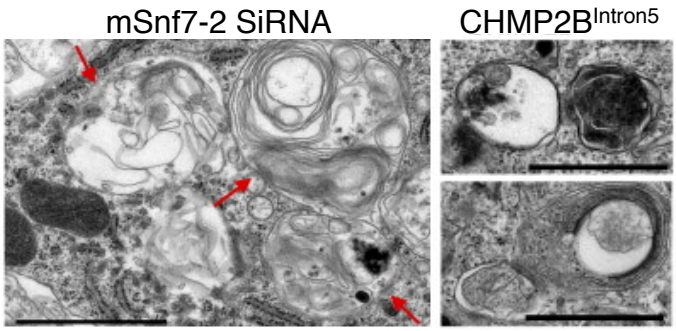

Figure 4.23. Depletion of ESCRT-III Function Induces Accumulation of Autophagosomes Comparable to the Multilamellar Structures Observed in *Rab8* Mutants
SiRNA mediated depletion of mSnf7-2 (the mouse orthologue of *Drosophila* Shrub) induced autophagosome accumulation in cortical neurons, as does *CHMP2B^{Intron5}* transfection of HEK293 cells. (Adapted from Lee et. al (2007)).

4.3.4 Ultrastructure Analysis Reveals Mitochondrial Aberrations

The final phenotype observed during ultrastructural analysis was that of abnormal mitochondrial morphology in the muscles of *Rab8* mutants. These mitochondria displayed significant morphological perturbation characterised by significant elongation, with a number of mitochondria appearing to be separated yet still attached by a long projection. Interestingly this phenotype shows a marked similarity to that observed in *C. elegans* Dynamin related protein 1 (Drp1) mutants (Fig. 4.24.) (Breckenridge et al., 2009). Drp1 is a GTPase that has a functional role in mitochondrial and peroxisome division as well as normal brain and neural tube development (Koch et al., 2003; Smirnova et al., 2001; Wakabayashi et al., 2009). It has also been shown to associate with mutant *htt*, which potentiates Drp1 enzymatic activity (Song et al., 2011). Htt in turn has been shown to associate with Rab8, via the Rab8 effector optineurin (Sahlender

et al., 2005). As such one may postulate that Rab8 may have a role in the regulation of normal mitochondrial fission and fusion events, potentially through Drp1. Future experimentation may look to elucidate this function through dissection of this potential pathway. S-nitrosylation of Drp1, mediated by the beta-amyloid protein, has also been shown to lead to the promotion of mitochondrial fission, synaptic loss and neuronal damage, implicating this as a potential target pathway in the study of Alzheimer's disease, and perhaps other neurodegenerative diseases (Cho et al., 2009).

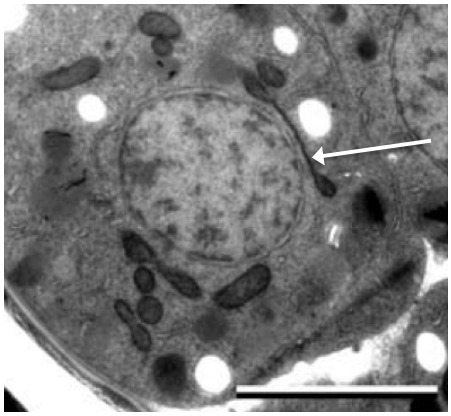

Figure 4.24. *Dynamin Related Protein 1* (*Drp1*) Mutant *C. elegans* Display Elongated Mitochondria Similar to Those Observed in *Rab8* Mutant *Drosophila*
Scale bar = 2 μm. (Adapted from Breckenridge et al. (2009)).

4.3.5. *Rab8* Mutants Display Impaired Physiology

Having observed significant perturbations to normal NMJ growth coupled with ultrastructural aberrations investigation looked to determine whether *Rab8* mutant synapses were physiologically functional. Observation of crawling speed revealed that the majority of *Rab8* transheterozygous mutants showed no perturbation to larval locomotion. As such it may be inferred that whilst overgrown, synapses are functionally normal. This may allude to overgrowth being a compensatory mechanism, growing larger with an increased number of synaptic terminals upon the muscle to compensate for a molecular dysfunction within the neuron.

The one transheterozygous combination displaying reduced larval locomotion is likely to result from the generation of both lines, by EMS, from the same

background stock in the same laboratory. As such second site mutations may be present in both stocks that are not complemented by outcrossing to each other. Alternatively it may be argued that this transheterozygous combination, $Rab8^{1}/Rab8^{3}$, contains the mutations that are both present in functional GTPase motifs and, as such, may display significant functional inactivity. However one may postulate this is unlikely to be the case as this combination shows no more significant perturbation to NMJ morphology, whilst the $Rab8^{1}$/Df(3L)ED228 transheterozygous mutant, which equates to $Rab8^{1}$/-, shows no perturbation to larval crawling speed. These findings suggest synaptic overgrowth does not directly correlate with a reduction or increase in crawling speed. For example in contrast to *Rab8* mutants *spin* mutants, which display synaptic overgrowth, display reduced crawling speed.

In contrast to the observation of limited perturbation to normal physiological function, in terms of larval crawling speed, *Rab8* mutant larvae display significant disruption to normal synaptic transmission (Bruno Marie, University of Puerto Rico). The reduced mEPSP amplitude observed suggests that either less neurotransmitter is released in response to presynaptic stimulation by an action potential or that the muscle is eliciting an attenuated response to the normal amount of neurotransmitter. The latter typically occurs due to a reduction in the size of the post-synaptic receptor field and a decrease in glutamate receptor abundance (Heckscher et al., 2007). However our previous observations suggest that there is no perturbation to normal GluR localisation and distribution and as such one may postulate that reduced mEPSP amplitude most likely associates with reduced neurotransmitter release. This also corroborates the findings that Rab8 has a predominantly pre-synaptic function, with pre-synaptic but not post-synaptic expression of *Rab8* capable of rescuing synaptic overgrowth. Future investigation shall look to determine the effects of pre- and post-synaptic rescues upon electrophysiological phenotypes in order to substantiate this hypothesis. Reduced mEPSP amplitude also supports the previous hypothesis that large vesicles observed in synaptic boutons are not synaptic vesicles and are in fact associated with endosomal recycling intermediates, similar to those associated with expression of dominant negative Rab5 (Wucherpfennig et al., 2003).

Rab8 mutants also presented with an increased EPSP, correlating with the synaptic overgrowth observed and suggesting that although synaptic bouton size is reduced the increased bouton number and cumulative bouton size elicits an increased evoked response in the postsynaptic muscle. A reduced quantal content is observed as a result of the reduction in mEPSP amplitude coupled with increased EPSP in *Rab8* mutants. Elevated EPSP may also contribute towards the reduction in mEPSP observed.

Interestingly the observed aberrations to synaptic function are in stark contrast to those observed in other models of synaptic overgrowth including *hiw*, which displays a marked reduction in quantal content and EPSP amplitude, and *spin* mutants, which display a 50 % reduction in quantal content but a normal EPSP amplitude (Sweeney and Davis, 2002; Wan et al., 2000). Taken together these findings support the hypothesis that synaptic overgrowth does not directly correlate with synaptic function, with different models of synaptic overgrowth displaying distinct physiological variance.

5. Unregulated Growth in *Rab8* Mutants Requires Synergistic JNK and TGFβ Signalling

5.1. Introduction

Growth, development and the continuous homeostatic modulation of the *Drosophila* NMJ, in response to both internal and external cues, is regulated by a series of interconnected, bi-directional, pre- and post-synaptic signalling pathways. These include both TGFβ and JNK signalling (see Chapter 1).

Both TGFβ and JNK signalling have been implicated in the growth and development of the *Drosophila* larval NMJ. For example a significant body of evidence exists demonstrating that the TGFβ ligand and BMP family protein Gbb is secreted by the muscle, binding pre-synaptically expressed TGFβ receptors and providing a retrograde signal to the developing pre-synaptic terminal (Marques, 2005; Marques et al., 2003; McCabe et al., 2003). Evidence suggests that ligand bound receptors are then endocytosed and trafficked to the cell body, where they induce activation and nuclear localisation of P-MAD allowing transduction of the TGFβ signal to promote synaptic growth (Smith et al., 2012). It has also been demonstrated that TGFβ signalling at the NMJ can be modulated by glia (Fuentes-Medel et al., 2012). Glia release the TGFβ ligand Maverick (Mav) which is thought to induce muscle expression of the TGFβ type-II receptor Punt, resulting in a potent modulation of retrograde Gbb release (Fuentes-Medel et al., 2012). Similarly a significant body of evidence has implicated JNK signalling in synaptic over-growth (Collins et al., 2006; Milton et al., 2011). JNK signalling has been implicated in stress responses within cells, responding to a range of endogenous and environmental insults (see Chapter 1). For example previous work in the Sweeney lab has demonstrated that JNK signalling is activated in response to an oxidative stress burden in *spin* mutants, leading to unrestricted synaptic growth (Milton et al., 2011). In addition research has shown that synaptic overgrowth in *hiw* mutants is associated with increased activation of the JNK signalling pathway (Collins et al., 2006). It has been demonstrated that hiw acts in the degradation of the JNKKK wnd and as such

hiw mutants display reduced restraint upon wnd leading to increased JNK activation (Collins et al., 2006).

Despite significant evidence implicating both TGFβ and JNK signalling in NMJ development, with both implicated in a number of synaptic overgrowth models, and despite significant evidence in other contexts demonstrating that these signalling pathways act synergistically there is currently little evidence supporting a synergistic mode of action at the *Drosophila* NMJ. Here evidence is provided to suggest that both TGFβ and JNK signalling contribute towards the synaptic overgrowth phenotype observed in *Rab8* transheterozygous mutants. In addition it is shown that TGFβ and JNK signalling act synergistically in the physiological regulation of NMJ growth. In keeping with this we propose a mechanism by which ectopic TGFβ signalling, resulting from perturbation to endosomal recycling in *Rab8* mutants, promotes JNK signalling via the JNKKK TAK1, scaffolding upon the endosomal JNK scaffolding protein POSH.

5.2. Results

5.2.1. TGFβ Activity is Up-regulated in *Rab8* Mutants and Required for Unrestricted NMJ Growth

Having demonstrated, in the previous chapter, that *Rab8* mutants display an unrestricted synaptic growth phenotype the focus of this chapter was to identify the molecular mechanism behind the overgrowth. Previous studies have demonstrated endocytic trafficking to play a critical role in regulating nervous system development through the modulation of growth factor receptors, including TGFβ (Fuentes-Medel et al., 2012; O'Connor-Giles et al., 2008; Rodal et al., 2011; Smith et al., 2012; Sweeney and Davis, 2002). For example it has been shown that activated TGFβ receptor complexes are endocytosed, in an activity dependent manner, at the synaptic terminal and retrogradely transported to the cell body where the TGFβ signal transduction cascade promotes transcription of factors involved in synaptic plasticity and NMJ growth (Smith et al., 2012). As such TGFβ signalling promotes synaptic modulation in an activity dependent manner. It has also been demonstrated that aberration to

normal endosomal trafficking can result in misrelated TGFβ signalling, leading to synaptic overgrowth at the *Drosophila* NMJ (Kim et al., 2010; Korolchuk et al., 2007; O'Connor-Giles et al., 2008; Rodal et al., 2011; Sweeney and Davis, 2002). For example Sweeney and Davis (2002) demonstrated that mutations in the gene encoding the late endosomal/lysosomal protein spin induce significant synaptic overgrowth associated with misregulated TGFβ signalling. Similarly mutations in other endosomal proteins including Ema and Vps35 elicit TGFβ dependent synaptic overgrowth (Kim et al., 2010; Korolchuk et al., 2007). It was also demonstrated that inhibition of *spicthyin,* an early endosomal protein involved in the endocytosis of BMP receptors, promotes up-regulation of BMP signalling leading to expansion of the *Drosophila* NMJ (Wang et al., 2007). In addition it was recently shown that mutations in *Brain tumor* (*Brat*), a regulator of synaptic endocytosis, and *Spartin,* which promotes endocytic degradation of Wit, elicit synaptic overgrowth at the *Drosophila* NMJ (Nahm et al., 2013; Shi et al., 2013). As such, having observed significant perturbation to normal endosomal markers it was asked whether this led to a disruption of normal TGFβ activity and whether TGFβ signalling contributed towards the unrestricted growth phenotype observed in *Rab8* mutants.

In the data presented here it is demonstrated that functional TGFβ signalling is required for the synaptic overgrowth phenotype observed in *Rab8* transheterozygous mutant larvae. Previous studies have shown that certain synaptic overgrowth phenotypes, such as that of *spin*, are associated with perturbed TGFβ signalling (Sweeney and Davis, 2002). Furthermore these studies show that overgrowth can be alleviated through inhibition of TGFβ signalling. Development and expansion of the *Drosophila* NMJ has been shown to be regulated by retrograde TGFβ signalling involving muscle secreted BMP Gbb binding the type-II TGFβ receptor Wit (Marques et al., 2003; McCabe et al., 2003). Wit in turn forms an active tetrameric receptor complex with Type-I receptors, including Tkv. As such TGFβ signalling at the NMJ can be inhibited by expression of *Tkv* loss of function mutants. Previous studies have shown that heterozygous, hypomorphic *Tkv* mutants elicits no alteration in NMJ size whilst transheterozygous or homozygous *Tkv* mutants induce an ~ 50 % reduction in bouton number (Sweeney and Davis, 2002). The same trend was also observed

for inhibition of TGFβ signalling using *sax* or *wit* mutants. Here these findings are recapitulated with the presence of mutant *Tkv* in a *Rab8* transheterozygous mutant background alleviating synaptic overgrowth in a dose dependent manner (Fig. 5.1.). For example Tkv^{7}/+ in a *Rab8* mutant background partially rescues overgrowth whilst the presence of Tkv^{7}/Tkv^{K16713} completely rescues *Rab8* mutant overgrowth to wildtype levels. The requirement of normal TGFβ signalling, signalling through the Tkv receptor, in *Rab8* mutant overgrowth is supported by analysis of muscle 4 where it is demonstrated that heterozygous Tkv^{K16713} in a transheterozygous *Rab8* mutant background is sufficient to completely rescue both increased bouton number and NMJ length (Fig. 5.2.A-B). Heterozygous Tkv^{K16713} also rescued the reduced synaptic bouton size seen in *Rab8* mutants (Fig. 5.2.C). Interestingly Tkv^{K16713}/+;$Rab8^{1}/Rab8^{B229}$ mutant larvae actually showed a bouton size significantly greater than that of wildtypes whilst Tkv^{K16713}/+ larvae showed boutons with a size no different to wildtype (Fig. 5.2.C). This study also revealed that whilst heterozygous *Rab8* mutants do not display synaptic overgrowth they do show a reduced synaptic bouton size comparable to that of *Rab8* transheterozygotes (Fig. 5.2.C.).

The role for TGFβ signalling in *Rab8* mutant overgrowth is further supported by the demonstration that inhibition of the inhibitory-SMAD Dad through heterozygous expression of the *Dad* loss of function mutant $Dad^{\Delta IEL}$ alongside heterozygous $Rab8^{1}$ is sufficient to induce a significant increase in synaptic bouton number at both muscle 6/7 and 4 (Fig. 5.1. and 5.2.). Heterozygotes of $Rab8^{1}$ and $Dad^{\Delta IEL}$ alone have no effect upon bouton number. Synaptic overgrowth in $Rab8^{1}/Dad^{\Delta IEL}$ double heterozygotes is further supported by a significant increase in NMJ length at muscle 4, again comparable to *Rab8* transheterozygous mutants (Fig. 5.2.B). $Rab8^{1}/Dad^{\Delta IEL}$ double heterozygotes also display a reduced mean normalised synaptic bouton size, however this is significantly larger than that of $Rab8^{1}$ heterozygotes and not significantly different to $Dad^{\Delta IEL}$ heterozygotes suggesting that reducing Dad inhibition of TGFβ signalling does not potentiate the reduced bouton size already observed in *Rab8* heterozygotes (Fig.5.2.C).

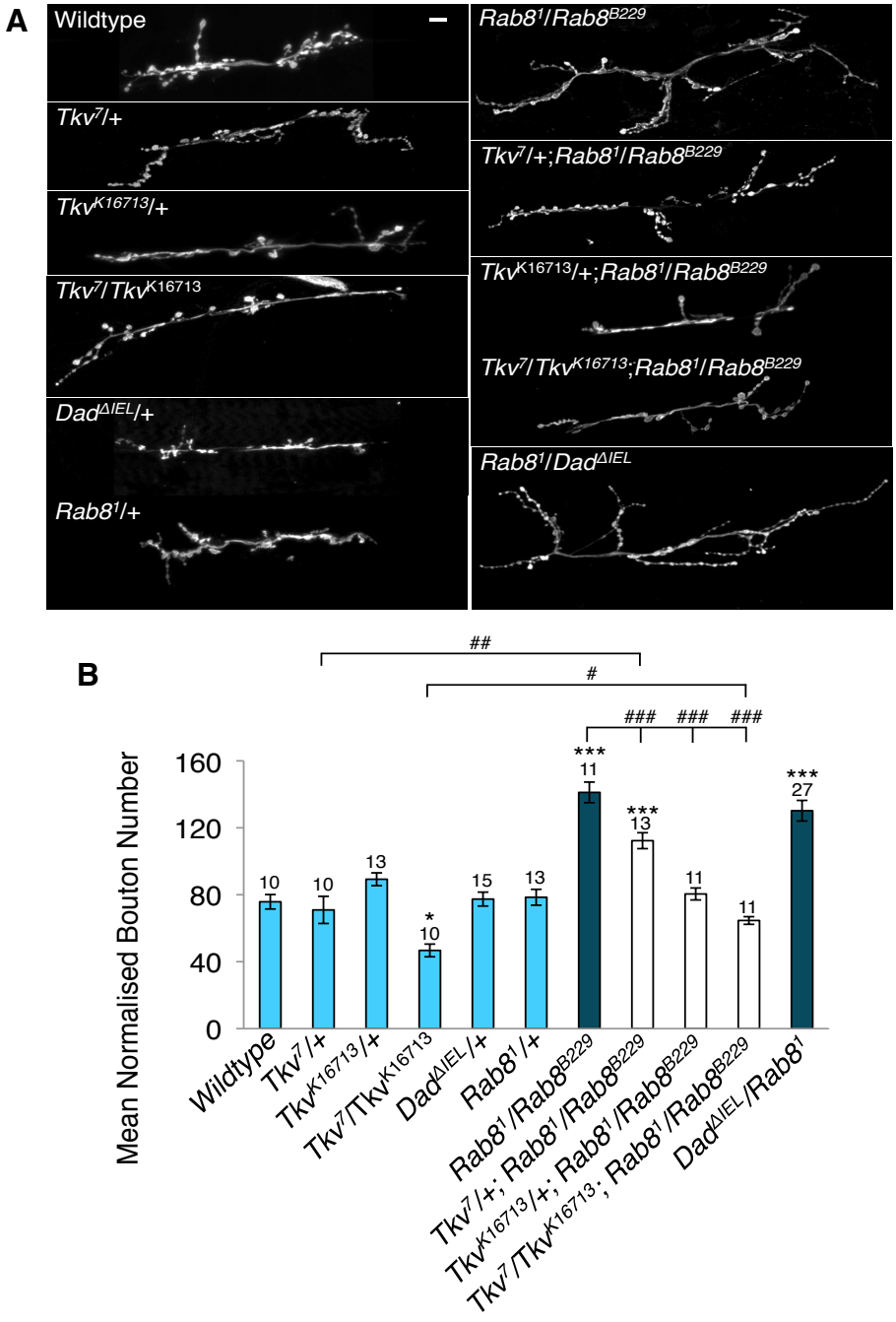

Figure 5.1. Increased Synaptic Bouton Number In *Rab8* Mutants Requires Functional TGFβ Signalling

(**A-B**) Inhibition of TGFβ signalling through expression of *Tkv* loss of function mutants in a *Rab8* transheterozygous mutant background rescues increased synaptic bouton number, in a dose dependent manner. Heterozygous expression of Tkv mutants in a wildtype background elicits no variance in bouton number whilst transheterozygous Tkv mutants display a 38.35 % reduction in synaptic bouton number, compared to wildtype. Suppression of TGFβ inhibition through heterozygous expression of a *Dad* loss of function mutant has no effect upon synaptic bouton number, however when combined with a heterozygous *Rab8* mutant induces a significant increase in bouton number comparable to *Rab8* transheterozygotes. Heterozygous *Rab8* mutants show no variance from wildtype. Scale bar = 10 µm. (ANOVA: $F(d.f.\ 10) = 27.8476$; $p < 0.001$ with post-hoc Dunnett's comparison to wildtype control *** $p < 0.001$, * $p < 0.05$ and student t-test comparison between genotypes ### $p < 0.001$, ## $p < 0.01$, # $p < 0.05$). 3rd instar larvae, muscle 6/7 hemi-segment A3.

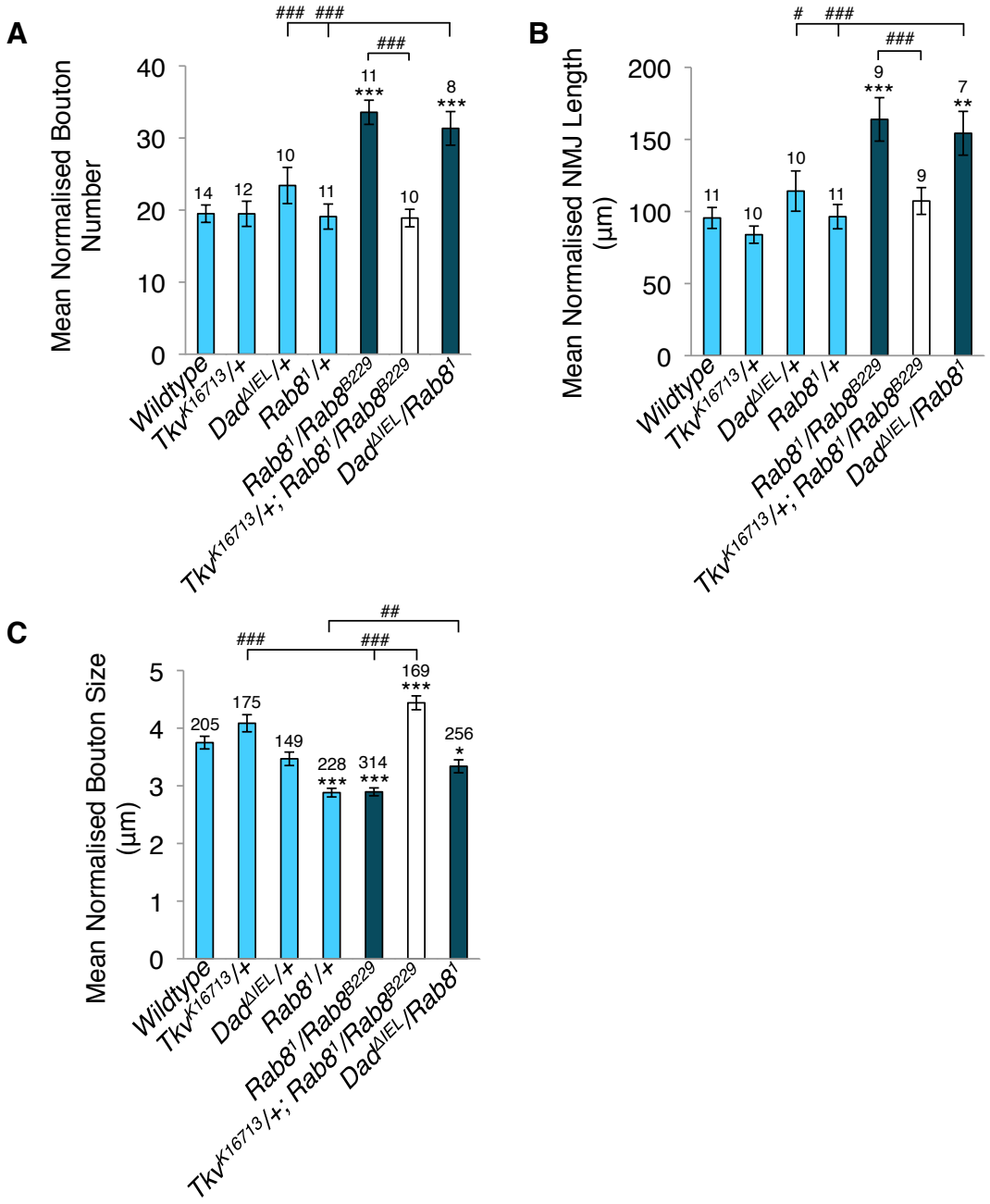

Figure 5.2. Unrestricted Growth In *Rab8* Mutants Requires Functional TGFβ Signalling
Corroborating observations at muscle 6/7 analysis of muscle 4, 3rd instar larvae hemi-segment A3, demonstrates that TGFβ signalling is essential for the overgrowth phenotypes observed in *Rab8* mutants. (**A**) Inhibition of TGFβ signalling in *Rab8* transheterozygous mutants, through heterozygous expression of the *Tkv* loss of function mutation Tkv^{K16713}, rescues increased bouton number. Heterozygous expression of Tkv^{K16713} in a wildtype background shows no variance from wildtype. Suppression of TGFβ inhibition through heterozygous expression of the *Dad* loss of function mutant $Dad^{\Delta IEL}$ in a *Rab8* heterozygous mutant background induced an increase in synaptic bouton number comparable to muscle 7 and *Rab8* transheterozygous mutants. Heterozygous $Rab8^{1}$ and $Dad^{\Delta IEL}$ alone show no variance from wildtype. (ANOVA: F(d.f. 6) = 24.9310; $p < 0.001$ with post-hoc Dunnett's comparison to wildtype control *** $p < 0.001$, and student t-test comparison between genotypes ### $p < 0.001$). (**B**) NMj length is affected in the same manner with heterozygous expression of Tkv^{K16713} in a transheterozygous *Rab8* mutant background rescuing increased NMJ length. $Rab8^{1}/Dad^{\Delta IEL}$ double mutants also display increased NMJ length comparable to *Rab8* transheterozygotes whilst heterozygous $Rab8^{1}$ and $Dad^{\Delta IEL}$ have no effect alone. (ANOVA: F(d.f. 6) = 7.5526; $p < 0.001$ with post-hoc Dunnett's comparison to wildtype control *** $p < 0.001$, ** $p < 0.01$ and student t-test comparison between genotypes ### $p < 0.001$, # $p < 0.05$). (**C**) Reduced bouton size in *Rab8* mutants can be alleviated by inhibition of TGFβ through heterozygous expression of Tkv^{K16713}, which alone shows no variance from wildtype. Similarly $Tkv^{K16713}/Rab8^{1}$ double mutants show

reduced bouton size. However whilst heterozygous $Dad^{\Delta IEL}$ shows no variance in bouton size from wildtype heterozygous $Rab8^{1}$ show a reduced bouton size comparable to *Rab8* transheterozygotes. (ANOVA: F(d.f. 6) = 71.3031; $p < 0.001$ with post-hoc Dunnett's comparison to wildtype control *** $p < 0.001$, * $p < 0.05$ and student t-test comparison between genotypes ### $p < 0.001$, ## $p < 0.01$).

Having demonstrated TGFβ signalling to be essential for the synaptic overgrowth phenotype observed in *Rab8* transheterozygous mutants it was then asked whether these mutants displayed an abnormal up-regulation of TGFβ signalling. The data presented here confirms TGFβ signalling to be up-regulated in *Rab8* mutants both at the cellular and transcriptional level. MAD is the *Drosophila* orthologue of the R-SMAD, SMAD1 and, as such, is activated by phosphorylation by Tkv in response to ligand mediated receptor activation (see section 1.3.9.). Therefore levels of phosphorylated MAD (p-MAD) can be used as an indicator of TGFβ activity. Here it is demonstrated that nuclear p-MAD levels, in eve positive motor-neurons, are increased by 99.53 % in *Rab8* mutants ($Rab8^{1}/Rab8^{B229}$), compared to wildtype (Fig. 5.3. A-B). This indicates an increase in TGFβ activity at the point of receptor phosphorylation of the R-SMAD. Analysis of p-MAD immunofluorescence also revealed an accumulation of p-MAD positive aggregates within the VNC and axon bundles of *Rab8* mutants. Such accumulations were not observed in wildtype animals (Fig.5.4.). It was also noted that these axonal p-MAD aggregates showed partial co-localisation with HRS, an endosomally localised ESCRT-0 component.

Having demonstrated increased TGFβ activity at the point of receptor phosphorylation of the R-SMAD, MAD it was then determined whether the TGFβ pathway was transcriptionally more active. As the TGFβ pathway transcriptionally activates the inhibitory SMAD, Dad, *Dad-LacZ* can be used as a reporter of TGFβ activity. Again TGFβ activity is shown to be up-regulated in *Rab8* mutants, displaying an 846.84 % increase in nuclear Dad-driven LacZ fluorescence within the larval VNC, when compared to wildtype (Fig. 5.3 C-D).

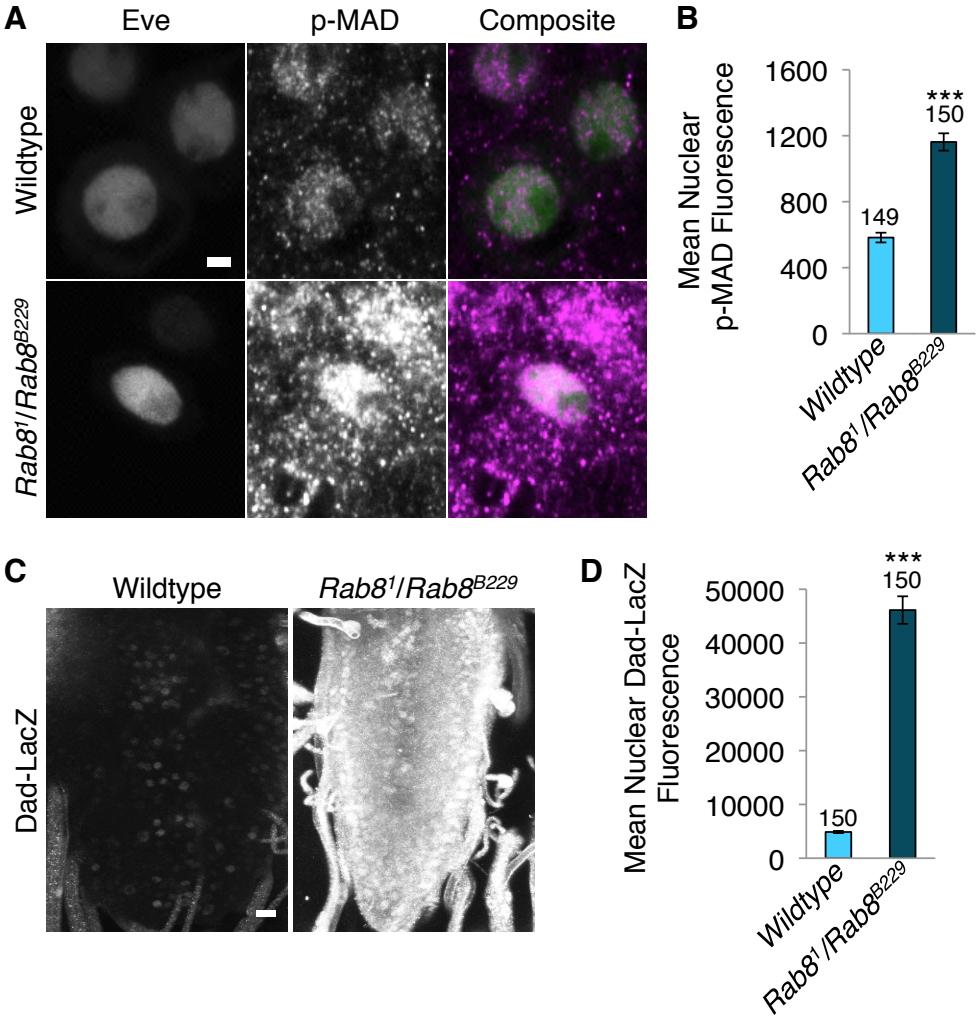

Figure 5.3. *Rab8* Mutants Display Increased Levels of TGFβ Activity
(**A-B**) *Rab8* mutants show a significant increase in nuclear phosphorylated MAD, *Drosophila* SMAD1, within eve positive motor neurons in 3rd instar larvae, when compared to wildtype. Scale Bar = 2 µm. (ANOVA: $F(d.f.\ 1) = 92.3468$; $p < 0.001$). (**C**) *Rab8* mutants also show a clear increase in levels of Dad, the Drosophila inhibitory-SMAD, which is transcriptionally activated by the TGFβ signalling pathway throughout the ventral nerve cord of 3rd instar larvae (Scale Bar = 10µm). (**D**) Quantification of Dad-LacZ levels reveals a significant increase in Dad-LacZ in Rab8 mutants, compared to wildtype. (ANOVA: $F(d.f.\ 1) = 257.76$; $p < 0.001$).

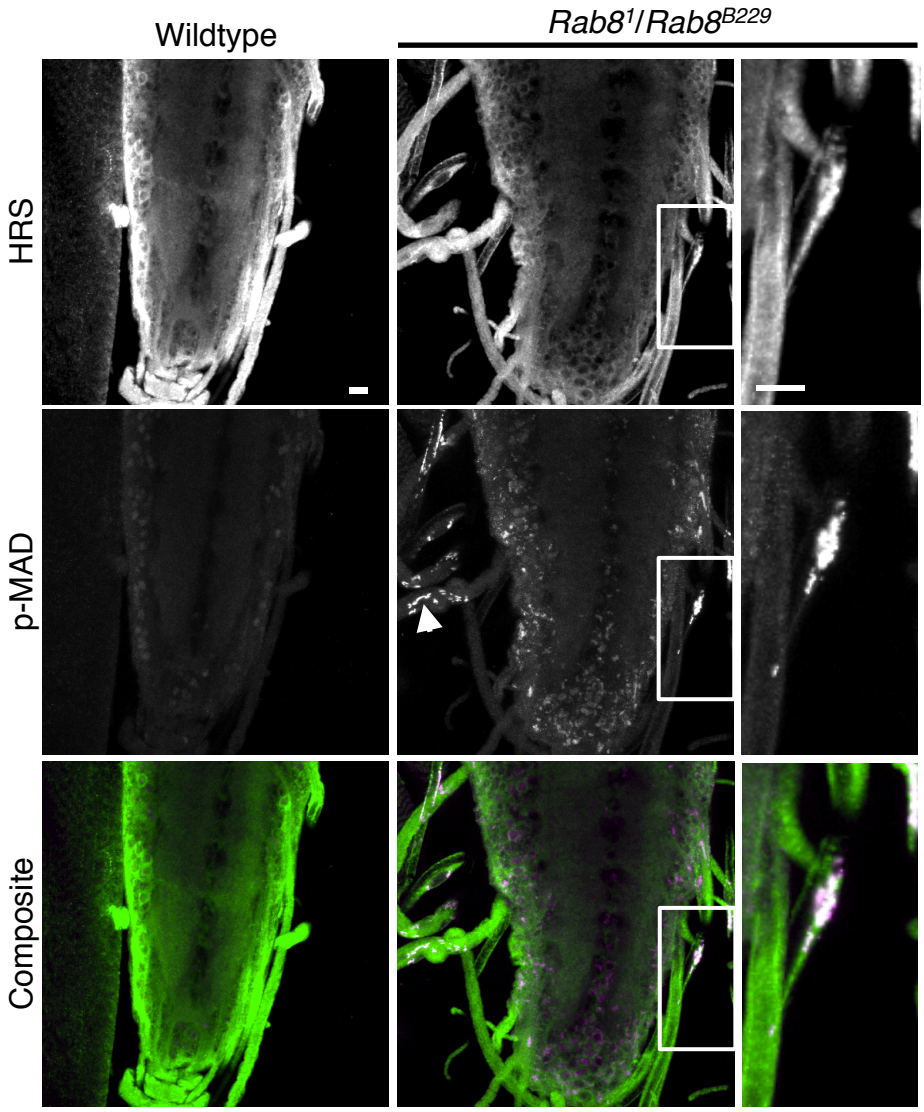

Figure 5.4. *Rab8* Mutants Display Accumulations of p-MAD Partially Co-localising With HRS In Axon Bundles.
Immunofluorescence imaging of p-MAD and HRS reveals that as well as showing increased nuclear p-MAD fluorescence Rab8 mutants show accumulations of p-MAD throughout the ventral nerve cord (VNC) and within axon bundles (arrow head and box) projecting from the VNC. P-MAD accumulations also co-localise with the endosomal protein HRS. Scale Bars = 10 μm.

During analysis to determine whether accumulations of p-MAD in *Rab8* mutant axon bundles co-localised with endosomes, using HRS and an endosomal marker, it was also noted that HRS fluorescence appeared reduced in the VNC of *Rab8* mutants. As such further analysis looked to quantify HRS levels. This analysis reveals a significant decrease in HRS within the cell bodies of eve positive motor neurons (Fig 5.5). This suggests that *Rab8* mutants present with

a depletion of HRS or that HRS is sequestered elsewhere, perhaps within axons where p-SMAD accumulations are observed partially co-localising with HRS.

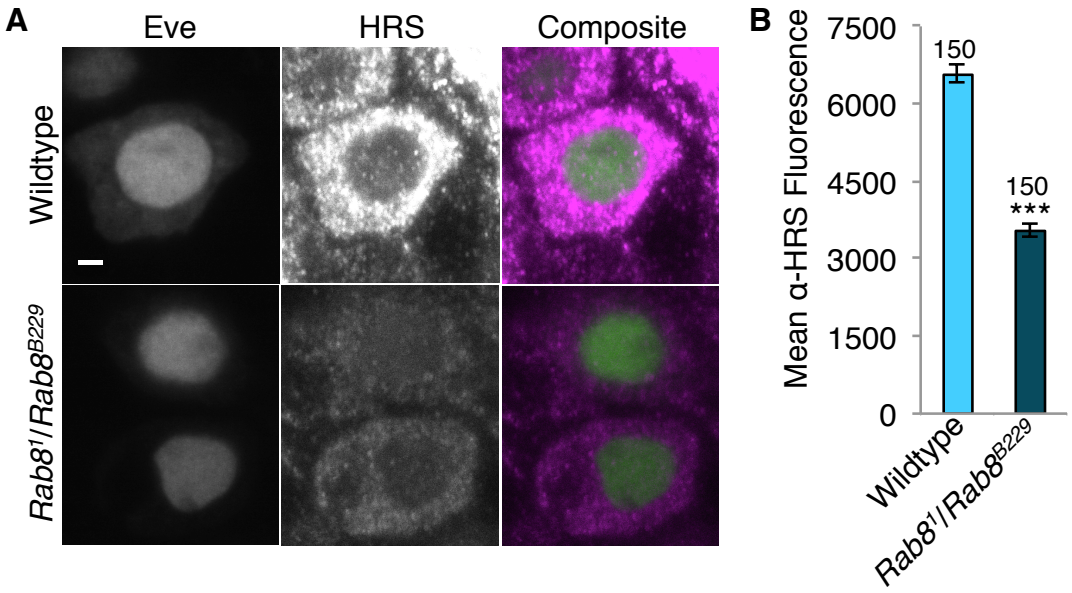

Figure 5.5. *Rab8* Mutants Show Reduced HRS Fluorescence Within Eve Positive Motor Neuronal Cell Bodies Within the Ventral Nerve Cord
(**A-B**) Immunohistochemical analysis of HRS in Drosophila eve positive motor neuronal cell bodies reveals a significant decrease in HRS within *Rab8* mutants. Eve positive motor neurons within the ventral nerve cord of 3rd instar larvae. Scale Bar = 2 µm. (ANOVA: F(d.f. 1) = 215.8528; $p < 0.001$).

5.2.2. JNK Signalling is Up-regulated in *Rab8* Mutants and Required for Unrestricted NMJ Growth

Synaptic growth and plasticity requires regulation by a multitude of intricate and interconnected signalling pathways. As such it was asked whether synaptic overgrowth in *Rab8* mutants was associated with perturbation to any other developmental pathways, other than TGFβ. One alternative pathway that has been implicated as a potent regulator of synaptic growth and development at the *Drosophila* NMJ is that of JNK/AP-1 signalling (Collins et al., 2006; Etter et al., 2005; Milton et al., 2011; Sanyal et al., 2002). AP-1 is a transcription factor comprised of hetro- or homo-dimers of Fos and Jun which, once activated, translocate to the nucleus promoting transcriptional activation of mediators of synaptic growth and function, as well as other tissue specific responses including apoptosis and autophagy (Collins et al., 2006; Milton et al., 2011;

Perkins et al., 1990). Genes encoding AP-1 components, including Fos and Jun, are classified as immediate-early genes, the transcription of which can be rapidly induced independently of *de novo* protein synthesis (Karin, 1996). JNK is a central component of the JNK signalling cascade leading to activation of AP-1 in response to a variety of both intracellular and extracellular cues, including oxidative stress (Derijard et al., 1994; Hibi et al., 1993; Milton et al., 2011; Pantos et al., 2003; Silverman et al., 2003; Yoshida et al., 2005). For example recent work in the Sweeney lab has shown that *spin* mutants display an oxidative stress burden, as a result of endosomal-lysosomal dysfunction, leading to up-regulated JNK/AP-1 signalling and eliciting a synaptic overgrowth phenotype (Milton et al., 2011). This overgrowth was shown to be alleviated by inhibition of the JNK/AP-1 pathway. With *Rab8* mutants presenting a synaptic overgrowth phenotype similar to that observed in *spin* mutants and with both mutant overgrowths showing the requirement for a permissive TGFβ signal it was asked whether JNK signalling contributed towards overgrowth in *Rab8* mutants, as with *spin.*

Through inhibition of JNK signalling using either pan-neuronal (nSyb-Gal4) or motor neuronal (OK6-Gal4) driven expression of a dominant negative form of Fos (UAS-Fos^{DN}) it was shown that functional JNK signalling was essential for the unrestricted synaptic growth phenotype observed in *Rab8* mutants. Pan-neuronal and motor neuronal expression of UAS-*Fos^{DN}* had no effect upon synaptic bouton number when expressed in a wildtype background (Fig. 5.6.). However when expressed in a *Rab8* transheterozygous mutant background both pan-neuronal and motor neuronal expression of *Fos^{DN}* was sufficient to completely rescue increased bouton number, showing no variance from wildtype but a significant difference to *Rab8^{1}*/*Rab8^{B229}* (Fig. 5.6.). In addition it was also shown that inhibition of puckered, a negative regulator of JNK signalling, using a heterozygous loss of function *Puc* mutant *Puc^{E69}* in a heterozygous *Rab8* mutant background induced an increase in synaptic bouton number comparable to both *Rab8* transheterozygotes and *Rab8^{1}*/*Dad$^{\Delta IEL}$* double heterozygotes (Fig. 5.6.). In contrast the presence of heterozygous *Puc^{E69}* or *Rab8^{1}* alone showed no variance in synaptic bouton number, compared to wildtype (Fig. 5.6.). Therefore as with TGFβ signalling JNK

signalling contributes towards the synaptic overgrowth phenotype observed in *Rab8* mutants.

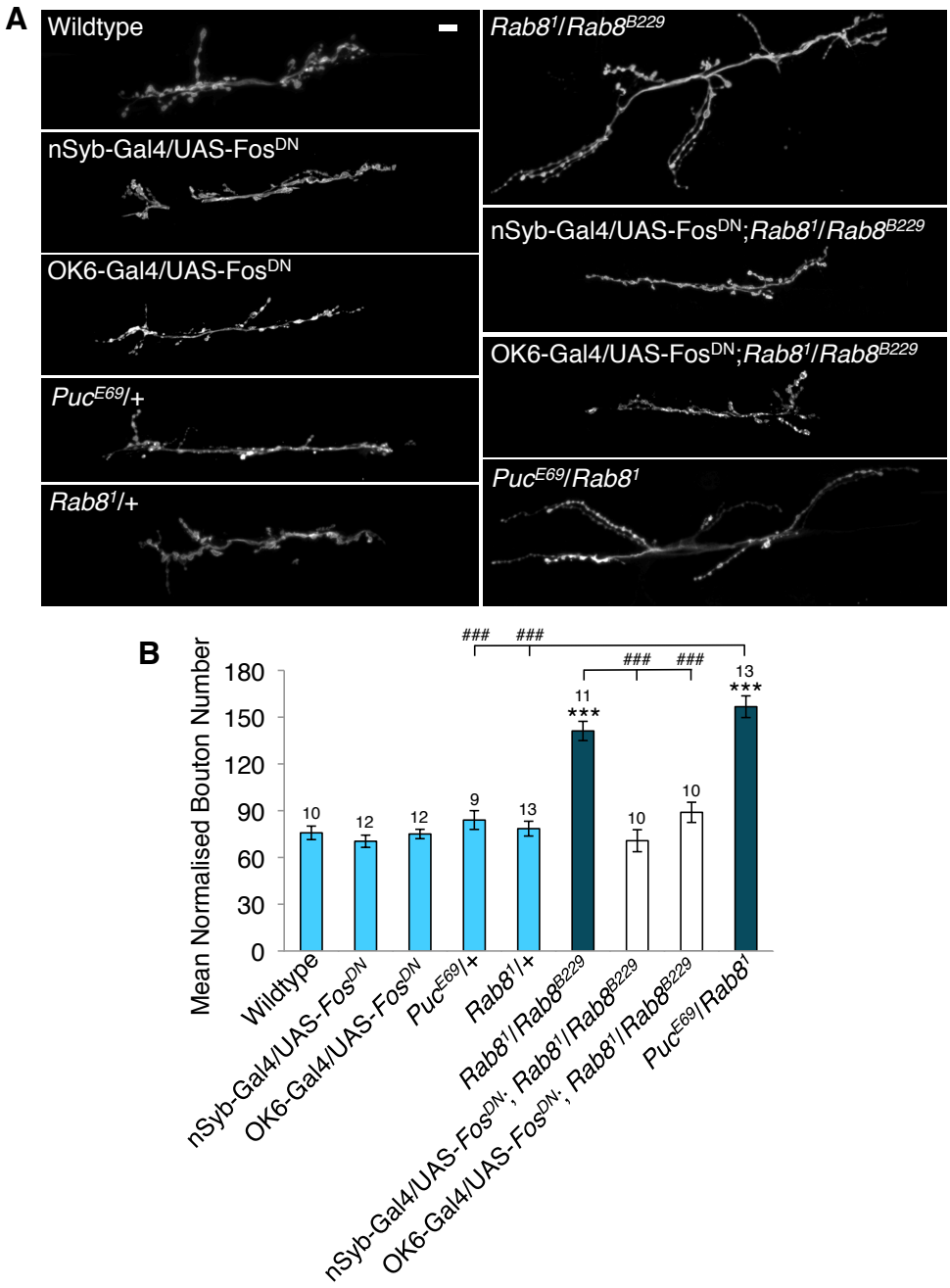

Figure 5.6. Unrestricted NMJ Growth in *Rab8* Mutants Requires Functional JNK Signalling

(**A-B**) Inhibition on JNK signalling through pan-neuronal (nSyb-Gal4) or Motor neuronal (OK6-Gal4) driven expression of a dominant negative Fos, UAS-Fos^{DN}, in a transheterozygous *Rab8* mutant background rescues the increased bouton number observed in *Rab8* transheterozygous mutants. Pan-neuronal and motor neuronal expression of UAS-Fos^{DN} in a wildtype backgrounds shows no variance in bouton number compared to wildtypes. Suppression of JNK inhibition through the presence of a heterozygous puckered loss of function mutant, Puc^{E69}, alongside heterozygous $Rab8^{1}$ induces an overgrowth phenotype comparable to that seen in *Rab8* transheterozygous mutants whilst heterozygous $Rab8^{1}$ and Puc^{E69} alone show no variance from wildtype. Scale bar = 10 µm. (ANOVA: F(d.f. 8) = 36.4999; $p < 0.001$ with post-hoc Dunnett's comparison to wildtype control *** $p < 0.001$ and student t-test comparison between genotypes ### $p < 0.001$).

In order to substantiate the observed role of JNK signalling in *Rab8* mutant NMJ overgrowth it was asked whether *Rab8* mutants display an increased activation of the JNK signalling pathway. Puc has been shown to be transcriptionally activated by the JNK/AP-1 pathway, providing a feedback loop in order to modulate JNK signalling (Martin-Blanco et al., 1998). As such Puc-LacZ can be used as a reporter of JNK activity. Here it is shown that transheterozygous *Rab8* mutants display a significant increase in JNK activity, displaying a clear increase in nuclear Puc driven –LacZ expression in eve positive motor neurons (Fig. 5.7. A-B).

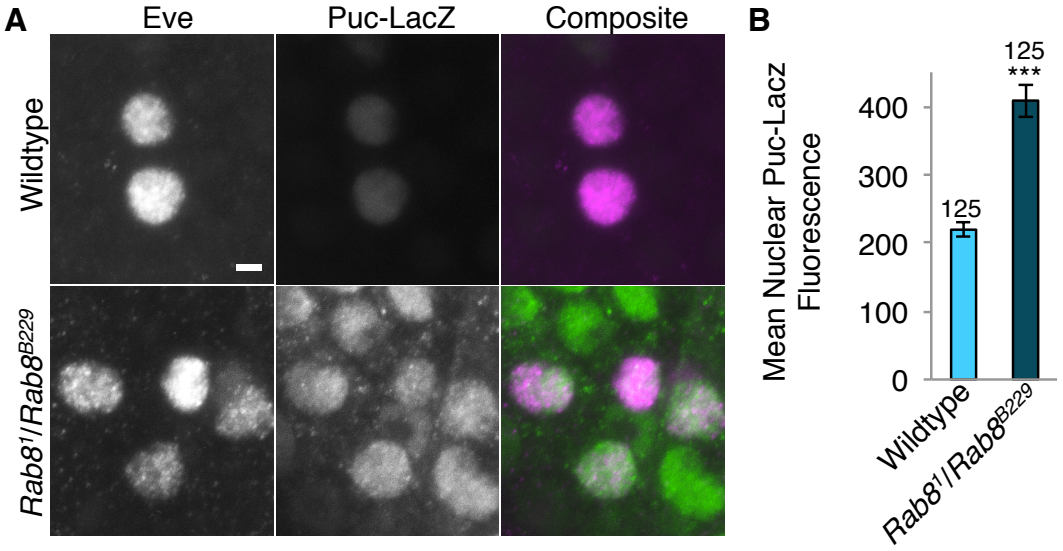

Figure 5.7. *Rab8* Mutants Display Increased Levels of JNK Activity
(**A**) *Rab8* mutants display a clear increase in nuclear Puckered-LacZ (puc-lacZ) staining, a reporter of JNK activity, within eve positive motor neurons in 3rd instar larval ventral nerve cords. Scale bar = 2 µm. (**B**) Quantification of nuclear puc-lacZ in eve positive motor neurons reveals a significant increase in *Rab8* mutants, compared to wildtypes (ANOVA: $F(d.f.\ 1) = 53.6294$; $p < 0.001$).

5.2.3. TGFβ and JNK Signalling Act Synergistically in Normal Physiological Regulation of NMJ Growth

Here it has been demonstrated that both TGFβ and JNK signalling are up-regulated in transheterozygous *Rab8* mutants. In addition it is shown that suppression of inhibition of JNK or TGFβ in a heterozygous *Rab8* mutant background induces synaptic overgrowth comparable to transheterozygous

Rab8 mutants. As such it was asked whether TGFβ and JNK signalling might act synergistically in the regulation of normal physiological NMJ growth. Previous studies have shown that, in other contexts, TGFβ and JNK signalling display direct and mutual interaction (Liu et al., 2012; Mao et al., 2011; Perlman et al., 2001; Sorrentino et al., 2008). For example it has been shown that TGFβ is capable of activating JNK in a SMAD-independent, TRAF6 and TAK1 dependent manner (Sorrentino et al., 2008). Operating in a mechanism that is proposed to show similarity to that of the Toll-like receptor pathway. Conversely it has been shown that JNK signalling can also activate TGFβ with AP-1 components directly interacting with SMAD's and that JNK can regulate TGFβ in a SMAD2 dependent manner (Derynck and Zhang, 2003; Engel et al., 1999). The results presented here provide support for the hypothesis that TGFβ and JNK signalling pathways may act synergistically in the regulation of developmental processes, including synaptic growth at the *Drosophila* NMJ. As mentioned previously, in sections 5.2.1. and 5.2.2., Dad and Puc act as negative mediators of TGFβ and JNK signalling, respectively. Furthermore if either is inhibited, through the heterozygous presence of a loss of function allele, in a *Rab8* heterozygous mutant background synaptic overgrowth is induced. Here it is shown that whilst neither heterozygous Puc^{E69} or $Dad^{\Delta IEL}$ loss of function mutants induce synaptic overgrowth $Puc^{E69}/Dad^{\Delta IEL}$ heterozygous double mutants display synaptic overgrowth comparable to that seen in $Puc^{E69}/Rab8^{1}$ and $Dad^{\Delta IEL}/Rab8^{1}$ double mutants, as well as in *Rab8* transheterozygous mutants (Fig. 5.8.). Synaptic overgrowth in $Puc^{E69}/Dad^{\Delta IEL}$ heterozygous double mutants is characterised by an increase in synaptic bouton number (Fig. 5.8.A-C), which is conserved across NMJ's at both muscle 6/7 and 4, as well as an increase in NMJ length (Fig. 5.8.D) and a reduction in synaptic bouton size (Fig. 5.8.E). Interestingly these results also demonstrate that whilst bouton number and NMJ length are unaffected bouton size is reduced in $Puc^{E69}/+$ heterozygous mutants (71.5 % of wildtype) to approximately the same degree as $Puc^{E69}/Dad^{\Delta IEL}$ double mutants (72.8 % of wildtype) as well as *Rab8* heterozygous (76.9 % of wildtype) and transheterozygous (77.2 % of wildtype) mutants observed previously. This suggests that JNK signalling may play a potent role in the regulation of bouton size and the reduced bouton size seen in *Rab8* mutants.

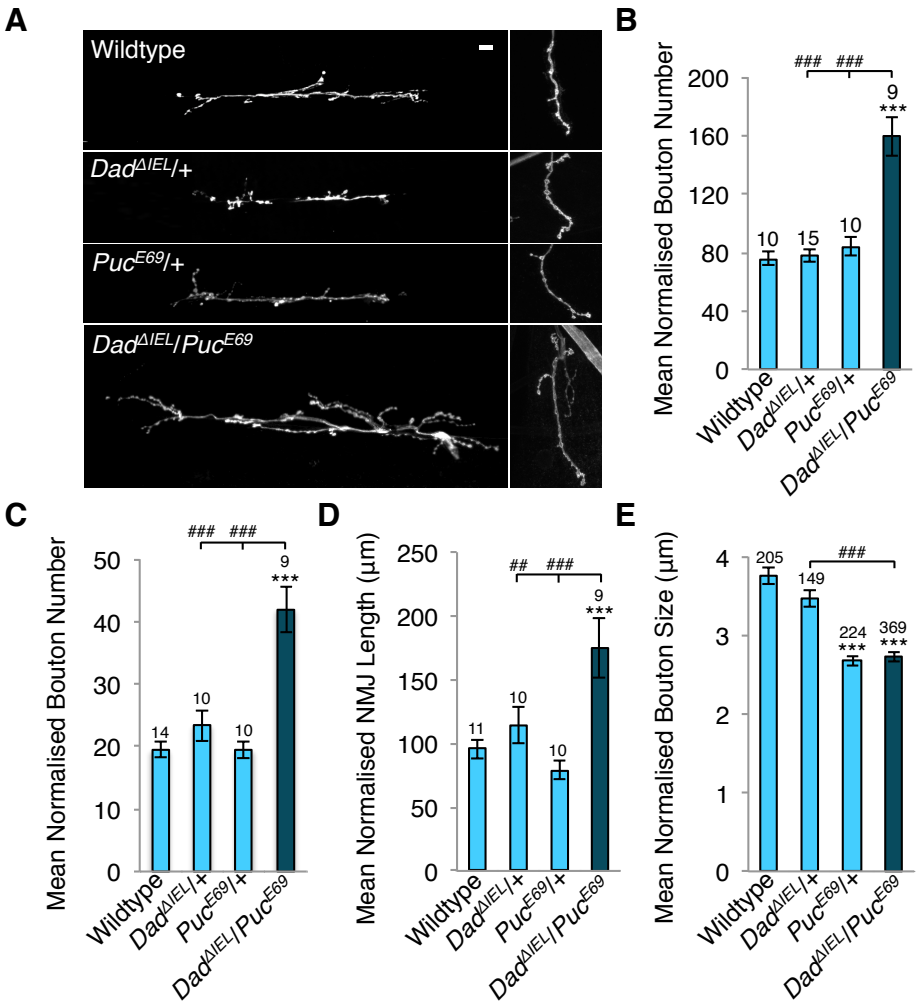

Figure 5.8. TGFβ and JNK Signalling Act Synergistically to Regulate Normal NMJ Growth
(**A**) Heterozygous combinations of *Dad* and *Puc* loss of function mutants together reduce Dad and Puc inhibition of the TGFβ and JNK signalling pathways, respectively. In doing so this elicits a clear synaptic overgrowth phenotype comparable to that seen in *Rab8* transheterozygous mutants. Images on the left represent muscle 6/7 and those on the right muscle 4, hemi-segment A3 of 3rd instar larvae. Scale bar = 10 µm. (**B**) Quantification of synaptic bouton number at muscle 6/7 reveals that $Dad^{\Delta IEL}/Puc^{E69}$ heterozygous double mutants show a significant increase in mean normalised synaptic bouton number compared to wildtype and heterozygous $Dad^{\Delta IEL}$ and Puc^{E69} single mutants, which show no variance from wildtype. (ANOVA: F(d.f. 3) = 28.0239; $p < 0.001$ with post-hoc Dunnett's comparison to wildtype control *** $p < 0.001$ and student t-test comparison between genotypes ### $p < 0.001$). (**C**) The same trend is observed at muscle 4 with $Dad^{\Delta IEL}/Puc^{E69}$ double mutants displaying a significant increase in mean normalised bouton number compared to wildtypes and both $Dad^{\Delta IEL}$ and Puc^{E69} single mutants, which display no variance from wildtype. (ANOVA: F(d.f. 3) = 21.5592; $p < 0.001$ with post-hoc Dunnett's comparison to wildtype control *** $p < 0.001$ and student t-test comparison between genotypes ### $p < 0.001$). (**D**) $Dad^{\Delta IEL}/Puc^{E69}$ double mutants also display a significant increase in mean normalised NMJ length when compared to wildtype and to both heterozygous single $Dad^{\Delta IEL}$ and Puc^{E69} mutants, which display no significant variance from wildtype. (ANOVA: F(d.f. 3) = 9.5010; $p < 0.001$ with post-hoc Dunnett's comparison to wildtype control *** $p < 0.001$ and student t-test comparison between genotypes ### $p < 0.001$, ## $p < 0.01$). (**E**) $Dad^{\Delta IEL}/Puc^{E69}$ double mutants also display a significantly reduced mean normalised synaptic bouton size compared to wildtypes and to $Dad^{\Delta IEL}$ heterozygotes, which show no variance from wildtype. However in contrast Puc^{E69} heterozygous mutants show a significantly reduced bouton size, compared to wildtype, equal to that of $Dad^{\Delta IEL}/Puc^{E69}$ double mutants.

5.2.4. *Rab8* Mutants Reveal a Role for the Endosomal JNK Scaffold POSH and the JNKKK TAK1 in Synapse Growth

Previous findings in this investigation demonstrate that *Rab8* mutants display unrestricted synaptic overgrowth associated with up-regulated TGFβ and JNK signalling, as well as perturbations to normal endosomal trafficking. Furthermore these results suggest that TGFβ and JNK signalling act synergistically to regulate synaptic growth. POSH has previously been identified as a potent regulator of JNK signalling acting both as a JNK scaffold and as a modulator of TAK1, a known JNKKK (Tapon et al., 1998; Tsuda et al., 2005; Tsuda et al., 2006; Xu et al., 2003). It has been demonstrated that POSH actively binds to TAK1, targeting it for proteasomal degradation through the E3 ubiquitin ligase activity of the POSH zinc finger ring domain (Tsuda et al., 2005). In addition in other contexts TAK1 has, as its names suggests, been shown to be directly activated by the TGFβ signalling pathway (Shibuya et al., 1998; Sorrentino et al., 2008; Yamaguchi et al., 1995). Ligand mediated activation of the TGFβ receptor complex promotes dimerisation and auto-ubiquitylation of TRAF6 leading to the ubiquitylation and activation of TAK1, which has been shown to associate directly with the TGFβ type-I receptor (Sorrentino et al., 2008). TAK1 is then capable of further auto-phosphorylation and activation of downstream JNK signalling. Alternatively it has been proposed that under un-stimulated conditions TAK1 stably associates with the TGFβ type-I receptor, however upon activation TAK1 dissociates and is activated via TAB-1 mediated auto-phosphorylation (Kim et al., 2009). Whilst the exact mechanism remains to be fully elucidated these previous findings suggest that TGFβ activation may lead to downstream activation of the JNK signalling pathway via TAK1, a protein that is regulated by the E3 ubiquitin ligase activity of the JNK scaffolding protein POSH. POSH has also been shown to associate with HRS on early endosomes, where it plays an essential role, through its E3 ubiquitin ligase activity, in the regulation of HRS stability (Kim et al., 2006). HRS in turn directly associates with TAK1 where it has been shown to be essential for both the localisation of TAK1 to the endosome and the activation of both TAK1 and TGFβ SMAD's (Miura and Mishina, 2011).

Based on the previously identified roles for POSH, and it's associated factors, it was proposed that POSH may act as a central point in the regulation of synaptic growth, acting to scaffold JNK signalling and conveying transduction of a signalling cascade from TGFβ to JNK, via TAK1. The results here provide support for this hypothesis demonstrating that both inhibition and neuronal overexpression of POSH rescue the synaptic overgrowth observed in *Rab8* transheterozygous mutants. Here it was demonstrated that inhibition of POSH through the use of *POSH* mutants $POSH^{EP1206}$ and $POSH^{EP2248}$ either homozygously or transheterozygously in a transheterozygous *Rab8* mutant background showed no significant variance in synaptic bouton number to their controls, in a wildtype background (Fig. 5.9.). In addition all *POSH Rab8* double mutants displayed a significantly reduced number of synaptic boutons compared to *Rab8* transheterozygous mutants. Furthermore, with the exception of homozygous $POSH^{EP1206}$, no allelic combination of *POSH* mutants displayed any variance from wildtype in either a wildtype or *Rab8* mutant background (Fig. 5.9.). As such, taken together, it can be inferred that inhibition of POSH is sufficient to alleviate increased synaptic bouton number in *Rab8* mutants. In addition it was also demonstrated that pan-neuronal expression of UAS-*POSH*, which showed no variance to wildtype in a wildtype background, was sufficient to completely rescue increased synaptic bouton number in a *Rab8* mutant background (Fig. 5.9.). nSyb-Gal4/UAS-*POSH*;$Rab8^{1}$/$Rab8^{B229}$ larvae showed no variance in synaptic bouton number to wildtype or the UAS-POSH control, yet a significant variance to the transheterozygous *Rab8* mutants (Fig. 5.9.). Taken together these results indicate a fundamental role for POSH in the regulation of synaptic growth.

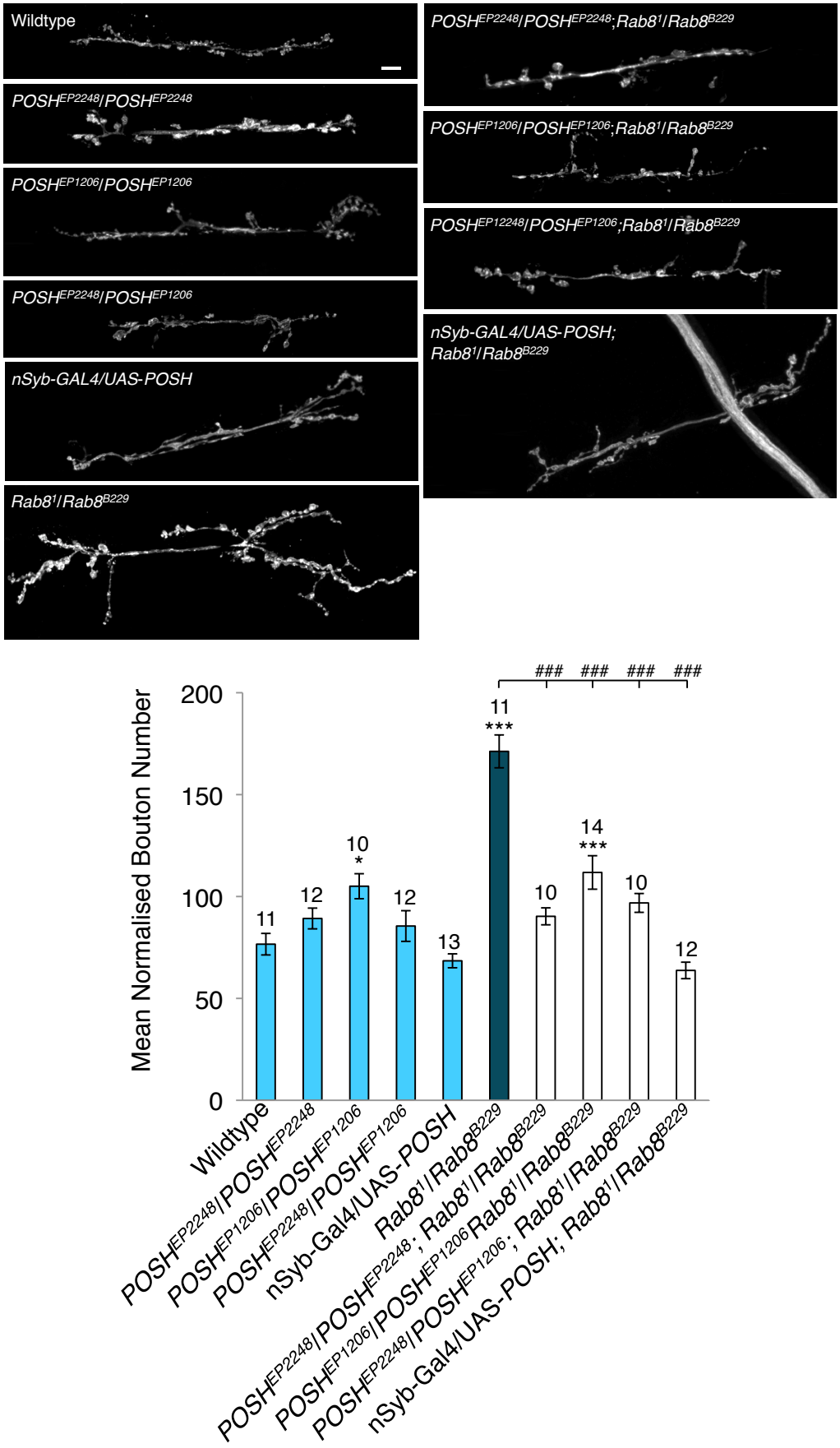

Figure 5.9. Perturbation of *POSH* Alleviates Increased Synaptic Bouton Number in *Rab8* Mutants

Increased normalised synaptic bouton number in *Rab8* transheterozygous mutants can be alleviated through expression of *POSH* mutants $POSH^{EP1206}$ and $POSH^{EP2248}$ either homozygously or transheterozygously in a *Rab8* mutant background. All *POSH Rab8* double mutants show a significant variance in synaptic bouton number to *Rab8* transheterozygous

mutants. In addition each displays no significant variance to its representative *POSH* mutant control (in a wildtype background). Both $POSH^{EP1206}/POSH^{EP1206}$;$Rab8^{1}/Rab8^{B229}$ double mutants and $POSH^{EP1206}/POSH^{EP1206}$ controls presented a small but significant variance to wildtype. All other double mutants and their controls showed no significant variance in synaptic bouton number to wildtype. Similarly overexpression of UAS-*POSH*, under the control of the pan-neuronal driver nSyb-Gal4, showed no effect upon synaptic bouton number alone, however was sufficient to completely rescue increased bouton number in a *Rab8* mutant background. Neuronal expression of UAS-*POSH* in a *Rab8* mutant background showed no significant variance to either the UAS-*POSH* control or wildtypes. Analysis was of muscle 6/7, hemi-segment A3 in 3rd instar wandering larvae. Scale bar = 10 μm. (ANOVA: $F(d.f.\ 9) = 24.0378$ $p < 0.001$ with post-hoc Dunnett's comparison to wildtype control *** $p < 0.001$ and student t-test comparison between genotypes ### $p < 0.001$).

Having demonstrated that both overexpression and inhibition of *POSH* in a *Rab8* transheterozygous mutant background is sufficient to rescue synaptic overgrowth analysis looked to determine whether there was any perturbation to normal POSH distribution in *Rab8* mutants. Here it is shown that in *Rab8* transheterozygous mutants POSH displays an altered distribution pattern, displaying increased intensity and accumulations within axon bundles projecting from the VNC (Fig. 5.10.).

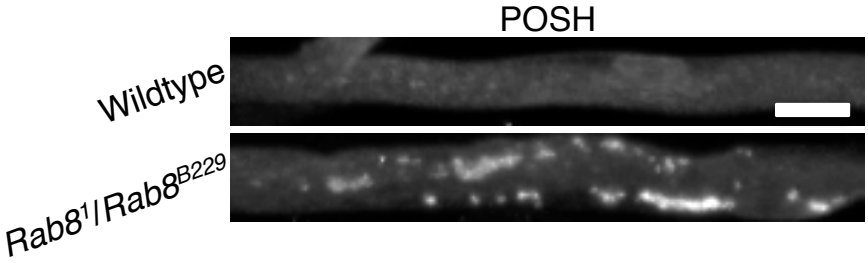

Figure 5.10. POSH Accumulates in Axons of Transheterozygous *Rab8* Mutants
Anti-POSH immunohistochemical staining reveals accumulations of POSH within axon bundles of transheterozygous *Rab8* mutant larvae. Accumulations were not seen in wildtype larvae. Scale bar = 10 μm.

Having identified a role for *POSH* in the regulation of synaptic growth, with both *POSH* mutants and neuronal expression of *POSH* alleviating synaptic overgrowth in *Rab8* mutants, it was asked whether either *TAK1* or *HRS* contribute towards synaptic growth. The results presented here demonstrate that *TAK1* acts as a potent regulator of synaptic growth. For example whilst heterozygous expression of the *TAK1* loss of function mutant $TAK1^{179}$ shows no variance in synaptic bouton number from wildtypes, introduction of $TAK1^{179}$/+ into a $Rab8^{1}/Rab8^{B229}$ mutant background shows a significant variance from $Rab8^{1}/Rab8^{B229}$ mutants and no variance from wildtypes (Fig. 5.11).

TAK1^{179}/+;*Rab8*^{1}/*Rab8*^{B229} mutants do, however show a small, but significant, variance from *TAK1*^{179}/+ controls suggesting this may not be a full rescue. This does however demonstrate that *TAK1* is essential for the overgrowth phenotype observed in *Rab8* transheterozygous mutants. Corroborating these findings it was also shown that neuronal (nSyb-Gal4) expression of either a *TAK1*-RNAi or a kinase dead *TAK1* dominant negative allele (UAS-*TAK1*^{K46R}, (Mihaly et al., 2001)) could completely alleviate increase synaptic bouton number in *Rab8* transheterozygotes (Fig. 5.11.). Neuronal expression of either in a *Rab8* mutant background showed a significant variance in synaptic bouton number from *Rab8* transheterozygous mutants but no variance to either wildtypes or nSyb driven *TAK1*-RNAi or *TAK1* dominant negative controls (Fig. 5.11.). In addition it was also shown that neuronal overexpression of wildtype *TAK1* could elicit a potent synaptic overgrowth phenotype (Fig. 5.11.). This overgrowth displayed phenotypic characteristics visibly comparable to *Rab8* mutants, including a prevalence of small boutons.

In addition to a role for *TAK1* in the regulation of synaptic growth these results also reveal a role for *HRS*. Here it is demonstrated that whilst presence of the heterozygous *HRS* loss of function mutant *HRS*^{D28} has no effect upon synaptic bouton number *HRS*^{D28}/*Rab8*^{1} transheterozygous mutants show a significant increase in synaptic bouton number, compared to wildtype (Fig. 5.11.). *Rab8*^{1} heterozygotes were again shown to have no effect upon synaptic bouton number in their own right (Fig. 5.11.). Synaptic overgrowth observed was not as severe as that seen in *Rab8* transheterozygotes. These results support previous findings that *Rab8* transheterozygous mutants display a significant reduction in HRS within motor neuronal cell bodies and suggest that *HRS* contributes towards the regulation of NMJ growth.

Taken together these results identify *POSH* and *TAK1* as novel regulators of synaptic growth. In addition they reveal a potential role for the POSH complex as a nexus in the regulation of growth signals, potentially modulating transduction of TGFβ signals, via TAK1, to JNK.

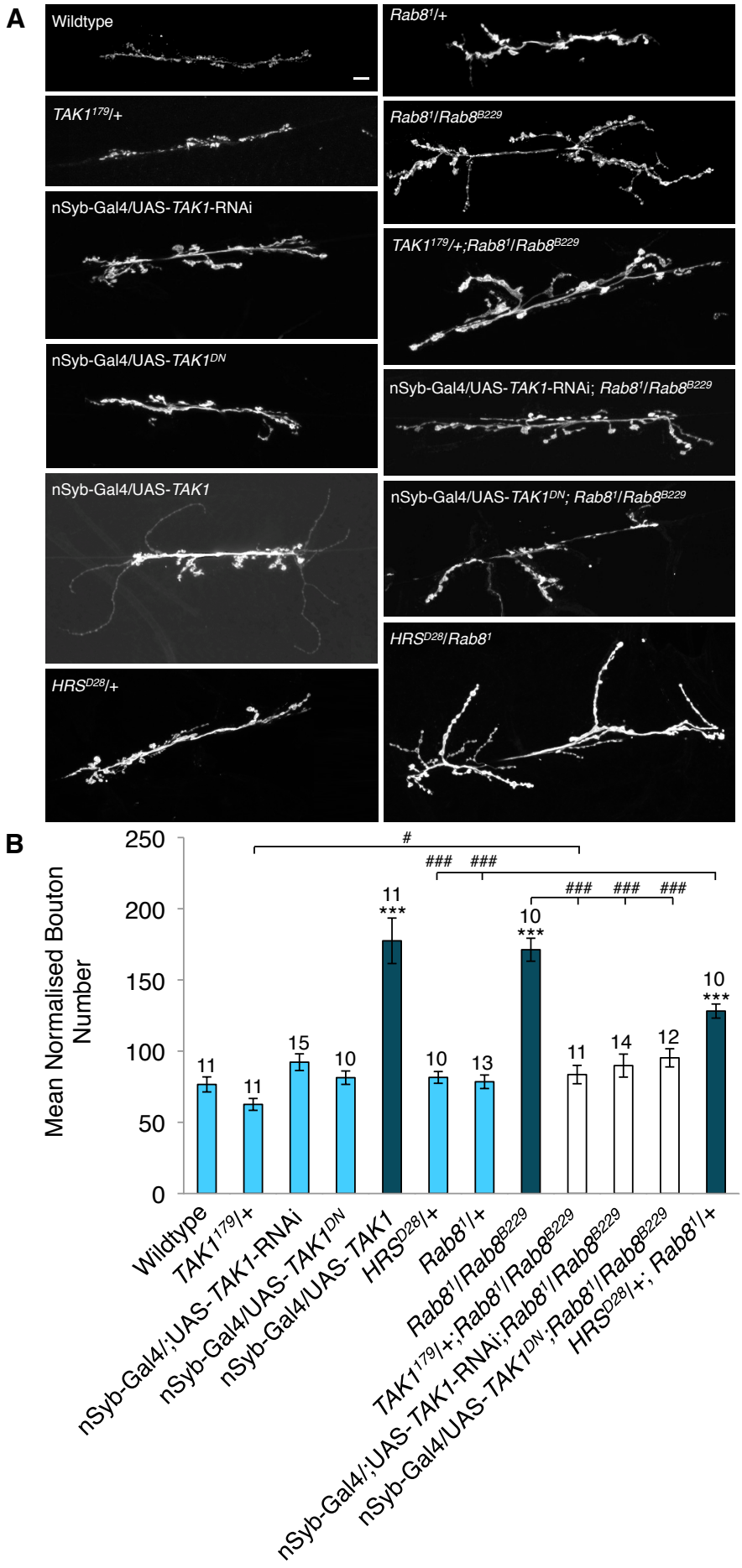

Figure 5.11. *TAK1* and *HRS* Contribute Towards Synaptic Overgrowth in *Rab8* Mutants
(A) Inhibition of *TAK1* via heterozygous expression of the loss of function mutation $TAK1^{179}$ or pan-neuronal expression of a dominant negative *TAK1* or a *TAK1*-RNAi in a transheterozygous

Rab8 mutant background alleviates the increase in synaptic bouton number seen in *Rab8* mutants. Overexpression of *TAK1* induces a synaptic overgrowth comparable to *Rab8* transheterozygotes. Similarly inhibition of *HRS* via transheterozygous expression of the loss of function mutant HRS^{D28} alongside $Rab8^{1}$ elicits a synaptic overgrowth phenotype. Heterozygous expression of either HRS^{D28} or $Rab8^{1}$ alone has no effect upon bouton number. Scale bar = 10 µm. (**B**) Quantification of synaptic bouton number. (ANOVA: $F(d.f.\ 11) = 24.2733$; $p < 0.001$ with post-hoc Dunnett's comparison to wildtype control *** $p < 0.001$ and student t-test comparison between genotypes ### $p < 0.001$, # $p < 0.05$).

5.3. Discussion

5.3.1. TGFβ and JNK Signalling Are Required for Unrestricted Growth in *Rab8* Mutants

Previous studies have demonstrated that both TGFβ and JNK signalling play a fundamental role in the development of the nervous system (Bjorkblom et al., 2005; Gomes et al., 2005; Kim et al., 2005a; Mecha et al., 2008; Sun et al., 2013; Unsicker and Strelau, 2000; Vogel et al., 2010). Furthermore they have shown that perturbations to either pathway can have significant implications upon neuronal development leading to neurodegeneration and neurodegenerative diseases. For example in a study by Lee et al. (2010) it was shown that TGFβ activity promoted aggregation of TGF-β1-induced anti-apoptotic factor (TIAF1) leading to the accumulation and aggregation of amyloid plaques, characteristic of Alzheimer's disease, and the induction of apoptotic cell death (Lee et al., 2010). Furthermore other studies have demonstrated that TGFβ signalling is up-regulated in the brains of Alzheimer's patients, although whether this is pathological or a neuroprotective response has yet to be fully elucidated (Chao et al., 1994; Flanders et al., 1995). Similarly studies have also shown that increased JNK signalling results in an aberrant accumulation of both amyloid and Tau aggregates in models of Alzheimer's disease (Dias-Santagata et al., 2007; Shen et al., 2008). Furthermore, as for TGFβ signalling, JNK signalling has been shown to be elevated in the brains of Alzheimer's patients (Bomfim et al., 2012; Zhu et al., 2003). Perturbations to both TGFβ and JNK signalling has also been observed in patients suffering from other neurodegenerative diseases including Parkinson's disease and ALS (Ilzecka et al., 2002; Mogi et al., 1995; Peng and Andersen, 2003). TGFβ and JNK

signalling have also been implicated in a broad array of processes essential for development of the nervous system including facilitation of dendritic development, synapse development, axon path-finding, development of the cerebellum and neuronal differentiation, and neuronal migration, apoptosis and development, for TGFβ and JNK respectively (Charron and Tessier-Lavigne, 2007; Constam et al., 1994; Heupel et al., 2008; Li et al., 2009a; Sun et al., 2007; Yi et al., 2010).

Studies in *Drosophila* have demonstrated that both the TGFβ and JNK signalling pathways display a contributory role in the regulation of normal NMJ assembly and function. For example inhibition of normal TGFβ signalling has been shown to elicit a significant synaptic undergrowth phenotype in wildtype larvae (Aberle et al., 2002; O'Connor-Giles et al., 2008; Sweeney and Davis, 2002). In addition a permissive TGFβ signal has been demonstrated to be essential in a number of synaptic overgrowth models, including *spin*, *nwk* and *Ema,* with inhibition of TGFβ alleviating overgrowth in a dose dependent manner (Kim et al., 2010; O'Connor-Giles et al., 2008; Sweeney and Davis, 2002). Similarly JNK has been revealed to be a positive regulator of NMJ growth with inhibition of JNK signalling alleviating NMJ overgrowth in both *spin* and *hiw* mutants (Collins et al., 2006; Milton et al., 2011). As such the observation that both TGFβ and JNK signalling are essential for the unregulated synaptic growth phenotype observed in *Rab8* mutants and that both pathways appear to be actively up-regulated in these mutants provides further support to a growing body of evidence for the involvement of these pathways in NMJ development. In addition to corroborating previous findings that both TGFβ and JNK signalling have a functional role in the regulation of NMJ development the results presented here reveal that NMJ expansion and synaptic bouton size appear to be regulated semi-autonomously from one another. For example it is demonstrated that whilst overgrowth phenotypes, including increased NMJ length and bouton number, require transheterozygous mutation of *Rab8*, reduced synaptic bouton size is observed in Rab8 *homozygotes*. In addition alleviating inhibition upon TGFβ signalling by inhibiting Dad, which potentiates all other unregulated growth phenotypes observed, does not potentiate reduced bouton size. Furthermore it was shown that heterozygous *puc* mutants, which

essentially show reduced JNK inhibition, display significantly reduced synaptic bouton sizes comparable to *Rab8* transhetrozygotes, but no overgrowth phenotypes. As such taken together these findings suggest that reduced synaptic bouton size, which is observed in numerous *Drosophila* mutants displaying unregulated NMJ growth and is a hallmark of *hiw* mutants, may be regulated semi-autonomously from NMJ expansion phenotypes and potentially by JNK signalling independently of TGFβ.

As well as elevated levels of TGFβ activity, indicated by significant increases in levels of nuclear P-MAD and nuclear Dad-LacZ, *Rab8* mutants were shown to display accumulations of P-MAD within axon bundles projecting from the VNC. In a recent study Smith et al. (2012) demonstrated that active TGFβ receptor complexes are endocytosed and trafficked, retrogradely and in an activity dependent manner, from the *Drosophila* NMJ to the cell body in order to modulate TGFβ activity at the synapse. As such one may postulate that accumulations of P-MAD visible within the axon may relate to P-MAD in complex with the active TGFβ receptor complex being trafficked from the synapse. However Smith et al. (2012) showed no evidence that P-MAD was transported along axons, inferring that P-MAD at the synaptic terminal and cell body represent two distinct populations. Indeed here we show no evidence of P-MAD in the axons of wildtype animals, suggesting that under normal physiological conditions P-MAD is not transported along axons, at least not at visible levels. As such it may be inferred that either *Rab8* mutants perturb normal P-MAD localisation resulting in axonal accumulations or that maybe such elevated levels of P-MAD in *Rab8* mutants allows for visualisation of axonally transported P-MAD. One may also propose that axonal accumulations may associate with the perturbation to normal endosomal trafficking previously observed in *Rab8* mutants (Chapter 4).

5.3.2. TGFβ and JNK Signalling Act Synergistically in The Regulation of NMJ Growth

As mentioned previously both TGFβ and JNK signalling have already been implicated in the regulation of *Drosophila* NMJ assembly and function. In fact it

has been shown that synaptic overgrowth in an increasing number of mutants, including *spin*, *hiw* and now *Rab8*, can be alleviated by inhibition of either pathway. However, despite this, there has been little evidence to date that TGFβ and JNK act synergistically during the regulation of NMJ growth. In contrast a significant body of evidence exists to show that in many other contexts TGFβ and JNK act synergistically, with significant degrees of crosstalk (Liu et al., 2012; Liu et al., 2007; Pardoux and Derynck, 2004; Shim et al., 2005; Ventura et al., 2004; Yamashita et al., 2008). For example Adachi-Yamada et al. (1999) demonstrated that, in *Drosophila*, overexpression of a constitutively active Tkv promoted JNK activation and induction of downstream apoptotic responses (Adachi-Yamada et al., 1999). Similarly Yang and Su (2011) demonstrated that ectopic TGFβ expression lead to JNK-dependent activation of apoptosis in *Drosophila* cardiac tissue (Yang and Su, 2011). Furthermore they showed that the TGFβ ligand (dpp) potentiated it's own expression, through TAK1, resulting in hyperactivity of JNK under pathological conditions. As such the observation, in this investigation, that under normal physiological conditions simultaneously reducing the restraint maintained upon both the TGFβ and JNK signalling pathways can elicit a synaptic overgrowth phenotype provides evidence that, as within other systems, TGFβ and JNK act synergistically in the regulation of NMJ development. Overgrowth observed in this investigation was characterised by a significant increase in both synaptic bouton number and NMJ length, as well as a reduction in synaptic bouton size, a phenotype comparable to that observed in *Rab8* mutants.

5.3.3. *Rab8* Mutants Reveal a Role for the Endosomal JNK Scaffold POSH and the JNKKK TAK1 in Synapse Growth

Numerous studies have implicated Rab8 as playing an essential role in the trafficking of endosomal cargo to the recycling endosome (Henry and Sheff, 2008; Linder et al., 2007; Vaibhava et al., 2012). In addition results presented previously in this investigation (Chapter 4) demonstrate that *Rab8* mutants display significant perturbation to endosomal trafficking. This included a significant reduction of the recycling endosomal marker Rab4. In a study by

Rodal et al. (2011) it was demonstrated that inhibition of endosomal recycling contributed towards aberrant accumulation of active, ligand bound, TGFβ receptors within the early endosome. Furthermore ectopic TGFβ signalling within the endosome promoted significant synaptic overgrowth. This observation supports a growing body of evidence demonstrating that TGFβ receptors continue to signal within the endosome and that this can contribute towards unrestricted synaptic growth in a number of mutant models displaying endosomal perturbation (Rodal et al., 2011; Sweeney and Davis, 2002; Wang et al., 2007). In fact it has also been shown that TGFβ signalling is actively up-regulated in the early endosome due to early-endosomal enrichment of SARA, a protein involved in trafficking R-SMAD's to the TGFβ receptors (Di Guglielmo et al., 2003; Hayes et al., 2002). As discussed earlier recent evidence also suggests that ligand bound TGFβ receptors are actively endocytosed at the synaptic terminal and transported to the cell body to convey signal transduction essential for the modulation of synaptic growth (Smith et al., 2012). As such it is clear that recycling of TGFβ receptors via the recycling endosome is essential to return receptors to the synaptic terminal, maintaining synaptic homeostasis. Assimilation of these previous findings with the observation that *Rab8* mutants display significantly elevated levels of TGFβ signalling, coupled with endosomal perturbation, provide support for the hypothesis that synaptic overgrowth in *Rab8* mutants is associated with aberrant endosomal processing of TGFβ. In addition to elevated TGFβ signalling *Rab8* mutants display significant up-regulation of JNK signalling, coupled with accumulation of the endosomal JNK scaffolding protein POSH within axonal projections. As such based upon previous literature and the results presented here we propose a model by which endosomal accumulation of active TGFβ receptors promotes synaptic overgrowth via transduction of ectopic expression via TAK1 to activate JNK, scaffolding upon the endosomal JNK scaffold POSH (Fig. 5.12.). We propose that ectopic TGFβ expression within early endosomes promotes activation of the JNKKK TAK1, as discussed previously in section 2.5.4.. TAK1 in turn associates with the JNK scaffold POSH promoting activation of JNK. This ectopic activation promotes unrestricted growth in *Rab8* mutants. In addition *TAK1* has been implicated in a feedback loop promoting TGFβ activation through interaction with the downstream SMAD proteins. As such this may

further potentiate ectopic expression of the TGFβ and JNK signalling pathways, potentiating synaptic growth. The observations made in this chapter support this model. For example TGFβ and JNK signalling were shown to be elevated in *Rab8* mutants and be required for synaptic overgrowth. In addition they were demonstrated to act synergistically in the regulation of synaptic growth. Furthermore inhibition of *TAK1* alleviates synaptic overgrowth in *Rab8* mutants whilst overexpression of *TAK1* in a wildtype background promotes synaptic overgrowth comparable to that seen in *Rab8* mutants. It was also shown that both inhibition and overexpression of *POSH* could alleviate overgrowth. This can be explained by the fact that inhibition of *POSH* inhibits the role of POSH as a central scaffold but also that if overexpressed POSH is likely to titrate out the associated factors reducing the ectopic induction of JNK at the endosome. Overexpression of POSH may also promote POSH mediated degradation of TAK1 via the E3-ubiquitin ligase activity of this protein (Tsuda et al., 2005). In order to provide support for this model future investigation shall look to ascertain levels of TGFβ and JNK signalling in *Rab8* transheterozygous mutants in a POSH null background. Similarly levels of TGFβ and JNK signalling should be determined in *TAK1,Rab8* double mutants. Unfortunately due to the generation times required this analysis could not be performed in time to contribute towards this data chapter.

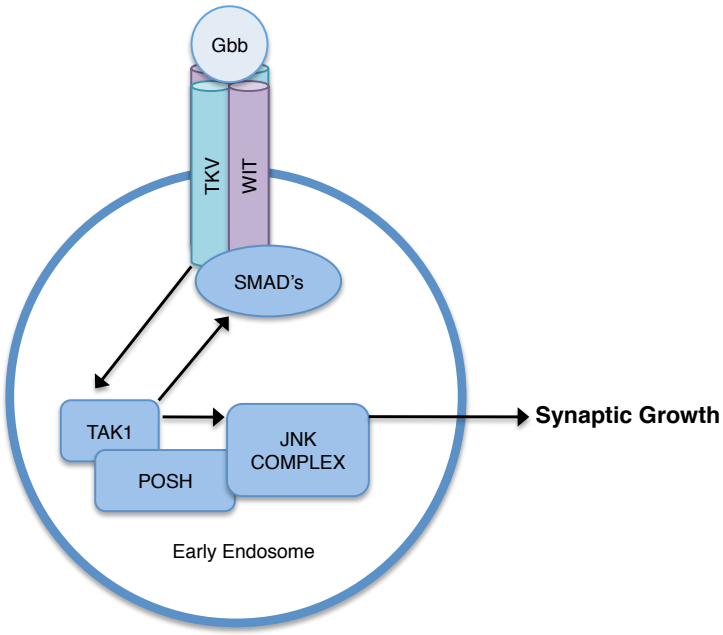

Figure 5.12. Proposed Model For POSH As a Regulator of Synaptic Growth
Mutations in *Rab8* induce perturbation to normal endosomal trafficking, potentially through disrupting Rab8's role in promoting endosomal traffic to the recycling endosome. This perturbation promotes accumulation of endocytosed ligand bound, active TGFβ receptors within

the early endosome. *Rab8* mutants also display accumulation of the early-endosomal protein POSH with axon bundles projecting from the ventral nerve cord. Active TGFβ receptors promote activation of the JNKKK TAK1, which, in complex with the JNK scaffold POSH promotes ectopic activation of the JNK signalling pathway. TAK1 may also promote activation of autophagy, which has also been implicated in JNK activation. TAK1 can also promote further TGFβ signalling, acting in a feedback loop via the SMAD proteins involved in TGFβ signal transduction. POSH has also been shown to act as an E3 ubiquitin ligase promoting the degradation of HRS. Ectopic degradation of HRS, alongside *Rab8* mutants creates a further burden upon the endosomal pathway inhibiting both endosomal-lysosomal degradation of ligand bound receptors and recycling via the recycling endosome. As such this potentiates TGFβ accumulation within early endosomes potentiating the pathological cycle.

In addition to the role of POSH as a JNK scaffold it has been demonstrated that POSH acts as an E3 ubiquitin ligase, promoting the degradation of HRS at early endosomes (Kim et al., 2006). The results presented in this chapter demonstrate that *Rab8* transheterozygous mutants display a significant reduction in motor neuronal HRS. In addition inhibition of *HRS* in a heterozygous *Rab8* mutant background was sufficient to promote synaptic overgrowth. As such one may postulate that accumulation of POSH in *Rab8* mutants promotes POSH mediated degradation of HRS, leading to the reduction in HRS observed. In a previous study by Rodal et al. (2011) it was demonstrated that whilst *HRS* mutants do not display any perturbation to synaptic growth alone, *HRS,Snx16* double mutants display a synaptic overgrowth phenotype. In this study they suggested that inhibition of Snx16 perturbed nwk dependent endosomal trafficking to the recycling endosome whilst HRS mutants inhibit MVB formation. As such double mutants prevent endosomal recycling and degradation of TGFβ receptors leading to an accumulation of active TGFβ receptors within the early endosome. In turn ectopic TGFβ signalling promoted synaptic overgrowth. With previous studies implicating *Rab8* in the recycling endosomal pathway taken together these findings support the proposed mechanism for synaptic overgrowth in *Rab8* mutants. This may also suggest why *Rab8* mutants potentiate *CHMP2B*^{Intron5} toxicity, as *Rab8 CHMP2B* double mutants would perturb both recycling endosomal traffic and MVB formation. In order to substantiate the role of POSH in the degradation of HRS, future investigation may look to determine whether heterozygous expression of a POSH null in a transheterozygous *Rab8* mutant

background is sufficient to rescue reduced motor neuronal HRS levels observed in *Rab8* mutants.

In a study by Criollo et al. (2011) it was demonstrated that TAK1 may act as a regulator of autophagy (Criollo et al., 2011). For example they demonstrated that TAK1 depletion or expression of a *TAK1* dominant negative inhibited autophagy in cell culture. In addition they reported that TAK1 was required for optimal induction of autophagy in response to a number of stimuli, including TGFβ signalling. Corroborating these findings a number of other studies have substantiated the role for TAK1 as a regulator of autophagy (Herrero-Martin et al., 2009; Shin et al., 2013). Previous studies have also shown that autophagy acts as a potent regulator of synaptic growth at the *Drosophila* NMJ (Milton et al., 2011; Shen and Ganetzky, 2009). For example it has been demonstrated that autophagy degrades *hiw,* relieving its inhibition upon JNK signalling, promoting synaptic overgrowth (Shen and Ganetzky, 2009). Furthermore inhibition of autophagy can alleviate synaptic overgrowth in *spin* mutants (Milton et al., 2011). As such one may postulate that autophagy may contribute towards synaptic overgrowth in *Rab8* mutants and future investigation should look to determine whether inhibition of autophagy could alleviate synaptic overgrowth in *Rab8* mutants. In fact preliminary evidence has shown that inhibition of autophagy by homozygous expression of a loss of function mutant of the essential autophagy gene *Atg7* can inhibit increased mean normalised synaptic bouton number in transheterozygous *Rab8* mutants (wt = 110.2 ± 3.7, n = 16. $Rab8^{1}/Rab8^{B229}$ = 199.8 ± 13.7, n = 10. $Atg7^{D77}/Atg7^{D77}$ = 99.1 ± 6.03, n = 5. $Rab8^{1}/Rab8^{B229}$; $Atg7^{D77}/Atg7^{D77}$ = 106.1 ± 7.9, n = 6). Future investigation shall look to build upon these preliminary findings by increasing the data set and including a range of autophagy related genes.

5.3.4. Summary

Taken together the results presented in this chapter demonstrate that synaptic overgrowth in *Rab8* mutants requires TGFβ and JNK signalling and that both of these signalling pathways are elevated in *Rab8* mutants. Furthermore they demonstrated that JNK and TGFβ signalling act synergistically in the regulation of synaptic growth and development. This synergism is potentially regulated by the activity of POSH as a central JNK scaffold, mediating a signal transduction pathway between TGFβ and JNK, via TAK1. Ectopic accumulation of POSH may also promote degradation of HRS, inhibiting MVB formation further potentiating ectopic TGFβ activity.

6. Characterisation of *CHMP2B*^{Intron5} and The Role of *Rab8* In *CHMP2B*^{Intron5} Toxicity

6.1. Introduction

Previous studies have implicated CHMP2B in the regulation of normal neuronal development and morphology, which is perturbed by the FTD associated *CHMP2B*^{Intron5} mutation (Belly et al., 2010; Lee et al., 2012; Lee et al., 2007). As such we asked whether neuronal expression of *CHMP2B*^{Intron5} in *Drosophila* larvae would elicit a perturbation to the normal assembly and function of the NMJ. In addition, having previously identified *Rab8* as both a potent regulator of NMJ growth and as a dominant enhancer of *CHMP2B*^{Intron5} expression in the fly eye, it was asked whether expression of *Rab8* could alleviate any *CHMP2B*^{Intron5} related perturbation observed. In this chapter we demonstrate that neuronal expression of *CHMP2B*^{Intron5} elicits a synaptic overgrowth phenotype at the *Drosophila* larval NMJ and that overexpression of *Rab8* is sufficient to alleviate all aspects of this overgrowth phenotype.

FTD-3 associated with the *CHMP2B*^{Intron5} mutation is classified, based upon the presence and composition of neuronal inclusions, as FTLD-UPS (Holm et al., 2009; Isaacs et al., 2011). That is to say that patients, and model organisms, displaying the *CHMP2B*^{Intron5} mutation typically present with ubiquitin-positive neuronal inclusions. The formation of such inclusions has typically been associated with perturbation to homeostatic protein quality control systems including the ubiquitin proteasome system and autophagy (Chen et al., 2011; Takalo et al., 2013). In addition previous studies have revealed that mutations in *CHMP2B*, and other ESCRT components, elicit significant aberration to normal autophagic processes (Filimonenko et al., 2007a; Lee et al., 2007; Lee and Gao, 2008). Autophagy itself can be defined simply as a homeostatic catabolic process by which cellular components are recycled through targeted degradation by the lysosome. It has been demonstrated to serve as an essential protective response during periods of cell stress (Altman and Rathmell, 2012). In addition it has been implicated as a potent regulator of

synaptic growth at the *Drosophila* NMJ (Milton et al., 2011; Shen and Ganetzky, 2009; West and Sweeney, 2012). However it is a matter of debate as to whether autophagy contributes towards the toxicity associated with the *CHMP2B*^{Intron5} mutation. As such in this chapter the investigation looks to determine whether autophagy contributes towards the toxicity of the *CHMP2B*^{Intron5} eye and NMJ phenotypes.

6.2. Results

6.2.1. Neuronal Expression of *CHMP2B*^{Intron5} Elicits a Synaptic Overgrowth Phenotype That Can be Alleviated by Rab8

Previous studies have shown that expression of the *CHMP2B*^{Intron5} mutant transgene within cultured neurons results in a significant perturbation to normal neuronal morphology, prior to neuronal death (Belly et al., 2010; Lee et al., 2007). For example Belly et al. (2011) demonstrated that transfection of primary rat hippocampal neurons with *CHMP2B*^{Intron5} induced a 25 % reduction in dendritic branching coupled with a 64 % increase in the density of dendritic spines. Spines were also, on average, 40 % smaller than those observed in wildtypes. In addition Lee et al. (2007) demonstrated that transfection of *CHMP2B*^{Intron5} into cultured cortical neurons elicited a significant dendritic retraction phenotype, presenting with an 80 % reduction in dendritic length prior to eventual neuron death within 2 - 3 days. In contrast, whilst *CHMP2B*^{Intron5} has been shown to induce a reduction in dendritic branching it has been demonstrated that mutations in the gene encoding the CHMP2B interacting protein Shrub elicit an increased branching phenotype in *Drosophila* larval class IV dendritic arborizing neurons (Sweeney et al., 2006). Increased branching was associated with a significant increase in the number of fine higher-order branches. With previous data implicating CHMP2B in the regulation of neuronal development analysis looked to determine whether expression of *CHMP2B*^{Intron5}, in an *in vivo Drosophila* model, would elicit perturbations to normal neuronal morphology, focusing on the NMJ. The results presented here demonstrate that neuronal expression of UAS-*CHMP2B*^{Intron5}, under the control

of the pan-neuronal driver nSyb-Gal4, induced a significant increase (35.3 %) in synaptic bouton number, when compared to wildtype, at muscle 6/7 hemi-segment A3 of 3rd instar larvae (Fig. 6.1.).

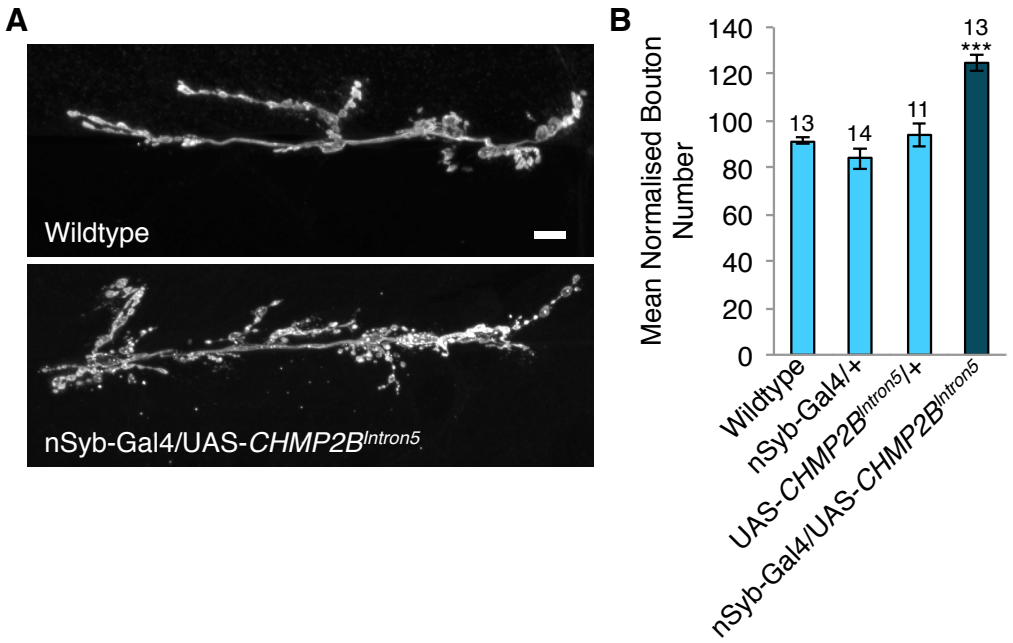

Figure 6.1. Neuronal Expression of *CHMP2B*^{Intron5} Elicits a Significant Increase in Synaptic Bouton Number
(**A-B)** Overexpression of the UAS-*CHMP2B*^{Intron5} mutant transgene under the control of the pan-neuronal driver nSyb-Gal4 induces a synaptic overgrowth phenotype characterised by a significant increase in synaptic bouton number. 3rd instar larvae muscle 6/7, hemi-segment A3. Scale Bar = 10 µm. (ANOVA: $F(d.f.\ 3) = 18.6926$; $p < 0.001$ with post-hoc Dunnett's comparison to wildtype control *** $p < 0.001$).

Having observed a significant increase in synaptic bouton number at muscle 6/7, hemi-segment A3, as result of pan-neuronal expression of the *CHMP2B*^{Intron5} mutant transgene, muscle 4 was used as a more amenable synapse to further characterise synaptic overgrowth. During the course of this investigation it has been demonstrated that *Rab8* mutants act as dominant enhancers of *CHMP2B*^{Intron5} toxicity (Chapter 3), whilst *Rab8* has been identified as a potent regulator of synaptic growth (Chapters 4 and 5). As such it was also asked whether expression of wildtype *Rab8* could alleviate the overgrowth phenotype observed as a result of neuronal *CHMP2B*^{Intron5} expression.

The results presented here demonstrate that the increased synaptic bouton number, associated with neuronal expression of *CHMP2B*^{Intron5}, observed at muscle 6/7 is conserved at muscle 4 (Fig. 6.2.). For example a significant increase in synaptic bouton number, compared to wildtype, was observed at

both muscle 6/7 and 4 (Fig. 6.2.). In addition it was demonstrated that co-expression of UAS-*Rab8*, which had no effect on synaptic bouton number alone, could alleviate increased bouton number associated with neuronal expression of the *CHMP2B*^{Intron5} mutant transgene (Fig. 6.2.). At muscle 6/7 a partial rescue was observed with nSyb-Gal4/UAS-*CHMP2B*^{Intron5};UAS-*Rab8*/+ NMJ's showing a synaptic bouton number significantly less than nSyb-Gal4/UAS-*CHMP2B*^{Intron5} NMJ's, however still significantly greater than both wildtype and nSyb-Gal4/+;UAS-*Rab8*/+ controls (Fig. 6.2.B). In contrast at muscle 4 a complete rescue was observed with Rab8 rescues showing a significantly lower bouton number than nSyb-Gal4/UAS-*CHMP2B*^{Intron5} NMJ's, and no significant variance from wildtypes (Fig. 6.2.A&C). Rescues did, however, show a small significant variance from nSyb-Gal4/+;UAS-*Rab8*/+ control's, which showed a slightly increased, but not significant, number of boutons compared to wildtype. Overall these results suggest that neuronal co-expression of wildtype *Rab8* is sufficient to curtail increased synaptic bouton number induced by expression of the *CHMP2B*^{Intron5} mutant transgene.

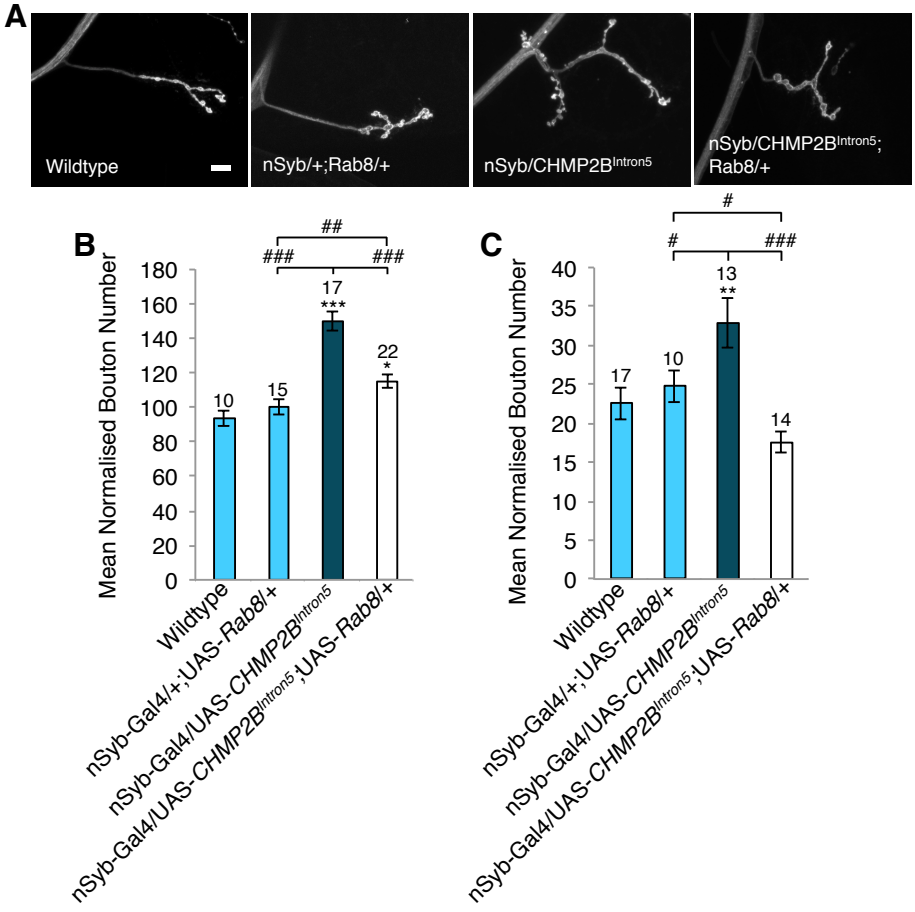

Figure 6.2. Co-Expression of Wildtype *Rab8* Can Alleviate Increased Synaptic Bouton Number Associated With Neuronal Expression of *CHMP2B*^{Intron5}

(**A**) Neuronal expression of UAS-*CHMP2B*^{Intron5} under the control of the pan-neuronal driver nSyb-Gal4 induces a significant synaptic overgrowth phenotype that can be rescued by co-expression of UAS-*Rab8.* Neuronal expression of UAS-*Rab8* alone does not affect NMJ growth. Scale bar = 10 µm. (**B-C**) Increased synaptic bouton number associated with neuronal expression of the *CHMP2B*^{Intron5} mutant transgene can be alleviated by co-expression of UAS-*Rab8* at both muscle 6/7 and muscle 4, hemi-segment A3, in 3rd instar larvae. **B:** ANOVA: $F(d.f.\ 3) = 25.2705$; $p < 0.001$ **C**: ANOVA: $F(d.f.\ 3) = 6.3774$; $p < 0.001$ with post-hoc Dunnett's comparison to wildtype controls *** $p < 0.001$, ** $p < 0.01$, * $p < 0.05$ and student's t-test between genotypes ### $p < 0.001$, ## $p < 0.01$, # $p < 0.05$).

Analysis of muscle 4 also demonstrated that neuronal expression of the *CHMP2B*^{Intron5} mutant transgene elicited other synaptic overgrowth phenotypes, in addition to increased synaptic bouton number. For example nSyb-Gal4 driven expression of UAS-*CHMP2B*^{Intron5} induced a significant increase in mean normalised NMJ length (Fig. 6.3.A). Increased NMJ length was completely rescued by co-expression of wildtype *Rab8*. In contrast to *Rab8* mutants' nSyb-Gal4/UAS-*CHMP2B*^{Intron5} larvae displayed a significant increase in NMJ branching (Fig. 6.3.B). This was, again, rescued by co-expression of *Rab8*. Comparable to *Rab8* mutants neuronal expression of *CHMP2B*^{Intron5} induced a proliferation in the mean number of satellite boutons observed (Fig. 6.3.C). In contrast to many endocytic mutants this increase in satellite boutons does not account, entirely, for the increase in total bouton number observed. As with the other synaptic overgrowth phenotypes displayed increased satellite bouton number could be rescued through co-expression of *Rab8* (Fig. 6.3.C). In contrast to *Rab8* mutants, which display a reduced synaptic bouton size, neuronal expression of *CHMP2B*^{Intron5} has no effect upon the synaptic bouton size observed (Fig.6.3.D). As such cumulative bouton size was not analysed. Interestingly neuronal co-expression of *Rab8* and the *CHMP2B*^{Intron5} mutant transgene elicited a significant increase in synaptic bouton number, compared to wildtype and UAS-Rab8 or UAS-CHMP2B^{Intron5} expressed alone (Fig.6.3.D).

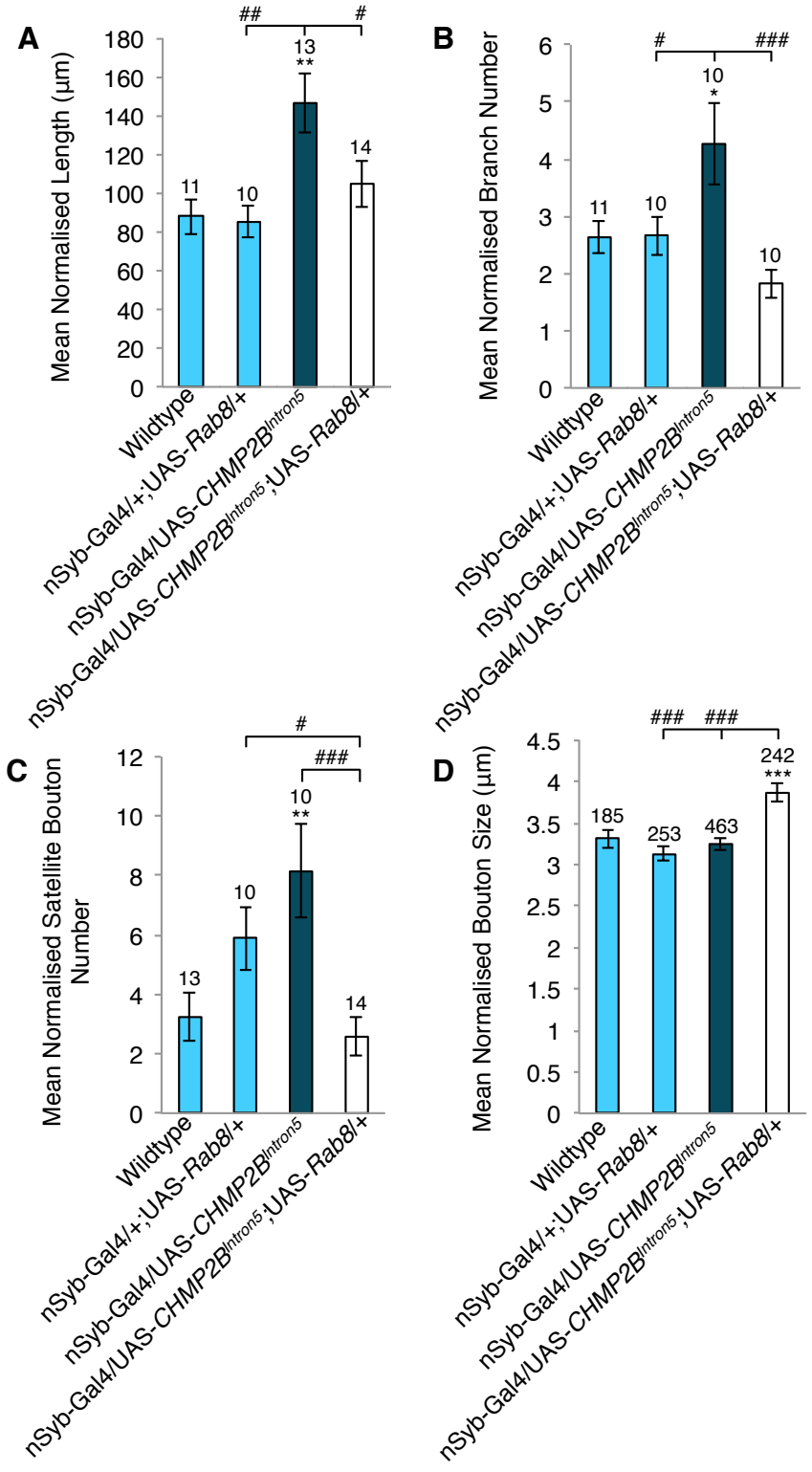

Figure 6.3. Neuronal Expression of *CHMP2B*^{Intron5} Induces Unrestricted Synaptic Growth That Can be Rescued Through Co-Expression of Wildtype Rab8

(**A**) Neuronal Expression of UAS-*CHMP2B*^{Intron5}, using the pan neuronal driver nSyb-Gal4, induces a significant increase in mean normalised NMJ length compared to wildtypes and neuronally expressed *Rab8*, which shows no variance from wildtype. Increased NMJ length is rescued by co-expression of UAS-*Rab8* with nSyb-Gal4/UAS-*CHMP2B*^{Intron5};UAS-*Rab8*/+ larvae showing no variance in NMJ length from wildtype or *Rab8* controls, yet a significant variance from neuronally expressed *CHMP2B*^{Intron5}. ANOVA: F(d.f. 3) = 5.4519; $p < 0.01$ with post-hoc Dunnett's comparison to wildtype controls ** $p < 0.01$ and student's t-test between genotypes ## $p < 0.01$, # $p < 0.05$. (**B**) Neuronal expression of UAS-*CHMP2B*^{Intron5} elicits a significant increase in mean normalised branch number compared to wildtype and neuronally expressed *Rab8* controls. Increased branching is also rescued by co-expression of *Rab8* with nSyb-Gal4/UAS-

CHMP2B^{Intron5};UAS-*Rab8*/+ larvae showing no variance in branch number from controls yet a significant variance from nSyb-Gal4/UAS-*CHMP2B*^{Intron5}. ANOVA: F(d.f. 3) = 5.4544; $p < 0.01$ with post-hoc Dunnett's comparison to wildtype controls * $p < 0.05$ and student's t-test between genotypes ### $p < 0.001$, # $p < 0.05$. (**C**) Neuronal expression of *CHMP2B*^{Intron5} promotes a proliferation of satellite boutons showing a significant increase in satellites compared to wildtypes but not nSyb-Gal4/+;UAS-*Rab8*/+ controls which show an increased, although not significantly different from wildtype, number of satellite boutons. Increased satellite bouton number can again be rescued by co-expression of *Rab8*. Rescues show no variance from wildtype and a significant variance from neuronally expressed *CHMP2B*^{Intron5}. Rescues also show a significant variance from nSyb-Gal4/+;UAS-*Rab8*/+ controls. ANOVA: F(d.f. 3) = 6.5642; $p < 0.001$ with post-hoc Dunnett's comparison to wildtype controls ** $p < 0.01$ and student's t-test between genotypes ### $p < 0.001$, # $p < 0.05$. (**D**) Neuronal expression of *CHMP2B*^{Intron5} has no effect upon synaptic bouton size showing no variance to wildtype of neuronally expressed *Rab8* controls. Neuronal co-expression of *Rab8* and *CHMP2B*^{Intron5} elicited an increase in mean normalised synaptic bouton size showing a mean bouton size significantly greater than all other genotypes. ANOVA: F(d.f. 3) = 12.9398; $p < 0.001$ with post-hoc Dunnett's comparison to wildtype controls *** $p < 0.001$ and student's t-test between genotypes ### $p < 0.001$. All analysis was performed on NMJ's at muscle 4, hemi-segment A3 in 3rd instar wandering larvae.

6.2.2. Neuronal Expression of *CHMP2B*^{Intron5} Induces Increased TGFβ Activity That Can be Rescued By Expression of *Rab8*

In the previous chapter it was shown that NMJ synaptic overgrowth in *Rab8* mutants required a permissive TGFβ signal and that mutants presented with increased TGFβ activity. Having demonstrated here that neuronal expression of the *CHMP2B*^{Intron5} mutant transgene elicited a synaptic overgrowth phenotype that could be rescued through expression of wildtype *Rab8* it was asked whether increased TGFβ activity was also observed as a result of neuronal expression of *CHMP2B*^{Intron5}. The results here show that pan-neuronal expression of *CHMP2B*^{Intron5}, under the control of nSyb-Gal4, results in a significant increase in nuclear p-MAD within eve positive motor neurons (Fig. 6.4.). In addition it was demonstrated that co-expression of wildtype *Rab8* alongside the *CHMP2B*^{Intron5} mutant transgene was sufficient to completely rescue elevated nuclear P-MAD (Fig. 6.4.). It is interesting to note that neuronal (nSyb) expression of *Rab8* alone resulted in the accumulation of P-MAD at a peri-nuclear localisation, although levels of nuclear P-MAD showed no variance from wildtype (Fig. 6.4.). In addition co-expression of *Rab8* and *CHMP2B*^{Intron5} rescues both reduced nuclear P-MAD in *CHMP2B*^{Intron5} and peri-nuclear accumulation of P-MAD associated with *Rab8* overexpression.

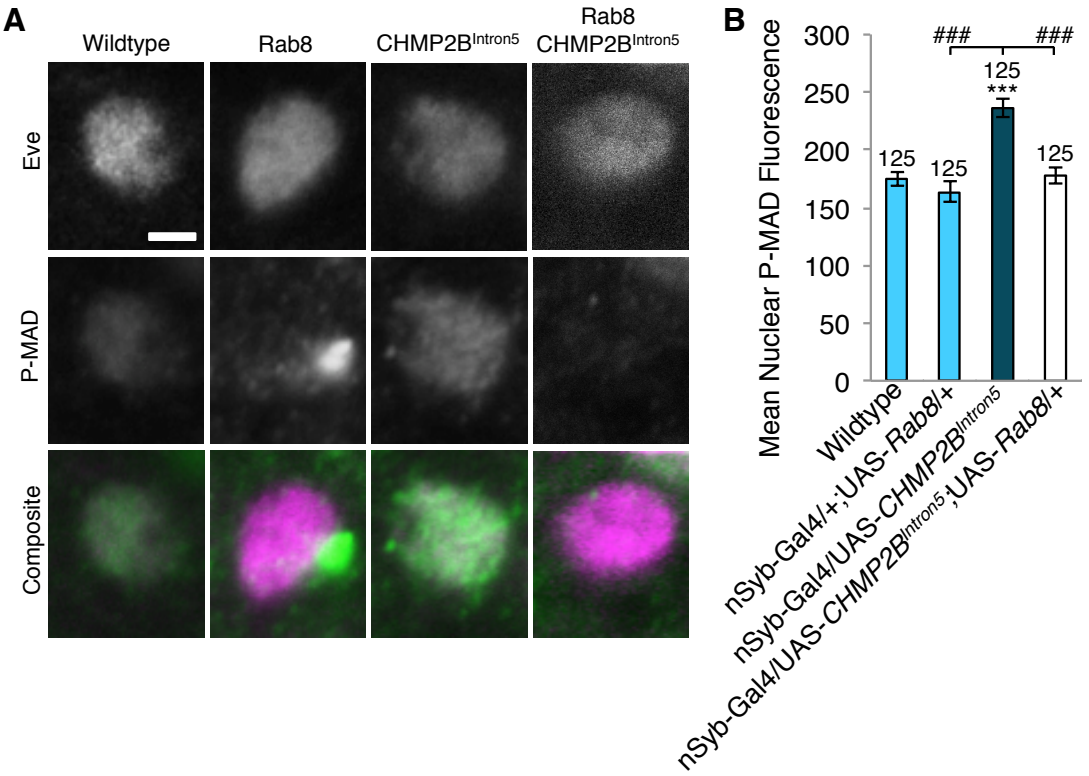

Figure 6.4. Neuronal Expression of *CHMP2B*^{Intron5} Induces Increased Levels of Nuclear P-MAD That Can be Alleviated by Co-Expression of Wildtype *Rab8*
(**A-B**) Neuronal Expression of *CHMP2B*^{Intron5} under the control of the pan-neuronal driver nSyb-Gal4 elicits a significant increase in levels of nuclear P-MAD within eve positive motor neurons, in 3rd instar larvae. Elevated levels of nuclear P-MAD can be alleviated by co-expression of wildtype Rab8. Whilst nuclear expression of *Rab8* shows no variance in nuclear levels of P-MAD compared to wildtype it does result in a peri-nuclear accumulation of P-MAD. This is not observed when co-expressed with *CHMP2B*^{Intron5}. Scale bar = 2 µm. ANOVA: F(d.f. 3) = 18.8731; $p < 0.001$ with post-hoc Dunnett's comparison to wildtype controls *** $p < 0.001$ and student's t-test between genotypes ### $p < 0.001$.

6.2.3. Neuronal Expression of *CHMP2B*^{Intron5} Induces a Locomotor Deficit That Can Not be Rescued By *Rab8*

Having observed a synaptic overgrowth phenotype associated with neuronal expression of the *CHMP2B*^{Intron5} mutant transgene it was asked whether synaptic overgrowth was associated with a perturbation to physiological function. As for *Rab8* mutants, see Chapter 4, NMJ functionality was assessed using a crawling assay to look at locomotor function. Whilst synaptic overgrowth in *Rab8* mutants was not associated with a reduction in locomotor function here it is observed that pan-neuronal expression of the *CHMP2B*^{Intron5} mutant transgene results in a 46.94 % reduction in larval velocity, compared to wildtype (Fig. 6.5.). Furthermore whilst synaptic overgrowth phenotypes and elevated levels of nuclear P-MAD in nSyb-Gal4/UAS-*CHMP2B*^{Intron5} larvae can be

rescued by overexpression of wildtype *Rab8* it is shown here that co-expression of wildtype *Rab8* alongside *CHMP2B*^{Intron5} is not sufficient to rescue the locomotor deficit, showing no variance from nSyb-Gal4/UAS-*CHMP2B*^{Intron5} mutants and a significant variance from wildtype. As such this suggests that the locomotor deficit observed in *CHMP2B*^{Intron5} mutants may not be directly associated with the synaptic overgrowth phenotype.

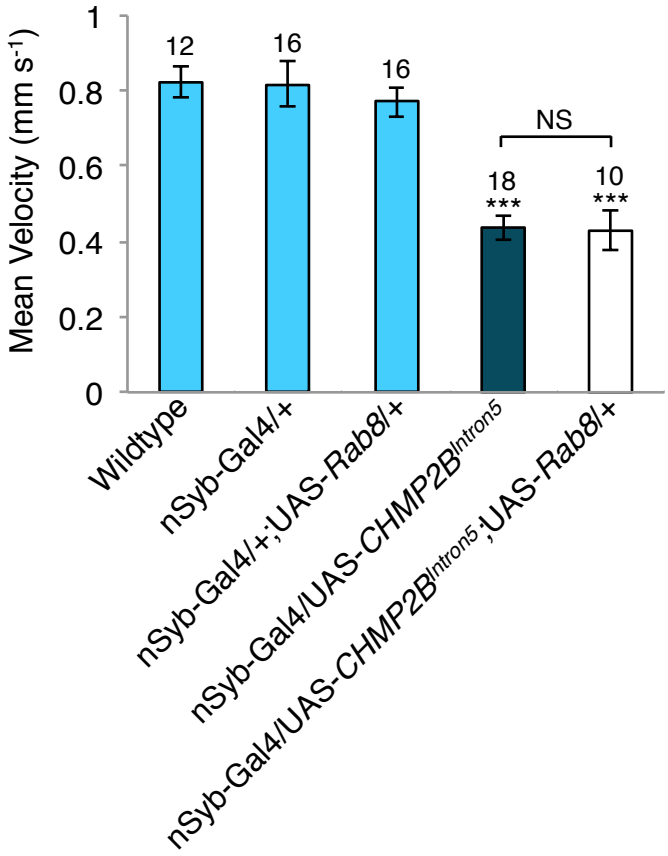

Figure 6.5. Neuronal Expression of CHMP2B^{Intron5} Induces a Locomotor Deficit That Can Not be Alleviated by Expression of Rab8.
Pan-neuronal expression of the *CHMP2B*^{Intron5} mutant transgene under the control of nSyb-Gal4 results in a locomotor deficit showing a significantly reduced mean crawling velocity of third instar larvae when compared to wildtype controls. Co-expression of wildtype *Rab8* does not rescue the reduced crawling velocity in *CHMP2B*^{Intron5} mutants. (ANOVA: $F(d.f.\ 4) = 19.7039$; $p < 0.001$ with post-hoc Dunnett's comparison to wildtype control *** $p < 0.001$ and student's t-test comparison between groups).

6.2.4. Neuronal Expression of *CHMP2B*^{Intron5} Induces Accumulation of Ubiquitinylated Proteins Within the Larval Ventral Nerve Cord

As mentioned previously, in Chapter 1, FTD is a highly heterogeneous disease that can, in part, be classified into neuropathological subtypes based upon the prevalence and composition of neuronal inclusions. FTD-3, associated with the *CHMP2B*^{Intron5} mutation, is classified as FTD-UPS; displaying tau-negative, TDP-43-negative, FUS-negative and ubiquitin-positive neuronal inclusions. As such it was asked whether neuronal expression of the *CHMP2B*^{Intron5} mutant transgene could induce an accumulation of ubiquitinylated protein aggregates within the larval brain. Here it is demonstrated that expression of *CHMP2B*^{Intron5} under the control of the pan-neuronal driver nSyb-Gal4 results in the accumulation of mono- and poly-ubiquitnylated proteins within cells of the larval VNC (Fig. 6.6.). Such aggregates were not observed within wildtype larval VNC's. It is also interesting to note that neuronal expression of *CHMP2B*^{Intron5} also led to a perturbation to HRP staining, which is used as a marker of the *Drosophila* nervous system. Anti-HRP was originally identified as being able to stain the nervous system of *Drosophila* and grasshoppers by Jan and Jan (1982), and has since become an essential tool in the study of the *Drosophila* nervous system (Jan and Jan, 1982). Subsequent studies have revealed the immunoreactivity of anti-HRP to be with the carbohydrate epitopes of the nervous system specific glycoprotein Nervana (Sun and Salvaterra, 1995a, b). Here it was shown that *CHMP2B*^{Intron5} expression lead to aggregation of anti-HRP staining within specific cells and that this partially co-localised with aggregates of mono- and poly-ubiquitinylated proteins.

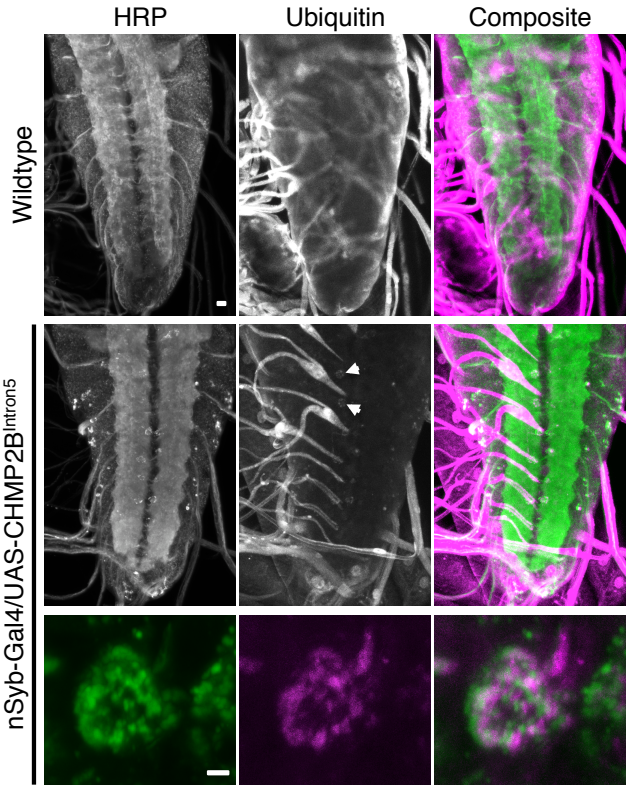

Figure 6.6. Ubiquitinylated Proteins Aggregate in The Ventral Nerve Cord of Larvae Neuronally Expressing *CHMP2B*^{Intron5}
Neuronal expression of *CHMP2B*^{Intro5} under the control of the pan-neuronal driver nSyb-Gal4 leads to the accumulation of mono- and poly-ubiquitinylated protein aggregates within cells of the larval ventral nerve cord (Arrow Heads and zoomed in box). Similar accumulations were not observed in wildtype animals where staining appeared diffuse. Expression of *CHMP2B*^{Intron5} also appears to perturb normal HRP staining, which marks the nervous system, with aggregates showing partial co-localisation with ubiquitin aggregates. Scale bars; whole VNC = 10 µm, close up of aggregates = 2 µm.

6.2.5. *CHMP2B*^{Intron5} Mutants Show Autophagic Defects

6.2.5.1. Inhibition of Autophagy Related Genes Alleviates *CHMP2B*^{Intron5} Toxicity in The *Drosophila* Eye

Abnormal accumulation and aggregation of proteins, forming neuronal inclusions, is seen as a hallmark of many neurodegenerative diseases, including Parkinson's, Huntington's, Alzheimer's, ALS and FTD (Adachi et al., 2009; Bigio et al., 2004; Pedersen and Heegaard, 2013; Ross and Poirier, 2004; Rosso et al., 2001). As such it has been proposed that impaired protein degradation and clearance may provide a conserved mechanism behind neurodegenerative diseases.

Previous studies have hypothesised that the accumulation of ubiquitin positive neuronal aggregates in FTD, associated with CHMP2B mutations, are the result of perturbations to the autophagic protein degradation pathway (Filimonenko et al., 2007a) (Lee et al., 2007). For example Lee et al. (2007) demonstrated that transfection of cortical neurons, in culture, with either *CHMP2B*^{Intron5} or mSnf7-2 siRNA resulted in the accumulation of autophagosomes and abnormal multi-lamellar structures. *CHMP2B*^{Intron5} expression also promoted sequestration of mSnf7-2 into ubiquitin positive endosomes. Similar observations were also seen through overexpression of either *CHMP2B*^{Intron5} or *Shrub*-RNAi within the *Drosophila* eye. In addition transfection of cortical neurons with *mSnf7-2* siRNA or *CHMP2B*^{Intron5} also promoted severe dendritic retraction and cell death. However, despite the observation of autophagic disruption in *CHMP2B* mutants it has been argued that perturbation to autophagy may not be the causative factor in *CHMP2B* associated neurodegeneration. For example it has been shown that other *CHMP2B* mutants including *CHMP2B*$^{\Delta 10}$ display autophagic disruption akin to that seen in *CHMP2B*^{Intron5} without presenting neurodegeneration and cell death (Belly et al., 2010; Filimonenko et al., 2007a). As such, having observed the accumulation of ubiquitin positive inclusions within the VNC of larvae neuronally expressing the *CHMP2B*^{Intron5} transgene, analysis looked to elucidate whether autophagy has a role in *CHMP2B*^{Intron5} associated neurodegeneration within this system.

Here the *Drosophila* eye is once again utilised as a model system to screen for modifiers of the *CHMP2B*^{Intron5} phenotype in a targeted screen of known autophagy genes. With previous studies showing *CHMP2B*^{Intron5} toxicity to be associated with an abnormal association between CHMP2B and Shrub and that *Shrub* inhibition promotes autophagic defects similar to *CHMP2B*^{Intron5} autophagy genes were also screened against the *Shrub*-GFP dominant negative eye phenotype (Ahmad et al., 2009; Lee et al., 2007; Lee and Gao, 2009).

The results presented here provide support for the hypothesis that autophagy contributes towards the toxicity observed in *CHMP2B*^{Intron5} and *shrub*-GFP mutants. For example reduction of autophagy via the introduction of

heterozygous mutations, or RNAi transgenes directed against the autophagy related genes (Atg's) results in a decrease in the severity of the *CHMP2B*^{Intron5} eye phenotype (Fig. 6.7.). For these experiments we targeted *Atg1*, *Atg7* and *Atg18*, which have all been identified as highly conserved and essential autophagy genes (Nakatogawa et al., 2009; Obara et al., 2008). Quantification of the *CHMP2B*^{intron5} eye phenotype revealed an increased prevalence of the mild (low; +) eye phenotype when the function of the *Atg* genes was reduced in a GMR-Gal4, UAS-*CHMP2B*^{Intron5} background. Reduction of Atg function alone showed no effect on eye development in the absence of *CHMP2B*^{Intron5}. Expression of *Atg18*-RNAi in the *CHMP2B*^{Intron5} eye showed the greatest alleviation of toxicity. Further supporting these findings it was observed that increasing autophagy through overexpression of UAS-*Atg1* potentiated the *CHMP2B*^{Intron5} eye phenotype. However it must be noted that *Atg1* overexpression in the absence of *CHMP2B*^{Intron5} induced a rough eye phenotype in its own right. Interestingly it was also observed that inhibition of *Rheb,* which is known to promote autophagy through alleviating Rheb mediated activation of TOR, an autophagic inhibitor, showed little effect upon *CHMP2B*^{Intron5} toxicity. In contrast overexpression of *Rheb*, which should inhibit autophagy, actually potentiated toxicity, demonstrating an opposing effect to inhibiting autophagy through inhibition of *Atg* genes.

In contrast to the results observed in the GMR-Gal4, UAS-*CHMP2B*^{Intron5} background, inhibition of *Atg* genes in a GMR-Gal4, UAS-*Shrub*-GFP background appeared to have little ability to reduce toxicity (Fig. 6.7.). In contrast overexpression of both Atg1 and Rheb potentiated toxicity. Inhibition of Rheb also potentiated toxicity, reducing the number of flies classified as presenting a low phenotype. These results suggest that *CHMP2B*^{Intron5} and the dominant negative *Shrub*-GFP may differentially affect autophagy.

Taken together these results suggest that autophagy may contribute to the degeneration observed in *CHMP2B*^{Intron5} mutants. However, our data suggests a possible discrepancy between the toxic effects of *CHMP2B*^{Intron5} and *Shrub*-GFP.

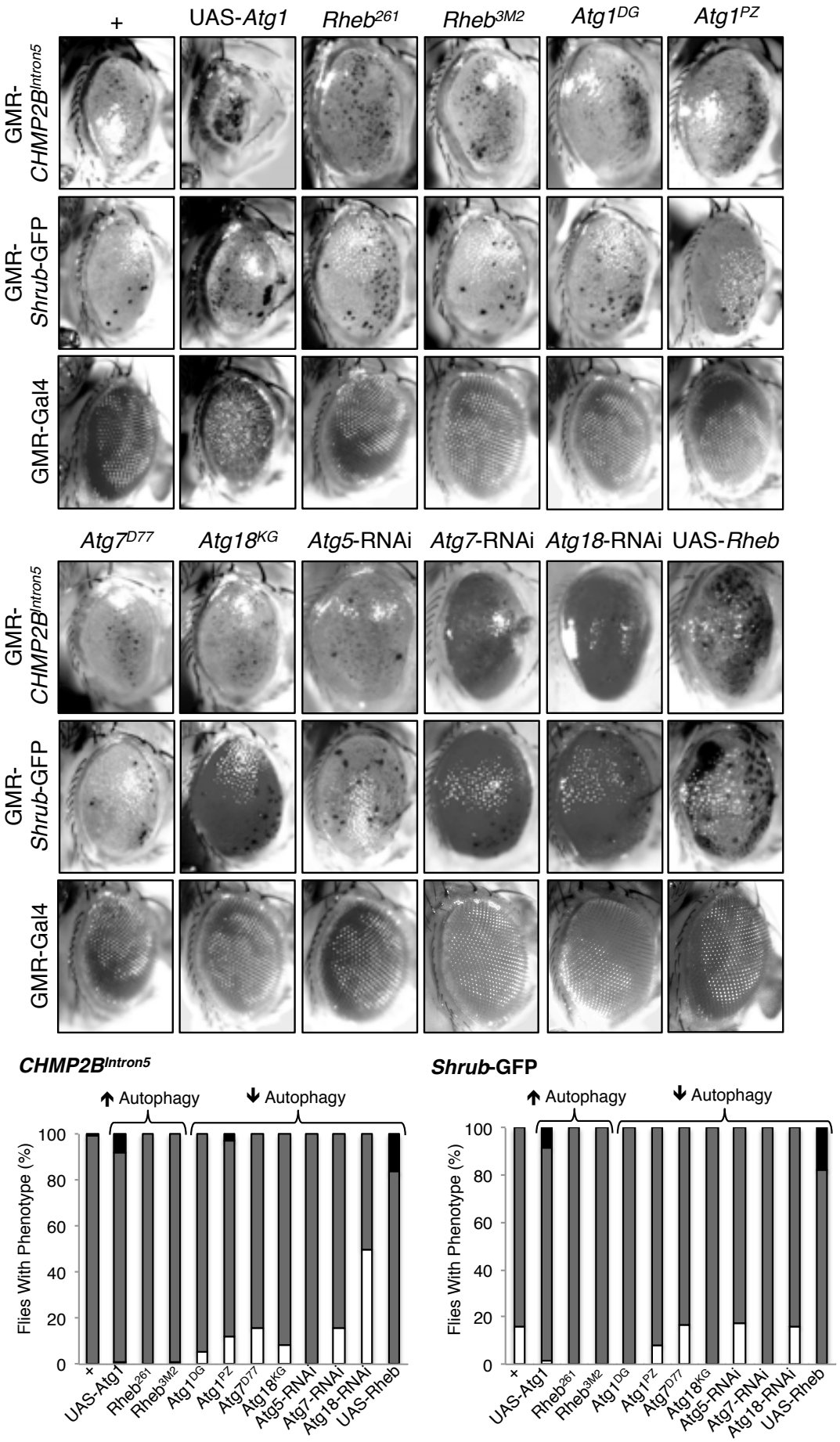

Figure 6.7. Inhibition of Atg Genes Alleviates *CHMP2B*^{Intron5} But Not *Shrub*-GFP Toxicity
A targeted modifier screen of known autophagy genes against GMR-Gal4, UAS-*CHMP2B*^{Intron5}/+ and GMR-Gal4, UAS-*Shrub*-GFP/+ reveals that inhibition of autophagy related genes (Atg's)

alleviates toxicity associated with *CHMP2B*^{Intron5} but not with *Shrub*-GFP. In contrast inhibition of autophagy through overexpression of Rheb potentiates toxicity associated with both. Potentiation of autophagy through overexpression of Atg1 potentiates both *Shrub*-GFP and *CHMP2B*^{Intron5} toxicity whilst Rheb mutants only potentiate *Shrub*-GFP. Quantification: White = low (+) phenotype (< 15 spots of melanisation), Grey = medium (++) phenotype (>15 spots of melanisation but < 50 % of the eye affected), Black = high (+++) phenotype (> 50 % of the eye affected by melanisation). n = 100 per genotype.

6.2.5.2. Expression of *CHMP2B*^{Intron5} in The *Drosophila* Eye Severely Perturbs The Internal Eye Structure and Distribution of Autophagic Markers

Having demonstrated that, in general, inhibition of autophagy alleviates the severity of the *CHMP2B*^{Intron5} eye phenotype, we used the autophagic marker Atg5-GFP to visualise autophagy within the *CHMP2B*^{Intron5} eye. Atg5 has previously been shown to play a fundamental role during normal autophagosome maturation (Chen and Zhong, 2012; Fujita et al., 2008). Following activation by Atg7 Atg5 forms a stable complex with Atg12 and Atg16 where it plays a functional role during elongation of the isolation membrane to form an autophagosome, although the mechanisms involved in this process remain unclear (Fujita et al., 2008). Here it is demonstrated that whilst Atg5-GFP displays an even, diffuse distribution throughout the *Drosophila* wildtype eye, expression of *CHMP2B*^{Intron5} severely perturbs the normal eye structure, resulting in a re-distribution of Atg5-GFP (Fig.6.8.). Due to the severity of the eye disruption it proves difficult to ascertain the effect of *CHMP2B*^{Intron5} upon Atg5-GFP distribution alone. It is, however, clear that Atg5-GFP re-distributes, predominantly surrounding areas where degeneration is most severe and melanisation is present.

Aside from autophagic perturbation these results also further reveal the severity of degeneration associated with expression of the *CHMP2B*^{Intron5} transgene. Rhodamine conjugated phalloidin was used to stain the actin rich rhabdomeres within the 8 photoreceptor neurons (R1-R8) of each ommatidium. Only 7 rhabdomeres are visible as R8 lies directly beneath R7, see Chapter 1. As such 7 clustered photoreceptors can be observed within each ommatidia, of which there are ~ 760, repeated in a highly organised manner across the wildtype eye.

In contrast GMR-Gal4 expression of *CHMP2B*^{Intron5} severely perturbs the normal internal eye structure, resulting in a complete loss of normal photoreceptor distribution and organisation (Fig. 6.8). It must be noted that whilst eye specific GMR-Gal4 drives expression within supporting cells and not just neurons. These results support previous light microscopy observations, demonstrating severe degeneration to the normal highly organised eye structure as a result of GMR-Gal4 driven expression of the *CHMP2B*^{Intron5} transgene.

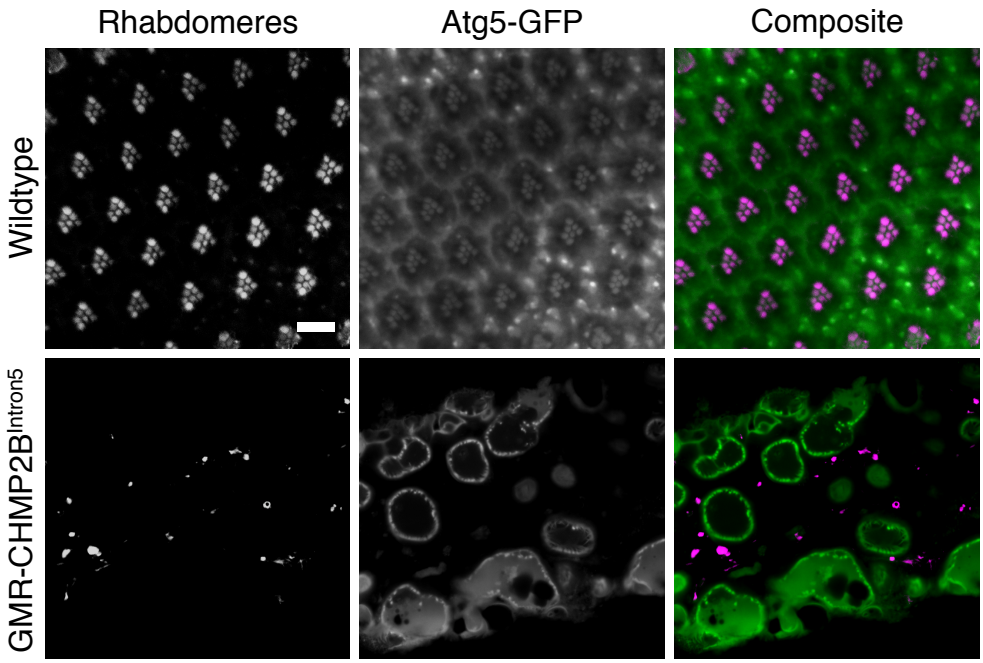

Figure 6.8. *CHMP2B*^{Intron5} Expression Perturbs Autophagy Within the *Drosophila* Eye
Expression of the *CHMP2B*^{Intron5} mutant transgene within the *Drosophila* eye, under the control of the eye specific driver GMR-Gal4, perturbs the normally highly regular and ordered internal structure of the eye. Rhodamine conjugated phalloidin was used to stain the actin rich rhabdomeres within each ommatidium of the flies photoreceptor neurons. This allowed visualisation of 7 distinct puncta clustered in a highly regular pattern repeating throughout the eye, as seen in wildtypes. Expression of *CHMP2B*^{Intron5} completely disrupts this normal distribution pattern. Atg5-GFP was used as a marker of autophagy and can be seen to be evenly and diffusely distributed throughout the wildtype eye. Expression of *CHMP2B*^{Intron5} perturbs this pattern with autophagic activity re-distributed to specific localisations, predominantly surrounding melanised spots. Scale bar = 10 μm.

6.2.5.3. Inhibition of Autophagy Alleviates Synaptic Overgrowth Associated With *CHMP2B*^{Intron5}

Having demonstrated that *CHMP2B*^{intron5} expression induced overgrowth at the larval neuromuscular synapse we looked to establish whether autophagy had a contributory role in the synaptic overgrowth observed. Previous studies have

demonstrated that autophagy acts as a potent regulator of synaptic growth. For example studies have shown that increasing autophagy promotes a synaptic overgrowth phenotype, whilst inhibition of autophagy reduces synaptic overgrowth (Milton et al., 2011; Shen and Ganetzky, 2009). In addition preliminary investigation demonstrated previously, in Chapter 5, that inhibition of autophagy alleviated synaptic overgrowth in *Rab8* mutants. As such it was asked, having demonstrated that inhibition of autophagy alleviated the *CHMP2B*^{Intron5} eye phenotype, whether inhibition of autophagy could rescue synaptic overgrowth. *Atg18* has been demonstrated to be an essential autophagy gene (Nakatogawa et al., 2009; Obara et al., 2008). In addition previous work by Milton et al. (2011) demonstrated that inhibition of *Atg18,* via the presence of the *Atg18* loss of function mutant *Atg18*^{KG} transheterozygously with a deficiency allele null for *Atg18* (Df(3L)Excel6112), was sufficient to rescue synaptic overgrowth in *spin* mutants. Here it is demonstrated that whilst *Atg18*^{KG}/Df(3L)Excel6112 larvae show no effect upon synaptic bouton number alone *Atg18*^{KG}/Df(3L)Excel6112 in the background of neuronally expressed *CHMP2B*^{Intron5} was sufficient to completely alleviate increase synaptic bouton number (Fig. 6.9). nSyb-Gal4/UAS-*CHMP2B*^{Intron5} larvae displayed a significant increase in synaptic bouton number compared to all other genotypes, which showed no significant variance from one another.

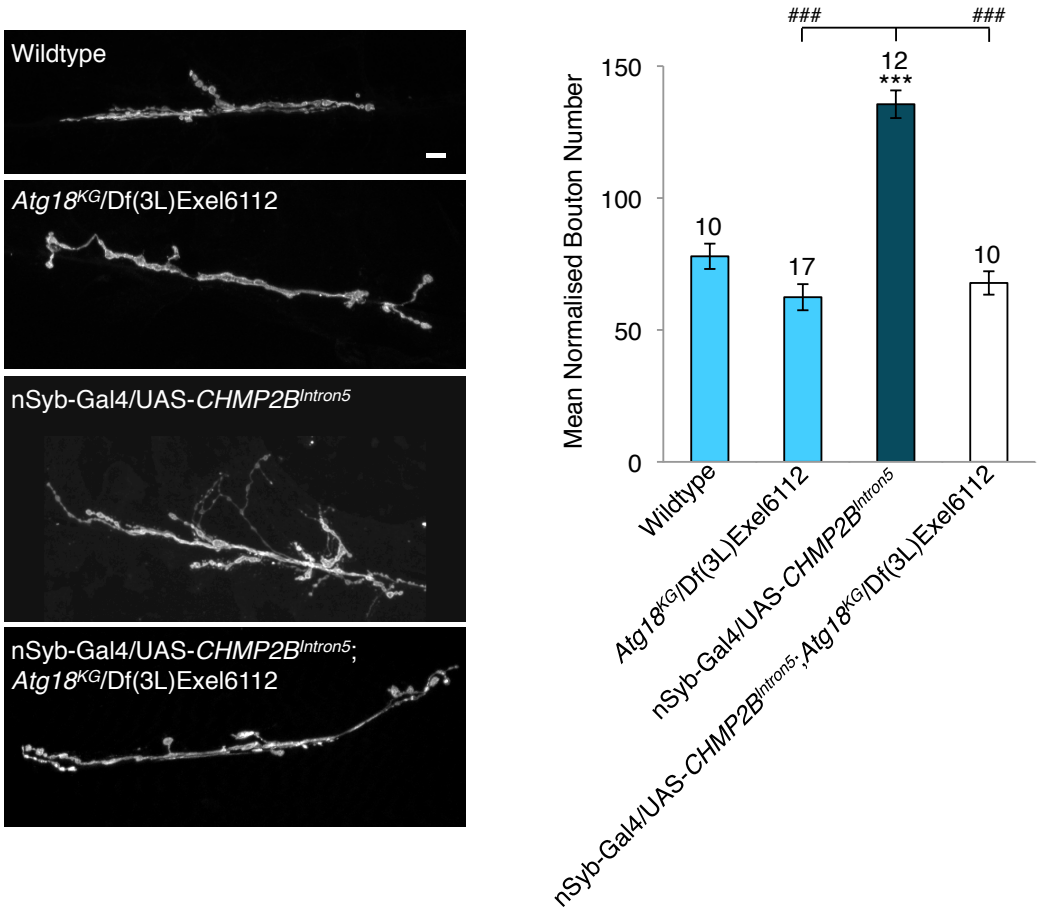

Figure 6.9. Inhibition of Autophagy Alleviates Increased Synaptic Bouton Number Associated With Neuronal Expression of *CHMP2B*^{Intron5}
Neuronal expression of *CHMP2B*^{Intron5}, under the control of the pan-neuronal driver nSyb-Gal4, induced a significant increase in synaptic bouton number in 3rd instar larvae at muscle 6/7, hemi-segment A3. Inhibition of *Atg18* by the introduction of the *Atg18*^{KG}/Df(3L)Excel6112 transheterozygous mutant combination had no effect upon synaptic bouton number alone, however alleviated increased bouton number in a nSyb-Gal4/UAS-*CHMP2B*^{Intron5} background. Scale bar = 10 µm. (ANOVA: F(d.f. 3) = 52.1556; $p < 0.001$ with post-hoc Dunnett's comparison to wildtype control *** $p < 0.001$ and student's t-test comparison between groups ### $p < 0.001$).

6.2.5.4. Rapamycin Induced Autophagy Potentiates Synaptic Overgrowth Associated With Expression of *Shrub*-GFP But Not *CHMP2B*^{Intron5}

Target of Rapamycin (TOR) has been identified as a conserved kinase and negative regulator of autophagy (Chang et al., 2009). It is the catalytic subunit of two TOR complexes (TORC), TORC1 and TORC2, of which TORC1 has been shown to be sensitive to rapamycin (Loewith et al., 2002). Treatment with rapamycin has been shown to inhibit TORC1, therefore reducing inhibition of autophagy. Furthermore potentiation of autophagy through rapamycin treatment

has been shown to induce synaptic overgrowth at the *Drosophila* NMJ in numerous studies (Knox et al., 2007; Shen and Ganetzky, 2009). The results presented here substantiate these previous findings demonstrating that rapamycin treatment elicits a synaptic overgrowth phenotype in wildtype larvae (Fig. 6.10). These results also demonstrate that, as for pan-neuronal expression, motor neuronal specific expression of both *CHMP2B*^{Intron5} and *Shrub*-GFP, using the motor neuronal driver OK6-Gal4, induce a significant increase in synaptic bouton number, when compared to wildtype. In addition it was demonstrated that whilst rapamycin treatment significantly potentiates increased bouton number associated with motor neuronal expression of *Shrub*-GFP, treatment elicits no effect upon *CHMP2B*^{Intron5} synaptic overgrowth. This in part supports modifier screen findings where activation of autophagy through inhibition of Rheb, a negative regulator of TOR, potentiated *Shrub*-GFP toxicity but not *CHMP2B*^{Intron5} toxicity.

Taken together this analysis of autophagy substantiates a role for autophagy in the toxicity associated with both *Shrub*-GFP and *CHMP2B*^{Intron5}. However it is clear that there are discrepancies between the observations for *Shrub*-GFP and those for *CHMP2B*$^{Intron5.}$

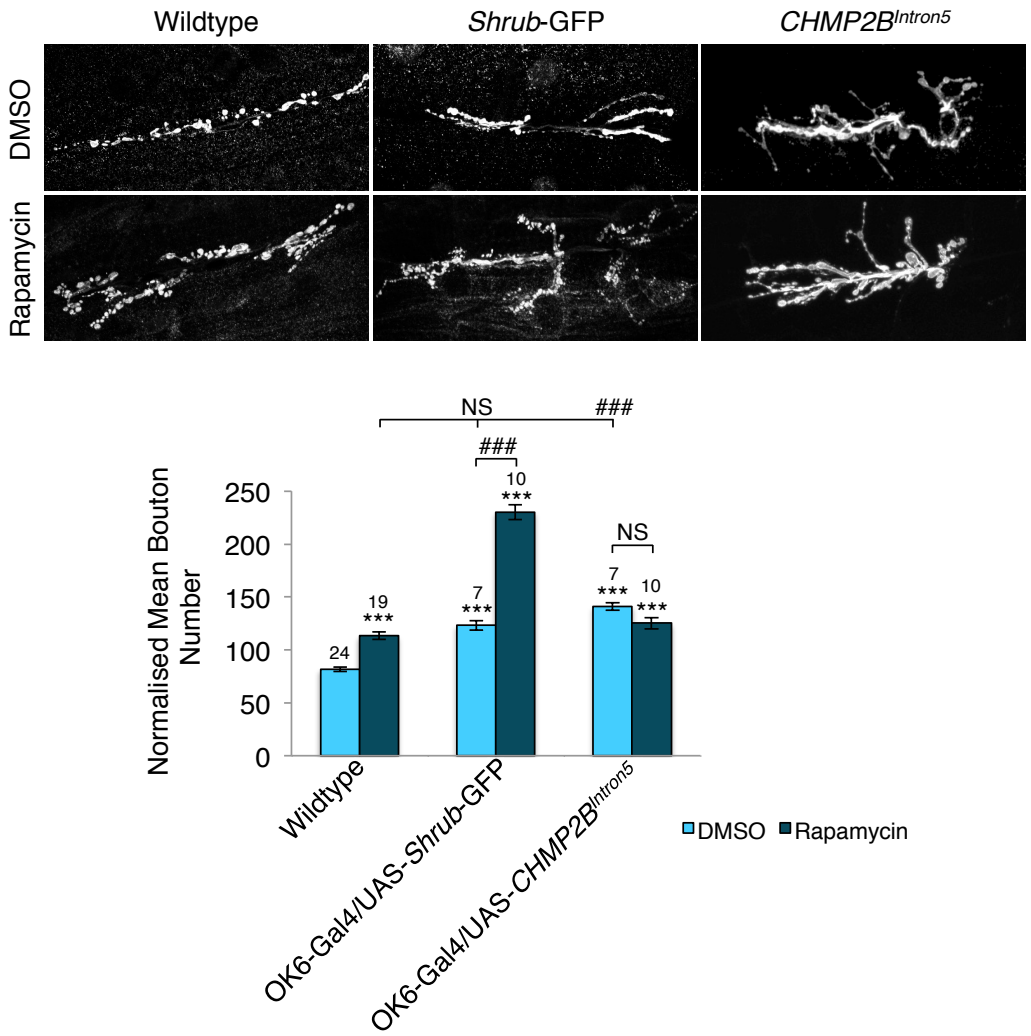

Figure 6.10. Activation of Autophagy by Rapamycin Treatment Potentiates *Shrub*-GFP but Not *CHMP2B*^{Intron5} Induced Synaptic Overgrowth

Drosophila larvae were raised on 4 µM Rapamycin (in DMSO 0.4 % v/v of food) or just DMSO (controls) until the 3rd instar wandering stage, at which point they were dissected. Rapamycin treatment elicits a synaptic overgrowth phenotype characterised by a significant increase in synaptic bouton number in wildtype larvae. Motor neuronal expression (OK6-Gal4) of *Shrub*-GFP induced an increase in bouton number equivalent to that of wildtypes. This overgrowth could be significantly potentiated by rapamycin treatment. Motor neuronal expression of *CHMP2B*^{Intron5} induced a significant increase in synaptic bouton compared to wildtype and rapamycin treated wildtype larvae. Rapamycin treatment had no effect upon of *CHMP2B*^{Intron5}, showing no significant variance between treated and untreated animals. Scale Bar = 10 µm. (ANOVA: $F(d.f.\ 5) = 128.1793$; $p < 0.001$ with post-hoc Dunnett's comparison to wildtype DMSO treated controls *** $p < 0.001$ and student's t-test comparison between groups # $p < 0.001$).

6.3. Discussion

6.3.1. *Rab8* Alleviates Synaptic Overgrowth Phenotypes But Not Deficits in Function Associated With Neuronal Expression of *CHMP2B*^{Intron5}

In the previous chapters *Rab8* was identified as a potent regulator of synaptic growth. It was shown that *Rab8* mutants display a significant synaptic overgrowth phenotype associated with endosomal perturbations and disruption to normal TGFβ and JNK signalling pathways. In addition *Rab8* was identified as a dominant enhancer of *CHMP2B*, with *Rab8* mutants potentiating toxicity associated with expression of the *CHMP2B*^{Intron5} mutant transgene. As such in this chapter it was asked whether neuronal expression of the *CHMP2B*^{Intron5} would perturb normal NMJ growth and if so whether expression of wildtype *Rab8* could alleviate this perturbation.

Here it is shown that pan-neuronal expression of *CHMP2B*^{Intron5} does elicit a synaptic overgrowth phenotype characterised by a significant increase in synaptic bouton number, NMJ length and satellite bouton number. Such phenotypes were also observed in *Rab8* mutants, however in contrast neuronal expression of *CHMP2B*^{Intron5} also induces a significant increase in branching. Increases in both branching and satellite bouton number are, as mentioned previously in Chapter 4, characteristic of endocytic mutants and, as such, are in keeping with the known role of CHMP2B within the endocytic pathway.

Despite variances in the synaptic overgrowth phenotypes observed between *Rab8* mutants and neuronally expressed *CHMP2B*^{Intron5} the results presented here demonstrate that co-expression of *Rab8* alongside *CHMP2B*^{Intron5} is sufficient to rescue all aspects of the synaptic overgrowth observed in *CHMP2B*^{Intron5}. These findings provide significant support for previous observation that *Rab8* acts as a potent regulator of synaptic growth and is a dominant modifier of *CHMP2B*.

Previously (Chapters 4 and 5) we have demonstrated that synaptic bouton size is sensitive to Rab8 perturbation, with *Rab8* mutants displaying a significant

reduction in synaptic bouton size, compared to wildtype. In addition the results presented suggest that synaptic bouton size may be more sensitive to inhibition of *Rab8* than other NMJ phenotypes, including bouton number. For example reduced bouton size was observed in heterozygous *Rab8* mutants whilst, in contrast, aberration to all other growth phenotypes including elevated bouton number and NMJ length were only observed when *Rab8* was transheterozygously mutated. It was also previously demonstrated that neuronal expression of UAS-*Rab8*, using a UAS-*Rab8* stock on the second chromosome, induced a mild increase in synaptic bouton size. This is in contrast to the observation seen here, using a UAS-*Rab8* on the third chromosome, that neuronal expression of *Rab8* has no effect upon bouton size. This may suggest that the UAS-*Rab8* used here is less potent than that used previously. Taken together these results suggest that Rab8 may regulate NMJ development in a dose dependent manner with bouton size being more sensitive to *Rab8* loss than other NMJ characteristics, such as bouton number, branching and NMJ length. Alternatively this may suggest that bouton size is regulated independently from other NMJ characteristics, although all are dependent upon Rab8. Support for this hypothesis may come from previous observations (Chapter 5) that heterozygous Puc mutants, which display reduced inhibition upon the JNK signalling pathway, show a significantly reduced synaptic bouton size but no other perturbations to NMJ growth. In contrast reducing inhibition upon both JNK and TGFβ signalling through puc^{E69}/Dad$^{\Delta IEL}$ double mutants elicits a general unregulated growth phenotype characterised by reduced bouton size, increased bouton number and increased NMJ length.

One may also postulate that increased bouton size observed when co-expressing *CHMP2B*^{Intron5} and *Rab8* relates to an ability of *Rab8* to rescue synaptic growth but not other aspects of cellular deficits. For example the role of *Rab8* as a potent regulator of synaptic growth may mean it can alleviate the general overgrowth phenotype without resolving aspects of the underlying endosomal trafficking deficit, leading to a manifestation of overgrowth as enlargement to synaptic boutons. Again this suggests that regulation of synaptic bouton size may be somewhat independent from general NMJ size and bouton number. Support for the hypothesis that *Rab8* acts to rescue growth

phenotypes without fully rescuing the molecular deficit associated with *CHMP2B*^{Intron5} comes from the observation that neuronal expression of *CHMP2B*^{Intron5} elicits a significant reduction in larval crawling velocity, a phenotype that cannot be rescued by co-expression of *Rab8*. In contrast Rab8 mutants show no perturbation to normal larval crawling. Further investigation may look to characterise synaptic function in larvae neuronally expressing *CHMP2B*^{Intron5} using electrophysiological recordings of muscle activity. This may provide a greater understanding of *Rab8's* function in alleviation of synaptic overgrowth.

6.3.2. *Rab8* Expression Alleviates Elevated P-MAD Associated With Neuronal Expression of *CHMP2B*^{Intron5}

Greater understanding of the role of *Rab8* as a regulator of synaptic growth may come from the observation that *Rab8* can alleviate elevated levels of nuclear P-MAD observed in motor neurons of larvae neuronally expressing *CHMP2B*^{Intron5}. Elevated levels of P-MAD are indicative of increased TGFβ activity, which has been shown to result in synaptic overgrowth in numerous *Drosophila* mutants, including in this study in *Rab8* mutants (Aberle et al., 2002; O'Connor-Giles et al., 2008; Rodal et al., 2011; Sweeney and Davis, 2002). As such these results suggest that both *CHMP2B* and *Rab8* play an essential role in the regulation of TGFβ. These findings support previous studies identifying endosomal trafficking as an essential pathway for the regulation of TGFβ signalling (Di Guglielmo et al., 2003; Miaczynska et al., 2004). For example it has been demonstrated that endocytic internalisation of active TGFβ receptor complexes is both essential to initiate downstream signalling processes but also for down-regulation of signalling (Miaczynska et al., 2004). In fact studies have revealed that early endosomes provide an environment that actively promotes TGFβ signalling, being enriched with SARA, a protein that facilitates R-SMAD association with the active receptor complex (Di Guglielmo et al., 2003; Itoh et al., 2002; Miaczynska et al., 2004; Tsukazaki et al., 1998). Early endosomes also facilitate down-regulation of signalling by targeting receptor cargo internalisation into MVB's, which in turn fuse with lysosomes to promote degradation (Di Guglielmo

et al., 2003; Kavsak et al., 2000). As such it is clear how the *CHMP2B*^{Intron5} mutation, which inhibits MVB formation, could promote aberrant elevated TGFβ activity by both inhibiting endosomal-lysosomal down-regulation of TGFβ and causing an accumulation of active TGFβ receptors within the early endosome. In addition it has been demonstrated that endosomes provide a route by which TGFβ receptors can be recycled back to the plasma membrane, via Rab11 positive recycling endosomes (Mitchell et al., 2004; Yin et al., 2013). In fact in a recent study Yin et al. (2013) showed that delivery of TGFβ receptors to recycling endosome was essential to maintain a polarized, steady-state expression of TGFβ within epithelial cells. As discussed previously, in Chapter 1, *Rab8* has been shown to play an important role in the endosomal recycling pathway with depletion of *Rab8* inhibiting endosomal trafficking to peri-nuclear recycling endosomes. Rab8 has also been shown to co-localise, and function in the same pathways, as Rab11. As such one may postulate that overexpression of *Rab8* may act to increase trafficking of TGFβ receptors from early endosomes into recycling endosomes, alleviating the burden induced by the *CHMP2B*^{Intron5} mutation and the inability to traffic TGFβ receptors to the lysosome.

The observation that overexpression of *Rab8* induces an accumulation of P-MAD at a peri-nuclear location poses an interesting question as to the role of *Rab8* in P-MAD localisation. Previous investigations have also shown that TGFβ signalling can be regulated through proteasomal degradation of SMAD1, the mammalian orthologue of MAD (Fuentealba et al., 2007; Gruendler et al., 2001). In these studies it was demonstrated that activated P-SMAD was targeted to a peri-nuclear location, proposed to be the centrosome, in order for proteasomal degradation to occur. As such it may be inferred that *Rab8* plays a regulatory role in the trafficking of P-MAD to the centrosome, promoting proteasomal degradation. This could explain why *Rab8* mutants show elevated levels of P-MAD, which contributes to synaptic overgrowth, and why overexpressing *Rab8* results in P-MAD accumulation at a peri-nuclear location. It has also been suggested that the proteasome is actually localised at a peri-nuclear location juxtaposed to the centrosome within what is termed an aggresome (Corboy et al., 2005; Olzmann et al., 2008; Pandit et al., 2009). It

has been suggested that aggresomes form a compartment in which misfolded proteins and protein aggregates are sequestered, both protecting the cell from the deleterious effect of such aggregates and bringing them into close association with the proteasome to promote degradation (Olzmann et al., 2008). Aggresomes can also be targeted for autophagic clearance by the cell, especially when the proteasome is impaired, further promoting degradation. As such one may propose that *Rab8* acts in the trafficking of components to, or the formation of, aggresomes. Support for this hypothesis comes from a study by Baron Gaillard et al. (2011) in which they demonstrated that *Rab8* complexes with peri-centriolar material protein 1 (PCM1) and Hook2, a protein that has been implicated in protein transport to peri-centrosomal aggresomes (Baron Gaillard et al., 2011). As such Rab8 may act to target P-MAD to aggresomes, where it can be sequestered and targeted for proteasomal degradation. In order to substantiate this hypothesis future investigation must look to determine whether P-MAD accumulations co-localise with aggresome markers, such as HSP70, HDAC6, proteasomal components and ubiquitinylated proteins.

6.3.3. Autophagy Contributes To *CHMP2B*^{Intron5} Toxicity

As with many neurodegenerative diseases the presence and composition of neuronal inclusions are a hallmark of FTD. In addition they have become a common method by which to classify FTD into neuropathological subtypes (Mackenzie et al., 2011; Mackenzie et al., 2010). In this investigation it was demonstrated that larvae pan-neuronally expressing the *CHMP2B*^{Intron5} mutant transgene presented with accumulations of mono- and poly-ubiquitinylated proteins with the VNC. Such an observation, mimicking the inclusion phenotype observed previously in cell culture, in mice models and within FTD-UPS patients, provides credence to this as a viable model of FTD-3.

Accumulation of neuronal inclusions, including ubiquitin positive aggregates observed in FTD, has been associated with perturbations to homeostatic protein quality control mechanisms within cells (Chen et al., 2011; Takalo et al., 2013). The two most significant of these mechanisms being the ubiquitin proteasome

system (UPS) and autophagy. In healthy cells it is estimated that up to 30 % of newly synthesised proteins are incorrectly processed and misfolded and, as such, require processing and recycling via either the UPS or autophagic-lysosomal degradative pathway (Schubert et al., 2000). Therefore inhibition or disruption to either pathway can elicit a significant accumulation of misfolded and aggregated proteins within cells. This in turn creates a burden of protein aggregates that overwhelm the degradative systems further potentiating the problem, inducing cellular stress and leading to the eventual cell death observed in neurodegenerative diseases. However, whilst it has been shown that *CHMP2B* mutations associated with FTD display ubiquitin positive aggregates, perturbation to autophagy and neuronal death it is a topic of debate as to whether or not autophagy actually contributes towards the toxicity of *CHMP2B*^{Intron5}. For example, as mentioned previously, other *CHMP2B* mutants have been shown to display perturbations to autophagy, akin to those seen in *CHMP2B*^{Intron5}, but in the absence of neurodegeneration.

Here it was demonstrated that inhibition of autophagy through the presence of either loss of function Atg mutants or Atg-RNAi's alleviated *CHMP2B*^{Intron5} toxicity within the *Drosophila* eye. This observation supports previous findings by Lee et al. (2009) where it was demonstrated that inhibition of autophagy via siRNA knock-down of Atg5 or Atg7 or the administration of an autophagy inhibitor significantly improved the survival rate of rat cortical neurons expressing *CHMP2B*^{Intron5}. Similarly they also showed that cortical neurons isolated from Atg5 -/- mice displayed greater resistance to *CHMP2B*^{Intron5} mediated cell death. As such one may infer that autophagy contributes towards the toxicity associated with the *CHMP2B*^{Intron5} mutation. This is further corroborated by the observation that activation of autophagy through overexpression of Atg1 potentiates toxicity in the *CHMP2B*^{Intron5} eye. However one must take into account that Atg1 expression in the eye, in the absence of *CHMP2B*^{Intron5}*,* elicits a rough eye phenotype when expressed alone.

Whilst inhibition of autophagy through expression of Atg mutants alleviated *CHMP2B*^{Intron5} toxicity in the *Drosophila* eye overexpression of Rheb, a negative

regulator of autophagy, actually potentiated *CHMP2B*^{Intron5} toxicity. Whilst this result appears somewhat paradoxical it actually supports previous findings showing that Rheb has a differential effect upon synaptic terminal growth to manipulation of autophagy (Knox et al., 2007). For example overexpression of Rheb, which should inhibit autophagy, within the *Drosophila* motor neuron induces synaptic overgrowth whilst Rheb mutants display synaptic undergrowth (Knox et al., 2007). In contrast inhibition of autophagy via mutations in essential autophagy genes induces mild synaptic undergrowth whilst overexpression of Atg1 or activation of autophagy through Rapamycin treatment induce overgrowth (Knox et al., 2007; Shen and Ganetzky, 2009). Currently the reason for the somewhat paradoxical effect of Rheb upon synaptic development is yet to be elucidated. In addition the general role of autophagy in neurodegeneration remains unclear and, like the role of Rheb, slightly paradoxical. For example inhibition of autophagy has been shown to both simulate neurodegenerative lysosomal storage disorders (LSD's) and alleviate LSD phenotypes (Sweeney Lab data) (Milton, 2011).

Substantiating the role of autophagy in *CHMP2B*^{Intron5} toxicity it was observed that inhibition of *Atg18* was sufficient to alleviate synaptic overgrowth associated with pan-neuronal expression of *CHMP2B*^{Intron5}. Whilst this indicates autophagy to be a contributory factor in *CHMP2B*^{Intron5} toxicity it also corroborates previous findings implicating autophagy as a potent regulator of synaptic growth (Milton et al., 2011; Shen and Ganetzky, 2009). For example Milton et al. (2011) demonstrated that introduction of autophagy mutants into a *spin* mutant background was sufficient to completely rescue synaptic overgrowth. In addition it has been shown that autophagy acts to degrade the E3 ubiquitin ligase *hiw* releasing its inhibition upon the JNKKK *wallenda (Collins et al., 2006).* Thus overexpression of autophagy promotes synaptic overgrowth via disinhibition of the JNK/AP-1 pathway. Therefore having observed neuronal expression of *CHMP2B*^{Intron5} to induce elevated levels of P-MAD coupled with synaptic overgrowth which can be alleviated by expression of *Rab8* or inhibition of autophagy one may propose JNK signalling is likely to contribute towards synaptic overgrowth in CHMP2B^{Intron5}. As such future investigation should look to combine the Puc-LacZ reporter with *CHMP2B*^{Intron5} mutant expression in

order to determine whether neuronal expression of *CHMP2B*^{Intron5} induces elevate JNK signalling as well as TGFβ. In addition these observations support previous preliminary findings demonstrating that inhibition of autophagy in a *Rab8* transheterozygous mutant background alleviates synaptic overgrowth. As such this further implicates autophagy as a regulator of synaptic growth, potentially contributing towards overactive JNK signalling.

Further corroborating a perturbation to normal autophagic processes in *CHMP2B*^{Intron5} mutants it was demonstrated that eye specific expression of *CHMP2B*^{Intron5} resulted in significant disruption to the autophagic marker Atg5-GFP. Whilst diffusely and evenly distributed throughout the wildtype eye Atg5-GFP appears to localise specifically surrounding regions of melanisation within the GMR-Gal4/UAS-*CHMP2B*^{Intron5} eye. Melanisation accompanied by autophagy is indicative of an innate immune response in *Drosophila*, supporting previous observations that CHMP2B mutant toxicity is associated with an innate immune response (Ahmad et al., 2009). Analysis of the internal structure of the *Drosophila* eye in response to *CHMP2B*^{Intron5} expression also revealed a significant disruption to the normal distribution and localisation of photoreceptor neurons. This observation indicates that degeneration observed across the eye surface is associated with more significant internal degeneration. Furthermore this supports previous observations that *CHMP2B*^{Intron5} toxicity is associated with perturbation to normal neuronal structures. It must also be considered that this degree of disruption is likely to account for some of the perturbation to Atg5-GFP localisation observed.

6.3.4. Autophagy Differentially Regulates Phenotypes Associated With *CHMP2B*^{Intron5} and *Shrub*-GFP Expression

Previous work in the Sweeny and Gao labs has demonstrated that the *Shrub*-GFP fusion protein acts as a dominant negative, antimorphic version of *Shrub*. It has also been demonstrated that the *CHMP2B*^{Intron5} mutation results in a failure of CHMP2B to dissociate from the ESCRT-III complex, forming an abnormally stable association with Shrub (Lee et al., 2007). In addition it has been shown that *Shrub*-GFP phenocopies *CHMP2B*^{Intron5} in a number of ways.

For example Ahmad et al. (2009) demonstrated that when expressed in the *Drosophila* eye Shrub-GFP and *CHMP2B*^{Intron5} display similar phenotypes, which were equally affected by the same genetic modifiers. Such an observation has also been made during the course of this investigation (see Chapter 3). They also demonstrated that both *Shrub*-GFP and *CHMP2B*^{Intron5} elicited an accumulation of cleaved späetzle protein, indicating Toll pathway activation. As such it has been proposed that *Shrub*-GFP directly phenocopies *CHMP2B*^{Intron5}. Here we provide further support for this hypothesis demonstrating that when expressed specifically within motor-neurons, under the control of OK6-Gal4, both *Shrub*-GFP and *CHMP2B*^{Intron5} display synaptic overgrowth comparable to each other. However treatment with rapamycin, which has previously been shown to induce autophagy and promote significant synaptic overgrowth at the *Drosophila* NMJ, significantly potentiated synaptic overgrowth in *Shrub*-GFP expressing and wildtype larvae but not *CHMP2B*^{Intron5} expressing larvae. As such this suggests autophagy affects *Shrub*-GFP and *CHMP2B*^{Intron5} differently, or at least to differing degrees. Interestingly a discrepancy between *Shrub*-GFP and *CHMP2B*^{Intron5} was also observed during modifier screens where inhibition of autophagy alleviated *CHMP2B*^{Intron5} toxicity but not that of *Shrub*-GFP. As *CHMP2B*^{Intron5} associated NMJ and eye phenotypes can be alleviated, to some degree, by inhibiting autophagy but not significantly potentiated by promoting autophagy and vice versa for *Shrub*-GFP one may postulate that autophagy may be more active in *CHMP2B*^{Intron5} than in *Shrub*-GFP expressing animals. As such it can be inferred that autophagy is likely to contribute towards toxicity in *CHMP2B*^{Intron5} and that Shrub-GFP does not directly phenocopy *CHMP2B*^{Intron5} in all aspects. Future investigation may look to further characterise the role of autophagy in *Shrub*-GFP, in comparison to *CHMP2B*^{Intron5} in order to elucidate the mechanism behind this variance. This may also be essential to ascertain the validity of *Shrub*-GFP as a comparable model to *CHMP2B*^{Intron5}. Due to the nature of the *Shrub*-GFP allele, acting as a dominant negative due to the GFP fusion, future investigation should also look to corroborate the findings of this investigation using Shrub loss of function alleles or Shrub-RNAi constructs.

7. Discussion and Future Research

7.1. Introduction

At the start of this investigation the following primary questions were asked:

1. Can a *Drosophila* Model of FTD in which the *CHMP2B*^{Intron5} mutant transgene is expressed in the *Drosophila* eye be used to identify novel modifiers of *CHMP2B*^{Intron5} Toxicity?
2. How do mutations in *Rab8*, modifiers of *CHMP2B*^{Intron5} toxicity, affect synaptic development and the nervous system?
3. What is the mechanism behind synaptic overgrowth observed in *Rab8* Mutants?
4. Does neuronal expression of *CHMP2B*^{Intron5} in *Drosophila* provide a representative model of FTD-3 and how does *Rab8* affect *CHMP2B*^{Intron5} mutant phenotypes?

This final chapter looks to determine which of these questions have been answered, providing a comprehensive, succinct overview of all the data generated as part of this investigation. It also looks to pose further questions and areas for future investigation.

7.2. Identification of Novel Modifiers of *CHMP2B*^{Intron5} Toxicity

There currently exists a growing body of evidence demonstrating that the *Drosophila* eye provides an elegant and powerful system in which modifiers of disease causing human mutations can be unbiasedly screened for (Jackson et al., 2002; Pandey et al., 2007; Shulman and Feany, 2003; St Johnston, 2002). Such approaches have already proven highly successful in the identification of novel interacting partners of α-syn, β-amyloid and tau (Butler et al., 2012; Jackson et al., 2002; Shulman and Feany, 2003; van de Hoef et al., 2009). Furthermore they have contributed significantly to the understanding of a range

of neurodegenerative disorders including Alzheimer's disease, Huntington's, IBMPFD and Parkinson's disease, to name a few (Butler et al., 2012; Jackson et al., 2002; Ritson et al., 2010; Shulman and Feany, 2003; van de Hoef et al., 2009; Zhang et al., 2010). During this investigation the *CHMP2B*^{Intron5} mutant transgene was expressed in the *Drosophila* eye generating a distinctive phenotype against which modifiers could be screened for. Using a combination of unbiased and targeted screens a number of potent modifiers of *CHMP2B*^{Intron5} toxicity were identified, one of which was *Rab8*. Subsequent characterisation during the course of this investigation demonstrated that *Rab8* acts as a potent regulator of synaptic development and neuronal morphology. It was also demonstrated that a number of other *CHMP2B* modifiers identified contribute towards the mechanism responsible for synaptic overgrowth in *Rab8* mutants. As such one may stipulate that modifier screens using *CHMP2B*^{Intron5} provide a versatile system by which to identify novel factors implicated in neuronal development and disease. In addition the identification of dominant modifiers during these screens provides an essential framework for further investigation into the molecular mechanisms associated with *CHMP2B*^{Intron5} toxicity and the role of the modifiers identified in the normal maintenance of neuronal development and function. Corroborating these observations and the versatility of modifier screens additional research in the Sweeney and Gao labs have utilised modifier screens of *CHMP2B*^{Intron5} as the foundation for characterising the involvement of both syntaxin 12/13 and serpin5 in *CHMP2B*^{Intron5} associated toxicity (Ahmad et al., 2009). Taken together the results of this investigation, alongside these other studies, provide credence to the power of modifier screens as a tool for identification of novel targets for investigation. As such future analysis must look to characterise the remaining positive "hits" from the modifier screens performed.

Whilst the results of this and previous investigations in the Sweeney and Gao labs have identified clear modifiers of *CHMP2B*^{Intron5} toxicity it is essential that, following characterisation of these modifiers in flies, future analysis looks to characterise their function in higher order models of FTD. For example in order to definitively implicate identified molecular pathways in FTD pathology we must

ascertain whether these pathways are similarly affected in both vertebrate models of FTD and, in the long term, in FTD patients.

7.3. Rab8, a Regulator of Synaptic Growth

The predominant focus of this investigation has been on characterisation of *Rab8* mutants, having identified them to be potent enhancers of *CHMP2B*^{Intron5} toxicity in the *Drosophila* eye. As a result we have clearly demonstrated that Rab8 acts as a potent pre-synaptic regulator of NMJ growth. In addition we have shown synaptic overgrowth to be associated with elevated and synergistic activity of the TGFβ and JNK signalling pathways. This observation contributes towards a significant, and growing, body of evidence demonstrating that TGFβ and JNK signalling act as regulators of NMJ development and plasticity (Collins et al., 2006; Marques, 2005; Marques et al., 2003; McCabe et al., 2003; Milton et al., 2011; O'Connor-Giles et al., 2008; Sweeney and Davis, 2002). However these findings provide a number of new insights into this regulation. For example despite significant evidence showing synergistic activity of the two pathways in other contexts and both pathways being implicated in numerous models of *Drosophila* NMJ overgrowth there has been little direct evidence indicating a synergistic activity of the two pathways within neurons (Liu et al., 2012; Mao et al., 2011; Perlman et al., 2001; Sorrentino et al., 2008). The observation in this study that the two pathways act synergistically supports previous findings in the Sweeney lab where it has been shown that activation of JNK, via oxidative stress, alone cannot induce synaptic overgrowth (Milton et al., 2011). However synaptic overgrowth is observed in *spin* mutants, which display an oxidative stress burden leading to elevated JNK signalling coupled with perturbed endosomal trafficking resulting in elevated TGFβ activity (Milton et al., 2011). In addition synaptic overgrowth in *Rab8* mutants also identifies POSH and TAK1 as novel regulators of synaptic growth, revealing POSH as a potential nexus linking TGFβ and JNK signalling, via TAK1. The involvement of the endosomal JNK scaffold POSH and the observation that *Rab8* mutants display perturbed endosomal-lysosomal trafficking also supports previous evidence indicating that perturbation of endosomal trafficking inhibits correct

processing and recycling of TGFβ receptors (Rodal et al., 2011; Sweeney and Davis, 2002; Wang et al., 2007). In order to further substantiate these observations future investigation shall look to determine whether TGFβ receptors can be observed to accumulate within endosomes of *Rab8* mutants.

In addition to the observation of synaptic overgrowth, associated with elevated TGFβ and JNK signalling, in *Rab8* mutants this study also demonstrated that overexpression of wildtype *Rab8* in a neuronally expressed *CHMP2B*^{Intron5} background could alleviate synaptic overgrowth and elevated levels of nuclear p-MAD. As such these findings implicate Rab8 as a potent regulator of synaptic growth and also of TGFβ signalling. Such observations provide further support for a role of normal endosomal trafficking in the homeostatic regulation of TGFβ signalling within neurons (Chen, 2009; O'Connor-Giles et al., 2008; Sweeney and Davis, 2002). In addition previous studies have shown that expression of Rab8 is also sufficient to alleviate neuronal cell death in models of Parkinson's disease (Gitler et al., 2008). As such this raises the question as to whether Rab8 has a neuro-protective function, potentially through its role in regulating endosomal traffic. In order to test this hypothesis future investigation shall look to determine whether overexpression of *Rab8* can alleviate toxicity associated with other *Drosophila* models of neurodegeneration. During the course of this investigation it was also observed that overexpression of wildtype *Rab8* alone resulted in aggregation of p-MAD at a peri-nuclear location within motor neurons. In order to determine the mechanism by which *Rab8* can alleviate toxicity associated with *CHMP2B*^{Intron5} and models of Parkinson's disease future investigation must look to determine the identity of this peri-nuclear organelle. One possibility, as discussed in Chapter 6, is that this represents an aggresome, an intermediate in the regulation of cellular proteostasis acting during periods of elevated stress upon the protein degradation systems within cells, and potentially under normal physiological conditions (Corboy et al., 2005; Olzmann et al., 2008; Pandit et al., 2009). Identification of this organelle as either an aggresome or an alternative structure may provide novel targets for both the study of disease and for the development of possible therapeutics.

Taken together the results of this investigation reveal *Rab8*, and its associated molecular pathways, as a novel regulator of NMJ growth and development and identify *Rab8* as a novel target for the study of neurodegenerative diseases in general.

7.4. Is Rab8 a Regulator of Innate Immune Responses in Neurons?

During the course of this investigation a number of factors implicated in innate immunity have been identified as either potent modifiers of *CHMP2B*^{Intron5} toxicity, in the *Drosophila* eye, or as factors involved in synaptic overgrowth in *Rab8* mutants. For example there exists a significant body of evidence demonstrating that both POSH and TAK1 act as regulators of innate immunity (Ajibade et al., 2013; Lennox and Stronach, 2010; Sato et al., 2005; Tsuda et al., 2005). In a study by Tsuda et al. (2005) POSH null mutants were shown to display immune defects, in response to bacterial infection, associated with a delayed induction followed by aberrantly sustained activation of JNK signalling. Furthermore they suggested that abnormal immune responses in POSH mutants associated with a perturbation of POSH E3 ubiquitin ligase mediated regulation of TAK1. TAK1 has, in turn, been identified as an upstream activator of immune signalling with previous investigations demonstrating that TAK1 is activated in response to the activation of Toll like receptors (TLR's) during immune responses (Irie et al., 2000; Sato et al., 2005). In addition the TAK1-JNK cascade has been identified as an essential signalling pathway in the activation of innate immune responses (Zhang et al., 2009). Previous work in the Sweeney and Gao labs has also demonstrated that CHMP2B may act as a mediator of innate immunity through regulation of Toll signalling (Ahmad et al., 2009). For example they demonstrated that Toll signalling was up-regulated when *CHMP2B*^{Intron5} was expressed in the fly eye and identified *Serpin5*, a regulator of Toll signalling, as a modifier of the *CHMP2B*^{Intron5} phenotype (Ahmad et al., 2009). As such having shown that *Rab8*, *POSH* and *TAK1* all act as modifiers of *CHMP2B*^{Intron5} and that TAK1 and POSH are essential for

synaptic overgrowth in *Rab8* mutants the results of this investigation suggest a potential role for Rab8 as a regulator of innate immune responses in neurons.

Having identified a potential association between Rab8 and the regulation of innate immune responses in neurons, as well as having demonstrated that JNK signalling is elevated in *Rab8* mutants and required for synaptic overgrowth here we suggest a potential mechanism for Rab8 in regulating the innate immune TAK1-JNK cascade. Previous studies have demonstrated that GTP-bound active Rab8 complexes with MAPK Kinase Kinase Kinase 2 (MAP4K2), also known as Rab8-interacting protein (Rab8ip) (Ren et al., 1996). In addition it has been demonstrated that whilst expression of wildtype *Rab8* in MDCK cells results in a nuclear localisation of MAP4K2, expression of a dominant negative form of Rab8, which fails to associate with MAP4K2, leads to a cytoplasmic localisation of MAP4K2 (Bruce, 2009). As previous findings have shown that MAP4K2 is inactivated by nuclear sequestration this suggests that Rab8 is acting to silence MAP4K2 activity (Bruce, 2009; Massa et al., 2011; Rees et al., 2012). As such one would expect that in *Rab8* mutants MAP4K2 activity would be elevated, leading to activation of the TAK1 mediated JNK signalling pathway. A BLAST (Basic Local Alignment Tool) analysis of the human MAP4K2 sequence identifies the *Drosophila* MAP4K's happyhour, hippo, germinal centre kinase 3 and misshapen (msn) to be the most likely *Drosophila* orthologues of MAP4K2. Msn has in turn been implicated in innate immune responses in *Drosophila* acting upstream of TAK1 (Takatsu et al., 2000). As such we propose that Rab8 may act to regulate TAK1 mediated JNK signalling, associated with innate immunity, in neurons via modulation of MAP4K2 activity (Fig. 7.1.) In order to test this hypothesis future investigation shall look to determine whether inhibition of any of the *Drosophila* MAP4K's can alleviate synaptic overgrowth in *Rab8* mutants. In addition we shall look to determine whether *Rab8* mutants display a redistribution of the relevant MAP4K to a cytoplasmic localisation and determine whether, if so, this promotes increased activation. Experimentation shall also look to use the TAP-tagged Rab8 constructs generated during this investigation to perform immunoprecipitation experiments. This shall hopefully allow conformation of Rab8 interaction with the relevant MAP4K under GTP-bound conditions.

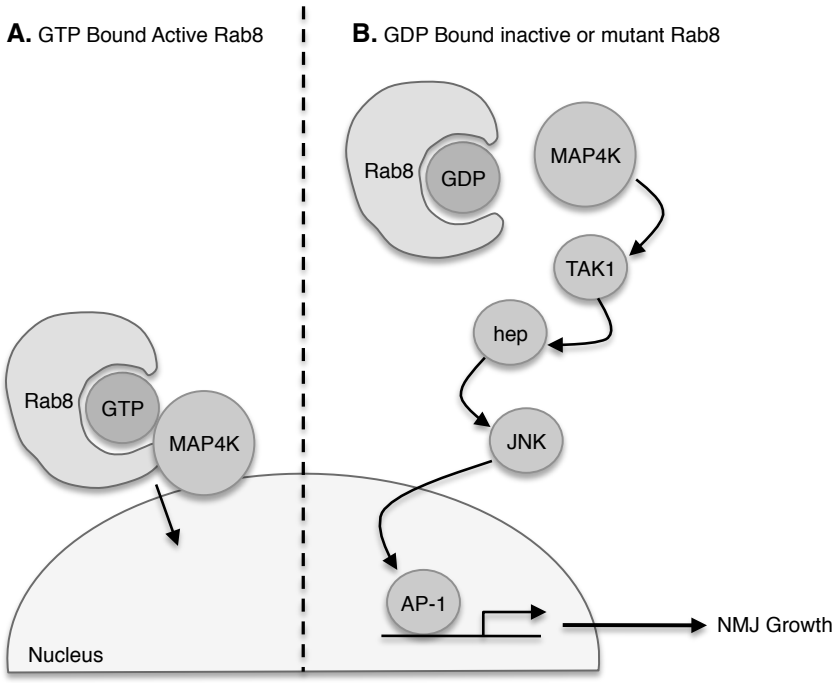

Figure 7.1. Proposed Mechanism for *Rab8* Mediated Regulation of The TAK1-JNK Cascade
A. GTP-bound active Rab8 associates with the *Drosophila* MAP4K2 orthologue promoting its nuclear sequestration and inhibition. **B.** In *Rab8* mutants or when GDP-bound, Rab8 fails to associate with MAP4K resulting in a cytosolic accumulation of MAP4K. MAP4K in turn activates the JNKKK TAK1, promoting activation of the JNKK hemipterous (hep), leading to activation of the *Drosophila* JNK (basket, bsk). JNK activation promotes activation of AP-1 leading to its translocation to the nucleus to promote transcription of downstream genes leading to induction downstream processes, including NMJ growth.

Supporting a role for Rab8 as a potential regulator of innate immunity in neurons work in the Sweeney lab has demonstrated that larvae presenting mutations in OCRL1, a Rab8 effector, display significant melanisation coupled with a reduction in the volume of the larval VNC. Preliminary findings also suggest a possible inappropriate activation of innate immunity leading to aberrant invasion of the VNC by immune cells. Future investigation shall look to determine whether this apparent activation of innate immunity associates with the identified interaction between OCRL1 and Rab8.

7.5. Does Expression of the *CHMP2B^{Intron5}* Mutant Transgene in *Drosophila* Provide a Representative Model of FTD?

During the course of this investigation, it has been demonstrated that expression of *CHMP2B^{Intron5}* in the *Drosophila* eye provides a robust model in

which we have been able to identify novel enhancers of *CHMP2B*^{Intron5} toxicity. In addition we have shown that many of the identified modifiers, including *Rab8*, and their associated molecular pathways have a role in the regulation of neuronal development. It was also demonstrated that neuronal expression of *CHMP2B*^{Intron5} perturbed normal synaptic growth, eliciting a synaptic overgrowth phenotype at the larval NMJ, coupled with a reduction in synaptic function, indicated by a locomotor deficit in larvae. However, despite this, it is important to remember that this is an overexpression model in an invertebrate system. As such here we discuss whether this system provides a representative model of FTD and ask how future investigation should look to substantiate the observations made during this investigation.

During this investigation we have demonstrated that larvae pan-neuronally expressing the *CHMP2B*^{Intron5} mutant transgene display a synaptic overgrowth phenotype coupled with elevated levels of nuclear P-MAD. In addition it was demonstrated that both these phenotypes could be rescued through expression of *Rab8*, mutants of which themselves display elevated TGFβ signalling and synaptic overgrowth. As such these findings implicate CHMP2B as a regulator of TGFβ signalling within neurons and suggest that neuronal pathology observed in FTD may associate with perturbations to normal endosomal regulation of TGFβ. Support for this hypothesis comes from observations that TGFβ levels have been shown to be elevated in patients suffering from a range of neurodegenerative diseases including Parkinson's, Alzheimer's and FTD (Chao et al., 1994; Flanders et al., 1995; Mogi et al., 1995; Sjogren et al., 2004). For example Sjörgen et al. (2004) demonstrated that TGFβ levels were elevated in the cerebrospinal fluid (CSF) of FTD patients (Sjogren et al., 2004). In order to corroborate the observations made in this *Drosophila* model of FTD-3, and substantiate its role as a representative model of the disease, future investigation shall look to determine whether *CHMP2B*^{Intron5} mutant mice also display elevated levels of TGFβ signalling. This could be determined through analysis of both brain tissue and CSF via histological staining and High-performance liquid chromatography. In addition, having observed a synergistic activity of TGFβ and JNK signalling in the regulation of NMJ growth in both *Rab8* mutants and under normal physiological conditions future analysis shall

also look to determine whether JNK signalling is elevated in both *Drosophila* and mice models of *CHMP2B*^{Intron5} associated FTD. In the long-term the same analysis could also be conducted using tissue or CSF from FTD-3 patients presenting with the *CHMP2B*^{Intron5} mutation. Such observations would help to determine the true versatility and reliability of this *Drosophila* model as a representative model of FTD.

In addition to elevated levels of TGFβ signalling larvae pan-neuronally expressing *CHMP2B*^{Intron5} were also show to display accumulations of ubiquitinylated proteins within the VNC. Such an observation provides support for the validity of this as a model of FTD-3, which has been identified as a UPS-FTD; displaying ubiquitin positive neuronal inclusions (Holm et al., 2009; Isaacs et al., 2011). Having demonstrated that expression of *Rab8* can alleviate synaptic overgrowth and elevated TGFβ associated with expression of *CHMP2B*^{Intron5} in *Drosophila,* future investigation shall look to determine whether expression of *Rab8* can also alleviate ubiquitinylated protein aggregates. Such an observation would support a role for Rab8 in regulating protein degradation pathways, possibly through the interaction of the endosomal-trafficking pathway with autophagy.

Taken as whole the observations of this investigation demonstrate that *Drosophila* can provide a robust model in which we can identify potential molecular mechanism associated with FTD pathology. Furthermore these observations provide testable hypotheses for analysis in higher order model organism or within human tissues. As such this suggests that whilst this model relies upon overexpression of *CHMP2B*^{Intron5} within an invertebrate system it can provide an essential tool for the elucidation of molecular mechanisms involved in FTD pathology.

7.6. Future Investigation

In addition to the experimental approaches listed for future investigation throughout the course of this dissertation the observations of this investigation as a whole pose interesting objectives for future investigation.

During initial modifier screens both *Rab8* and the Rab8 effector *OCRL1* were identified as potent modifiers of the FTD *CHMP2B*^{Intron5} *Drosophila* eye phenotype. As mentioned previously *OCRL1* encodes an inositol phosphatase, a protein essential for the regulation of phosphoinositide (PI) lipids (Pirruccello and De Camilli, 2012). PI's have been demonstrated to play a plethora of diverse and essential roles throughout the cell including signal transduction, membrane trafficking, exocytosis and endocytosis (Pirruccello and De Camilli, 2012). As such perturbation of inositol phosphatases has been implicated in a range of disparate human pathologies, including cancer, diabetes and neurodegenerative disease (Choudhury et al., 2005; Coon et al., 2012; Hou et al., 2011; Pirruccello and De Camilli, 2012). For example, as discussed in Chapters 1 and 3, mutations in *OCRL1* have been implicate in the neurodevelopmental disorder Lowe Syndrome (LS) (Choudhury et al., 2005; Coon et al., 2012; Hou et al., 2011). In addition to a number of studies showing that Rab8 and OCRL1 form a physical interaction it has also been demonstrated that certain OCRL1 mutations, associated with LS, inhibit this interaction (Hou et al., 2011). As such this indicates that the physical association between Rab8 and its effector OCRL1 plays an essential role in the regulation of normal neuronal health. Despite this the physiological role of this interaction remains to be elucidated. Having demonstrated, during the course of this investigation, both *OCRL1* and Rab8 to be dominant enhancers of *CHMP2B*^{Intron5} toxicity and having identified Rab8 to be a potent regulator of neuronal development we further implicate the interaction between Rab8 and OCRL1 as a potential target for the study of neurodegeneration and as a key interaction in the maintenance of neuronal health. Having developed a range of tools for the study of both Rab8 and OCRL1 and possessing a range of both *Rab8* and *OCRL1* alleles we are in advantageous position for studying the role

of the Rab8-OCRL1 interaction and the importance of this interaction in endosomal trafficking events associated with neuronal development and function. As such I propose that future investigation should look to characterise the nature of this interaction utilising a number of approaches demonstrated throughout this investigation. For example investigation could look to characterise the effect of the *OCRL1* F668V mutant, which elicits a 5.8 fold reduction in Rab8 binding affinity, upon synaptic development, analysing the NMJ and CNS at both a histological and ultrastructural level (Hou et al., 2011).

In addition study in the Sweeney lab has demonstrated that *OCRL1* mutant larvae display what appears to be an aberrant innate immune response, displaying melanisation throughout the larvae. As such any future investigation into the role of the Rab8-OCRL1 interaction should also look to determine whether neuronal dysfunction and pathology associates with an activation of innate immune response, potentially acting through the TAK1-JNK cascade. Overall I believe that future investigation into the role of the OCRL1-Rab8 interaction may provide great insight into the molecular mechanisms underlying pathology in both FTD and LS and, therefore, help to elucidate molecular pathways associated with neuronal pathology in a range of neurological, neuro-developmental and neurodegenerative diseases.

7.7. Summary

The key results and conclusions of this study are summarised as follows:

1. Expression of the *CHMP2B*^{Intron5} mutant transgene in the *Drosophila* eye provides a robust model for conducting modifier screens, identifying novel enhancers and suppressors of a model of FTD.

2. *Rab8* mutants dominantly enhance *CHMP2B*^{Intron5} toxicity.

3. Rab8 is a potent, pre-synaptic, regulator of neuronal growth and development with mutants displaying unregulated growth at the *Drosophila* larval NMJ.
4. *Rab8* mutants display a significant disruption to normal endosomal-lysosomal trafficking, most likely associated with Rab8's role in recycling endosomal trafficking

5. *Rab8* mutants display elevated TGFβ signalling, which is essential for the unregulated synaptic growth phenotypes observed.

6. *Rab8* mutants display elevated JNK signalling, which is essential for the unregulated synaptic growth phenotypes observed.

7. TGFβ and JNK signalling act synergistically to regulate synaptic development under normal physiological conditions.

8. The endosomal JNK scaffold POSH and associated JNKKK TAK1 are essential for unregulated NMJ growth in *Rab8* mutants. As such this observation identifies novel regulators of NMJ growth and provides a mechanism for endosomal synergistic activity of TGFβ and JNK in synaptic overgrowth.

9. Rab8 alleviates synaptic overgrowth associated with neuronal expression of *CHMP2B*^{Intron5}

10. Rab8 may act as a regulator of JNK signalling in response to innate immune activation in neurons.

Appendices

Appendix 1. Muscle 6/7 Bouton Numbers and MSA's

		Mean Bouton Number		MSA		Mean Normalised Bouton Number		
Figure	**Genotype**	**Number**	**SEM**	**MSA (μm^2)**	**SEM**	**Number**	**SEM**	**n**
Fig.4.6.	*w*$^-$ (WT)	110.19	3.75	78704.43	2254.96			16
	Rab8^1/*Rab8*^{2}	146.08	4.33	64807.39	3669.02	182.41	9.78	12
	Rab8^1/*Rab8*^{3}	149.44	5.58	64279.49	2931.12	185.34	9.03	9
	Rab8^1/*Rab8*^{Z3007}	193.89	12.77	71153.24	4764.09	223.97	21.57	9
	Rab8^1/*Rab8*^{B229}	186.60	6.81	76540.78	5648.26	199.83	13.72	10
	Rab8^1/Df(3L)*ED228*	157.33	6.66	73156.17	2467.23	170.94	10.19	9
	Rab8^2/*Rab8*^{3}	128.50	4.11	66621.42	3115.65	155.48	10.13	10
	Rab8^2/*Rab8*^{Z3007}	193.33	5.00	83125.83	5527.39	186.60	11.43	6
	Rab8^2/*Rab8*^{B229}	157.25	5.53	89367.03	3609.99	143.22	9.06	16
	Rab8^2/Df(3L)*ED228*	158.07	7.85	68128.31	1700.72	161.13	10.29	10
	Rab8^3/*Rab8*^{Z3007}	181.00	4.71	94816.57	2533.56	151.08	5.75	9
	Rab8^3/*Rab8*^{B229}	162.88	3.30	88690.26	5045.49	147.64	8.40	8
	Rab8^3/Df(3L)*ED228*	157.29	3.43	83473.04	5016.93	152.08	11.22	7
	Rab8^{Z3007}/*Rab8*^{B229}	152.91	9.18	78842.15	2489.86	153.93	10.67	11
	Rab8^{Z3007}/Df(3L)*ED228*	172.63	7.12	75135.52	3321.20	183.96	12.71	8
	Rab8^{B229}/Df(3L)*ED228*	170.50	5.37	89360.33	2182.09	150.39	4.77	6
Fig.4.7.	*CS*/*w*$^-$	91.85	4.95	86103.90	2747.84			14
	act-GAL4/UAS-*Rab8*;*Rab8*^{1}/*Rab8*^{B229}	87.50	3.48	82552.02	1541.03	91.22	2.94	10
	act-GAL4/UAS-*Rab8*	77.53	3.30	81498.42	2729.90	83.77	4.73	19
	nsyb-GAL4/UAS-*Rab8*	84.36	4.72	72068.27	3141.27	100.68	7.29	14

Appendix 1. Muscle 6/7 Bouton Numbers and MSA's

		Mean Bouton Number		MSA		Mean Normalised Bouton Number		
Figure	**Genotype**	**Number**	**SEM**	**MSA (μm^2)**	**SEM**	**Number**	**SEM**	**n**
	nSyb-GAL4/UAS-*Rab8*;*Rab8*^{1}/*Rab8*^{B229}	89.30	6.86	90024.34	2174.91	86.22	7.27	10
	Rab8^{1}/*Rab8*^{B229}	186.60	6.81	76540.78	5648.26	218.61	15.01	10
	UAS-*Rab8*/+; +/MHC-GAL4	70.92	4.22	78981.53	2663.66	77.78	4.40	13
	UAS-*Rab8*/+; MHC-GAL4,*Rab8*^{B229}/*Rab8*^{1}	123.33	5.44	95673.86	2864.16	112.82	6.84	12
Fig.5.1.	*CS*/*w*$^{-}$	75.80	4.33	80863.85	4153.72			10
	Tkv^{7}/+	78.30	8.03	89562.38	1884.31	70.93	8.11	10
	Tkv^{k16713}/+	87.00	5.81	78984.32	2243.15	89.27	3.83	11
	Tkv^{7}/*Tkv*^{k16713}	45.10	2.86	80381.12	4906.80	46.73	3.79	10
	Dad$^{\Delta IEL}$/+	79.47	4.44	83485.52	2713.06	77.41	4.16	15
	Rab8^{1}/+	78.23	3.09	82083.26	2716.88	78.49	4.75	13
	Rab8^{1}/*Rab8*^{B229}	143.73	5.21	81541.12	3050.38	141.16	6.16	11
	Tkv^{7}/+;*Rab8*^{1}/*Rab8*^{B229}	104.00	4.49	75562.63	3014.65	112.31	4.75	13
	Tkv^{k16713}/+;*Rab*^{1}/*Rab8*^{B229}	86.64	6.89	87026.61	4308.22	80.44	3.35	11
	Tkv^{7}/*Tkv*^{k16713};*Rab*^{1}/*Rab8*^{B229}	66.09	3.20	82987.38	2873.68	64.62	2.29	11
	Dad$^{\Delta IEL}$/*Rab8*^{1}	138.33	5.83	87477.40	2735.39	130.21	6.16	27
Fig.5.6.	*CS*/*w*$^{-}$	75.80	4.33	80863.85	4153.72			10
	nSyb-Gal4/UAS-FOSDN	79.75	4.04	92494.61	3297.05	70.40	3.91	12
	OK6-Gal4/UAS-FOSDN	68.42	2.34	74016.46	1396.04	75.06	3.01	12
	Puc^{E69}/+	86.00	4.73	83338.40	1935.46	84.01	6.03	9
	Rab8^{1}/+	78.23	3.09	82083.26	2716.88	78.49	4.75	13
	Rab8^{1}/*Rab8*^{B229}	143.73	5.21	81541.12	3050.38	141.16	6.16	11
	nSyb-Gal4/UAS-FOSDN;*Rab8*^{1}/*Rab8*^{B229}	68.80	3.90	84748.00	7828.09	70.75	7.07	10
	OK6-Gal4/UAS-FOSDN;*Rab8*^{1}/*Rab8*^{B229}	83.00	4.85	76540.98	2805.56	88.95	6.48	10
	Rab8^{1}/*Puc*^{E69}	150.92	5.24	78425.50	1721.76	156.71	6.96	13

Appendix 1. Muscle 6/7 Bouton Numbers and MSA's

		Mean Bouton Number		MSA		Mean Normalised Bouton Number		
Figure	**Genotype**	**Number**	**SEM**	**MSA (μm^2)**	**SEM**	**Number**	**SEM**	**n**
Fig.5.8.	*cs*/*w*$^-$	75.80	4.33	80863.85	4153.72			10
	Dad$^{\Delta IEL}$/+	79.47	4.44	83485.52	2713.06	77.41	4.16	15
	Puc^{E69}/+	86.00	4.73	83338.40	1935.46	84.01	6.03	9
	Puc^{E69}/ *Dad*$^{\Delta IEL}$	142.30	5.47	75600.75	4892.19	159.68	13.48	10
Fig.5.9.	*CS*/*w*$^-$	76.61	5.29	80859.33	848.59			11
	POSH^{EP1206}/*POSH*^{EP1206}	92.30	5.65	71263.36	2234.03	105.05	6.13	10
	POSH^{EP2248}/*POSH*^{EP2248}	73.83	3.18	67718.39	1469.48	89.22	5.10	12
	POSH^{EP2248}/*POSH*^{EP1206}	72.92	5.66	70693.15	4040.47	85.52	7.53	12
	nSyb-GAL4/UAS-*POSH*	84.69	3.86	101543.38	4206.43	68.45	3.42	13
	Rab8^1/*Rab8*^{B229}	155.40	6.13	74126.50	2948.01	171.22	8.07	10
	POSH^{EP1206}/*POSH*^{EP1206};*Rab8*^{1}/*Rab8*^{B229}	94.50	8.18	67971.30	2103.63	111.80	8.22	14
	POSH^{EP2248}/*POSH*^{EP2248};*Rab8*^{1}/*Rab8*^{B229}	83.40	4.99	74655.60	2839.92	90.27	4.16	10
	POSH^{EP2248}/*POSH*^{EP1206};*Rab8*^{1}/*Rab8*^{B229}	98.50	5.50	82160.36	1913.35	96.85	4.62	10
	nSyb-GAL4/UAS-*POSH*;*Rab8*^{1}/*Rab8*^{B229}	74.58	5.15	94655.08	2429.82	63.73	4.05	12
Fig.5.11.	*CS*/*w*$^-$	76.61	5.29	80859.33	848.59			11
	TAK1^{179}/+	66.36	3.34	87614.70	4191.05	62.59	4.17	11
	nSyb-GAL4-*TAK1*-RNAi	99.93	6.69	87732.40	2113.24	92.23	5.86	15
	nSyb-*TAK1DN*	77.80	7.13	76946.94	3995.27	81.35	4.70	10
	nSyb-*TAK1*	130.27	9.51	60521.87	2189.13	177.48	15.97	11
	HRS$^{\Delta 28}$/+	89.60	6.57	88520.02	2689.01	81.54	4.13	10
	Rab8^1/+	78.23	3.09	82083.26	2716.88	78.49	4.75	13
	Rab8^1/*Rab8*^{B229}	155.40	6.13	74126.50	2948.01	171.22	8.07	10
	TAK1^{179}/+;*Rab8*^{1}/*Rab8*^{B229}	96.91	6.57	95052.49	3554.07	83.54	6.45	11
	nSyb-GAL4-*TAK1*-DN;*Rab8*^{1}/*Rab8*^{B229}	89.17	6.43	76892.81	3702.22	95.29	6.38	12

Appendix 1. Muscle 6/7 Bouton Numbers and MSA's

		Mean Bouton Number		MSA		Mean Normalised Bouton Number		
Figure	**Genotype**	**Number**	**SEM**	**MSA (μm^2)**	**SEM**	**Number**	**SEM**	**n**
	nSyb-GAL4-*TAK1*-RNAi;*Rab8*^{1}/*Rab8*^{B229}	89.14	7.38	81661.76	1886.03	89.83	8.08	14
	HRS$^{\Delta 28}$/+;*Rab8*^{1}/+	135.50	6.68	85269.37	2011.78	128.14	4.94	10
Fig.6.1.	*CS*/*w*$^{-}$	93.07	3.22	85356.83	2331.64			16
	nSyb-GAL4-UAS-*CHMP2B*^{Intron5}	134.92	3.37	78414.07	2495.31	148.02	4.41	13
	nSyb-GAL4/+	100.43	5.83	86103.90	2747.84	99.62	5.37	14
	UAS-*CHMP2B*^{Intron5}/+	97.82	4.94	75706.29	2885.37	111.34	5.82	11
Fig.6.2.	*CS*/*w*$^{-}$	93.5	4.66	89387.87	1917.01			10
	nsyb-Gal4/+;UAS-*Rab8*/+	88.73	3.65	80472.34	3058.53	99.83	4.35	15
	nsyb-Gal4/UAS-*CHMP2B*^{Intron5}	128.00	4.01	79581.75	3066.97	149.79	5.79	17
	nsyb-Gal4/UAS-*CHMP2B*^{Intron5};UAS-*Rab8*/+	100.09	3.37	78492.23	1975.21	114.89	3.99	22
Fig.6.9.	*CS*/*w*$^{-}$	93.50	4.66	89387.87	1917.01			10
	nsyb-Gal4/UAS-*CHMP2B*^{Intron5}	130.82	3.90	79037.47	2671.74	149.79	5.79	17
	nsyb-Gal4/+;UAS-*Rab8*/+	88.73	3.65	80472.34	3058.53	99.83	4.35	15
	nsyb-Gal4/UAS-*CHMP2B*^{Intron5};UAS-*Rab8*/+	100.09	3.37	78492.23	1975.21	114.89	3.99	22
	CS/*w*$^{-}$	77.91	4.80	80890.07	3084.52			10
	nsyb-Gal4/UAS-*CHMP2B*^{Intron5}	130.82	3.90	79037.47	2244.71	135.55	5.24	17
	Atg18/Df(3L)*Exel6112*	71.75	5.21	94206.78	2995.77	62.42	4.95	12
	nsyb-Gal4/UAS-*CHMP2B*^{Intron5};*Atg18*/Df(3L)*Exel6112*	76.44	4.92	91701.30	2104.27	67.81	4.43	10
Fig.6.10.	*w*$^{-}$ (DMSO)	81.71	2.08	75755.92	1823.81			24
	w^{-} (Rapamycin)	107.74	3.60	72019.06	2390.42	113.33	3.78	19
	OK6-Gal4/UAS-*Shrub*-GFP (DMSO)	122.00	4.41	75061.93	4084.46	123.13	4.45	7
	OK6-Gal4/UAS-*Shrub*-GFP (Rapamycin)	195.10	7.01	64208.41	1833.90	230.19	8.28	10
	OK6-Gal4/UAS-*CHMP2B*^{Intron5} (DMSO)	108.29	3.48	58242.69	4133.66	140.85	4.52	7
	OK6-Gal4/UAS-*CHMP2B*^{Intron5} (Rapamycin)	112.13	5.81	67870.72	6676.73	125.15	6.48	8

Appendix 2. Muscle 4 Bouton Numbers and MSA's

		Mean Bouton Number		MSA		Mean Normalised Bouton Number		
Figure	**Genotype**	**Number**	**SEM**	**MSA (μm^2)**	**SEM**	**Number**	**SEM**	**n**
Fig.4.7.	*CS*/*w*$^-$	23.13	2.17	59605.83	2203.45			15
	Rab8^1/*Rab8*^{B229}	43.81	2.02	59035.38	1467.24	44.94	2.71	16
	act-GAL4/UAS-*Rab8*;*Rab8*^{1}/*Rab8*^{B229}	21.75	1.37	55775.50	1932.60	23.34	1.33	14
	nsyb-Gal4/UAS-*Rab8; Rab8*^{1}/*Rab8*^{B229}	24.20	1.72	59234.54	2876.80	24.58	1.86	10
	UAS-*Rab8*/+; MHC-GAL4,*Rab8*^{B229}/*Rab8*^{1}	39.55	4.66	65638.86	3230.70	35.90	2.88	11
	nsyb-Gal4/UAS-*Rab8*	20.33	1.93	61336.18	2774.42	19.90	1.26	12
	act-Gal4, UAS-*Rab8*	21.69	1.89	63996.76	2827.40	20.65	1.56	13
	UAS-*Rab8*/+; +/MHC-GAL4	20.40	2.29	57514.18	3866.51	21.46	1.95	10
Fig.5.2.	*CS*/*w*$^-$	19.50	1.21	55748.16	1765.22			14
	Rab8^1/*Rab8*^{B229}	35.36	2.57	59234.58	2223.92	33.57	1.68	11
	Tkv^{k16713}/+	18.75	1.84	53493.82	1585.27	19.48	1.75	12
	Tkv^{k16713}/+;*Rab*^{1}/*Rab8*^{B229}	19.00	1.00	56854.89	2689.94	18.89	1.22	10
	Dad$^{\Delta IEL}$/+	23.30	2.11	57510.52	3001.22	23.41	2.51	10
	Dad$^{\Delta IEL}$/Rab8^1	32.25	1.40	58493.07	2523.80	31.34	2.33	8
	Rab8^1/+	20.73	2.41	61734.38	2830.39	19.10	1.74	11
Fig.5.8.	*CS*/*w*$^-$	19.50	1.21	55748.16	1765.22			14
	Dad$^{\Delta IEL}$/+	23.30	2.11	57510.52	3001.22	23.41	2.51	10
	Puc^{E69}/+	22.50	1.34	66396.44	3801.50	19.41	1.37	10
	Puc^{E69}/*Dad*$^{\Delta IEL}$	40.78	3.44	54520.38	931.12	41.90	3.74	10
Fig.6.2.	*CS*/*w*$^-$	22.53	2.02					17
	nsyb-GAL4/*Rab8*	25.40	2.01	66934.40	4287.16	24.73	2.01	10
	nsyb-GAL4/UAS-*CHMP2B*^{Intron5}	34.31	2.75	66446.84	2378.43	32.88	3.17	13
	nsyb-GAL4/UAS-*CHMP2B*^{Intron5};UAS-*Rab8*	17.29	1.27	62417.20	2116.69	17.53	1.37	14

Appendix 3. Muscle 4 NMJ Lengths and MSA's

		Mean NMJ Length				Mean Normalised NMJ Length		
Figure	**Genotype**	**Length (μm^2)**	**SEM**	**MSA (μm^2)**	**SEM**	**Length (μm^2)**	**SEM**	**n**
Fig.4.7.	*CS*/*w*$^-$	88.94	9.41	61164.76	2052.23			11
	Rab8^1/*Rab8*^{B229}	157.49	6.70	61673.74	1461.63	157.51	8.85	10
	act-GAL4/UAS-*Rab8*;*Rab8*^{1}/*Rab8*^{B229}	105.17	9.44	57942.99	1082.90	114.91	9.50	10
	nsyb-Gal4/UAS-*Rab8; Rab8*^{1}/*Rab8*^{B229}	118.86	11.05	59234.54	2876.80	123.66	10.96	10
	UAS-*Rab8*/+; MHC-GAL4,*Rab8*^{B229}/*Rab8*^{1}	139.37	13.87	65638.86	3230.70	131.83	15.80	11
	nsyb-Gal4/UAS-*Rab8*	103.10	11.58	61586.01	3335.34	118.26	9.32	11
	act-Gal4, UAS-*Rab8*	108.96	8.61	64885.34	2744.38	104.10	10.05	10
	UAS-*Rab8*/+; +/MHC-GAL4	89.85	13.14	57514.18	3866.51	96.41	11.09	10
Fig.5.2.	*CS*/*w*$^-$	95.52	7.28	56585.38	2102.45			11
	Rab8^1/*Rab8*^{B229}	168.00	13.53	57939.67	1513.73	166.36	15.31	9
	Tkv^{k16713}/+	79.02	4.78	53247.20	1742.30	85.17	6.05	12
	Tkv^{k16713}/+;*Rab*^{1}/*Rab8*^{B229}	105.50	7.65	55897.96	2666.47	108.89	9.43	9
	Dad$^{\Delta IEL}$/+	116.06	13.09	57510.52	3001.22	115.88	14.17	10
	Dad$^{\Delta IEL}$/Rab8^1	157.32	12.54	58493.07	2523.80	156.58	15.42	7
	Rab8^1/+	104.18	7.23	61734.38	2830.39	97.86	8.56	11
Fig.5.8.	*CS*/*w*$^-$	95.52	7.28	56585.38	2102.45			11
	Dad$^{\Delta IEL}$/+	116.06	13.09	57510.52	3001.22	114.16	13.96	10
	Puc^{E69}/+	92.46	7.92	66396.44	3801.50	79.01	7.04	10
	Puc^{E69}/*Dad*$^{\Delta IEL}$	170.54	22.77	54520.38	931.12	174.84	23.20	10
Fig.6.2.	*CS*/*w*$^-$	87.87	9.25	63419.92	2401.31			11
	nsyb-GAL4/*Rab8*	87.88	6.84	66934.40	2988.98	86.51	8.06	10
	nsyb-GAL4/UAS-*CHMP2B*^{Intron5}	153.24	14.27	66488.64	2366.26	146.47	15.43	13
	nsyb-GAL4/UAS-*CHMP2B*^{Intron5};UAS-*Rab8*	100.85	8.43	62417.20	2116.69	106.51	12.14	14

Appendix 4. Muscle 4 Branch Numbers and MSA's

		Mean Branch Number				Mean Normalised Branch Number		
Figure	**Genotype**	**Number**	**SEM**	**MSA (μm^2)**	**SEM**	**Number**	**SEM**	**n**
Fig.4.7.	*CS*/*w*$^-$	2.53	0.24	59605.83	2203.45			15
	Rab8^1/*Rab8*^{B229}	3.30	0.37	61673.74	1461.63	3.23	0.41	10
	act-GAL4/UAS-*Rab8*;*Rab8*^{1}/*Rab8*^{B229}	2.83	0.21	55775.50	1932.60	3.08	0.26	12
	nsyb-Gal4/UAS-*Rab8; Rab8*^{1}/*Rab8*^{B229}	2.80	0.20	59234.54	2876.80	2.89	0.26	10
	UAS-*Rab8*/+; MHC-GAL4,*Rab8*^{B229}/*Rab8*^{1}	3.36	0.42	65638.86	3230.70	3.07	0.39	11
	nsyb-Gal4/UAS-*Rab8*	2.58	0.34	61164.20	3138.30	2.56	0.29	12
	act-Gal4, UAS-*Rab8*	2.00	0.21	64885.34	2744.38	1.86	0.25	10
	UAS-*Rab8*/+; +/MHC-GAL4	2.40	0.22	57514.18	3866.51	2.51	0.21	10
Fig.6.2.	*CS*/*w*$^-$	2.60	0.31	61312.30	3009.17			11
	nsyb-GAL4/*Rab8*	2.70	0.30	66934.40	4287.16	2.61	0.32	10
	nsyb-GAL4/UAS-*CHMP2B*^{Intron5}	4.30	10.00	63818.84	2487.00	4.19	0.71	10
	nsyb-GAL4/UAS-*CHMP2B*^{Intron5};UAS-*Rab8*	1.80	0.25	62012.40	2775.25	1.80	0.25	10

Appendix 5. Muscle 4 Satellite Bouton Numbers and MSA's

		Mean Satellite Bouton Number				Mean Normalised Satellite Bouton Number		
Figure	**Genotype**	**Number**	**SEM**	**MSA (μm^2)**	**SEM**	**Number**	**SEM**	**n**
Fig.4.7.	*CS*/*w*$^-$	2.50	0.70	61723.62	2479.20			10
	Rab8^1/*Rab8*^{B229}	8.40	1.41	61284.39	1061.78	8.51	1.45	10
	act-GAL4/UAS-*Rab8*;*Rab8*^{1}/*Rab8*^{B229}	4.67	0.74	55775.50	1932.60	4.91	0.77	12
	nsyb-Gal4/UAS-*Rab8; Rab8*^{1}/*Rab8*^{B229}	5.80	1.14	59234.54	2876.80	6.16	1.39	10
	UAS-*Rab8*/+; MHC-GAL4,*Rab8*^{B229}/*Rab8*^{1}	9.64	2.87	65638.86	3230.70	8.84	2.43	12
	nsyb-Gal4/UAS-*Rab8*	6.07	0.84	63186.83	2350.89	5.92	0.77	14
	act-Gal4, UAS-*Rab8*	4.36	1.09	64007.11	2822.47	4.43	1.22	11
	UAS-*Rab8*/+; +/MHC-GAL4	9.64	2.87	65638.86	3230.70	8.84	2.43	11
Fig.6.2.	*CS*/*w*$^-$	3.23	0.79	65403.36	2444.50			13
	nsyb-GAL4/*Rab8*	6.00	1.04	66934.40	2988.98	6.16	1.11	10
	nsyb-GAL4/UAS-*CHMP2B*^{Intron5}	8.00	1.34	63818.84	2487.00	8.53	1.65	10
	nsyb-GAL4/UAS-*CHMP2B*^{Intron5};UAS-*Rab8*	2.64	0.66	62417.20	2116.69	2.70	0.66	14

Appendix 6. Muscle 4 Bouton Sizes and MSA's

		Mean Bouton Size				Mean Normalised Bouton Size		
Figure	Genotype	Size (μm)	SEM	MSA (μm^2)	SEM	Size (μm)	SEM	n
Fig.4.7.	*CS*/*w*$^-$	3.31	0.11	63419.92	2401.31			185
	Rab8^1/*Rab8*^{B229}	2.87	0.07	61284.39	1061.78	3.00	0.07	358
	act-GAL4/UAS-*Rab8*;*Rab8*^{1}/*Rab8*^{B229}	3.49	0.13	56729.97	425.89	3.91	0.15	157
	nsyb-Gal4/UAS-*Rab8; Rab8*^{1}/*Rab8*^{B229}	3.40	0.10	59234.54	2876.80	3.69	0.12	242
	UAS-*Rab8*/+; MHC-GAL4,*Rab8*^{B229}/*Rab8*^{1}	2.52	0.05	65638.86	3230.70	2.30	0.05	435
	nsyb-Gal4/UAS-*Rab8*	4.53	0.13	61325.77	3138.30	4.67	0.15	162
	act-Gal4, UAS-*Rab8*	3.95	0.13	64682.62	2791.88	3.97	0.13	121
	UAS-*Rab8*/+; +/MHC-GAL4	1.27	0.09	57514.18	3866.51	3.26	0.10	214
Fig.5.2.	*CS*/*w*$^-$	3.75	0.11	56585.38	2102.45			205
	Rab8^1/*Rab8*^{B229}	2.97	0.07	57939.67	1513.73	2.94	0.07	314
	Tkv^{k16713}/+	3.88	0.13	53247.20	1742.30	4.15	0.15	175
	Tkv^{k16713}/+;*Rab*^{1}/*Rab8*^{B229}	4.36	0.11	55897.96	2666.47	4.51	0.12	172
	Dad$^{\Delta IEL}$/+	3.28	0.10	57510.52	3001.22	3.52	0.12	149
	Dad$^{\Delta IEL}$/Rab8^1	3.43	0.11	58493.07	2523.80	3.39	0.11	256
	Rab8^1/+	3.11	0.07	61734.38	2830.39	2.93	0.08	228
Fig.5.8.	*CS*/*w*$^-$	3.75	0.11	56585.38	2102.45			205
	Dad$^{\Delta IEL}$/+	3.28	0.10	57510.52	3001.22	3.52	0.12	149
	Puc^{E69}/+	3.12	0.07	66396.44	3801.50	2.68	0.06	224
	Puc^{E69}/*Dad*$^{\Delta IEL}$	2.65	0.06	54520.38	931.12	2.73	0.06	369
Fig.6.2.	*CS*/*w*$^-$	3.31	0.11	63419.92	2401.31			185
	nsyb-GAL4/*Rab8*	3.13	0.08	66934.40	2988.98	3.19	0.09	253
	nsyb-GAL4/UAS-*CHMP2B*^{Intron5}	3.36	0.07	65875.83	2274.82	3.25	0.07	463
	nsyb-GAL4/UAS-*CHMP2B*^{Intron5};UAS-*Rab8*	3.76	0.09	62417.20	2116.69	3.86	0.11	242

Abbreviations

αSyn	**A**lpha-**Syn**uclein
aCC	**a**nterior **C**orner **C**ell
AD	**A**lzheimer's **D**isease
ADBE	**A**ctivity-**D**ependent **B**ulk **E**ndocytosis
Ahi1	**A**belson's **h**elper **i**ntegration **1**
ALG	**A**poptosis **L**inked **G**ene
ALIX	**A**poptosis **L**inked gene-2- **I**nteracting protein **X**
ALS	**A**myotrophic **L**ateral **S**clerosis
AMPA	α-**A**mino-3-hydroxy-5-**M**ethyl-4-isox**a**zole**p**ropionate
ANOVA	**An**alysis **O**f **Va**riance
AP-1	**A**ctivator **P**rotein-**1**
ApoE	**Apo**liprprotein **E**
APP	**A**myloid **P**recursor **P**rotein
Arf6	**A**denosine diphosphate-**r**ibosylation **f**actor **6**
ATG	**Au**tophagy related **G**ene
BDMA	**Di**methyl**b**enzyl**a**mine
BES	**B**acterial artificial chromosome **E**nd **S**equences
BMP	**B**one **M**orphogenic **P**rotein
bp	**b**ase **p**airs
bvFTD	**b**ehavioural **v**ariant **F**ronto**t**emporal **D**ementia
C9ORF72	**C**hromosome **9** **O**pen **R**eading **F**rame **72**
Caz	**Ca**be**x**a
CBD	**C**orticobasal **D**egeneration
cDNA	**c**omplementary **DNA**
CG	**C**omputed **G**ene
CHMP	**Ch**arged **M**ultivesicular body **P**rotein
CHMP2B	**Ch**arged **M**ultivesicular body **P**rotein **2B**
Ci	**C**ubitus **i**nterruptus
CLN3	**C**eroid-**L**ipofuscinosis, **N**euronal **3**
CMT2B	**C**harcot-**M**arie-**T**ooth Disease type **2B**
CNS	**C**entral **N**ervous **S**ystem
co-SMAD	**co**-factor-**S** **M**other's **A**gainst **D**ecapentaplegic
CPG	**C**entral **P**attern **G**enerator
CTCF	**C**orrected **T**otal **C**ell **F**luorescence
CTNF	**C**orrected **T**otal **N**uclear immuno**f**luorescence
Cy3	**Cy**anine **3**
CyO	**C**urly of **O**ster
Dad	**D**aughters **A**gainst **D**ecapentaplegic
ddH_2O	**d**ouble **d**istilled water
DDSA	**D**o**d**ecenyl **S**uccinic **A**nhydride
dH_2O	**d**istilled water
Dlg	**D**iscs **L**ar**g**e
DMF	**Di**methyl**f**ormamide
DMSO	**Di**methyl **S**ulph**o**xide
dNTP	**d**eoxyribo**n**ucleotide **Tri**p**h**osphate
DPP	**D**eca**p**enta**p**legic
Drp1	**D**ynamin **r**elated **p**rotein **1**

EAP	**E**bony **A**ctivating **P**rotein
EDTA	**E**thylene**d**iamine**t**etra**a**cetic acid
eGFP	**e**nhance **G**reen **F**luorescent **P**rotein
EHD	EH Domain containing protein
eIF-2Bε	**e**ukaryotic **I**nitiation **F**actor **2B**-**e**psilon
Ema	**E**ndosomal **ma**turation defective
EMS	**E**thyl **M**ethane **S**ulphonate
EPSP	**E**xcitatory **P**ost-**S**ynaptic **P**otential
ER	**E**ndoplasmic **R**eticulum
ERC	**E**ndosomal **R**ecycling **C**ompartment
ESCRT	**E**ndosomal **S**orting **C**omplex **R**equired for **T**ransport
EtOH	Ethanol
Fas II	**Fas**ciclin II
FM	**F**requency-**M**odulated
fpCC	**f**riend of **p**osterior **C**orner **C**ell
FTD	**F**ronto**t**emporal **D**ementia
FTD-3	**F**ronto**t**emporal **D**ementia associated with chromosome **3**
FTLD	**F**ronto**t**emporal **L**obar **D**egeneration
FTLD-FUS	**FTLD-Fu**sed in **S**arcoma
FTLD-Tau	**FTLD-Tau**
FTLD-TDP	**FTLD-T**rans-activation response **D**NA-binding **P**rotein 43
FTLD-UPS	**FTLD**-Ubiquitin Proteasome System
FUS	**Fu**sed in **S**arcoma
GAP	**G**TPase **A**ctivating **P**roteins
Gbb	**G**lass **b**ottom **b**oat
GDF	**G**uanosin diphosphate-Dissociation Inhibitors **D**isplacement **F**actors
GDI	**G**uanosin diphosphate-**D**issociation **I**nhibitors
GDP	**G**uanosin **Di**phosphate
GEF	**G**uanine nucleotide **E**xchange **F**actor
GFP	**G**reen **F**luorescent **P**rotein
GluR	**Glu**tamate **R**eceptor
GMR	**G**lass **M**ultimer **R**eporter
GRN/PGRN	Pro**gr**anuli**n**
GSK-3	**G**lycogen **S**ynthase **K**inase **3**
GST	**G**lutathione **S**-**T**ransferase
GTP	**G**uanosin-5'-**Tri**p**h**osphate
HDAC	**H**istone **De**a**c**etylase
HGS	**H**epatocyte **G**rowth factor-regulated tyrosine kinase **S**ubstrate
hiw	**hi**gh**w**ire
HL3	**H**emolymph **L**ike-**3** saline
HRP	**H**orse**r**adish **P**eroxidase
HRS	**H**epatocyte growth factor-**R**egulated tyrosine kinase **S**ubstrate
HSE	**H**eat **S**hock **E**lements
HSP	**H**eat **S**hock **P**rotein
Htt	**H**un**t**ing**t**in
IGF	**I**nsulin-like **G**rowth **F**actor
ILV	**I**ntra**l**uminal **V**esicles

Imp	**I**GF-II **m**RNA binding **p**rotein
IPIP27	27 kDa Inositol Polyphosphate phosphatase-Interacting Protein
ISN	**I**nter**s**egmental motor **N**erve
JNK	**J**un **N**-terminal **K**inase
JNKKK	**J**un **N**-terminal **K**inase **K**inase **K**inase
Jra	**J**un-**r**elated **a**ntigen
kb	**k**ilo**b**ase
LB	**L**uria **B**roth
LBPA	**L**yso**b**is**p**hosphatidic **A**cid
LS	**L**owe **S**yndrome
LSD's	**L**ysosomal **S**torage **D**isorders
Lsn	**L**ar**s**e**n**
LTP	**L**ong **T**erm **P**otentiation
MAD	**M**others **A**gainst **D**ecapentalegic
MAPK	**M**itogen-**A**ctivated **P**rotein **K**inase
MAPT	**M**icrotubule **A**ssociated **P**rotein **T**au
Mav	**Mav**erick
mEPSP	**m**ini **E**xcitatory **P**ost-**S**ynaptic **P**otential
MHC	**M**ajor **H**istocompatibility **C**omplex
MICAl3	**Mi**crotubule-associated monoxygenase, **cal**ponin and LIM domain containing **3**
MIM	**M**icrotubule interacting and transport **I**nteracting **M**otif
MIT	**M**icrotubule **I**nteracting and **T**ransport
MND	**M**otor **N**euron **D**isease
mRNA	**m**essenger **RNA**
MSA	**M**uscle **S**urface **A**rea
MT1-MMP	Type **I** **T**rans**m**embrane **M**atrix **M**etallo**p**roteinase
MVB	**M**ulti**v**esicular **B**odies
Myo5-b & -c	**Myo**sin**V-b** & **-c**
NFκB	**N**uclear **F**actor **k**appa-**B**
NMJ	**N**euro**m**uscular **J**unction
NPC	**N**iemann **P**ick **C**
NSF	**N**-ethylmaleimide-**S**ensative **F**actor
nSyb	**n**euronal **Sy**napto**b**revin
NTAP	**N**-terminal **T**andem **A**ffinity **P**urification
nwk	**n**ervous **wrec**k
OCRL1	**O**culo**c**erbro**r**enal syndrome of **L**owe **1**
OK6	**O**'**K**ane 6
PBS	**P**hosphate **B**uffered **S**aline
PBS-T	**P**hosphate **B**uffered **S**aline with detergent **T**ween 20
PBT	**P**hosphate **B**uffered Saline with detergent **T**ween 20
pCC	**p**osterior **C**orner **C**ell
PCM1	**P**eri-**C**entriolar **M**aterial protein **1**
PCR	**P**olymerase **C**hain **R**eaction
PD	**P**arkinson's **D**isease
PDZ	**P**ost synaptic density protein**, D**rosophila disc large tumor suppressor, **Z**onula occludens-1 protein
PEL	**P**ost **E**gg **L**aying
PKC	**P**rotein **K**inase **C**

P-MAD	**P**hospho-/**P**hosphorylated- **M**others **A**gainst **D**ecapentaplegic
PNFA	**P**rogressive **N**on-**F**luent **A**phasia
POSH	**P**lenty **O**f **SH**3's
PS	**P**osition **S**pecific
PSD	**P**ost **S**ynaptic **D**ensity
PSEN1	**Pre**sen**e**illin-**1**
PSP	**P**rogressive **S**upranuclear **P**alsy
Puc	**Puc**kered
Rab	**Ra**s related in **B**rain
RabGGT	**Rab G**eranyl **G**eranyl **T**ransferase
REP	**R**ab **E**scort **P**rotein
RNAi	**RNA i**nterference
ROS	**R**eactive **O**xygen **S**pecies
R-SMADs	**R**eceptor **SMAD**
RT	**R**oom **T**emperature
SARA	**S**MAD **A**nchor for **R**eceptor **A**ctivation
sax	**Sax**ophone
SCA3	**S**pino**c**erebella **A**taxia type-**3**
SD	**S**emantic **D**ementia
SDS	**S**odium **D**odecyl **S**ulphate
SEM	**S**tandard **E**rror of **M**ean
Ses	**Ses**quipedalian
SH3TC2	**SH3** domain and **T**etratricopeptide repeats-**C**ontaining protein **2**
siRNA	**s**mall **i**nterferring **RNA**
SMAD	SMA + MAD
SmD3	**Sm**all nuclear ribonucleoprotein **D3** polypeptide 18 kDa
SNa-d	**S**egmental **N**erves **a-d**
SNARE	**S**oluble **N**-ethylmaleimide-sensitive factor attachment protein **Re**ceptor
SNX	**S**orting **Nex**in
SOC	**S**uper **O**ptimal broth with **C**atabolite repression
SOD	**S**uper**o**xide **D**ismutase
spin	**spin**ster
SSR	**S**ub**s**ynaptic **R**eticulum
STAM	**S**ignal **T**ransducing **A**daptor **M**olecule
TAB	**T**ransforming Growth Factor Beta **A**ctivated Kinase 1 **b**inding Protein
TAK	**T**ransforming growth factor beta-**A**ctivated **K**inase
TAP	**T**andem **A**ffinity **P**urification
TAR	**T**rans-**A**ctivation **R**esponse
TARDBP	**T**rans-**A**ctivation **R**esponse **D**NA-**B**inding **P**rotein 43
TBPH	**T**rans-activation response DNA **B**inding **P**rotein 43 **H**omolog
TDP-43	**T**rans-activation response **D**NA-binding **P**rotein **43**
TE Buffer	**T**ris-**E**DTA Buffer
TEM	**T**ransmission **E**lectron **M**icroscopy
TER	**T**ransitional **E**ndoplasmic **R**eticulum
TOR	**T**arget **o**f **R**apamaycin

TORC	**T**arget **o**f **R**apamaycin **C**omplex
Tfn	**T**rans**f**erri**n**
TfnR	**T**rans**f**errin **R**eceptor
TGFβ	**T**ransforming **G**rowth **F**actor **Beta**
TGN	**T**rans-**G**olgi **N**etwork
TIAF1	**T**ransforming Growth Factor Beta**1** **I**nduced **A**ntiapoptotic **F**actor
Tkv	**T**hic**k** **V**eins
T_m	**m**elting **T**emperature
TN	**T**ransverse **N**erve
TRAF	**T**umor **N**ecrosis **F**actor **R**eceptor
Tris-HCl	**tris**(hydroxymethyl)aminomethane hydrochloride
TSG101	**T**umour **S**usceptibility **G**ene **101**
UAS	**U**pstream **A**ctivator **S**equence
UPS	**U**biquitin **P**roteasome **S**ystem
VCP	**V**alosin **C**ontaining **P**rotein
VNC	**V**entral **N**erve **C**ord
Vps	**V**acuolar **P**rotein **S**orting
Vsp	**V**ery **s**mall **p**uparia
Wit	**Wi**shful **T**hinking
Wnd	**W**alle**nd**a
WT	**W**ildtype

References

Aberle, H., Haghighi, A.P., Fetter, R.D., McCabe, B.D., Magalhaes, T.R., and Goodman, C.S. (2002). wishful thinking encodes a BMP type II receptor that regulates synaptic growth in Drosophila. Neuron *33*, 545-558.

Adachi, H., Katsuno, M., Waza, M., Minamiyama, M., Tanaka, F., and Sobue, G. (2009). Heat shock proteins in neurodegenerative diseases: pathogenic roles and therapeutic implications. International journal of hyperthermia : the official journal of European Society for Hyperthermic Oncology, North American Hyperthermia Group *25*, 647-654.

Adachi-Yamada, T., Fujimura-Kamada, K., Nishida, Y., and Matsumoto, K. (1999). Distortion of proximodistal information causes JNK-dependent apoptosis in Drosophila wing. Nature *400*, 166-169.

Adams, M.D., Celniker, S.E., Holt, R.A., Evans, C.A., Gocayne, J.D., Amanatides, P.G., Scherer, S.E., Li, P.W., Hoskins, R.A., Galle, R.F.*, et al.* (2000). The genome sequence of Drosophila melanogaster. Science *287*, 2185-2195.

Adams, M.D., and Sekelsky, J.J. (2002). From sequence to phenotype: reverse genetics in Drosophila melanogaster. Nature reviews Genetics *3*, 189-198.

Agola, J.O., Jim, P.A., Ward, H.H., Basuray, S., and Wandinger-Ness, A. (2011). Rab GTPases as regulators of endocytosis, targets of disease and therapeutic opportunities. Clinical genetics *80*, 305-318.

Ahmad, S.T., Sweeney, S.T., Lee, J.A., Sweeney, N.T., and Gao, F.B. (2009). Genetic screen identifies serpin5 as a regulator of the toll pathway and CHMP2B toxicity associated with frontotemporal dementia. Proceedings of the National Academy of Sciences of the United States of America *106*, 12168-12173.

Ajibade, A.A., Wang, H.Y., and Wang, R.F. (2013). Cell type-specific function of TAK1 in innate immune signaling. Trends in immunology *34*, 307-316.

Alexandrov, K., Horiuchi, H., Steele-Mortimer, O., Seabra, M.C., and Zerial, M. (1994). Rab escort protein-1 is a multifunctional protein that accompanies newly prenylated rab proteins to their target membranes. The EMBO journal *13*, 5262-5273.

Ali, B.R., Wasmeier, C., Lamoreux, L., Strom, M., and Seabra, M.C. (2004). Multiple regions contribute to membrane targeting of Rab GTPases. Journal of cell science *117*, 6401-6412.

Aligianis, I.A., Johnson, C.A., Gissen, P., Chen, D., Hampshire, D., Hoffmann, K., Maina, E.N., Morgan, N.V., Tee, L., Morton, J.*, et al.* (2005). Mutations of the catalytic subunit of RAB3GAP cause Warburg Micro syndrome. Nature genetics *37*, 221-223.

Aligianis, I.A., Morgan, N.V., Mione, M., Johnson, C.A., Rosser, E., Hennekam, R.C., Adams, G., Trembath, R.C., Pilz, D.T., Stoodley, N.*, et al.* (2006). Mutation in Rab3 GTPase-activating protein (RAB3GAP) noncatalytic subunit in a kindred with Martsolf syndrome. American journal of human genetics *78*, 702-707.

Altman, B.J., and Rathmell, J.C. (2012). Metabolic stress in autophagy and cell death pathways. Cold Spring Harbor perspectives in biology *4*, a008763.

Amorim, M.J., Bruce, E.A., Read, E.K., Foeglein, A., Mahen, R., Stuart, A.D., and Digard, P. (2011). A Rab11- and microtubule-dependent mechanism for cytoplasmic transport of influenza A virus viral RNA. Journal of virology *85*, 4143-4156.

Ang, A.L., Taguchi, T., Francis, S., Folsch, H., Murrells, L.J., Pypaert, M., Warren, G., and Mellman, I. (2004). Recycling endosomes can serve as intermediates during transport from the Golgi to the plasma membrane of MDCK cells. The Journal of cell biology *167*, 531-543.

Ariumi, Y., Kuroki, M., Maki, M., Ikeda, M., Dansako, H., Wakita, T., and Kato, N. (2011). The ESCRT system is required for hepatitis C virus production. PloS one *6*, e14517.

Armstrong, J., Thompson, N., Squire, J.H., Smith, J., Hayes, B., and Solari, R. (1996). Identification of a novel member of the Rab8 family from the rat basophilic leukaemia cell line, RBL.2H3. Journal of cell science *109 (Pt 6)*, 1265-1274.

Armstrong, R.A., Carter, D., and Cairns, N.J. (2012). A quantitative study of the neuropathology of 32 sporadic and familial cases of frontotemporal lobar degeneration with TDP-43 proteinopathy (FTLD-TDP). Neuropathology and applied neurobiology *38*, 25-38.

Arvanitakis, Z. (2010). Update on frontotemporal dementia. Neurologist *16*, 16-22.

Ataman, B., Ashley, J., Gorczyca, D., Gorczyca, M., Mathew, D., Wichmann, C., Sigrist, S.J., and Budnik, V. (2006a). Nuclear trafficking of Drosophila Frizzled-2 during synapse development requires the PDZ protein dGRIP. Proceedings of the National Academy of Sciences of the United States of America *103*, 7841-7846.

Ataman, B., Budnik, V., and Thomas, U. (2006b). Scaffolding proteins at the Drosophila neuromuscular junction. International review of neurobiology *75*, 181-216.

Atwood, H.L., Govind, C.K., and Wu, C.F. (1993). Differential ultrastructure of synaptic terminals on ventral longitudinal abdominal muscles in Drosophila larvae. Journal of neurobiology *24*, 1008-1024.

Bachmann-Gagescu, R., Phelps, I.G., Stearns, G., Link, B.A., Brockerhoff, S.E., Moens, C.B., and Doherty, D. (2011). The ciliopathy gene cc2d2a controls zebrafish photoreceptor outer segment development through a role in Rab8-dependent vesicle trafficking. Human molecular genetics *20*, 4041-4055.

Baines, R.A., and Bate, M. (1998). Electrophysiological development of central neurons in the Drosophila embryo. The Journal of neuroscience : the official journal of the Society for Neuroscience *18*, 4673-4683.

Bajorek, M., Schubert, H.L., McCullough, J., Langelier, C., Eckert, D.M., Stubblefield, W.M., Uter, N.T., Myszka, D.G., Hill, C.P., and Sundquist, W.I. (2009). Structural basis for ESCRT-III protein autoinhibition. Nature structural & molecular biology *16*, 754-762.

Bak, T.H., and Hodges, J.R. (2001). Motor neurone disease, dementia and aphasia: coincidence, co-occurrence or continuum? Journal of neurology *248*, 260-270.

Baker, M., Mackenzie, I.R., Pickering-Brown, S.M., Gass, J., Rademakers, R., Lindholm, C., Snowden, J., Adamson, J., Sadovnick, A.D., Rollinson, S.*, et al.* (2006). Mutations in progranulin cause tau-negative frontotemporal dementia linked to chromosome 17. Nature *442*, 916-919.

Baron Gaillard, C.L., Pallesi-Pocachard, E., Massey-Harroche, D., Richard, F., Arsanto, J.P., Chauvin, J.P., Lecine, P., Kramer, H., Borg, J.P., and Le Bivic, A. (2011). Hook2 is involved in the morphogenesis of the primary cilium. Molecular biology of the cell *22*, 4549-4562.

Bathgate, D., Snowden, J.S., Varma, A., Blackshaw, A., and Neary, D. (2001). Behaviour in frontotemporal dementia, Alzheimer's disease and vascular dementia. Acta neurologica Scandinavica *103*, 367-378.

BDGP, T.B.D.G.P. (2013). Rab8 Gene Expression Report.

Belly, A., Bodon, G., Blot, B., Bouron, A., Sadoul, R., and Goldberg, Y. (2010). CHMP2B mutants linked to frontotemporal dementia impair maturation of dendritic spines. Journal of cell science *123*, 2943-2954.

Ben El Kadhi, K., Emery, G., and Carreno, S. (2012). The unexpected role of Drosophila OCRL during cytokinesis. Communicative & integrative biology *5*, 291-293.

Bentley, A., MacLennan, B., Calvo, J., and Dearolf, C.R. (2000). Targeted recovery of mutations in Drosophila. Genetics *156*, 1169-1173.

Bernardi, L., Anfossi, M., Gallo, M., Geracitano, S., Cola, R., Puccio, G., Curcio, S.A., Frangipane, F., Mirabelli, M., Clodomiro, A.*, et al.* (2011). PSEN1 and PRNP gene mutations: co-occurrence makes onset very early in a family with FTD phenotype. Journal of Alzheimer's disease : JAD *24*, 415-419.

Bigio, E.H., Johnson, N.A., Rademaker, A.W., Fung, B.B., Mesulam, M.M., Siddique, N., Dellefave, L., Caliendo, J., Freeman, S., and Siddique, T. (2004). Neuronal ubiquitinated intranuclear inclusions in familial and non-familial frontotemporal dementia of the motor neuron disease type associated with amyotrophic lateral sclerosis. Journal of neuropathology and experimental neurology *63*, 801-811.

Bilen, J., and Bonini, N.M. (2007). Genome-wide screen for modifiers of ataxin-3 neurodegeneration in Drosophila. PLoS genetics *3*, 1950-1964.

Bjorkblom, B., Ostman, N., Hongisto, V., Komarovski, V., Filen, J.J., Nyman, T.A., Kallunki, T., Courtney, M.J., and Coffey, E.T. (2005). Constitutively active cytoplasmic c-Jun N-terminal kinase 1 is a dominant regulator of dendritic architecture: role of microtubule-associated protein 2 as an effector. The Journal of neuroscience : the official journal of the Society for Neuroscience *25*, 6350-6361.

Blumenstiel, J.P., Noll, A.C., Griffiths, J.A., Perera, A.G., Walton, K.N., Gilliland, W.D., Hawley, R.S., and Staehling-Hampton, K. (2009). Identification of EMS-induced mutations in Drosophila melanogaster by whole-genome sequencing. Genetics *182*, 25-32.

Bodon, G., Chassefeyre, R., Pernet-Gallay, K., Martinelli, N., Effantin, G., Hulsik, D.L., Belly, A., Goldberg, Y., Chatellard-Causse, C., Blot, B.*, et al.* (2011a). Charged multivesicular body protein 2B (CHMP2B) of the endosomal sorting complex required for transport-III (ESCRT-III) polymerizes into helical structures deforming the plasma membrane. The Journal of biological chemistry *286*, 40276-40286.

Bomfim, T.R., Forny-Germano, L., Sathler, L.B., Brito-Moreira, J., Houzel, J.C., Decker, H., Silverman, M.A., Kazi, H., Melo, H.M., McClean, P.L.*, et al.* (2012). An anti-diabetes agent protects the mouse brain from defective insulin signaling caused by Alzheimer's disease- associated Abeta oligomers. The Journal of clinical investigation *122*, 1339-1353.

Bonner, J.M., and Boulianne, G.L. (2011). Drosophila as a model to study age-related neurodegenerative disorders: Alzheimer's disease. Experimental gerontology *46*, 335-339.

Borroni, B., Alberici, A., Grassi, M., Turla, M., Zanetti, O., Bianchetti, A., Dalla Volta, G., Rozzini, R., Gilberti, N., Bellelli, G.*, et al.* (2010). Is frontotemporal lobar degeneration a rare disorder? Evidence from a preliminary study in Brescia county, Italy. Journal of Alzheimer's disease : JAD *19*, 111-116.

Borroni, B., Bonvicini, C., Alberici, A., Buratti, E., Agosti, C., Archetti, S., Papetti, A., Stuani, C., Di Luca, M., Gennarelli, M.*, et al.* (2009). Mutation within TARDBP leads to frontotemporal dementia without motor neuron disease. Human mutation *30*, E974-983.

Bossing, T., Udolph, G., Doe, C.Q., and Technau, G.M. (1996). The embryonic central nervous system lineages of Drosophila melanogaster. I. Neuroblast lineages derived from the ventral half of the neuroectoderm. Developmental biology *179*, 41-64.

Bourne, H.R., Sanders, D.A., and McCormick, F. (1991). The GTPase superfamily: conserved structure and molecular mechanism. Nature *349*, 117-127.

Boxer, A.L., Gold, M., Huey, E., Gao, F.B., Burton, E.A., Chow, T., Kao, A., Leavitt, B.R., Lamb, B., Grether, M.*, et al.* (2013). Frontotemporal degeneration, the next therapeutic frontier: molecules and animal models for frontotemporal degeneration drug development. Alzheimer's & dementia : the journal of the Alzheimer's Association *9*, 176-188.

Boylan, K.L., Mische, S., Li, M., Marques, G., Morin, X., Chia, W., and Hays, T.S. (2008). Motility screen identifies Drosophila IGF-II mRNA-binding protein--zipcode-binding protein acting in oogenesis and synaptogenesis. PLoS genetics *4*, e36.

Brambati, S.M., Rankin, K.P., Narvid, J., Seeley, W.W., Dean, D., Rosen, H.J., Miller, B.L., Ashburner, J., and Gorno-Tempini, M.L. (2009). Atrophy progression in semantic dementia with asymmetric temporal involvement: a tensor-based morphometry study. Neurobiology of aging *30*, 103-111.

Brand, A.H., and Perrimon, N. (1993). Targeted gene expression as a means of altering cell fates and generating dominant phenotypes. Development *118*, 401-415.

Bravo-Cordero, J.J., Marrero-Diaz, R., Megias, D., Genis, L., Garcia-Grande, A., Garcia, M.A., Arroyo, A.G., and Montoya, M.C. (2007). MT1-MMP proinvasive activity is regulated by a novel Rab8-dependent exocytic pathway. The EMBO journal *26*, 1499-1510.

Breckenridge, D.G., Kang, B.H., and Xue, D. (2009). Bcl-2 proteins EGL-1 and CED-9 do not regulate mitochondrial fission or fusion in Caenorhabditis elegans. Current biology : CB *19*, 768-773.

Broadie, K., and Bate, M. (1993a). Muscle development is independent of innervation during Drosophila embryogenesis. Development *119*, 533-543.

Broadie, K.S., and Bate, M. (1993b). Development of the embryonic neuromuscular synapse of Drosophila melanogaster. The Journal of neuroscience : the official journal of the Society for Neuroscience *13*, 144-166.

Broadus, J., Skeath, J.B., Spana, E.P., Bossing, T., Technau, G., and Doe, C.Q. (1995). New neuroblast markers and the origin of the aCC/pCC neurons in the Drosophila central nervous system. Mechanisms of development *53*, 393-402.

Brown, T.C., Correia, S.S., Petrok, C.N., and Esteban, J.A. (2007a). Functional compartmentalization of endosomal trafficking for the synaptic delivery of AMPA receptors during long-term potentiation. The Journal of neuroscience : the official journal of the Society for Neuroscience *27*, 13311-13315.

Bruce, T.L.F. (2009). Functional interaction of RacF2 and the WASp family protein, SCAR, in the Rab8 signaling pathway of the social amoeba, Dictyostelium discoideum.

Bruckner, S.R., Tammariello, S.P., Kuan, C.Y., Flavell, R.A., Rakic, P., and Estus, S. (2001). JNK3 contributes to c-Jun activation and apoptosis but not oxidative stress in nerve growth factor-deprived sympathetic neurons. Journal of neurochemistry *78*, 298-303.

Bucci, C., Parton, R.G., Mather, I.H., Stunnenberg, H., Simons, K., Hoflack, B., and Zerial, M. (1992). The small GTPase rab5 functions as a regulatory factor in the early endocytic pathway. Cell *70*, 715-728.

Budnik, V. (2006). The fly neuromuscular junction: structure and function. Academic Press *75*.

Burstein, E.S., and Macara, I.G. (1992). Interactions of the ras-like protein p25rab3A with Mg2+ and guanine nucleotides. The Biochemical journal *282 (Pt 2)*, 387-392.

Butler, E.K., Voigt, A., Lutz, A.K., Toegel, J.P., Gerhardt, E., Karsten, P., Falkenburger, B., Reinartz, A., Winklhofer, K.F., and Schulz, J.B. (2012). The mitochondrial chaperone protein TRAP1 mitigates alpha-Synuclein toxicity. PLoS genetics *8*, e1002488.

Calero, M., Chen, C.Z., Zhu, W., Winand, N., Havas, K.A., Gilbert, P.M., Burd, C.G., and Collins, R.N. (2003). Dual prenylation is required for Rab protein localization and function. Molecular biology of the cell *14*, 1852-1867.

Campbell, M., and Ganetzky, B. (2012). Extensive morphological divergence and rapid evolution of the larval neuromuscular junction in Drosophila. Proceedings of the National Academy of Sciences of the United States of America *109*, E648-655.

Cao, W., Song, H.J., Gangi, T., Kelkar, A., Antani, I., Garza, D., and Konsolaki, M. (2008). Identification of novel genes that modify phenotypes induced by Alzheimer's beta-amyloid overexpression in Drosophila. Genetics *178*, 1457-1471.

Carlton, J. (2010). The ESCRT machinery: a cellular apparatus for sorting and scission. Biochemical Society transactions *38*, 1397-1412.

Chakraborty, R., Vepuri, V., Mhatre, S.D., Paddock, B.E., Miller, S., Michelson, S.J., Delvadia, R., Desai, A., Vinokur, M., Melicharek, D.J.*, et al.* (2011). Characterization of a Drosophila Alzheimer's disease model: pharmacological rescue of cognitive defects. PloS one *6*, e20799.

Chan, C.C., Scoggin, S., Wang, D., Cherry, S., Dembo, T., Greenberg, B., Jin, E.J., Kuey, C., Lopez, A., Mehta, S.Q.*, et al.* (2011). Systematic discovery of Rab GTPases with synaptic functions in Drosophila. Current biology : CB *21*, 1704-1715.

Chan, D., Fox, N.C., Scahill, R.I., Crum, W.R., Whitwell, J.L., Leschziner, G., Rossor, A.M., Stevens, J.M., Cipolotti, L., and Rossor, M.N. (2001). Patterns of temporal lobe atrophy in semantic dementia and Alzheimer's disease. Annals of neurology *49*, 433-442.

Chang, Y.Y., Juhasz, G., Goraksha-Hicks, P., Arsham, A.M., Mallin, D.R., Muller, L.K., and Neufeld, T.P. (2009). Nutrient-dependent regulation of autophagy through the target of rapamycin pathway. Biochemical Society transactions *37*, 232-236.

Chao, C.C., Hu, S., Frey, W.H., 2nd, Ala, T.A., Tourtellotte, W.W., and Peterson, P.K. (1994). Transforming growth factor beta in Alzheimer's disease. Clinical and diagnostic laboratory immunology *1*, 109-110.

Charron, F., and Tessier-Lavigne, M. (2007). The Hedgehog, TGF-beta/BMP and Wnt families of morphogens in axon guidance. Advances in experimental medicine and biology *621*, 116-133.

Chauvire, V., Even, C., Thuile, J., Rouillon, F., and Guelfi, J.D. (2007). [Frontotemporal dementia: a review]. L'Encephale *33*, 933-940.

Chavrier, P., Gorvel, J.P., Stelzer, E., Simons, K., Gruenberg, J., and Zerial, M. (1991). Hypervariable C-terminal domain of rab proteins acts as a targeting signal. Nature *353*, 769-772.

Chen, B., Retzlaff, M., Roos, T., and Frydman, J. (2011). Cellular strategies of protein quality control. Cold Spring Harbor perspectives in biology *3*, a004374.

Chen, D., and Zhong, Q. (2012). A tethering coherent protein in autophagosome maturation. Autophagy *8*, 985-986.

Chen, S., Liang, M.C., Chia, J.N., Ngsee, J.K., and Ting, A.E. (2001). Rab8b and its interacting partner TRIP8b are involved in regulated secretion in AtT20 cells. The Journal of biological chemistry *276*, 13209-13216.

Chen, Y.G. (2009). Endocytic regulation of TGF-beta signaling. Cell research *19*, 58-70.

Chevallier, J., Chamoun, Z., Jiang, G., Prestwich, G., Sakai, N., Matile, S., Parton, R.G., and Gruenberg, J. (2008). Lysobisphosphatidic acid controls endosomal cholesterol levels. The Journal of biological chemistry *283*, 27871-27880.

Chiba, S., Amagai, Y., Homma, Y., Fukuda, M., and Mizuno, K. (2013). NDR2-mediated Rabin8 phosphorylation is crucial for ciliogenesis by switching binding specificity from phosphatidylserine to Sec15. The EMBO journal *32*, 874-885.

Chintapalli, V.R., Wang, J., and Dow, J.A. (2007). Using FlyAtlas to identify better Drosophila melanogaster models of human disease. Nature genetics *39*, 715-720.

Cho, D.H., Nakamura, T., Fang, J., Cieplak, P., Godzik, A., Gu, Z., and Lipton, S.A. (2009). S-nitrosylation of Drp1 mediates beta-amyloid-related mitochondrial fission and neuronal injury. Science *324*, 102-105.

Choudhury, A., Sharma, D.K., Marks, D.L., and Pagano, R.E. (2004). Elevated endosomal cholesterol levels in Niemann-Pick cells inhibit rab4 and perturb membrane recycling. Molecular biology of the cell *15*, 4500-4511.

Choudhury, R., Diao, A., Zhang, F., Eisenberg, E., Saint-Pol, A., Williams, C., Konstantakopoulos, A., Lucocq, J., Johannes, L., Rabouille, C*., et al.* (2005). Lowe syndrome protein OCRL1 interacts with clathrin and regulates protein trafficking between endosomes and the trans-Golgi network. Molecular biology of the cell *16*, 3467-3479.

Chow, T.W., Miller, B.L., Hayashi, V.N., and Geschwind, D.H. (1999a). Inheritance of frontotemporal dementia. Archives of neurology *56*, 817-822.

Chung, W.S., and Barres, B.A. (2009). Selective remodeling: refining neural connectivity at the neuromuscular junction. PLoS biology *7*, e1000185.

Clarke, G.L., Chen, J., and Nishimune, H. (2012). Presynaptic Active Zone Density during Development and Synaptic Plasticity. Frontiers in molecular neuroscience *5*, 12.

Collins, C.A., and DiAntonio, A. (2007). Synaptic development: insights from Drosophila. Current opinion in neurobiology *17*, 35-42.

Collins, C.A., Wairkar, Y.P., Johnson, S.L., and DiAntonio, A. (2006). Highwire restrains synaptic growth by attenuating a MAP kinase signal. Neuron *51*, 57-69.

Colodner, K.J., and Feany, M.B. (2010). Glial fibrillary tangles and JAK/STAT-mediated glial and neuronal cell death in a Drosophila model of glial tauopathy. The Journal of neuroscience : the official journal of the Society for Neuroscience *30*, 16102-16113.

Constam, D.B., Schmid, P., Aguzzi, A., Schachner, M., and Fontana, A. (1994). Transient production of TGF-beta 2 by postnatal cerebellar neurons and its effect on neuroblast proliferation. The European journal of neuroscience *6*, 766-778.

Coon, B.G., Hernandez, V., Madhivanan, K., Mukherjee, D., Hanna, C.B., Barinaga-Rementeria Ramirez, I., Lowe, M., Beales, P.L., and Aguilar, R.C. (2012). The Lowe syndrome protein OCRL1 is involved in primary cilia assembly. Human molecular genetics *21*, 1835-1847.

Cooper, A.A., Gitler, A.D., Cashikar, A., Haynes, C.M., Hill, K.J., Bhullar, B., Liu, K., Xu, K., Strathearn, K.E., Liu, F.*, et al.* (2006). Alpha-synuclein blocks ER-Golgi traffic and Rab1 rescues neuron loss in Parkinson's models. Science *313*, 324-328.

Cooper, J.L., Greene, E.A., Till, B.J., Codomo, C.A., Wakimoto, B.T., and Henikoff, S. (2008). Retention of induced mutations in a Drosophila reverse-genetic resource. Genetics *180*, 661-667.

Corboy, M.J., Thomas, P.J., and Wigley, W.C. (2005). Aggresome formation. Methods in molecular biology *301*, 305-327.

Criollo, A., Niso-Santano, M., Malik, S.A., Michaud, M., Morselli, E., Marino, G., Lachkar, S., Arkhipenko, A.V., Harper, F., Pierron, G.*, et al.* (2011). Inhibition of autophagy by TAB2 and TAB3. The EMBO journal *30*, 4908-4920.

Cruts, M., Gijselinck, I., van der Zee, J., Engelborghs, S., Wils, H., Pirici, D., Rademakers, R., Vandenberghe, R., Dermaut, B., Martin, J.J.*, et al.* (2006). Null mutations in progranulin cause ubiquitin-positive frontotemporal dementia linked to chromosome 17q21. Nature *442*, 920-924.

Currie, D.A., Truman, J.W., and Burden, S.J. (1995). Drosophila glutamate receptor RNA expression in embryonic and larval muscle fibers. Developmental dynamics : an official publication of the American Association of Anatomists *203*, 311-316.

D'Adamo, P., Menegon, A., Lo Nigro, C., Grasso, M., Gulisano, M., Tamanini, F., Bienvenu, T., Gedeon, A.K., Oostra, B., Wu, S.K.*, et al.* (1998). Mutations in GDI1 are responsible for X-linked non-specific mental retardation. Nature genetics *19*, 134-139.

Dai, P., Akimaru, H., and Ishii, S. (2003). A hedgehog-responsive region in the Drosophila wing disc is defined by debra-mediated ubiquitination and lysosomal degradation of Ci. Developmental cell *4*, 917-928.

Dalfo, E., Barrachina, M., Rosa, J.L., Ambrosio, S., and Ferrer, I. (2004). Abnormal alpha-synuclein interactions with rab3a and rabphilin in diffuse Lewy body disease. Neurobiology of disease *16*, 92-97.

De Luca, A., Progida, C., Spinosa, M.R., Alifano, P., and Bucci, C. (2008). Characterization of the Rab7K157N mutant protein associated with Charcot-Marie-Tooth type 2B. Biochemical and biophysical research communications *372*, 283-287.

DeJesus-Hernandez, M., Mackenzie, I.R., Boeve, B.F., Boxer, A.L., Baker, M., Rutherford, N.J., Nicholson, A.M., Finch, N.A., Flynn, H., Adamson, J.*, et al.* (2011). Expanded GGGGCC hexanucleotide repeat in noncoding region of C9ORF72 causes chromosome 9p-linked FTD and ALS. Neuron *72*, 245-256.

Del Bo, R., Tiloca, C., Pensato, V., Corrado, L., Ratti, A., Ticozzi, N., Corti, S., Castellotti, B., Mazzini, L., Soraru, G.*, et al.* (2011). Novel optineurin mutations in patients with familial and sporadic amyotrophic lateral sclerosis. Journal of neurology, neurosurgery, and psychiatry *82*, 1239-1243.

del Toro, D., Alberch, J., Lazaro-Dieguez, F., Martin-Ibanez, R., Xifro, X., Egea, G., and Canals, J.M. (2009). Mutant huntingtin impairs post-Golgi trafficking to lysosomes by delocalizing optineurin/Rab8 complex from the Golgi apparatus. Molecular biology of the cell *20*, 1478-1492.

Derijard, B., Hibi, M., Wu, I.H., Barrett, T., Su, B., Deng, T., Karin, M., and Davis, R.J. (1994). JNK1: a protein kinase stimulated by UV light and Ha-Ras that binds and phosphorylates the c-Jun activation domain. Cell *76*, 1025-1037.

Derynck, R., and Zhang, Y.E. (2003). Smad-dependent and Smad-independent pathways in TGF-beta family signalling. Nature *425*, 577-584.

Di Guglielmo, G.M., Le Roy, C., Goodfellow, A.F., and Wrana, J.L. (2003). Distinct endocytic pathways regulate TGF-beta receptor signalling and turnover. Nature cell biology *5*, 410-421.

DiAntonio, A., Petersen, S.A., Heckmann, M., and Goodman, C.S. (1999). Glutamate receptor expression regulates quantal size and quantal content at the Drosophila neuromuscular junction. The Journal of neuroscience : the official journal of the Society for Neuroscience *19*, 3023-3032.

Dias-Santagata, D., Fulga, T.A., Duttaroy, A., and Feany, M.B. (2007). Oxidative stress mediates tau-induced neurodegeneration in Drosophila. The Journal of clinical investigation *117*, 236-245.

Dickman, D.K., Lu, Z., Meinertzhagen, I.A., and Schwarz, T.L. (2006). Altered synaptic development and active zone spacing in endocytosis mutants. Current biology : CB *16*, 591-598.

Diehl-Schmid, J., Bornschein, S., Pohl, C., Forstl, H., Kurz, A., and Jahn, T. (2011). Cognitive decline in the behavioral variant of frontotemporal dementia. International psychogeriatrics / IPA *23*, 230-237.

Diekmann, Y., Seixas, E., Gouw, M., Tavares-Cadete, F., Seabra, M.C., and Pereira-Leal, J.B. (2011). Thousands of rab GTPases for the cell biologist. PLoS computational biology *7*, e1002217.

Dietzl, G., Chen, D., Schnorrer, F., Su, K.C., Barinova, Y., Fellner, M., Gasser, B., Kinsey, K., Oppel, S., Scheiblauer, S.*, et al.* (2007). A genome-wide transgenic RNAi library for conditional gene inactivation in Drosophila. Nature *448*, 151-156.

Dirac-Svejstrup, A.B., Sumizawa, T., and Pfeffer, S.R. (1997). Identification of a GDI displacement factor that releases endosomal Rab GTPases from Rab-GDI. The EMBO journal *16*, 465-472.

Dong, C., Yang, L., Zhang, X., Gu, H., Lam, M.L., Claycomb, W.C., Xia, H., and Wu, G. (2010). Rab8 interacts with distinct motifs in alpha2B- and beta2-adrenergic receptors and differentially modulates their transport. The Journal of biological chemistry *285*, 20369-20380.

Dressman, M.A., Olivos-Glander, I.M., Nussbaum, R.L., and Suchy, S.F. (2000). Ocrl1, a PtdIns(4,5)P(2) 5-phosphatase, is localized to the trans-Golgi network of fibroblasts and epithelial cells. The journal of histochemistry and cytochemistry : official journal of the Histochemistry Society *48*, 179-190.

Eaton, B.A., Fetter, R.D., and Davis, G.W. (2002). Dynactin is necessary for synapse stabilization. Neuron *34*, 729-741.

Eggenschwiler, J.T., Espinoza, E., and Anderson, K.V. (2001). Rab23 is an essential negative regulator of the mouse Sonic hedgehog signalling pathway. Nature *412*, 194-198.

Elia, N., Sougrat, R., Spurlin, T.A., Hurley, J.H., and Lippincott-Schwartz, J. (2011). Dynamics of endosomal sorting complex required for transport (ESCRT) machinery during cytokinesis and its role in abscission. Proceedings of the National Academy of Sciences of the United States of America *108*, 4846-4851.

Elliott, D.A., and Brand, A.H. (2008). The GAL4 system : a versatile system for the expression of genes. Methods in molecular biology *420*, 79-95.

Engel, M.E., McDonnell, M.A., Law, B.K., and Moses, H.L. (1999). Interdependent SMAD and JNK signaling in transforming growth factor-beta-mediated transcription. The Journal of biological chemistry *274*, 37413-37420.

Esseltine, J.L., Ribeiro, F.M., and Ferguson, S.S. (2012). Rab8 modulates metabotropic glutamate receptor subtype 1 intracellular trafficking and signaling in a protein kinase C-dependent manner. The Journal of neuroscience : the official journal of the Society for Neuroscience *32*, 16933-16942a.

Etter, P.D., Narayanan, R., Navratilova, Z., Patel, C., Bohmann, D., Jasper, H., and Ramaswami, M. (2005). Synaptic and genomic responses to JNK and AP-1 signaling in Drosophila neurons. BMC neuroscience *6*, 39.

Fabrikant, G., Lata, S., Riches, J., Briggs, J., Weissenhorn, W., and Kozlov, M. (2009). Computational model of membrane fission catalyzed by ESCRT-III. PLoS computational biology *5*.

Featherstone, D.E., Rushton, E., and Broadie, K. (2002). Developmental regulation of glutamate receptor field size by nonvesicular glutamate release. Nature neuroscience *5*, 141-146.

Featherstone, D.E., Rushton, E., Rohrbough, J., Liebl, F., Karr, J., Sheng, Q., Rodesch, C.K., and Broadie, K. (2005). An essential Drosophila glutamate receptor subunit that functions in both central neuropil and neuromuscular junction. The Journal of neuroscience : the official journal of the Society for Neuroscience *25*, 3199-3208.

Fernandes, C., and Rao, Y. (2011). Genome-wide screen for modifiers of Parkinson's disease genes in Drosophila. Molecular brain *4*, 17.

Filimonenko, M., Stuffers, S., Raiborg, C., Yamamoto, A., Malerod, L., Fisher, E.M., Isaacs, A., Brech, A., Stenmark, H., and Simonsen, A. (2007a). Functional multivesicular bodies are required for autophagic clearance of protein aggregates associated with neurodegenerative disease. The Journal of cell biology *179*, 485-500.

Fisher, R.D., Chung, H.Y., Zhai, Q., Robinson, H., Sundquist, W.I., and Hill, C.P. (2007). Structural and biochemical studies of ALIX/AIP1 and its role in retrovirus budding. Cell *128*, 841-852.

Flanders, K.C., Lippa, C.F., Smith, T.W., Pollen, D.A., and Sporn, M.B. (1995). Altered expression of transforming growth factor-beta in Alzheimer's disease. Neurology *45*, 1561-1569.

Follit, J.A., Li, L., Vucica, Y., and Pazour, G.J. (2010). The cytoplasmic tail of fibrocystin contains a ciliary targeting sequence. The Journal of cell biology *188*, 21-28.

Fraldi, A., Annunziata, F., Lombardi, A., Kaiser, H.J., Medina, D.L., Spampanato, C., Fedele, A.O., Polishchuk, R., Sorrentino, N.C., Simons, K.*, et al.* (2010). Lysosomal fusion and SNARE function are impaired by cholesterol accumulation in lysosomal storage disorders. The EMBO journal *29*, 3607-3620.

Fuentealba, L.C., Eivers, E., Ikeda, A., Hurtado, C., Kuroda, H., Pera, E.M., and De Robertis, E.M. (2007). Integrating patterning signals: Wnt/GSK3 regulates the duration of the BMP/Smad1 signal. Cell *131*, 980-993.

Fuentes-Medel, Y., Ashley, J., Barria, R., Maloney, R., Freeman, M., and Budnik, V. (2012). Integration of a retrograde signal during synapse formation by glia-secreted TGF-beta ligand. Current biology : CB *22*, 1831-1838.

Fuentes-Medel, Y., Logan, M.A., Ashley, J., Ataman, B., Budnik, V., and Freeman, M.R. (2009). Glia and muscle sculpt neuromuscular arbors by engulfing destabilized synaptic boutons and shed presynaptic debris. PLoS biology *7*, e1000184.

Fujita, N., Itoh, T., Omori, H., Fukuda, M., Noda, T., and Yoshimori, T. (2008). The Atg16L complex specifies the site of LC3 lipidation for membrane biogenesis in autophagy. Molecular biology of the cell *19*, 2092-2100.

Fukui, T. (2009). [Clinical types of FTLD: progressive nonfluent aphasia; comparative discussions on the associated clinical presentations]. Brain Nerve *61*, 1252-1258.

Galimberti, D., and Scarpini, E. (2010). Genetics and biology of Alzheimer's disease and frontotemporal lobar degeneration. Int J Clin Exp Med *3*, 129-143.

Ganley, I.G., and Pfeffer, S.R. (2006). Cholesterol accumulation sequesters Rab9 and disrupts late endosome function in NPC1-deficient cells. The Journal of biological chemistry *281*, 17890-17899.

Gerges, N.Z., Backos, D.S., and Esteban, J.A. (2004a). Local control of AMPA receptor trafficking at the postsynaptic terminal by a small GTPase of the Rab family. The Journal of biological chemistry *279*, 43870-43878.

Ginsberg, S.D., Mufson, E.J., Alldred, M.J., Counts, S.E., Wuu, J., Nixon, R.A., and Che, S. (2011). Upregulation of select rab GTPases in cholinergic basal forebrain neurons in mild cognitive impairment and Alzheimer's disease. Journal of chemical neuroanatomy *42*, 102-110.

Ginsberg, S.D., Mufson, E.J., Counts, S.E., Wuu, J., Alldred, M.J., Nixon, R.A., and Che, S. (2010). Regional selectivity of rab5 and rab7 protein upregulation in mild cognitive impairment and Alzheimer's disease. Journal of Alzheimer's disease : JAD *22*, 631-639.

Gitler, A.D., Bevis, B.J., Shorter, J., Strathearn, K.E., Hamamichi, S., Su, L.J., Caldwell, K.A., Caldwell, G.A., Rochet, J.C., McCaffery, J.M.*, et al.* (2008). The Parkinson's disease protein alpha-synuclein disrupts cellular Rab homeostasis. Proceedings of the National Academy of Sciences of the United States of America *105*, 145-150.

Gjorgjieva, J., Berni, J., Evers, J.F., and Eglen, S.J. (2013). Neural circuits for peristaltic wave propagation in crawling Drosophila larvae: analysis and modeling. Frontiers in computational neuroscience *7*, 24.

Glodowski, D.R., Chen, C.C., Schaefer, H., Grant, B.D., and Rongo, C. (2007). RAB-10 regulates glutamate receptor recycling in a cholesterol-dependent endocytosis pathway. Molecular biology of the cell *18*, 4387-4396.

Goedert, M., Ghetti, B., and Spillantini, M.G. (2012). Frontotemporal dementia: implications for understanding Alzheimer disease. Cold Spring Harbor perspectives in medicine *2*, a006254.

Goldman, J.S., Farmer, J.M., Wood, E.M., Johnson, J.K., Boxer, A., Neuhaus, J., Lomen-Hoerth, C., Wilhelmsen, K.C., Lee, V.M., Grossman, M.*, et al.* (2005). Comparison of family histories in FTLD subtypes and related tauopathies. Neurology *65*, 1817-1819.

Gomes, F.C., Sousa Vde, O., and Romao, L. (2005). Emerging roles for TGF-beta1 in nervous system development. International journal of developmental neuroscience : the official journal of the International Society for Developmental Neuroscience *23*, 413-424.

Gramates, L.S., and Budnik, V. (1999). Assembly and maturation of the Drosophila larval neuromuscular junction. International review of neurobiology *43*, 93-117.

Grant, B.D., and Donaldson, J.G. (2009). Pathways and mechanisms of endocytic recycling. Nature reviews Molecular cell biology *10*, 597-608.

Grigoriev, I., Yu, K.L., Martinez-Sanchez, E., Serra-Marques, A., Smal, I., Meijering, E., Demmers, J., Peranen, J., Pasterkamp, R.J., van der Sluijs, P.*, et al.* (2011a). Rab6, Rab8, and MICAL3 cooperate in controlling docking and fusion of exocytotic carriers. Current biology : CB *21*, 967-974.

Grosshans, B.L., Ortiz, D., and Novick, P. (2006). Rabs and their effectors: achieving specificity in membrane traffic. Proceedings of the National Academy of Sciences of the United States of America *103*, 11821-11827.

Gruenberg, J., and Stenmark, H. (2004a). The biogenesis of multivesicular endosomes. Nature reviews Molecular cell biology *5*, 317-323.

Gruendler, C., Lin, Y., Farley, J., and Wang, T. (2001). Proteasomal degradation of Smad1 induced by bone morphogenetic proteins. The Journal of biological chemistry *276*, 46533-46543.

Guillaumot, P., Luquain, C., Malek, M., Huber, A.L., Brugiere, S., Garin, J., Grunwald, D., Regnier, D., Petrilli, V., Lefai, E.*, et al.* (2010). Pdro, a protein associated with late endosomes and lysosomes and implicated in cellular cholesterol homeostasis. PloS one *5*, e10977.

Guo, Y., Chang, C., Huang, R., Liu, B., Bao, L., and Liu, W. (2012). AP1 is essential for generation of autophagosomes from the trans-Golgi network. Journal of cell science *125*, 1706-1715.

Guruharsha, K.G., Rual, J.F., Zhai, B., Mintseris, J., Vaidya, P., Vaidya, N., Beekman, C., Wong, C., Rhee, D.Y., Cenaj, O.*, et al.* (2011). A protein complex network of Drosophila melanogaster. Cell *147*, 690-703.

Halazonetis, T.D., Georgopoulos, K., Greenberg, M.E., and Leder, P. (1988). c-Jun dimerizes with itself and with c-Fos, forming complexes of different DNA binding affinities. Cell *55*, 917-924.

Hammond, S.M., Caudy, A.A., and Hannon, G.J. (2001). Post-transcriptional gene silencing by double-stranded RNA. Nature reviews Genetics *2*, 110-119.

Han, D.D., Stein, D., and Stevens, L.M. (2000). Investigating the function of follicular subpopulations during Drosophila oogenesis through hormone-dependent enhancer-targeted cell ablation. Development *127*, 573-583.

Han, J.H., Ryu, H.H., Jun, M.H., Jang, D.J., and Lee, J.A. (2012). The functional analysis of the CHMP2B missense mutation associated with neurodegenerative diseases in the endo-lysosomal pathway. Biochemical and biophysical research communications *421*, 544-549.

Hanson, P.I., Roth, R., Lin, Y., and Heuser, J.E. (2008). Plasma membrane deformation by circular arrays of ESCRT-III protein filaments. The Journal of cell biology *180*, 389-402.

Hattula, K., Furuhjelm, J., Tikkanen, J., Tanhuanpaa, K., Laakkonen, P., and Peranen, J. (2006). Characterization of the Rab8-specific membrane traffic route linked to protrusion formation. Journal of cell science *119*, 4866-4877.

Hattula, K., and Peranen, J. (2000). FIP-2, a coiled-coil protein, links Huntingtin to Rab8 and modulates cellular morphogenesis. Current biology : CB *10*, 1603-1606.

Hayes, S., Chawla, A., and Corvera, S. (2002). TGF beta receptor internalization into EEA1-enriched early endosomes: role in signaling to Smad2. The Journal of cell biology *158*, 1239-1249.

Heckscher, E.S., Fetter, R.D., Marek, K.W., Albin, S.D., and Davis, G.W. (2007). NF-kappaB, IkappaB, and IRAK control glutamate receptor density at the Drosophila NMJ. Neuron *55*, 859-873.

Heckscher, E.S., Lockery, S.R., and Doe, C.Q. (2012). Characterization of Drosophila larval crawling at the level of organism, segment, and somatic body wall musculature. The Journal of neuroscience : the official journal of the Society for Neuroscience *32*, 12460-12471.

Heidrych, P., Zimmermann, U., Bress, A., Pusch, C.M., Ruth, P., Pfister, M., Knipper, M., and Blin, N. (2008). Rab8b GTPase, a protein transport regulator, is an interacting partner of otoferlin, defective in a human autosomal recessive deafness form. Human molecular genetics *17*, 3814-3821.

Henne, W.M., Buchkovich, N.J., and Emr, S.D. (2011). The ESCRT pathway. Developmental cell *21*, 77-91.

Henne, W.M., Stenmark, H., and Emr, S.D. (2013). Molecular Mechanisms of the Membrane Sculpting ESCRT Pathway. Cold Spring Harbor perspectives in biology *5*.

Henry, L., and Sheff, D.R. (2008). Rab8 regulates basolateral secretory, but not recycling, traffic at the recycling endosome. Molecular biology of the cell *19*, 2059-2068.

Herrero-Martin, G., Hoyer-Hansen, M., Garcia-Garcia, C., Fumarola, C., Farkas, T., Lopez-Rivas, A., and Jaattela, M. (2009). TAK1 activates AMPK-dependent cytoprotective autophagy in TRAIL-treated epithelial cells. The EMBO journal *28*, 677-685.

Heupel, K., Sargsyan, V., Plomp, J.J., Rickmann, M., Varoqueaux, F., Zhang, W., and Krieglstein, K. (2008). Loss of transforming growth factor-beta 2 leads to impairment of central synapse function. Neural development *3*, 25.

Hibi, M., Lin, A., Smeal, T., Minden, A., and Karin, M. (1993). Identification of an oncoprotein- and UV-responsive protein kinase that binds and potentiates the c-Jun activation domain. Genes & development *7*, 2135-2148.

Hirth, F. (2010). Drosophila melanogaster in the study of human neurodegeneration. CNS & neurological disorders drug targets *9*, 504-523.

Hoang, B., and Chiba, A. (2001). Single-cell analysis of Drosophila larval neuromuscular synapses. Developmental biology *229*, 55-70.

Holm, I.E., Englund, E., Mackenzie, I.R., Johannsen, P., and Isaacs, A.M. (2007). A reassessment of the neuropathology of frontotemporal dementia linked to chromosome 3. Journal of neuropathology and experimental neurology *66*, 884-891.

Holm, I.E., Isaacs, A.M., and Mackenzie, I.R. (2009). Absence of FUS-immunoreactive pathology in frontotemporal dementia linked to chromosome 3 (FTD-3) caused by mutation in the CHMP2B gene. Acta neuropathologica *118*, 719-720.

Horgan, C.P., Hanscom, S.R., Jolly, R.S., Futter, C.E., and McCaffrey, M.W. (2010). Rab11-FIP3 links the Rab11 GTPase and cytoplasmic dynein to mediate transport to the endosomal-recycling compartment. Journal of cell science *123*, 181-191.

Hou, X., Hagemann, N., Schoebel, S., Blankenfeldt, W., Goody, R.S., Erdmann, K.S., and Itzen, A. (2011). A structural basis for Lowe syndrome caused by mutations in the Rab-binding domain of OCRL1. The EMBO journal *30*, 1659-1670.

Hsiao, Y.C., Tong, Z.J., Westfall, J.E., Ault, J.G., Page-McCaw, P.S., and Ferland, R.J. (2009). Ahi1, whose human ortholog is mutated in Joubert syndrome, is required for Rab8a localization, ciliogenesis and vesicle trafficking. Human molecular genetics *18*, 3926-3941.

Huang, X., Suyama, K., Buchanan, J., Zhu, A.J., and Scott, M.P. (2005). A Drosophila model of the Niemann-Pick type C lysosome storage disease: dnpc1a is required for molting and sterol homeostasis. Development *132*, 5115-5124.

Huber, L.A., Dupree, P., and Dotti, C.G. (1995a). A deficiency of the small GTPase rab8 inhibits membrane traffic in developing neurons. Molecular and cellular biology *15*, 918-924.

Huber, L.A., Pimplikar, S., Parton, R.G., Virta, H., Zerial, M., and Simons, K. (1993). Rab8, a small GTPase involved in vesicular traffic between the TGN and the basolateral plasma membrane. The Journal of cell biology *123*, 35-45.

Hughes, C.L., and Thomas, J.B. (2007). A sensory feedback circuit coordinates muscle activity in Drosophila. Molecular and cellular neurosciences *35*, 383-396.

Hutagalung, A.H., and Novick, P.J. (2011). Role of Rab GTPases in membrane traffic and cell physiology. Physiological reviews *91*, 119-149.

Hutton, M., Lendon, C.L., Rizzu, P., Baker, M., Froelich, S., Houlden, H., Pickering-Brown, S., Chakraverty, S., Isaacs, A., Grover, A.*, et al.* (1998). Association of missense and 5'-splice-site mutations in tau with the inherited dementia FTDP-17. Nature *393*, 702-705.

Hyvola, N., Diao, A., McKenzie, E., Skippen, A., Cockcroft, S., and Lowe, M. (2006). Membrane targeting and activation of the Lowe syndrome protein OCRL1 by rab GTPases. The EMBO journal *25*, 3750-3761.

Ichikawa, H., and Kawamura, M. (2009). [Symptoms of frontotemporal dementia]. Brain Nerve *61*, 1227-1235.

Ilzecka, J., Stelmasiak, Z., and Dobosz, B. (2002). Transforming growth factor-Beta 1 (tgf-Beta 1) in patients with amyotrophic lateral sclerosis. Cytokine *20*, 239-243.

Imlach, W., and McCabe, B.D. (2009). Electrophysiological methods for recording synaptic potentials from the NMJ of Drosophila larvae. Journal of visualized experiments : JoVE.

Irie, T., Muta, T., and Takeshige, K. (2000). TAK1 mediates an activation signal from toll-like receptor(s) to nuclear factor-kappaB in lipopolysaccharide-stimulated macrophages. FEBS letters *467*, 160-164.

Isaacs, A.M., Johannsen, P., Holm, I., and Nielsen, J.E. (2011). Frontotemporal dementia caused by CHMP2B mutations. Curr Alzheimer Res *8*, 246-251.

Itoh, F., Divecha, N., Brocks, L., Oomen, L., Janssen, H., Calafat, J., Itoh, S., and Dijke Pt, P. (2002). The FYVE domain in Smad anchor for receptor activation (SARA) is sufficient for localization of SARA in early endosomes and regulates TGF-beta/Smad signalling. Genes to cells : devoted to molecular & cellular mechanisms *7*, 321-331.

Jackson, G.R., Wiedau-Pazos, M., Sang, T.K., Wagle, N., Brown, C.A., Massachi, S., and Geschwind, D.H. (2002). Human wild-type tau interacts with wingless pathway components and produces neurofibrillary pathology in Drosophila. Neuron *34*, 509-519.

Jan, L.Y., and Jan, Y.N. (1982). Antibodies to horseradish peroxidase as specific neuronal markers in Drosophila and in grasshopper embryos. Proceedings of the National Academy of Sciences of the United States of America *79*, 2700-2704.

Janssen, J.C., Schott, J.M., Cipolotti, L., Fox, N.C., Scahill, R.I., Josephs, K.A., Stevens, J.M., and Rossor, M.N. (2005). Mapping the onset and progression of atrophy in familial frontotemporal lobar degeneration. Journal of neurology, neurosurgery, and psychiatry *76*, 162-168.

Jenkins, D., Seelow, D., Jehee, F.S., Perlyn, C.A., Alonso, L.G., Bueno, D.F., Donnai, D., Josifova, D., Mathijssen, I.M., Morton, J.E.*, et al.* (2007). RAB23 mutations in Carpenter syndrome imply an unexpected role for hedgehog signaling in cranial-suture development and obesity. American journal of human genetics *80*, 1162-1170.

Jin, S., Pan, L., Liu, Z., Wang, Q., Xu, Z., and Zhang, Y.Q. (2009). Drosophila Tubulin-specific chaperone E functions at neuromuscular synapses and is required for microtubule network formation. Development *136*, 1571-1581.

Joberty, G., Tavitian, A., and Zahraoui, A. (1993). Isoprenylation of Rab proteins possessing a C-terminal CaaX motif. FEBS letters *330*, 323-328.

Johansen, J., Halpern, M.E., Johansen, K.M., and Keshishian, H. (1989). Stereotypic morphology of glutamatergic synapses on identified muscle cells of Drosophila larvae. The Journal of neuroscience : the official journal of the Society for Neuroscience *9*, 710-725.

Josephs, K.A., Hodges, J.R., Snowden, J.S., Mackenzie, I.R., Neumann, M., Mann, D.M., and Dickson, D.W. (2011). Neuropathological background of phenotypical variability in frontotemporal dementia. Acta neuropathologica *122*, 137-153.

Josephs, K.A., Petersen, R.C., Knopman, D.S., Boeve, B.F., Whitwell, J.L., Duffy, J.R., Parisi, J.E., and Dickson, D.W. (2006). Clinicopathologic analysis of frontotemporal and corticobasal degenerations and PSP. Neurology *66*, 41-48.

Josephs, K.A., Whitwell, J.L., Parisi, J.E., Petersen, R.C., Boeve, B.F., Jack, C.R., Jr., and Dickson, D.W. (2010). Caudate atrophy on MRI is a characteristic feature of FTLD-FUS. European journal of neurology : the official journal of the European Federation of Neurological Societies *17*, 969-975.

Jung, J., and Bonini, N. (2007). CREB-binding protein modulates repeat instability in a Drosophila model for polyQ disease. Science *315*, 1857-1859.

Kametani, F., Usami, M., Tanaka, K., Kume, H., and Mori, H. (2004a). Mutant presenilin (A260V) affects Rab8 in PC12D cell. Neurochemistry international *44*, 313-320.

Kane, M., and Cook, L. (2013). Dementia 2013: The hidden voice of loneliness. Alzheimer's Society.

Karin, M. (1996). The regulation of AP-1 activity by mitogen-activated protein kinases. Philosophical transactions of the Royal Society of London Series B, Biological sciences *351*, 127-134.

Kavsak, P., Rasmussen, R.K., Causing, C.G., Bonni, S., Zhu, H., Thomsen, G.H., and Wrana, J.L. (2000). Smad7 binds to Smurf2 to form an E3 ubiquitin ligase that targets the TGF beta receptor for degradation. Molecular cell *6*, 1365-1375.

Kelleher, R.J., 3rd, Govindarajan, A., Jung, H.Y., Kang, H., and Tonegawa, S. (2004). Translational control by MAPK signaling in long-term synaptic plasticity and memory. Cell *116*, 467-479.

Keshishian, H., Broadie, K., Chiba, A., and Bate, M. (1996). The drosophila neuromuscular junction: a model system for studying synaptic development and function. Annual review of neuroscience *19*, 545-575.

Keshishian, H., Chiba, A., Chang, T.N., Halfon, M.S., Harkins, E.W., Jarecki, J., Wang, L., Anderson, M., Cash, S., Halpern, M.E*., et al.* (1993). Cellular mechanisms governing synaptic development in Drosophila melanogaster. Journal of neurobiology *24*, 757-787.

Khandelwal, P., Prakasam, H.S., Clayton, D.R., Ruiz, W.G., Gallo, L.I., van Roekel, D., Lukianov, S., Peranen, J., Goldenring, J.R., and Apodaca, G. (2013). A Rab11a-Rab8a-Myo5B network promotes stretch-regulated exocytosis in bladder umbrella cells. Molecular biology of the cell *24*, 1007-1019.

Khodosh, R., Augsburger, A., Schwarz, T.L., and Garrity, P.A. (2006). Bchs, a BEACH domain protein, antagonizes Rab11 in synapse morphogenesis and other developmental events. Development *133*, 4655-4665.

Khokhar, A., Chen, N., Yuan, J.P., Li, Y., Landis, G.N., Beaulieu, G., Kaur, H., and Tower, J. (2008). Conditional switches for extracellular matrix patterning in Drosophila melanogaster. Genetics *178*, 1283-1293.

Kim, G.H., Park, E., and Han, J.K. (2005a). The assembly of POSH-JNK regulates Xenopus anterior neural development. Developmental biology *286*, 256-269.

Kim, G.H., Park, E., Kong, Y.Y., and Han, J.K. (2006). Novel function of POSH, a JNK scaffold, as an E3 ubiquitin ligase for the Hrs stability on early endosomes. Cellular signalling *18*, 553-563.

Kim, J., Sitaraman, S., Hierro, A., Beach, B.M., Odorizzi, G., and Hurley, J.H. (2005b). Structural basis for endosomal targeting by the Bro1 domain. Developmental cell *8*, 937-947.

Kim, S., Wairkar, Y.P., Daniels, R.W., and DiAntonio, A. (2010). The novel endosomal membrane protein Ema interacts with the class C Vps-HOPS complex to promote endosomal maturation. The Journal of cell biology *188*, 717-734.

Kim, S.I., Kwak, J.H., Na, H.J., Kim, J.K., Ding, Y., and Choi, M.E. (2009). Transforming growth factor-beta (TGF-beta1) activates TAK1 via TAB1-mediated autophosphorylation, independent of TGF-beta receptor kinase activity in mesangial cells. The Journal of biological chemistry *284*, 22285-22296.

Kim, Y.J., Bao, H., Bonanno, L., Zhang, B., and Serpe, M. (2012). Drosophila Neto is essential for clustering glutamate receptors at the neuromuscular junction. Genes & development *26*, 974-987.

Knapp, M. (2007). Dementia UK - The full report. London School of Economics, King's College London.

Knodler, A., Feng, S., Zhang, J., Zhang, X., Das, A., Peranen, J., and Guo, W. (2010). Coordination of Rab8 and Rab11 in primary ciliogenesis. Proceedings of the National Academy of Sciences of the United States of America *107*, 6346-6351.

Knox, S., Ge, H., Dimitroff, B.D., Ren, Y., Howe, K.A., Arsham, A.M., Easterday, M.C., Neufeld, T.P., O'Connor, M.B., and Selleck, S.B. (2007). Mechanisms of TSC-mediated control of synapse assembly and axon guidance. PloS one *2*, e375.

Kobayashi, T., Stang, E., Fang, K.S., de Moerloose, P., Parton, R.G., and Gruenberg, J. (1998). A lipid associated with the antiphospholipid syndrome regulates endosome structure and function. Nature *392*, 193-197.

Kobuna, H., Inoue, T., Shibata, M., Gengyo-Ando, K., Yamamoto, A., Mitani, S., and Arai, H. (2010). Multivesicular body formation requires OSBP-related proteins and cholesterol. PLoS genetics *6*.

Koch, A., Thiemann, M., Grabenbauer, M., Yoon, Y., McNiven, M.A., and Schrader, M. (2003). Dynamin-like protein 1 is involved in peroxisomal fission. The Journal of biological chemistry *278*, 8597-8605.

Koch, D., Spiwoks-Becker, I., Sabanov, V., Sinning, A., Dugladze, T., Stellmacher, A., Ahuja, R., Grimm, J., Schuler, S., Muller, A.*, et al.* (2011). Proper synaptic vesicle formation and neuronal network activity critically rely on syndapin I. The EMBO journal *30*, 4955-4969.

Kohsaka, H., Takasu, E., and Nose, A. (2007). In vivo induction of postsynaptic molecular assembly by the cell adhesion molecule Fasciclin2. The Journal of cell biology *179*, 1289-1300.

Koon, A.C., Ashley, J., Barria, R., DasGupta, S., Brain, R., Waddell, S., Alkema, M.J., and Budnik, V. (2011). Autoregulatory and paracrine control of synaptic and behavioral plasticity by octopaminergic signaling. Nature neuroscience *14*, 190-199.

Korolchuk, V.I., Schutz, M.M., Gomez-Llorente, C., Rocha, J., Lansu, N.R., Collins, S.M., Wairkar, Y.P., Robinson, I.M., and O'Kane, C.J. (2007). Drosophila Vps35 function is necessary for normal endocytic trafficking and actin cytoskeleton organisation. Journal of cell science *120*, 4367-4376.

Kottler, B., Lampin-Saint-Amaux, A., Comas, D., Preat, T., and Goguel, V. (2011). Debra, a protein mediating lysosomal degradation, is required for long-term memory in Drosophila. PloS one *6*, e25902.

Kouranti, I., Sachse, M., Arouche, N., Goud, B., and Echard, A. (2006). Rab35 regulates an endocytic recycling pathway essential for the terminal steps of cytokinesis. Current biology : CB *16*, 1719-1725.

Kumar, V., Fricke, R., Bhar, D., Reddy-Alla, S., Krishnan, K.S., Bogdan, S., and Ramaswami, M. (2009). Syndapin promotes formation of a postsynaptic membrane system in Drosophila. Molecular biology of the cell *20*, 2254-2264.

Kyriakakis, P., Tipping, M., Abed, L., and Veraksa, A. (2008). Tandem affinity purification in Drosophila: the advantages of the GS-TAP system. Fly *2*, 229-235.

Lakey, L., Chandaria, K., Quince, C., and Kane, M. (2012). Dementia 2012: A National Challenge. Alzheimer's Society.

Landgraf, M., Bossing, T., Technau, G.M., and Bate, M. (1997). The origin, location, and projections of the embryonic abdominal motorneurons of Drosophila. The Journal of neuroscience : the official journal of the Society for Neuroscience *17*, 9642-9655.

Landgraf, M., Jeffrey, V., Fujioka, M., Jaynes, J.B., and Bate, M. (2003a). Embryonic origins of a motor system: motor dendrites form a myotopic map in Drosophila. PLoS biology *1*, E41.

Landgraf, M., Sanchez-Soriano, N., Technau, G.M., Urban, J., and Prokop, A. (2003b). Charting the Drosophila neuropile: a strategy for the standardised characterisation of genetically amenable neurites. Developmental biology *260*, 207-225.

Landgraf, M., and Thor, S. (2006). Development and structure of motoneurons. International review of neurobiology *75*, 33-53.

Lau, A.S., and Mruk, D.D. (2003). Rab8B GTPase and junction dynamics in the testis. Endocrinology *144*, 1549-1563.

Lauricella, M., Emanuele, S., D'Anneo, A., Calvaruso, G., Vassallo, B., Carlisi, D., Portanova, P., Vento, R., and Tesoriere, G. (2006). JNK and AP-1 mediate apoptosis induced by bortezomib in HepG2 cells via FasL/caspase-8 and mitochondria-dependent pathways. Apoptosis : an international journal on programmed cell death *11*, 607-625.

Lee, J., Giordano, S., and Zhang, J. (2012). Autophagy, mitochondria and oxidative stress: cross-talk and redox signalling. The Biochemical journal *441*, 523-540.

Lee, J.A., Beigneux, A., Ahmad, S.T., Young, S.G., and Gao, F.B. (2007). ESCRT-III dysfunction causes autophagosome accumulation and neurodegeneration. Current biology : CB *17*, 1561-1567.

Lee, J.A., and Gao, F.B. (2008). Roles of ESCRT in autophagy-associated neurodegeneration. Autophagy *4*, 230-232.

Lee, J.A., and Gao, F.B. (2009). Inhibition of autophagy induction delays neuronal cell loss caused by dysfunctional ESCRT-III in frontotemporal dementia. The Journal of neuroscience : the official journal of the Society for Neuroscience *29*, 8506-8511.

Lee, M.H., Lin, S.R., Chang, J.Y., Schultz, L., Heath, J., Hsu, L.J., Kuo, Y.M., Hong, Q., Chiang, M.F., Gong, C.X.*, et al.* (2010). TGF-beta induces TIAF1 self-aggregation via

type II receptor-independent signaling that leads to generation of amyloid beta plaques in Alzheimer's disease. Cell death & disease *1*, e110.

Lennox, A.L., and Stronach, B. (2010). POSH misexpression induces caspase-dependent cell death in Drosophila. Developmental dynamics : an official publication of the American Association of Anatomists *239*, 651-664.

Leung, K.F., Baron, R., Ali, B.R., Magee, A.I., and Seabra, M.C. (2007). Rab GTPases containing a CAAX motif are processed post-geranylgeranylation by proteolysis and methylation. The Journal of biological chemistry *282*, 1487-1497.

Lewis, E.B.B., B. (1968). Method of feeding ethyl methane sulfonate (EMS) to *Drosophila* males. Drosophila Information Service *43*.

Leyton, C.E., and Hodges, J.R. (2010). Frontotemporal dementias: Recent advances and current controversies. Ann Indian Acad Neurol *13*, S74-80.

Li, G., and Liang, Z. (2001). Phosphate-binding loop and Rab GTPase function: mutations at Ser29 and Ala30 of Rab5 lead to loss-of-function as well as gain-of-function phenotype. The Biochemical journal *355*, 681-689.

Li, L.M., Liu, Q.H., Qiao, J.T., and Zhang, C. (2009a). Abeta(31-35)-induced neuronal apoptosis is mediated by JNK-dependent extrinsic apoptosis pathway. Neuroscience bulletin *25*, 361-366.

Li, X., Sapp, E., Chase, K., Comer-Tierney, L.A., Masso, N., Alexander, J., Reeves, P., Kegel, K.B., Valencia, A., Esteves, M.*, et al.* (2009b). Disruption of Rab11 activity in a knock-in mouse model of Huntington's disease. Neurobiology of disease *36*, 374-383.

Li, X., Standley, C., Sapp, E., Valencia, A., Qin, Z.H., Kegel, K.B., Yoder, J., Comer-Tierney, L.A., Esteves, M., Chase, K.*, et al.* (2009c). Mutant huntingtin impairs vesicle formation from recycling endosomes by interfering with Rab11 activity. Molecular and cellular biology *29*, 6106-6116.

Linder, M.D., Uronen, R.L., Holtta-Vuori, M., van der Sluijs, P., Peranen, J., and Ikonen, E. (2007). Rab8-dependent recycling promotes endosomal cholesterol removal in normal and sphingolipidosis cells. Molecular biology of the cell *18*, 47-56.

Lindquist, S.G., Braedgaard, H., Svenstrup, K., Isaacs, A.M., Nielsen, J.E., and Consortium, F.R. (2008). Frontotemporal dementia linked to chromosome 3 (FTD-3)--current concepts and the detection of a previously unknown branch of the Danish FTD-3 family. European journal of neurology : the official journal of the European Federation of Neurological Societies *15*, 667-670.

Liu, Q., Zhang, Y., Mao, H., Chen, W., Luo, N., Zhou, Q., Chen, W., and Yu, X. (2012). A crosstalk between the Smad and JNK signaling in the TGF-beta-induced epithelial-mesenchymal transition in rat peritoneal mesothelial cells. PloS one *7*, e32009.

Liu, S., Xu, S.W., Kennedy, L., Pala, D., Chen, Y., Eastwood, M., Carter, D.E., Black, C.M., Abraham, D.J., and Leask, A. (2007). FAK is required for TGFbeta-induced JNK phosphorylation in fibroblasts: implications for acquisition of a matrix-remodeling phenotype. Molecular biology of the cell *18*, 2169-2178.

Lnenicka, G.A., and Keshishian, H. (2000). Identified motor terminals in Drosophila larvae show distinct differences in morphology and physiology. Journal of neurobiology *43*, 186-197.

Loewith, R., Jacinto, E., Wullschleger, S., Lorberg, A., Crespo, J.L., Bonenfant, D., Oppliger, W., Jenoe, P., and Hall, M.N. (2002). Two TOR complexes, only one of which is rapamycin sensitive, have distinct roles in cell growth control. Molecular cell *10*, 457-468.

Lomen-Hoerth, C. (2004). Characterization of amyotrophic lateral sclerosis and frontotemporal dementia. Dementia and geriatric cognitive disorders *17*, 337-341.

Longatti, A., Lamb, C.A., Razi, M., Yoshimura, S., Barr, F.A., and Tooze, S.A. (2012). TBC1D14 regulates autophagosome formation via Rab11- and ULK1-positive recycling endosomes. The Journal of cell biology *197*, 659-675.

Luan, P., Heine, A., Zeng, K., Moyer, B., Greasely, S.E., Kuhn, P., Balch, W.E., and Wilson, I.A. (2000). A new functional domain of guanine nucleotide dissociation inhibitor (alpha-GDI) involved in Rab recycling. Traffic *1*, 270-281.

Luiro, K., Yliannala, K., Ahtiainen, L., Maunu, H., Jarvela, I., Kyttala, A., and Jalanko, A. (2004). Interconnections of CLN3, Hook1 and Rab proteins link Batten disease to defects in the endocytic pathway. Human molecular genetics *13*, 3017-3027.

Ma, L., and Jarman, A.P. (2011). Dilatory is a Drosophila protein related to AZI1 (CEP131) that is located at the ciliary base and required for cilium formation. Journal of cell science *124*, 2622-2630.

Macia, E., Partisani, M., Paleotti, O., Luton, F., and Franco, M. (2012). Arf6 negatively controls the rapid recycling of the beta2 adrenergic receptor. Journal of cell science *125*, 4026-4035.

Mackenzie, I.R., Baker, M., Pickering-Brown, S., Hsiung, G.Y., Lindholm, C., Dwosh, E., Gass, J., Cannon, A., Rademakers, R., Hutton, M.*, et al.* (2006). The neuropathology of frontotemporal lobar degeneration caused by mutations in the progranulin gene. Brain : a journal of neurology *129*, 3081-3090.

Mackenzie, I.R., Neumann, M., Baborie, A., Sampathu, D.M., Du Plessis, D., Jaros, E., Perry, R.H., Trojanowski, J.Q., Mann, D.M., and Lee, V.M. (2011). A harmonized classification system for FTLD-TDP pathology. Acta neuropathologica *122*, 111-113.

Mackenzie, I.R., Neumann, M., Bigio, E.H., Cairns, N.J., Alafuzoff, I., Kril, J., Kovacs, G.G., Ghetti, B., Halliday, G., Holm, I.E.*, et al.* (2010). Nomenclature and nosology for neuropathologic subtypes of frontotemporal lobar degeneration: an update. Acta neuropathologica *119*, 1-4.

Maguire, E.A., Kumaran, D., Hassabis, D., and Kopelman, M.D. (2010). Autobiographical memory in semantic dementia: a longitudinal fMRI study. Neuropsychologia *48*, 123-136.

Mahul-Mellier, A.L., Hemming, F.J., Blot, B., Fraboulet, S., and Sadoul, R. (2006). Alix, making a link between apoptosis-linked gene-2, the endosomal sorting complexes required for transport, and neuronal death in vivo. The Journal of neuroscience : the official journal of the Society for Neuroscience *26*, 542-549.

Mann, D.M. (1998). Dementia of frontal type and dementias with subcortical gliosis. Brain pathology *8*, 325-338.

Mao, R., Fan, Y., Mou, Y., Zhang, H., Fu, S., and Yang, J. (2011). TAK1 lysine 158 is required for TGF-beta-induced TRAF6-mediated Smad-independent IKK/NF-kappaB and JNK/AP-1 activation. Cellular signalling *23*, 222-227.

Margulies, C., Tully, T., and Dubnau, J. (2005). Deconstructing memory in Drosophila. Current biology : CB *15*, R700-713.

Marques, G. (2005). Morphogens and synaptogenesis in Drosophila. Journal of neurobiology *64*, 417-434.

Marques, G., Bao, H., Haerry, T.E., Shimell, M.J., Duchek, P., Zhang, B., and O'Connor, M.B. (2002). The Drosophila BMP type II receptor Wishful Thinking regulates neuromuscular synapse morphology and function. Neuron *33*, 529-543.

Marques, G., Haerry, T.E., Crotty, M.L., Xue, M., Zhang, B., and O'Connor, M.B. (2003). Retrograde Gbb signaling through the Bmp type 2 receptor wishful thinking regulates systemic FMRFa expression in Drosophila. Development *130*, 5457-5470.

Marsh, J.L., Pallos, J., and Thompson, L.M. (2003). Fly models of Huntington's disease. Human molecular genetics *12 Spec No 2*, R187-193.

Martin-Blanco, E., Gampel, A., Ring, J., Virdee, K., Kirov, N., Tolkovsky, A.M., and Martinez-Arias, A. (1998). puckered encodes a phosphatase that mediates a feedback loop regulating JNK activity during dorsal closure in Drosophila. Genes & development *12*, 557-570.

Massa, M.L., Gagliardino, J.J., and Francini, F. (2011). Liver glucokinase: An overview on the regulatory mechanisms of its activity. IUBMB life *63*, 1-6.

Matsumoto, K., Toh-e, A., and Oshima, Y. (1978). Genetic control of galactokinase synthesis in Saccharomyces cerevisiae: evidence for constitutive expression of the positive regulatory gene gal4. Journal of bacteriology *134*, 446-457.

Matsuo, H., Chevallier, J., Mayran, N., Le Blanc, I., Ferguson, C., Faure, J., Blanc, N.S., Matile, S., Dubochet, J., Sadoul, R.*, et al.* (2004). Role of LBPA and Alix in multivesicular liposome formation and endosome organization. Science *303*, 531-534.

McCabe, B.D., Hom, S., Aberle, H., Fetter, R.D., Marques, G., Haerry, T.E., Wan, H., O'Connor, M.B., Goodman, C.S., and Haghighi, A.P. (2004). Highwire regulates presynaptic BMP signaling essential for synaptic growth. Neuron *41*, 891-905.

McCabe, B.D., Marques, G., Haghighi, A.P., Fetter, R.D., Crotty, M.L., Haerry, T.E., Goodman, C.S., and O'Connor, M.B. (2003). The BMP homolog Gbb provides a retrograde signal that regulates synaptic growth at the Drosophila neuromuscular junction. Neuron *39*, 241-254.

McCray, B.A., Skordalakes, E., and Taylor, J.P. (2010). Disease mutations in Rab7 result in unregulated nucleotide exchange and inappropriate activation. Human molecular genetics *19*, 1033-1047.

McGuire, S.E., Deshazer, M., and Davis, R.L. (2005). Thirty years of olfactory learning and memory research in Drosophila melanogaster. Progress in neurobiology *76*, 328-347.

Mecha, M., Rabadan, M.A., Pena-Melian, A., Valencia, M., Mondejar, T., and Blanco, M.J. (2008). Expression of TGF-betas in the embryonic nervous system: analysis of interbalance between isoforms. Developmental dynamics : an official publication of the American Association of Anatomists *237*, 1709-1717.

Mercer, J., and Helenius, A. (2009). Virus entry by macropinocytosis. Nature cell biology *11*, 510-520.

Merrilees, J., Klapper, J., Murphy, J., Lomen-Hoerth, C., and Miller, B.L. (2010). Cognitive and behavioral challenges in caring for patients with frontotemporal dementia and amyotrophic lateral sclerosis. Amyotrophic lateral sclerosis : official publication of the World Federation of Neurology Research Group on Motor Neuron Diseases *11*, 298-302.

Merrill, S.A., and Hanson, P.I. (2010). Activation of human VPS4A by ESCRT-III proteins reveals ability of substrates to relieve enzyme autoinhibition. The Journal of biological chemistry *285*, 35428-35438.

Miaczynska, M., Pelkmans, L., and Zerial, M. (2004). Not just a sink: endosomes in control of signal transduction. Current opinion in cell biology *16*, 400-406.

Mihaly, J., Kockel, L., Gaengel, K., Weber, U., Bohmann, D., and Mlodzik, M. (2001). The role of the Drosophila TAK homologue dTAK during development. Mechanisms of development *102*, 67-79.

Milton, V., Jarrett, H., Gowers, K., Chalak, S., Briggs, L., Robinson, I., and Sweeney, S. (2011). Oxidative stress induces overgrowth of the Drosophila neuromuscular junction. Proceedings of the National Academy of Sciences of the United States of America *108*, 17521-17527.

Milton, V.U.o.Y. (2011). The effects of oxidative stress on synapse development in Drosphila.

Mishra, M., and Knust, E. (2013). Analysis of the Drosophila compound eye with light and electron microscopy. Methods in molecular biology *935*, 161-182.

Misra, S., and Rio, D.C. (1990). Cytotype control of Drosophila P element transposition: the 66 kd protein is a repressor of transposase activity. Cell *62*, 269-284.

Mitchell, H., Choudhury, A., Pagano, R.E., and Leof, E.B. (2004). Ligand-dependent and -independent transforming growth factor-beta receptor recycling regulated by clathrin-mediated endocytosis and Rab11. Molecular biology of the cell *15*, 4166-4178.

Miura, S., and Mishina, Y. (2011). Hepatocyte growth factor-regulated tyrosine kinase substrate (Hgs) is involved in BMP signaling through phosphorylation of SMADS and TAK1 in early mouse embryo. Developmental dynamics : an official publication of the American Association of Anatomists *240*, 2474-2481.

Mogi, M., Harada, M., Kondo, T., Narabayashi, H., Riederer, P., and Nagatsu, T. (1995). Transforming growth factor-beta 1 levels are elevated in the striatum and in ventricular cerebrospinal fluid in Parkinson's disease. Neuroscience letters *193*, 129-132.

Moloney, A., Sattelle, D.B., Lomas, D.A., and Crowther, D.C. (2010). Alzheimer's disease: insights from Drosophila melanogaster models. Trends in biochemical sciences *35*, 228-235.

Momeni, P., Rogaeva, E., Van Deerlin, V., Yuan, W., Grafman, J., Tierney, M., Huey, E., Bell, J., Morris, C.M., Kalaria, R.N.*, et al.* (2006). Genetic variability in CHMP2B and frontotemporal dementia. Neuro-degenerative diseases *3*, 129-133.

Moressis, A., Friedrich, A.R., Pavlopoulos, E., Davis, R.L., and Skoulakis, E.M. (2009). A dual role for the adaptor protein DRK in Drosophila olfactory learning and memory. The Journal of neuroscience : the official journal of the Society for Neuroscience *29*, 2611-2625.

Moritz, O.L., Tam, B.M., Hurd, L.L., Peranen, J., Deretic, D., and Papermaster, D.S. (2001). Mutant rab8 Impairs docking and fusion of rhodopsin-bearing post-Golgi membranes and causes cell death of transgenic Xenopus rods. Molecular biology of the cell *12*, 2341-2351.

Muller, H.J. (1927). Artificial Transmutation of the Gene. Science *66*, 84-87.

Murray, J.L., Mavrakis, M., McDonald, N.J., Yilla, M., Sheng, J., Bellini, W.J., Zhao, L., Le Doux, J.M., Shaw, M.W., Luo, C.C.*, et al.* (2005). Rab9 GTPase is required for replication of human immunodeficiency virus type 1, filoviruses, and measles virus. Journal of virology *79*, 11742-11751.

Nachury, M.V., Loktev, A.V., Zhang, Q., Westlake, C.J., Peranen, J., Merdes, A., Slusarski, D.C., Scheller, R.H., Bazan, J.F., Sheffield, V.C.*, et al.* (2007a). A core complex of BBS proteins cooperates with the GTPase Rab8 to promote ciliary membrane biogenesis. Cell *129*, 1201-1213.

Nagabhushana, A., Chalasani, M.L., Jain, N., Radha, V., Rangaraj, N., Balasubramanian, D., and Swarup, G. (2010). Regulation of endocytic trafficking of transferrin receptor by optineurin and its impairment by a glaucoma-associated mutant. BMC cell biology *11*, 4.

Nahm, M., Lee, M.J., Parkinson, W., Lee, M., Kim, H., Kim, Y.J., Kim, S., Cho, Y.S., Min, B.M., Bae, Y.C.*, et al.* (2013). Spartin regulates synaptic growth and neuronal survival by inhibiting BMP-mediated microtubule stabilization. Neuron *77*, 680-695.

Nakatogawa, H., Suzuki, K., Kamada, Y., and Ohsumi, Y. (2009). Dynamics and diversity in autophagy mechanisms: lessons from yeast. Nature reviews Molecular cell biology *10*, 458-467.

Neumann, M., Rademakers, R., Roeber, S., Baker, M., Kretzschmar, H.A., and Mackenzie, I.R. (2009). A new subtype of frontotemporal lobar degeneration with FUS pathology. Brain : a journal of neurology *132*, 2922-2931.

Ng, E.L., and Tang, B.L. (2008). Rab GTPases and their roles in brain neurons and glia. Brain Res Rev *58*, 236-246.

Nishino, I., Fu, J., Tanji, K., Yamada, T., Shimojo, S., Koori, T., Mora, M., Riggs, J.E., Oh, S.J., Koga, Y.*, et al.* (2000). Primary LAMP-2 deficiency causes X-linked vacuolar cardiomyopathy and myopathy (Danon disease). Nature *406*, 906-910.

Noakes, C.J., Lee, G., and Lowe, M. (2011). The PH domain proteins IPIP27A and B link OCRL1 to receptor recycling in the endocytic pathway. Molecular biology of the cell *22*, 606-623.

Nusslein-Volhard, C., and Wieschaus, E. (1980). Mutations affecting segment number and polarity in Drosophila. Nature *287*, 795-801.

O'Connor-Giles, K.M., Ho, L.L., and Ganetzky, B. (2008). Nervous wreck interacts with thickveins and the endocytic machinery to attenuate retrograde BMP signaling during synaptic growth. Neuron *58*, 507-518.

O'Kane, C.J., and Gehring, W.J. (1987). Detection in situ of genomic regulatory elements in Drosophila. Proceedings of the National Academy of Sciences of the United States of America *84*, 9123-9127.

O'Shea, E.K., Rutkowski, R., Stafford, W.F., 3rd, and Kim, P.S. (1989). Preferential heterodimer formation by isolated leucine zippers from fos and jun. Science *245*, 646-648.

Obara, K., Sekito, T., Niimi, K., and Ohsumi, Y. (2008). The Atg18-Atg2 complex is recruited to autophagic membranes via phosphatidylinositol 3-phosphate and exerts an essential function. The Journal of biological chemistry *283*, 23972-23980.

Ofstad, T.A., Zuker, C.S., and Reiser, M.B. (2011). Visual place learning in Drosophila melanogaster. Nature *474*, 204-207.

Ohira, M., Oshitani, N., Hosomi, S., Watanabe, K., Yamagami, H., Tominaga, K., Watanabe, T., Fujiwara, Y., Maeda, K., Hirakawa, K.*, et al.* (2009). Dislocation of Rab13 and vasodilator-stimulated phosphoprotein in inactive colon epithelium in patients with Crohn's disease. International journal of molecular medicine *24*, 829-835.

Okai, T., Araki, Y., Tada, M., Tateno, T., Kontani, K., and Katada, T. (2004). Novel small GTPase subfamily capable of associating with tubulin is required for chromosome segregation. Journal of cell science *117*, 4705-4715.

Okumura, M., Ichioka, F., Kobayashi, R., Suzuki, H., Yoshida, H., Shibata, H., and Maki, M. (2009). Penta-EF-hand protein ALG-2 functions as a Ca2+-dependent adaptor that bridges Alix and TSG101. Biochemical and biophysical research communications *386*, 237-241.

Olzmann, J.A., Li, L., and Chin, L.S. (2008). Aggresome formation and neurodegenerative diseases: therapeutic implications. Current medicinal chemistry *15*, 47-60.

Orso, G., Martinuzzi, A., Rossetto, M.G., Sartori, E., Feany, M., and Daga, A. (2005). Disease-related phenotypes in a Drosophila model of hereditary spastic paraplegia are ameliorated by treatment with vinblastine. The Journal of clinical investigation *115*, 3026-3034.

Packard, M., Koo, E.S., Gorczyca, M., Sharpe, J., Cumberledge, S., and Budnik, V. (2002). The Drosophila Wnt, wingless, provides an essential signal for pre- and postsynaptic differentiation. Cell *111*, 319-330.

Pan, X.D., and Chen, X.C. (2013). Clinic, neuropathology and molecular genetics of frontotemporal dementia: a mini-review. Translational neurodegeneration *2*, 8.

Pandey, U.B., Nie, Z., Batlevi, Y., McCray, B.A., Ritson, G.P., Nedelsky, N.B., Schwartz, S.L., DiProspero, N.A., Knight, M.A., Schuldiner, O.*, et al.* (2007). HDAC6 rescues neurodegeneration and provides an essential link between autophagy and the UPS. Nature *447*, 859-863.

Pandit, L., Kolodziejska, K.E., Zeng, S., and Eissa, N.T. (2009). The physiologic aggresome mediates cellular inactivation of iNOS. Proceedings of the National Academy of Sciences of the United States of America *106*, 1211-1215.

Pantos, C., Malliopoulou, V., Mourouzis, I., Moraitis, P., Tzeis, S., Thempeyioti, A., Paizis, I., Cokkinos, A., Carageorgiou, H., Varonos, D.D.*, et al.* (2003). Involvement of p38 MAPK and JNK in heat stress-induced cardioprotection. Basic research in cardiology *98*, 158-164.

Pardoux, C., and Derynck, R. (2004). JNK regulates expression and autocrine signaling of TGF-beta1. Molecular cell *15*, 170-171.

Parkhitko, C.A., Favorova, C.O., and Henske, E.P. (2011). Rabin8 Protein Interacts with GTPase Rheb and Inhibits Phosphorylation of Ser235/Ser236 in Small Ribosomal Subunit Protein S6. Acta naturae *3*, 71-76.

Pedersen, J.T., and Heegaard, N.H. (2013). Analysis of protein aggregation in neurodegenerative disease. Analytical chemistry *85*, 4215-4227.

Peng, J., and Andersen, J.K. (2003). The role of c-Jun N-terminal kinase (JNK) in Parkinson's disease. IUBMB life *55*, 267-271.

Peranen, J. (2011). Rab8 GTPase as a regulator of cell shape. Cytoskeleton *68*, 527-539.

Peränen, J., Auvinen, P., Virta, H., Wepf, R., and Simons, K. (1996). Rab8 promotes polarized membrane transport through reorganization of actin and microtubules in fibroblasts. The Journal of cell biology *135*, 153-167.

Perkins, K.K., Admon, A., Patel, N., and Tjian, R. (1990). The Drosophila Fos-related AP-1 protein is a developmentally regulated transcription factor. Genes & development *4*, 822-834.

Perlman, R., Schiemann, W.P., Brooks, M.W., Lodish, H.F., and Weinberg, R.A. (2001). TGF-beta-induced apoptosis is mediated by the adapter protein Daxx that facilitates JNK activation. Nature cell biology *3*, 708-714.

Pfeffer, S.R. (2001). Rab GTPases: specifying and deciphering organelle identity and function. Trends Cell Biol *11*, 487-491.

Pfeffer, S.R. (2005). Structural clues to Rab GTPase functional diversity. The Journal of biological chemistry *280*, 15485-15488.

Piguet, O., Petersen, A., Yin Ka Lam, B., Gabery, S., Murphy, K., Hodges, J.R., and Halliday, G.M. (2011). Eating and hypothalamus changes in behavioral-variant frontotemporal dementia. Annals of neurology *69*, 312-319.

Piper, R.C., and Katzmann, D.J. (2007a). Biogenesis and function of multivesicular bodies. Annu Rev Cell Dev Biol *23*, 519-547.

Piper, R.C., and Katzmann, D.J. (2007b). Biogenesis and function of multivesicular bodies. Annu Rev Cell Dev Biol *23*, 519-547.

Pirruccello, M., and De Camilli, P. (2012). Inositol 5-phosphatases: insights from the Lowe syndrome protein OCRL. Trends in biochemical sciences *37*, 134-143.

Prokop, A. (2006). Organization of the efferent system and structure of neuromuscular junctions in Drosophila. International review of neurobiology *75*, 71-90.

Prokop, A., Landgraf, M., Rushton, E., Broadie, K., and Bate, M. (1996). Presynaptic development at the Drosophila neuromuscular junction: assembly and localization of presynaptic active zones. Neuron *17*, 617-626.

Puri, C., Renna, M., Bento, C.F., Moreau, K., and Rubinsztein, D.C. (2013). Diverse autophagosome membrane sources coalesce in recycling endosomes. Cell *154*, 1285-1299.

Quaid, K.A. (2011). Genetic Counseling for Frontotemporal Dementias. J Mol Neurosci.

Quan, A., and Robinson, P.J. (2013). Syndapin - a membrane remodelling and endocytic F-BAR protein. The FEBS journal.

Rabinovici, G.D., and Miller, B.L. (2010). Frontotemporal lobar degeneration: epidemiology, pathophysiology, diagnosis and management. CNS drugs *24*, 375-398.

Raghu, S.V., and Borst, A. (2011). Candidate glutamatergic neurons in the visual system of Drosophila. PloS one *6*, e19472.

Rak, A., Pylypenko, O., Durek, T., Watzke, A., Kushnir, S., Brunsveld, L., Waldmann, H., Goody, R.S., and Alexandrov, K. (2003). Structure of Rab GDP-dissociation inhibitor in complex with prenylated YPT1 GTPase. Science *302*, 646-650.

Rascovsky, K., Hodges, J.R., Knopman, D., Mendez, M.F., Kramer, J.H., Neuhaus, J., van Swieten, J.C., Seelaar, H., Dopper, E.G., Onyike, C.U.*, et al.* (2011). Sensitivity of revised diagnostic criteria for the behavioural variant of frontotemporal dementia. Brain : a journal of neurology *134*, 2456-2477.

Ratnavalli, E., Brayne, C., Dawson, K., and Hodges, J.R. (2002). The prevalence of frontotemporal dementia. Neurology *58*, 1615-1621.

Rauscher, F.J., 3rd, Cohen, D.R., Curran, T., Bos, T.J., Vogt, P.K., Bohmann, D., Tjian, R., and Franza, B.R., Jr. (1988). Fos-associated protein p39 is the product of the jun proto-oncogene. Science *240*, 1010-1016.

Rawson, J.M., Lee, M., Kennedy, E.L., and Selleck, S.B. (2003). Drosophila neuromuscular synapse assembly and function require the TGF-beta type I receptor saxophone and the transcription factor Mad. Journal of neurobiology *55*, 134-150.

Rees, M.G., Wincovitch, S., Schultz, J., Waterstradt, R., Beer, N.L., Baltrusch, S., Collins, F.S., and Gloyn, A.L. (2012). Cellular characterisation of the GCKR P446L variant associated with type 2 diabetes risk. Diabetologia *55*, 114-122.

Reiter, L.T., Potocki, L., Chien, S., Gribskov, M., and Bier, E. (2001). A systematic analysis of human disease-associated gene sequences in Drosophila melanogaster. Genome research *11*, 1114-1125.

Ren, M., Zeng, J., De Lemos-Chiarandini, C., Rosenfeld, M., Adesnik, M., and Sabatini, D.D. (1996). In its active form, the GTP-binding protein rab8 interacts with a stress-activated protein kinase. Proceedings of the National Academy of Sciences of the United States of America *93*, 5151-5155.

Renton, A.E., Majounie, E., Waite, A., Simon-Sanchez, J., Rollinson, S., Gibbs, J.R., Schymick, J.C., Laaksovirta, H., van Swieten, J.C., Myllykangas, L.*, et al.* (2011). A hexanucleotide repeat expansion in C9ORF72 is the cause of chromosome 9p21-linked ALS-FTD. Neuron *72*, 257-268.

Ritson, G.P., Custer, S.K., Freibaum, B.D., Guinto, J.B., Geffel, D., Moore, J., Tang, W., Winton, M.J., Neumann, M., Trojanowski, J.Q.*, et al.* (2010). TDP-43 mediates degeneration in a novel Drosophila model of disease caused by mutations in VCP/p97. The Journal of neuroscience : the official journal of the Society for Neuroscience *30*, 7729-7739.

Roberts, R.C., Peden, A.A., Buss, F., Bright, N.A., Latouche, M., Reilly, M.M., Kendrick-Jones, J., and Luzio, J.P. (2010). Mistargeting of SH3TC2 away from the recycling endosome causes Charcot-Marie-Tooth disease type 4C. Human molecular genetics *19*, 1009-1018.

Robinson, S.W., Herzyk, P., Dow, J.A., and Leader, D.P. (2013). FlyAtlas: database of gene expression in the tissues of Drosophila melanogaster. Nucleic acids research *41*, D744-750.

Rodal, A.A., Blunk, A.D., Akbergenova, Y., Jorquera, R.A., Buhl, L.K., and Littleton, J.T. (2011). A presynaptic endosomal trafficking pathway controls synaptic growth signaling. The Journal of cell biology *193*, 201-217.

Rohrer, J.D., Rossor, M.N., and Warren, J.D. (2010). Syndromes of nonfluent primary progressive aphasia: a clinical and neurolinguistic analysis. Neurology *75*, 603-610.

Roland, J.T., Kenworthy, A.K., Peranen, J., Caplan, S., and Goldenring, J.R. (2007). Myosin Vb interacts with Rab8a on a tubular network containing EHD1 and EHD3. Molecular biology of the cell *18*, 2828-2837.

Roote, J., and Prokop, A. (2013). How to design a genetic mating scheme: a basic training package for Drosophila genetics. G3 *3*, 353-358.

Rosen, H.J., Perry, R.J., Murphy, J., Kramer, J.H., Mychack, P., Schuff, N., Weiner, M., Levenson, R.W., and Miller, B.L. (2002). Emotion comprehension in the temporal variant of frontotemporal dementia. Brain : a journal of neurology *125*, 2286-2295.

Ross, C.A., and Poirier, M.A. (2004). Protein aggregation and neurodegenerative disease. Nature medicine *10 Suppl*, S10-17.

Rosso, S.M., Donker Kaat, L., Baks, T., Joosse, M., de Koning, I., Pijnenburg, Y., de Jong, D., Dooijes, D., Kamphorst, W., Ravid, R.*, et al.* (2003a). Frontotemporal dementia in The Netherlands: patient characteristics and prevalence estimates from a population-based study. Brain : a journal of neurology *126*, 2016-2022.

Rosso, S.M., Kamphorst, W., de Graaf, B., Willemsen, R., Ravid, R., Niermeijer, M.F., Spillantini, M.G., Heutink, P., and van Swieten, J.C. (2001). Familial frontotemporal dementia with ubiquitin-positive inclusions is linked to chromosome 17q21-22. Brain : a journal of neurology *124*, 1948-1957.

Rowe, R.K., Suszko, J.W., and Pekosz, A. (2008). Roles for the recycling endosome, Rab8, and Rab11 in hantavirus release from epithelial cells. Virology *382*, 239-249.

Rubin, G.M., and Spradling, A.C. (1982). Genetic transformation of Drosophila with transposable element vectors. Science *218*, 348-353.

Ryder, E., Ashburner, M., Bautista-Llacer, R., Drummond, J., Webster, J., Johnson, G., Morley, T., Chan, Y.S., Blows, F., Coulson, D.*, et al.* (2007). The DrosDel deletion collection: a Drosophila genomewide chromosomal deficiency resource. Genetics *177*, 615-629.

Ryder, E., and Russell, S. (2003). Transposable elements as tools for genomics and genetics in Drosophila. Briefings in functional genomics & proteomics *2*, 57-71.

Ryter, S.W., Cloonan, S.M., and Choi, A.M. (2013). Autophagy: a critical regulator of cellular metabolism and homeostasis. Molecules and cells *36*, 7-16.

Sahlender, D.A., Roberts, R.C., Arden, S.D., Spudich, G., Taylor, M.J., Luzio, J.P., Kendrick-Jones, J., and Buss, F. (2005). Optineurin links myosin VI to the Golgi complex and is involved in Golgi organization and exocytosis. The Journal of cell biology *169*, 285-295.

Sanchez-Soriano, N., and Prokop, A. (2005). The influence of pioneer neurons on a growing motor nerve in Drosophila requires the neural cell adhesion molecule homolog FasciclinII. The Journal of neuroscience : the official journal of the Society for Neuroscience *25*, 78-87.

Sang, T.K., and Jackson, G.R. (2005). Drosophila models of neurodegenerative disease. NeuroRx : the journal of the American Society for Experimental NeuroTherapeutics *2*, 438-446.

Sanyal, S., Sandstrom, D.J., Hoeffer, C.A., and Ramaswami, M. (2002). AP-1 functions upstream of CREB to control synaptic plasticity in Drosophila. Nature *416*, 870-874.

Sarthi, J., and Elefant, F. (2011). dTip60 HAT activity controls synaptic bouton expansion at the Drosophila neuromuscular junction. PloS one *6*, e26202.

Sato, S., Sanjo, H., Takeda, K., Ninomiya-Tsuji, J., Yamamoto, M., Kawai, T., Matsumoto, K., Takeuchi, O., and Akira, S. (2005). Essential function for the kinase TAK1 in innate and adaptive immune responses. Nature immunology *6*, 1087-1095.

Sato, T., Mushiake, S., Kato, Y., Sato, K., Sato, M., Takeda, N., Ozono, K., Miki, K., Kubo, Y., Tsuji, A.*, et al.* (2007a). The Rab8 GTPase regulates apical protein localization in intestinal cells. Nature *448*, 366-369.

Schenkel, H., Hanke, S., De Lorenzo, C., Schmitt, R., and Mechler, B.M. (2002). P elements inserted in the vicinity of or within the Drosophila snRNP SmD3 gene nested in the first intron of the Ornithine Decarboxylase Antizyme gene affect only the expression of SmD3. Genetics *161*, 763-772.

Schmidt, O., and Teis, D. (2012). The ESCRT machinery. Current biology : CB *22*, R116-120.

Schneider, L., and Zhang, J. (2010). Lysosomal function in macromolecular homeostasis and bioenergetics in Parkinson's disease. Molecular neurodegeneration *5*, 14.

Schollenberger, L., Gronemeyer, T., Huber, C.M., Lay, D., Wiese, S., Meyer, H.E., Warscheid, B., Saffrich, R., Peranen, J., Gorgas, K.*, et al.* (2010). RhoA regulates peroxisome association to microtubules and the actin cytoskeleton. PloS one *5*, e13886.

Schubert, U., Anton, L.C., Gibbs, J., Norbury, C.C., Yewdell, J.W., and Bennink, J.R. (2000). Rapid degradation of a large fraction of newly synthesized proteins by proteasomes. Nature *404*, 770-774.

Schuster, C.M., Davis, G.W., Fetter, R.D., and Goodman, C.S. (1996). Genetic dissection of structural and functional components of synaptic plasticity. I. Fasciclin II controls synaptic stabilization and growth. Neuron *17*, 641-654.

Schwartz, S.L., Cao, C., Pylypenko, O., Rak, A., and Wandinger-Ness, A. (2007). Rab GTPases at a glance. Journal of cell science *120*, 3905-3910.

Schwarz, T.L. (2006). Transmitter release at the neuromuscular junction. International review of neurobiology *75*, 105-144.

Seelaar, H., Rohrer, J.D., Pijnenburg, Y.A., Fox, N.C., and van Swieten, J.C. (2011). Clinical, genetic and pathological heterogeneity of frontotemporal dementia: a review. Journal of neurology, neurosurgery, and psychiatry *82*, 476-486.

Seelaar, H., Schelhaas, H.J., Azmani, A., Kusters, B., Rosso, S., Majoor-Krakauer, D., de Rijk, M.C., Rizzu, P., ten Brummelhuis, M., van Doorn, P.A.*, et al.* (2007). TDP-43 pathology in familial frontotemporal dementia and motor neuron disease without Progranulin mutations. Brain : a journal of neurology *130*, 1375-1385.

Seeley, W.W., Bauer, A.M., Miller, B.L., Gorno-Tempini, M.L., Kramer, J.H., Weiner, M., and Rosen, H.J. (2005). The natural history of temporal variant frontotemporal dementia. Neurology *64*, 1384-1390.

Seripa, D., Bizzarro, A., Panza, F., Acciarri, A., Pellegrini, F., Pilotto, A., and Masullo, C. (2011). The APOE gene locus in frontotemporal dementia and primary progressive aphasia. Archives of neurology *68*, 622-628.

Sharma, M., Giridharan, S.S., Rahajeng, J., Caplan, S., and Naslavsky, N. (2010). MICAL-L1: An unusual Rab effector that links EHD1 to tubular recycling endosomes. Communicative & integrative biology *3*, 181-183.

Sharma, M., Giridharan, S.S., Rahajeng, J., Naslavsky, N., and Caplan, S. (2009). MICAL-L1 links EHD1 to tubular recycling endosomes and regulates receptor recycling. Molecular biology of the cell *20*, 5181-5194.

Shaulian, E., and Karin, M. (2001). AP-1 in cell proliferation and survival. Oncogene *20*, 2390-2400.

Shen, C., Chen, Y., Liu, H., Zhang, K., Zhang, T., Lin, A., and Jing, N. (2008). Hydrogen peroxide promotes Abeta production through JNK-dependent activation of gamma-secretase. The Journal of biological chemistry *283*, 17721-17730.

Shen, W., and Ganetzky, B. (2009). Autophagy promotes synapse development in Drosophila. The Journal of cell biology *187*, 71-79.

Shi, W., Chen, Y., Gan, G., Wang, D., Ren, J., Wang, Q., Xu, Z., Xie, W., and Zhang, Y.Q. (2013). Brain tumor regulates neuromuscular synapse growth and endocytosis in Drosophila by suppressing mad expression. The Journal of neuroscience : the official journal of the Society for Neuroscience *33*, 12352-12363.

Shibuya, H., Iwata, H., Masuyama, N., Gotoh, Y., Yamaguchi, K., Irie, K., Matsumoto, K., Nishida, E., and Ueno, N. (1998). Role of TAK1 and TAB1 in BMP signaling in early Xenopus development. The EMBO journal *17*, 1019-1028.

Shim, J.H., Xiao, C., Paschal, A.E., Bailey, S.T., Rao, P., Hayden, M.S., Lee, K.Y., Bussey, C., Steckel, M., Tanaka, N.*, et al.* (2005). TAK1, but not TAB1 or TAB2, plays an essential role in multiple signaling pathways in vivo. Genes & development *19*, 2668-2681.

Shin, J.H., Min, S.H., Kim, S.J., Kim, Y.I., Park, J., Lee, H.K., and Yoo, O.J. (2013). TAK1 regulates autophagic cell death by suppressing the phosphorylation of p70 S6 kinase 1. Scientific reports *3*, 1561.

Shtanko, O., Watanabe, S., Jasenosky, L.D., Watanabe, T., and Kawaoka, Y. (2011). ALIX/AIP1 is required for NP incorporation into Mopeia virus Z-induced virus-like particles. Journal of virology *85*, 3631-3641.

Shulman, J.M., and Feany, M.B. (2003). Genetic modifiers of tauopathy in Drosophila. Genetics *165*, 1233-1242.

Silverman, N., Zhou, R., Erlich, R.L., Hunter, M., Bernstein, E., Schneider, D., and Maniatis, T. (2003). Immune activation of NF-kappaB and JNK requires Drosophila TAK1. The Journal of biological chemistry *278*, 48928-48934.

Sjogren, M., Folkesson, S., Blennow, K., and Tarkowski, E. (2004). Increased intrathecal inflammatory activity in frontotemporal dementia: pathophysiological implications. Journal of neurology, neurosurgery, and psychiatry *75*, 1107-1111.

Skibinski, G., Parkinson, N.J., Brown, J.M., Chakrabarti, L., Lloyd, S.L., Hummerich, H., Nielsen, J.E., Hodges, J.R., Spillantini, M.G., Thusgaard, T.*, et al.* (2005). Mutations in the endosomal ESCRTIII-complex subunit CHMP2B in frontotemporal dementia. Nature genetics *37*, 806-808.

Smirnova, E., Griparic, L., Shurland, D.L., and van der Bliek, A.M. (2001). Dynamin-related protein Drp1 is required for mitochondrial division in mammalian cells. Molecular biology of the cell *12*, 2245-2256.

Smith, R.B., Machamer, J.B., Kim, N.C., Hays, T.S., and Marques, G. (2012). Relay of retrograde synaptogenic signals through axonal transport of BMP receptors. Journal of cell science *125*, 3752-3764.

Snowden, J.S., Bathgate, D., Varma, A., Blackshaw, A., Gibbons, Z.C., and Neary, D. (2001). Distinct behavioural profiles in frontotemporal dementia and semantic dementia. Journal of neurology, neurosurgery, and psychiatry *70*, 323-332.

Snowden, J.S., Neary, D., and Mann, D.M. (2002). Frontotemporal dementia. The British journal of psychiatry : the journal of mental science *180*, 140-143.

Song, W., Chen, J., Petrilli, A., Liot, G., Klinglmayr, E., Zhou, Y., Poquiz, P., Tjong, J., Pouladi, M.A., Hayden, M.R.*, et al.* (2011). Mutant huntingtin binds the mitochondrial fission GTPase dynamin-related protein-1 and increases its enzymatic activity. Nature medicine *17*, 377-382.

Sorrentino, A., Thakur, N., Grimsby, S., Marcusson, A., von Bulow, V., Schuster, N., Zhang, S., Heldin, C.H., and Landstrom, M. (2008). The type I TGF-beta receptor engages TRAF6 to activate TAK1 in a receptor kinase-independent manner. Nature cell biology *10*, 1199-1207.

Spradling, A.C., and Rubin, G.M. (1982). Transposition of cloned P elements into Drosophila germ line chromosomes. Science *218*, 341-347.

St Johnston, D. (2002). The art and design of genetic screens: Drosophila melanogaster. Nature reviews Genetics *3*, 176-188.

Stein, M., Pilli, M., Bernauer, S., Habermann, B.H., Zerial, M., and Wade, R.C. (2012). The interaction properties of the human Rab GTPase family--comparative analysis reveals determinants of molecular binding selectivity. PloS one *7*, e34870.

Steinert, J.R., Kuromi, H., Hellwig, A., Knirr, M., Wyatt, A.W., Kidokoro, Y., and Schuster, C.M. (2006). Experience-dependent formation and recruitment of large vesicles from reserve pool. Neuron *50*, 723-733.

Stenmark, H. (2009). Rab GTPases as coordinators of vesicle traffic. Nature reviews Molecular cell biology *10*, 513-525.

Strack, B., Calistri, A., Craig, S., Popova, E., and Gottlinger, H.G. (2003). AIP1/ALIX is a binding partner for HIV-1 p6 and EIAV p9 functioning in virus budding. Cell *114*, 689-699.

Stroupe, C., and Brunger, A.T. (2000). Crystal structures of a Rab protein in its inactive and active conformations. Journal of molecular biology *304*, 585-598.

Stuchell-Brereton, M.D., Skalicky, J.J., Kieffer, C., Karren, M.A., Ghaffarian, S., and Sundquist, W.I. (2007). ESCRT-III recognition by VPS4 ATPases. Nature *449*, 740-744.

Stuffers, S., Brech, A., and Stenmark, H. (2009). ESCRT proteins in physiology and disease. Exp Cell Res *315*, 1619-1626.

Sun, B., and Salvaterra, P.M. (1995a). Characterization of nervana, a Drosophila melanogaster neuron-specific glycoprotein antigen recognized by anti-horseradish peroxidase antibodies. Journal of neurochemistry *65*, 434-443.

Sun, B., and Salvaterra, P.M. (1995b). Two Drosophila nervous system antigens, Nervana 1 and 2, are homologous to the beta subunit of Na+,K(+)-ATPase. Proceedings of the National Academy of Sciences of the United States of America *92*, 5396-5400.

Sun, T., Yu, N., Zhai, L.K., Li, N., Zhang, C., Zhou, L., Huang, Z., Jiang, X.Y., Shen, Y., and Chen, Z.Y. (2013). c-Jun NH2-terminal kinase (JNK)-interacting protein-3 (JIP3) regulates neuronal axon elongation in a kinesin- and JNK-dependent manner. The Journal of biological chemistry *288*, 14531-14543.

Sun, Y., Yang, T., and Xu, Z. (2007). The JNK pathway and neuronal migration. Journal of genetics and genomics = Yi chuan xue bao *34*, 957-965.

Sweeney, N.T., Brenman, J.E., Jan, Y.N., and Gao, F.B. (2006). The coiled-coil protein shrub controls neuronal morphogenesis in Drosophila. Current biology : CB *16*, 1006-1011.

Sweeney, S.T., and Davis, G.W. (2002). Unrestricted synaptic growth in spinster-a late endosomal protein implicated in TGF-beta-mediated synaptic growth regulation. Neuron *36*, 403-416.

Sykiotis, G.P., and Bohmann, D. (2008). Keap1/Nrf2 signaling regulates oxidative stress tolerance and lifespan in Drosophila. Developmental cell *14*, 76-85.

Sykiotis, G.P., and Bohmann, D. (2010). Stress-activated cap'n'collar transcription factors in aging and human disease. Science signaling *3*, re3.

Takalo, M., Salminen, A., Soininen, H., Hiltunen, M., and Haapasalo, A. (2013). Protein aggregation and degradation mechanisms in neurodegenerative diseases. American journal of neurodegenerative disease *2*, 1-14.

Takatsu, Y., Nakamura, M., Stapleton, M., Danos, M.C., Matsumoto, K., O'Connor, M.B., Shibuya, H., and Ueno, N. (2000). TAK1 participates in c-Jun N-terminal kinase signaling during Drosophila development. Molecular and cellular biology *20*, 3015-3026.

Talbot, K., and Ansorge, O. (2006). Recent advances in the genetics of amyotrophic lateral sclerosis and frontotemporal dementia: common pathways in neurodegenerative disease. Human molecular genetics *15 Spec No 2*, R182-187.

Tamai, K., Tanaka, N., Nakano, T., Kakazu, E., Kondo, Y., Inoue, J., Shiina, M., Fukushima, K., Hoshino, T., Sano, K.*, et al.* (2010). Exosome secretion of dendritic cells is regulated by Hrs, an ESCRT-0 protein. Biochemical and biophysical research communications *399*, 384-390.

Tamai, K., Toyoshima, M., Tanaka, N., Yamamoto, N., Owada, Y., Kiyonari, H., Murata, K., Ueno, Y., Ono, M., Shimosegawa, T.*, et al.* (2008). Loss of hrs in the central nervous system causes accumulation of ubiquitinated proteins and neurodegeneration. The American journal of pathology *173*, 1806-1817.

Tapon, N., Nagata, K., Lamarche, N., and Hall, A. (1998). A new rac target POSH is an SH3-containing scaffold protein involved in the JNK and NF-kappaB signalling pathways. The EMBO journal *17*, 1395-1404.

Teis, D., Saksena, S., and Emr, S.D. (2008). Ordered assembly of the ESCRT-III complex on endosomes is required to sequester cargo during MVB formation. Developmental cell *15*, 578-589.

Thong, F.S., Bilan, P.J., and Klip, A. (2007). The Rab GTPase-activating protein AS160 integrates Akt, protein kinase C, and AMP-activated protein kinase signals regulating GLUT4 traffic. Diabetes *56*, 414-423.

Tomancak, P., Beaton, A., Weiszmann, R., Kwan, E., Shu, S., Lewis, S.E., Richards, S., Ashburner, M., Hartenstein, V., Celniker, S.E.*, et al.* (2002). Systematic determination of patterns of gene expression during Drosophila embryogenesis. Genome biology *3*, RESEARCH0088.

Tomancak, P., Berman, B.P., Beaton, A., Weiszmann, R., Kwan, E., Hartenstein, V., Celniker, S.E., and Rubin, G.M. (2007). Global analysis of patterns of gene expression during Drosophila embryogenesis. Genome biology *8*, R145.

Torroja, L., Chu, H., Kotovsky, I., and White, K. (1999). Neuronal overexpression of APPL, the Drosophila homologue of the amyloid precursor protein (APP), disrupts axonal transport. Current biology : CB *9*, 489-492.

Tsai, P.I., Wang, M., Kao, H.H., Cheng, Y.J., Lin, Y.J., Chen, R.H., and Chien, C.T. (2012). Activity-dependent retrograde laminin A signaling regulates synapse growth at Drosophila neuromuscular junctions. Proceedings of the National Academy of Sciences of the United States of America *109*, 17699-17704.

Tsuda, M., Langmann, C., Harden, N., and Aigaki, T. (2005). The RING-finger scaffold protein Plenty of SH3s targets TAK1 to control immunity signalling in Drosophila. EMBO reports *6*, 1082-1087.

Tsuda, M., Seong, K.H., and Aigaki, T. (2006). POSH, a scaffold protein for JNK signaling, binds to ALG-2 and ALIX in Drosophila. FEBS letters *580*, 3296-3300.

Tsukazaki, T., Chiang, T.A., Davison, A.F., Attisano, L., and Wrana, J.L. (1998). SARA, a FYVE domain protein that recruits Smad2 to the TGFbeta receptor. Cell *95*, 779-791.

Ultanir, S.K., Hertz, N.T., Li, G., Ge, W.P., Burlingame, A.L., Pleasure, S.J., Shokat, K.M., Jan, L.Y., and Jan, Y.N. (2012). Chemical genetic identification of NDR1/2 kinase substrates AAK1 and Rabin8 Uncovers their roles in dendrite arborization and spine development. Neuron *73*, 1127-1142.

Unsicker, K., and Strelau, J. (2000). Functions of transforming growth factor-beta isoforms in the nervous system. Cues based on localization and experimental in vitro and in vivo evidence. European journal of biochemistry / FEBS *267*, 6972-6975.

Urano, J., Tabancay, A.P., Yang, W., and Tamanoi, F. (2000). The Saccharomyces cerevisiae Rheb G-protein is involved in regulating canavanine resistance and arginine uptake. The Journal of biological chemistry *275*, 11198-11206.

Urwin, H., Authier, A., Nielsen, J.E., Metcalf, D., Powell, C., Froud, K., Malcolm, D.S., Holm, I., Johannsen, P., Brown, J.*, et al.* (2010a). Disruption of endocytic trafficking in frontotemporal dementia with CHMP2B mutations. Human molecular genetics *19*, 2228-2238.

Urwin, H., Josephs, K.A., Rohrer, J.D., Mackenzie, I.R., Neumann, M., Authier, A., Seelaar, H., Van Swieten, J.C., Brown, J.M., Johannsen, P.*, et al.* (2010b). FUS pathology defines the majority of tau- and TDP-43-negative frontotemporal lobar degeneration. Acta neuropathologica *120*, 33-41.

Va, D.P., Sa, A.A., and Paul, S.F.D. (2009). WONDER ANIMAL MODEL FOR GENETIC STUDIES-Drosophila Melanogaster–ITS LIFE CYCLE AND BREEDING METHODS–A REVIEW. Sri Ramachandra Journal of Medicine, 33.

Vaibhava, V., Nagabhushana, A., Chalasani, M.L., Sudhakar, C., Kumari, A., and Swarup, G. (2012). Optineurin mediates a negative regulation of Rab8 by the GTPase-activating protein TBC1D17. Journal of cell science *125*, 5026-5039.

Valente, E.M., Brancati, F., Silhavy, J.L., Castori, M., Marsh, S.E., Barrano, G., Bertini, E., Boltshauser, E., Zaki, M.S., Abdel-Aleem, A.*, et al.* (2006). AHI1 gene mutations cause specific forms of Joubert syndrome-related disorders. Annals of neurology *59*, 527-534.

van de Hoef, D.L., Hughes, J., Livne-Bar, I., Garza, D., Konsolaki, M., and Boulianne, G.L. (2009). Identifying genes that interact with Drosophila presenilin and amyloid precursor protein. Genesis *47*, 246-260.

van der Zee, J., Urwin, H., Engelborghs, S., Bruyland, M., Vandenberghe, R., Dermaut, B., De Pooter, T., Peeters, K., Santens, P., De Deyn, P.P.*, et al.* (2008). CHMP2B C-truncating mutations in frontotemporal lobar degeneration are associated with an aberrant endosomal phenotype in vitro. Human molecular genetics *17*, 313-322.

Van Langenhove, T., van der Zee, J., Sleegers, K., Engelborghs, S., Vandenberghe, R., Gijselinck, I., Van den Broeck, M., Mattheijssens, M., Peeters, K., De Deyn, P.P.*, et al.* (2010). Genetic contribution of FUS to frontotemporal lobar degeneration. Neurology *74*, 366-371.

Vanderzeypen, F., Bier, J.C., Genevrois, C., Mendlewicz, J., and Lotstra, F. (2003). [Frontal dementia or dementia praecox? A case report of a psychotic disorder with a severe decline]. L'Encephale *29*, 172-180.

Ventura, J.J., Kennedy, N.J., Flavell, R.A., and Davis, R.J. (2004). JNK regulates autocrine expression of TGF-beta1. Molecular cell *15*, 269-278.

Vergarajauregui, S., Connelly, P.S., Daniels, M.P., and Puertollano, R. (2008). Autophagic dysfunction in mucolipidosis type IV patients. Human molecular genetics *17*, 2723-2737.

Vergarajauregui, S., and Puertollano, R. (2008). Mucolipidosis type IV: the importance of functional lysosomes for efficient autophagy. Autophagy *4*, 832-834.

Verhoeven, K., De Jonghe, P., Coen, K., Verpoorten, N., Auer-Grumbach, M., Kwon, J.M., FitzPatrick, D., Schmedding, E., De Vriendt, E., Jacobs, A.*, et al.* (2003). Mutations in the small GTP-ase late endosomal protein RAB7 cause Charcot-Marie-Tooth type 2B neuropathy. American journal of human genetics *72*, 722-727.

Verstreken, P., Ohyama, T., and Bellen, H.J. (2008). FM 1-43 labeling of synaptic vesicle pools at the Drosophila neuromuscular junction. Methods in molecular biology *440*, 349-369.

Vogel, T., Ahrens, S., Buttner, N., and Krieglstein, K. (2010). Transforming growth factor beta promotes neuronal cell fate of mouse cortical and hippocampal progenitors in vitro and in vivo: identification of Nedd9 as an essential signaling component. Cerebral cortex *20*, 661-671.

Votteler, J., Iavnilovitch, E., Fingrut, O., Shemesh, V., Taglicht, D., Erez, O., Sorgel, S., Walther, T., Bannert, N., Schubert, U.*, et al.* (2009). Exploring the functional interaction between POSH and ALIX and the relevance to HIV-1 release. BMC biochemistry *10*, 12.

Wakabayashi, J., Zhang, Z., Wakabayashi, N., Tamura, Y., Fukaya, M., Kensler, T.W., Iijima, M., and Sesaki, H. (2009). The dynamin-related GTPase Drp1 is required for embryonic and brain development in mice. The Journal of cell biology *186*, 805-816.

Wan, H.I., DiAntonio, A., Fetter, R.D., Bergstrom, K., Strauss, R., and Goodman, C.S. (2000). Highwire regulates synaptic growth in Drosophila. Neuron *26*, 313-329.

Wang, X., Shaw, W.R., Tsang, H.T., Reid, E., and O'Kane, C.J. (2007). Drosophila spichthyin inhibits BMP signaling and regulates synaptic growth and axonal microtubules. Nature neuroscience *10*, 177-185.

Watson, M.R., Lagow, R.D., Xu, K., Zhang, B., and Bonini, N.M. (2008). A drosophila model for amyotrophic lateral sclerosis reveals motor neuron damage by human SOD1. The Journal of biological chemistry *283*, 24972-24981.

Watts, G.D., Wymer, J., Kovach, M.J., Mehta, S.G., Mumm, S., Darvish, D., Pestronk, A., Whyte, M.P., and Kimonis, V.E. (2004). Inclusion body myopathy associated with Paget disease of bone and frontotemporal dementia is caused by mutant valosin-containing protein. Nature genetics *36*, 377-381.

Weiss, K.R., Kimura, Y., Lee, W.C., and Littleton, J.T. (2012). Huntingtin aggregation kinetics and their pathological role in a Drosophila Huntington's disease model. Genetics *190*, 581-600.

West, R.J., and Sweeney, S.T. (2012). Oxidative stress and autophagy: Mediators of synapse growth? Autophagy *8*.

Westlake, C.J., Baye, L.M., Nachury, M.V., Wright, K.J., Ervin, K.E., Phu, L., Chalouni, C., Beck, J.S., Kirkpatrick, D.S., Slusarski, D.C*., et al.* (2011). Primary cilia membrane assembly is initiated by Rab11 and transport protein particle II (TRAPPII) complex-dependent trafficking of Rabin8 to the centrosome. Proceedings of the National Academy of Sciences of the United States of America *108*, 2759-2764.

Whitworth, A.J. (2011). Drosophila models of Parkinson's disease. Advances in genetics *73*, 1-50.

Whitworth, A.J., Wes, P.D., and Pallanck, L.J. (2006). Drosophila models pioneer a new approach to drug discovery for Parkinson's disease. Drug discovery today *11*, 119-126.

Wild, P., Farhan, H., McEwan, D.G., Wagner, S., Rogov, V.V., Brady, N.R., Richter, B., Korac, J., Waidmann, O., Choudhary, C*., et al.* (2011). Phosphorylation of the autophagy receptor optineurin restricts Salmonella growth. Science *333*, 228-233.

Williamson, W.R., and Hiesinger, P.R. (2010). Preparation of developing and adult Drosophila brains and retinae for live imaging. Journal of visualized experiments : JoVE.

Winkler, S., Schwabedissen, A., Backasch, D., Bokel, C., Seidel, C., Bonisch, S., Furthauer, M., Kuhrs, A., Cobreros, L., Brand, M*., et al.* (2005). Target-selected mutant screen by TILLING in Drosophila. Genome research *15*, 718-723.

Wollert, T., and Hurley, J.H. (2010). Molecular mechanism of multivesicular body biogenesis by ESCRT complexes. Nature *464*, 864-869.

Wollert, T., Wunder, C., Lippincott-Schwartz, J., and Hurley, J.H. (2009a). Membrane scission by the ESCRT-III complex. Nature *458*, 172-177.

Wollert, T., Yang, D., Ren, X., Lee, H.H., Im, Y.J., and Hurley, J.H. (2009b). The ESCRT machinery at a glance. Journal of cell science *122*, 2163-2166.

Wolpert, L. (2007). Principles of development, 3rd edn (Oxford ; New York: Oxford University Press).

Wu, H., Xiong, W.C., and Mei, L. (2010). To build a synapse: signaling pathways in neuromuscular junction assembly. Development *137*, 1017-1033.

Wu, X., Bradley, M.J., Cai, Y., Kummel, D., De La Cruz, E.M., Barr, F.A., and Reinisch, K.M. (2011). Insights regarding guanine nucleotide exchange from the structure of a DENN-domain protein complexed with its Rab GTPase substrate. Proceedings of the National Academy of Sciences of the United States of America *108*, 18672-18677.

Wucherpfennig, T., Wilsch-Brauninger, M., and Gonzalez-Gaitan, M. (2003). Role of Drosophila Rab5 during endosomal trafficking at the synapse and evoked neurotransmitter release. The Journal of cell biology *161*, 609-624.

Xu, Z., Kukekov, N.V., and Greene, L.A. (2003). POSH acts as a scaffold for a multiprotein complex that mediates JNK activation in apoptosis. The EMBO journal *22*, 252-261.

Yamaguchi, K., Shirakabe, K., Shibuya, H., Irie, K., Oishi, I., Ueno, N., Taniguchi, T., Nishida, E., and Matsumoto, K. (1995). Identification of a member of the MAPKKK family as a potential mediator of TGF-beta signal transduction. Science *270*, 2008-2011.

Yamashita, M., Fatyol, K., Jin, C., Wang, X., Liu, Z., and Zhang, Y.E. (2008). TRAF6 mediates Smad-independent activation of JNK and p38 by TGF-beta. Molecular cell *31*, 918-924.

Yang, S.A., and Su, M.T. (2011). Excessive Dpp signaling induces cardial apoptosis through dTAK1 and dJNK during late embryogenesis of Drosophila. Journal of biomedical science *18*, 85.

Yang, Y., Hentati, A., Deng, H.X., Dabbagh, O., Sasaki, T., Hirano, M., Hung, W.Y., Ouahchi, K., Yan, J., Azim, A.C*., et al.* (2001). The gene encoding alsin, a protein with three guanine-nucleotide exchange factor domains, is mutated in a form of recessive amyotrophic lateral sclerosis. Nature genetics *29*, 160-165.

Yi, J.J., Barnes, A.P., Hand, R., Polleux, F., and Ehlers, M.D. (2010). TGF-beta signaling specifies axons during brain development. Cell *142*, 144-157.

Yin, X., Murphy, S.J., Wilkes, M.C., Ji, Y., and Leof, E.B. (2013). Retromer maintains basolateral distribution of the type II TGF-beta receptor via the recycling endosome. Molecular biology of the cell *24*, 2285-2298.

Yoshida, K., Yamaguchi, T., Natsume, T., Kufe, D., and Miki, Y. (2005). JNK phosphorylation of 14-3-3 proteins regulates nuclear targeting of c-Abl in the apoptotic response to DNA damage. Nature cell biology *7*, 278-285.

Yoshihara, M., Rheuben, M.B., and Kidokoro, Y. (1997). Transition from growth cone to functional motor nerve terminal in Drosophila embryos. The Journal of neuroscience : the official journal of the Society for Neuroscience *17*, 8408-8426.

Yoshimura, S., Egerer, J., Fuchs, E., Haas, A.K., and Barr, F.A. (2007). Functional dissection of Rab GTPases involved in primary cilium formation. The Journal of cell biology *178*, 363-369.

Yu, Z., and Bonini, N.M. (2011). Modeling human trinucleotide repeat diseases in Drosophila. International review of neurobiology *99*, 191-212.

Zamborlini, A., Usami, Y., Radoshitzky, S.R., Popova, E., Palu, G., and Gottlinger, H. (2006). Release of autoinhibition converts ESCRT-III components into potent inhibitors of HIV-1 budding. Proceedings of the National Academy of Sciences of the United States of America *103*, 19140-19145.

Zerial, M., and McBride, H. (2001). Rab proteins as membrane organizers. Nature reviews Molecular cell biology *2*, 107-117.

Zhai, R.G., and Bellen, H.J. (2004). The architecture of the active zone in the presynaptic nerve terminal. Physiology *19*, 262-270.

Zhang, B., Li, M., Chen, L., Yang, K., Shan, Y., Zhu, L., Sun, S., Li, L., and Wang, C. (2009). The TAK1-JNK cascade is required for IRF3 function in the innate immune response. Cell research *19*, 412-428.

Zhang, B., and Stewart, B. (2010). Electrophysiological recording from Drosophila larval body-wall muscles. Cold Spring Harbor protocols *2010*, pdb prot5487.

Zhang, B., Zhang, Y., Wang, Z., and Zheng, Y. (2000). The role of Mg2+ cofactor in the guanine nucleotide exchange and GTP hydrolysis reactions of Rho family GTP-binding proteins. The Journal of biological chemistry *275*, 25299-25307.

Zhang, S., Binari, R., Zhou, R., and Perrimon, N. (2010). A genomewide RNA interference screen for modifiers of aggregates formation by mutant Huntingtin in Drosophila. Genetics *184*, 1165-1179.

Zhang, Y., Guo, H., Kwan, H., Wang, J.W., Kosek, J., and Lu, B. (2007). PAR-1 kinase phosphorylates Dlg and regulates its postsynaptic targeting at the Drosophila neuromuscular junction. Neuron *53*, 201-215.

Zhu, X., Ogawa, O., Wang, Y., Perry, G., and Smith, M.A. (2003). JKK1, an upstream activator of JNK/SAPK, is activated in Alzheimer's disease. Journal of neurochemistry *85*, 87-93.

Zhu, Y., Hu, L., Zhou, Y., Yao, Q., Liu, L., and Shao, F. (2010). Structural mechanism of host Rab1 activation by the bifunctional Legionella type IV effector SidM/DrrA. Proceedings of the National Academy of Sciences of the United States of America *107*, 4699-4704.

Zito, K., Parnas, D., Fetter, R.D., Isacoff, E.Y., and Goodman, C.S. (1999). Watching a synapse grow: noninvasive confocal imaging of synaptic growth in Drosophila. Neuron *22*, 719-729.